Identification and Characterisation of Human Cytomegalovirus-Mediated Degradation of Helicase-Like Transcription Factor

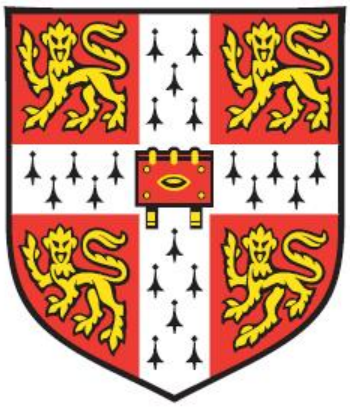

Kai-Min Lin

Department of Medicine

Cambridge Institute for Medical Research

University of Cambridge

This dissertation is submitted for the degree of

Doctor of Philosophy

Fitzwilliam College

September 2020

Declaration

I hereby declare, that except where specific reference is made to the work of others, the contents of this dissertation are original and have not been submitted in whole or in part for consideration for any other degree of qualification in this, or any other university.

This dissertation is the result of my own work and includes nothing which is the outcome of work done in collaboration except as where specified in the text and acknowledgments.

This dissertation does not exceed the specified word limit of 60,000 words as defined by the Degree Committee, excluding figures, photographs, tables, appendices and bibliography.

Kai-Min Lin

September, 2020

Summary

Identification and characterisation of human cytomegalovirus-mediated degradation of helicase-like transcription factor

Kai-Min Lin

Viruses are known to degrade host factors that are important in innate antiviral immunity in order to infect successfully. To systematically identify host proteins targeted for early degradation by human cytomegalovirus (HCMV), the lab developed orthogonal screens using high resolution multiplexed mass spectrometry. Taking advantage of broad and selective proteasome and lysosome inhibitors, proteasomal degradation was found to be heavily exploited by HCMV. Several known antiviral restriction factors, including components of cellular promyelocytic leukemia (PML) were enriched in a shortlist of proteasomally degraded proteins during infection.

A particularly robust novel 'hit' was helicase-like transcription factor (HLTF), a DNA repair protein that participates in error-free repair of stalled replication forks. HLTF was found degraded very early during infection, and its expression remained low throughout the course of HCMV lytic cycle. *De novo* expression of UL145, a previously uncharacterized viral protein, was found necessary and sufficient to degrade HLTF via recruitment of the cullin 4/DDB1 E3 ligase complex.

HLTF degradation was reported in human immunodeficiency virus (HIV) infection, however the interaction between HLTF and viruses remain largely elusive. The roles of UL145 were explored in hopes of understanding functions of HLTF in HCMV infection. UL145 was identified as a non-essential immediate early protein, however had a possible role in type I interferon (IFN) induction regulation in later stages of HCMV lytic progression. As the key host protein to be rescued by UL145 deletion, depletion of HLTF was found to transiently impair IFNβ transcription and HCMV infection. I hypothesise that HLTF is an undiscovered nuclear viral DNA sensor that triggers an antiviral interferon response during viral DNA replication.

Additionally, work presented here expands the range of powerful screening technologies to identify HCMV restriction factor candidates by identifying virally degraded host proteins. Further investigation of these candidates will contribute to our

understanding of how HCMV modulates host protein expression to evade antiviral factors.

Acknowledgments

Firstly, I would like to express my sincere gratitude to my supervisor Dr. Mike Weekes, for his everlasting support, guidance, and encouragement throughout the pursuit of this degree. I was blessed with this opportunity for he patiently reviewed a PhD application coming abruptly. His instruction was fundamental to this thesis and helped me develop as a research scientist. Without his scientific acumen and aweing diligence, it was nearly impossible to move this challenging project forward.

I would also like to thank everyone in the Weekes lab, who created the most enjoyable working environment in the world that I was almost reluctant to leave. Many of them contributed a lot to this project, especially Dr. Katie Nightingale, who laid a firm foundation for the entire protein degradation project and generously provided helpful discussions. I really appreciate Dr. Luis Nobre, Alice Fletcher-Etherington, and Dr. Ben Ravenhill for providing me the many cell lines and plasmids I needed for my experiments, and Dr. Lior Soday for the help on processing the proteomics data. All members of the Weekes lab were truly the highlights of my PhD. I will deeply miss the wise decisions from Katie, reliable solutions from Luis, warm support from Lior, friendly chats with Colin, evening enlightenments from Ben, prodigious work from Alice, wee comedies from Leah, insider gossips from Cassie, and of course, having Martin to check on my wellbeing.

Our collaborators at Cardiff University, particularly Dr. Rich Stanton, had unfailingly supplied us with all kinds of HCMV strains. His expertise in HCMV provided reliable protocols and useful advice that helped overcome many hurdles.

My research involved many equipment from CIMR core facility. I would like to thank Dr. Robin Antrobus from the proteomics core, Dr. Reiner Schulte from the flow cytometry core, Mark Bowen from the Microscopy core, and Mark Smallwood the level coordinator for maintaining the state of the art facilities and the help making the experimental plans into reality.

I am very fortunate to receive this opportunity to study at the University of Cambridge as an oversea fee status student. I would like to thank the Cambridge Commonwealth, European & International Trust and the Ministry of Education of Taiwan for setting up

and running the Taiwan-Cambridge scholarship programme, which funded my tuition, fee, and stipend in Cambridge.

Finally, I will not be able to complete this without the unconditional support I have received from my friends and family, no matter from Cambridge, the EBV group of National Taiwan University, National Tsing-Hua University, or anywhere else I have ever called home. I would like to thank Julia Woitischek and Ragini Medhi for accompanying me on this PhD journey. I am also very grateful to Chin-Wen Liang and Chung-Ying Huang for bearing with me during all the ups and downs tirelessly in the past decade.

Table of Contents

List of Figures

Chapter 1. Introduction

Chapter 2. Materials and Methods

Chapter 3. HLTF degradation mechanism during HCMV infection

Chapter 4. Function of HLTF during HCMV infection

Chapter 5. Refining protein degradation screens

Chapter 6. Discussion

List of Tables

Abbreviations

4EHP	translation initiation factor 4E homologous protein
ADAMST1	a disintegrin and metalloproteinase with thrombospondin motifs 1
AGC	automatic gain control
AHR	aryl hydrocarbon receptor
AIDS	acquired immunodeficiency syndrome
AJUBA	LIM domain-containing protein ajuba
AMP	adenosine monophosphate
ANAPC	anaphase-promoting complex
AP-1	activator protein 1
APC	anaphase-promoting complex
ARHGAP35	Rho GTPase-activating protein 35
ARMC9	LisH domain-containing protein ARMC9
ASC	apoptosis-associated speck-like protein containing a caspase recruitment domain
ATG	autophagy
ATM	ataxia telangiectasia-mutated
ATR	ATM and Rad3-related
ATRX	alpha-thalassemia/mental retardation X-linked
BACmid	bacterial artificial chromosome plasmid
BCA	bicinchoninic acid
BEAF	Drosophilia boundary element associated factor
BECN1	Beclin 1
BED	BEAF and DREF containing domain
BEND3	BEN domain containing 3
BGLF4	EBV BamH1 digested, G fragment, left, forward 4

BRCA1	DSB repair proteins breast cancer 1
BTB	bric-a-brac-tramtrack-broad complex
BTLA	B and T lymphocyte attenuator
C18	octadecyl carbon chain
CASP8	caspase 8
Cbl-b	Casitas B-lineage lymphoma proto-oncogene-b
CBP	CREB-binding protein
CCDC71L	coiled-coil domain-containing protein 71L
CCMV	chimpanzee cytomegalovirus
CD14	cluster of differentiation 14
CD34	cluster of differentiation 34
CDC25A	cell division control protein 25 homolog A
CDC25A	cell division control protein 25 homolog C
CDC2A	cell division control protein 2 homolog A
CDC42EP3	CDC42 effector protein 3
CDK1	cyclin-dependent kinase 1
CDK2	cyclin-dependent kinase 2
cDNA	complement DNA
CFLAR	CASP8 and FADD-like apoptosis regulator
CFP	cyan fluorescent protein
cGAMP	cyclic-GMP-AMP
cGAS	cyclic GMP-AMP synthase
ChIP	chromatin immunoprecipitation
CHK1	checkpoint kinase 1
CHK2	checkpoint kinase 2
CHST14	carbohydrate sulfotransferase 14

CITED2	CBP/p300 interacting transactivator with Glu/Asp rich carboxy-terminal domain 2
CNTNAP1	contactin-associated protein 1
CP	core protein
CREB	cAMP-response element binding protein
CRISPR	clustered regularly interspaced short palindromic repeats
CRL	cullin RING E3 ligase
CTGF	connective tissue growth factor
CUL	cullin
CXCL1	C-X-C motif chemokine ligand 1
CXCL10	C-X-C motif chemokine ligand 10
DAI	DNA-dependent activator of interferon, also known as ZBP1
DAPI	4’,6-diamidino-2-phenylindole
DAPK2	death-associated protein kinase 2
DAVID	database for annotation, visualisation and integrated discovery
DAXX	death-domain associated protein
DCAF	DDB1- and CUL4-associated factor
DDB1	DNA damage-binding protein 1
ddH_2O	double-distilled water
DDR	DNA damage response
DDX41	DEAD-box helicase 41
DENN	differentially expressed in normal and neoplastic cells
DENND2A	DENN domain-containing protein 2A
DHX36	DEAH-box helicase 36
DHX9	DEAH-box helicase 9
DIMT1	probable dimethyladenosine transferase

DKK3	Dickkopf-related protein 3
DLC1	Rho GTPase-activating protein 7
Dlg	Drosophila discs-large
DMEM	Dulbecco's modified eagle medium
DMSO	dimethyl sulfoxide
DNA-PK	DNA-dependent protein kinase
DREF	Drosophilia DNA replication-related element factor
DSB	double strand break
dsDNA	double-strand DNA
DTT	dithiothreitol
dUTPase	deoxyuridine triphosphate nucleotidohydrolase
Dvl	Drosophilia dishevelled
E. coli	Escherichia coli
E6AP	HPV E6 protein associated protein
EA-D	EBV early antigen diffuse component
EBER	EBV-encoded small RNAs
EBNA1	EBV nuclear antigen 1
EBV	Epstein-Barr virus
EGFR	epidermal growth factor receptor
ELISA	enzyme-linked immunosorbent assay
ER	endoplasmic reticulum
ERGIC	ER-Golgi intermediate compartment
ERK1/2	extracellular signal-regulated kinases 1/2
ESCRT	endosomal sorting complex for transport
FADD	Fas-associated protein with death domain
FAM101B	filamin-interacting protein FAM101B, refilin B

FAM126A	filamin-interacting protein FAM126A, hyccin
FCS	foetal calf serum
FERM	4.1 protein, ezrin, radixin, and moesin
FITC	fluorescein isothiocyanate
FRET	fluorescence resonance energy transfer
FRMD6	FERM domain containing 6
GAPDH	glyceraldehyde 3-phosphate dehydrogenase
GAS	IFNγ-activated site
GFP	green fluorescent protein
GLG1	Golgi glycoprotein 1
GLS3	glutaminase isoform 3
GLT8D1	glycosyltransferase 8 domain-containing protein 1
GM-CSF	granulocyte macrophage colony-stimulating factor
GMP	guanosine monophosphate
H2AX	H2A histone family member X
HACD1	Very-long-chain (3R)-3-hydroxyacyl-CoA dehydratase 1
HBx	hepatitis B virus X protein
HCD	higher energy collisional dissociation
HCMV	human cytomegalovirus
HDAC	histone deacetylase
HECT	E6AP C terminus
HEK293	human embryonic kidney cells 293
HEK293T	SV40 large T transformed HEK293
HEPES	4-(2-hydroxyethyl)-1-piperazineethanesulfonic acid
HERC	HECT and RLD-containing
HFFF	Human foetal foreskin fibroblast

HFFF-TERT	human telomerase reverse transcriptase immortalized HFFF
HGBP	human globin β promoter
HHARI	human homolog of Ariadne
HHV6	human herpesvirus 6
HHV7	human herpesvirus 7
HIN	hematopoietic expression, interferon-inducible nature, and nuclear localization
HIRAN	HIP116 Rad5p N-terminal
HIV1	human immunodeficiency virus type 1
HLTF	helicase-like transcription factor
HNRNPU	heterogeneous nuclear ribonucleoprotein U
HOIL	heme-oxidized IRP2 ubiquitin ligase 1
HOIP	HOIL-1-interacting protein
HOXA11	homeobox protein Hox-A11
HOXA13	homeobox protein Hox-A13
hpi	hour(s) post infection
HPLC	high-performance liquid chromatography
HpRP	high pH reversed phase fractionation
HPV	human papillomavirus
HR	homologous recombination
HRP	horseradish peroxidase
HSV1	herpes simplex viruses 1
HSV2	herpes simplex viruses 2
HUWE1	HECT, UBA and WWE domain containing 1
IAA	iodoacetamide
IBR	in-between-ring

ICP0	HSV1 infected cell protein 0
ICP27	HSV1 infected-cell protein 27
ID	internal diameter
IE1	HCMV immediate early 1
IE2	HCMV immediate early 2
IFIT1	interferon-induced protein with tetratricopeptide repeats 1
IFIT2	interferon-induced protein with tetratricopeptide repeats 2
IFIT3	interferon-induced protein with tetratricopeptide repeats 3
IFN	interferon
IKKε	IκB kinase ε
IKKβ	inhibitor of NFκB kinase β subunit
IL1	interleukin 1
IL6	interleukin 6
IL12	interleukin 12
IL18	Interleukin 18
IL28	interleukin 28
IL29	interleukin 29
IRF3	IFN regulatory factor 3
IRF9	interferon regulatory factor 9
IRL	internal repeat long
IRP2	iron regulatory protein 2
ISG	interferon-stimulated gene
ISG15	interferon stimulated gene 15
ISGF3	IFN-stimulated gene factor 3
ISRE	IFN-stimulated response element
ITCH	Itchy homolog

IκB	inhibitor of NFκB
JAK1	Janus activated kinase 1
JNK	c-Jun N-terminal kinase
kDa	kilo Dalton
KSHV	Kaposi's sarcoma-associated herpesvirus
LAMP	lysosome-associated membrane protein
LANA	KSHV latency-associated nuclear antigen 1
LAYN	layilin
LB	Luria-Bertani
LC3	light chain 3
LisH	lis homology domain
LMAN2L	lectin, mannose binding 2 like; VIP36-like protein
LMP	lysosomal membrane protein
LUBAC	linear ubiquitin chain assembly complex
LUNA	HCMV latency unique natural antigen
MAP3K2	mitogen-activated protein kinase kinase kinase 2
MAPK	mitogen-activated protein kinase
MAVS	mitochondrial antiviral signalling protein
MCLB	mammalian cell lysis buffer
MCMV	murine cytomegalovirus
MDA5	melanoma differentiation-associated gene 5
MDC1	mediator of DNA damage checkpoint protein 1
MDM2	murine double minute 2
MDMX	murine double minute X
MED20	mediator of RNA polymerase II transcription subunit 20
MEN1	menin 1

MHC	major histocompatibility complex
MHV68	murine gammaherpesvirus 68
MIC	MHC class I-related chain
MICA	MHC class-I chain-related proteins A
MIEP	major immediate early promoter
MLKL	mixed lineage kinase domain like pseudokinase
MOI	multiplicity of infection
MORC3	microrchidia CW-type zinc finger 3
MRN	MRE11, RAD50, NBS1
mRNA	messenger RNA
MS	mass spectrometry
MSK2	mitogen- and stress-activated kinase 2
mTOR	mammalian target of rapamycin
MuHV-4	murid herpesvirus-4
MVB	multivesicular bodies
MyD88	myeloid differentiation primary response gene 88
NACC2	nucleus accumbens-associated protein 2
NBS1	Nijmegen breakage syndrome 1
NCE	normalised collision energy
ND10	nuclear domain 10
NEDD4	neural precursor cell expressed, developmentally down-regulated 4
NEDD4L	NEDD4-like
NEMO	NFκB essential modulator
NFκB	nuclear factor kappa B
NHEJ	non-homologous end joining
NKG2DL	natural killer group 2D ligand

NLGN2	neuroligin 2
NTase	nucleotidyltransferase
O/N	overnight
OAS1	2’-5’-oligoadenylate synthase 1
OAS2	2’-5’-oligoadenylate synthase 2
ORF	open reading frame
oriLyt	HCMV origin of DNA replication
PAGE	polyacrylamide gel electrophoresis
PAMP	pathogen-associated molecular pattern
PARK2	Parkin 2
PBS	phosphate-buffered saline
PCDHGB2	protocadherin gamma-B2
PCDHGB5	protocadherin gamma-B5
PCDHGC3	Protocadherin gamma-C3
PCNA	proliferating cell nuclear antigen
PCR	polymerase chain reaction
pDC	plasmacytoid dendritic cell
PDZ	PSD-95/Dlg/ZO-1
PDZD11	PDZ domain containing protein 11
PE	phosphatidylethanolamine
PE	phycoerythrin
pfu	plaque forming unit
PI3K	phosphoinositide 3-kinase
PI3KC3–C1	class III phosphatidylinositol 3-kinase complex I
PIC	Protease Inhibitor Cocktail
PKNOX1	Homeobox protein PKNOX1

PML	promyelocytic leukemia
pol	polymerase
pp65	phosphoprotein 65
pp71	phosphoprotein 71
PRR	pattern-recognition receptor
PSD-95	Postsynaptic density protein 95
pSFFV	spleen focus-forming virus promoter
pSILAC	pulsed SILAC
PSM	peptide spectral matches
PTPN14	tyrosine-protein phosphatase non-receptor type 14
PVDF	polyvinylidene fluoride
RALGPS2	Ras-specific guanine nucleotide-releasing factor RalGPS2
RBM4	RNA binding motif protein 4
RBPMS	RNA-binding protein with multiple splicing
RBR	RING-between-RING
RBX1	RING box 1
RBX2	RING box 2
RGCC	regulator of cell cycle RGCC
RGL2	Ral guanine nucleotide dissociation stimulator like 2
RhCMV	Rhesus cytomegalovirus
RHIM	receptor-interacting protein homotypic interaction motif
RIG-I	RNA helicases retinoic acid-inducible gene I
RING	really interesting gene
RIPA	radioimmunoprecipitation assay
RIPK1	receptor-interacting serine/threonine protein kinases 1
RIPK3	receptor-interacting serine/threonine protein kinases 3

RLD	regulator of chromatin condensation 1 like domains
RNA	ribonucleic acid
RNF150	RING finger protein 150
RNF168	RING finger 168
RNF8	RING finger 8
ROC1	regulator of cullin 1
ROC2	regulator of cullin 2
RP	regulatory particle
RPA	replication protein A
RPS6KA4	ribosomal protein S6 kinase A4
rRNA	ribosomal RNA
RS	rapid separation
RSV	respiratory syncytial virus
RT	room temperature
RTK	receptor tyrosine kinase
SAM	sterile alpha motif
SAMHD1	SAM And HD domain containing deoxynucleoside triphosphate triphosphohydrolase 1
SA	streptavidin
SCCMV	simian cytomegalovirus
SCID	severe combined immunodeficiency
SDS	sodium dodecyl sulphate
SD	standard deviation
SEM	standard error of the mean
SETX	senataxin
SeV	Sendai virus

SF	serum-free
shRNA	small hairpin RNA
SigA	significance A
SigB	significance B
SILAC	stable isotope labelling by amino acids in cell culture
siRNA	small interfering RNA
SKP1	S phase kinase-associated protein 1
SMARCA3	SWI/SNF-related matrix-associated actin-dependent regulator of chromatin subfamily A member 3
SNAP	N-ethylmaleimide-sensitive attachment protein
SNARE	SNAP receptor
SNX16	sorting nexin 16
SOCS	suppressor of cytokine signalling box
SP100	speckled protein 100 kDa
SQSTM1	sequestosome 1, also known as p62
ssDNA	single strand DNA
STAT	signal transducer and activator of transcription
STING	stimulator of IFN gene
STK32B	serine/threonine kinase 32B
STNB1	syntrophin beta 1
SUGP2	SURP and G-patch domain-containing protein 2
SURP	suppressor of white-apricot homolog, SWAP
SV40	simian virus 40
SV5	simian virus V protein 5
SWI/SNF	switch/sucrose non-fermentable
TADA1	transcriptional adapter 1

TANK	TRAF-associated NFκB activator
TBK1	TANK-binding kinase-1
TCA	trichloroacetic acid
TCEAL4	transcription elongation factor A protein-like 4
TE	Tris-EDTA
tet	tetracycline
TFAP4	transcription factor AP-4
TLR	toll-like receptor
TMB	tetramethyl-benzidine
TMT	tandem mass tag
TNFα	tumour necrosis factor α
TOX	thymocyte selection-associated high mobility group box protein TOX
TP53BP1	p53 binding protein 1
TRAF	tumour necrosis factor receptor associated factor
TRAF6	tumour necrosis factor receptor-associated factor 6
TRIM32	tripartite motif-containing protein 32
TRIM56	tripartite motif-containing protein 56
TRIM5α	tripartite motif containing 5 alpha
TRL	terminal repeat long
tRNA	transfer RNA
TYK2	tyrosine kinase 2
Ub	ubiquitin
UBC13	ubiquitin-conjugating enzyme 13
UHPLC	ultrahigh performance liquid chromatography
UL	HCMV unique long
ULBPs	HCMV UL16 binding proteins

ULK1	unc-51-like autophagy activating kinase 1
UNG2	uracil-DNA glycosylase 2
US	HCMV unique short
UV	ultraviolet
VACV	vaccinia virus
V-ATPase	vacuolar ATPase
vIL10	HCMV viral interleukin 10
VIP36	vesicular integral-membrane protein VIP36
Vpr	HIV viral protein R
VSP16	vacuolar protein sorting-associated protein 16
VSV	vesicular stomatitis virus
VZV	varicella-zoster virus
wnt	wingless
WT	wild-type
WWP2	NEDD4-like E3 ubiquitin-protein ligase WWP2
Xcorr	cross-correlation score
XPA	Xeroderma pigmentosum complementation group A
YAP1	yes-associated protein 1
YFP	yellowish-green fluorescent protein
ZBED1	zinc finger BED-type containing 1
ZBP1	Z-form DNA/RNA-binding protein 1
ZFP36L2	mRNA decay activator protein ZFP36L2
ZMYND11	zinc finger MYND-type containing 11
ZNF668	zinc finger protein 668
ZO-1	zonula occludens-1

Chapter 1. Introduction

1.1. Human Cytomegalovirus

1.1.1. Herpesvirdae family

Herpesviridae are a family of linear, double-stranded DNA viruses that disseminate broadly in nature, infecting a wide range of animals, including mammals, birds, and reptiles (Pellett and Roizman, 2013). There are 8 types of herpesviruses having human as the primary host, all of which belong to one of the three subfamilies of Herpesvirdae (Table 1.1): The Alphaherpesvirinae, the Betaherpesvirinae, and the Gammaherpesvirinae (Pellett and Roizman, 2013).

Alphaherpesviruses have the most variable hosts among herpesviruses, replicate relatively fast, and establish latency primarily in sensory ganglia (Smith, 2012). This subfamily includes *Simplexviruses* and *Varicelloviruses* that have mammalian hosts, *Mardiviruses* and *Iltoviruses* that have avian hosts, and several reptilian herpesviruses that are not classified to any current genus (McGeoch and Gatherer, 2005). Herpes simplex viruses (HSV1, HSV2) and varicella-zoster virus (VZV) from this subfamily have man as the natural host (Bloom, 2016).

In comparison, betaherpesviruses, such as human cytomegalovirus (HCMV), human herpesvirus 6 (HHV6), and human herpesvirus 7 (HHV7) have restricted host range and a prolonged replication cycle (Santos, 2016). Cells infected with primate betaherpesviruses frequently become enlarged (cytomegalia) due to the presence of intranuclear inclusion bodies. Betaherpesviruses can establish latency in secretory glands, lymphoreticular cells, and kidneys (Mocarski, 2007).

Gammaherpesviruses have the most restricted host range among the three subfamilies, mainly have primates and mice as their natural host (Cesarman, 2011). In this subfamily Epstein-Barr virus (EBV) and Kaposi's sarcoma-associated herpesvirus (KSHV) are associated with tumour formation (Cesarman, 2011). All gammaherpesviruses can

lytically infect in lymphoblastoid cells, and latency is frequently established in lymphoid tissue (Tibbetts et al., 2003).

Even though different herpesviruses have distinct gene expression programs leading to diverse pathogenic effects, all members of herpesvirdae share several biological properties. Firstly, they all encode viral enzymes for nucleic acid metabolism, DNA synthesis, and post-translational protein modification; secondly, virus gene transcription, synthesis of viral DNA, and nucleocapsid assembly of herpesviruses occur in the host nucleus, and thirdly, herpesviruses establish lifelong latency in their hosts.

Table 1.1. Classification of the human herpesviruses.

Subfamily	Genus	Virus
Alphaherpesvirinae	Simplexvirus	Herpes simplex virus 1 (HSV1/HHV1)
		Herpes simplex virus 2 (HSV2/HHV2)
	Varicellovirus	Varicella-zoster virus (VZV/HHV3)
Betaherpesvirinae	Cytomegalovirus	Human cytomegalovirus (HCMV/HHV5)
	Roseolovirus	Human betaherpesvirus 6A (HHV6A)
		Human betaherpesvirus 6B (HHV6B)
		Human betaherpesvirus 7 (HHV7)
Gammaherpesvirinae	Lymphocryptovirus	Epstein-Barr virus (EBV/HHV4)
	Rhadinovirus	Kaposi's sarcoma-associated herpesvirus (KSHV/HHV8)

1.1.2. Human Cytomegalovirus

Human cytomegalovirus (HCMV) is a ubiquitous betaherpesvirus that persistently infects the vast majority of the human population worldwide. The prevalence of HCMV

infection is >80% in Africa, Asia and South America, and 40%-70% in Europe and North America (Cannon et al., 2010). The virus has a wide range of tissue tropism including endothelial cells, fibroblasts, smooth muscle, and hematopoietic cells, and possesses the potential to spread through the circulation system to many organs (Griffiths et al., 2015). Although primary infection is mostly asymptomatic in healthy individuals, HCMV is still the leading cause of congenital infection and may lead to life-threatening diseases in immunocompromised patients. Upon primary infection, HCMV effectively evades host innate and adaptive immunity and establishes life-long latency, making it an ideal model to investigate viral immune evasion (Jackson et al., 2011; Powers et al., 2008). Only a few antiviral drugs are currently available in clinical practice, and there is still a high demand for antiviral vaccines and safer antiviral treatments to reduce the global public health burden caused by HCMV (Anderholm et al., 2016).

1.1.3. Virion structure

HCMV shares structural properties with other herpesviruses (Figure 1.1). The double-stranded viral DNA is packed in a stable icosahedral protein nucleocapsid, which is surrounded by a thick layer of tegument proteins. HCMV capsids are encapsulated by an envelope consisting of host-derived lipid bilayer membrane and viral glycoproteins which mediate the attachment and entry to host cells. For instance, the trimeric complex gH:gL:gO allows virus to infect fibroblasts while the pentamer gH:gL:pUL128:pUL130:pUL131A facilitates entry into epithelial and endothelial cells (Vanarsdall and Johnson, 2012).

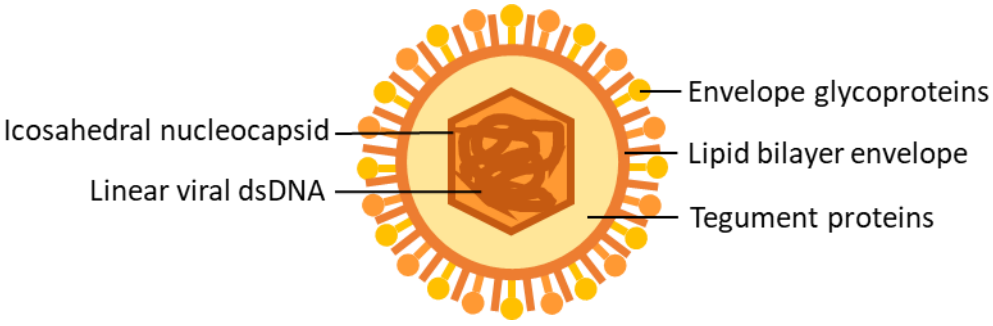

Figure 1.1. Structure of HCMV virion.

1.1.4. Viral genome

Among all the viruses that have human as the primary host, HCMV has the largest genome, with an approximate length of 230 kb (Dolan et al., 2004) and consisting of a unique long (UL) region and a unique short (US) region flanked by terminal and internal repeats (Figure 1.2). The terminal and internal repeats are reverse complementary to each other. The paired sequences flanking UL are known as "b" (terminal repeat long, TRL) and " b' " (internal repeat long, IRL), and the sequences flanking US are " c' " (IRS) and "c" (TRS), resulting in an overall configuration TRL-UL-IRL-IRS-US-TRS. A short redundant region called "a" sequence may come in multiple copies in some strains, occurs at both ends of HCMV genome and inversely at the IRL–IRS junction (Mocarski et al., 2013).

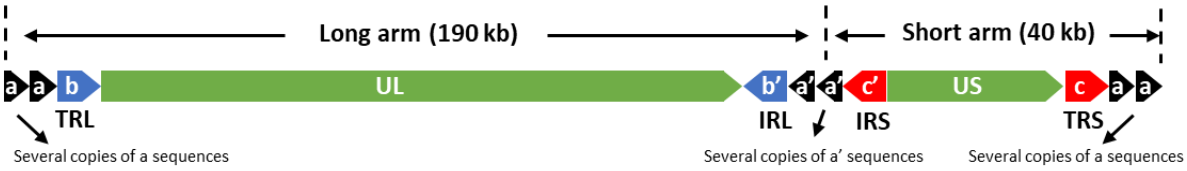

Figure 1.2. HCMV genome structure.
HCMV genome is comprised of long and short arms. Unique long (UL) sequence is flanked by copies of the b sequence (TRL) and inverted b sequence (b', IRL). Unique short (US) sequence is flanked by copies of c sequence (TRS) and inverted c sequence (c', IRS). One or several copies of the a sequence are found at both ends or the long/short junction (as inverted a, a' sequence) where the long and short arms join.

Generally, HCMV genes and their products are named in an orderly fashion based on their position in the genome, from left to right. However, some viral proteins are given names according to their chemical posttranslational modification and molecular weight, for example phosphorylated major tegument protein pp65 (UL83), or even the temporal

expression during the course of infection (immediate early proteins IE1 and IE2) (Chee et al., 1990; Spaete et al., 1994).

HCMV encodes for 171 canonical genes, several of which are known to be involved in steps of HCMV life cycle, yet the function of many viral gene products remains unknown (Van Damme and Van Loock, 2014). Adding to the complexity of HCMV biology, using ribosome profiling and transcript analysis, more than 600 previously unreported open reading frames were identified and verified, with a proportion verified by protein mass spectrometry at the time of study and since (Nightingale et al., 2018; Nobre et al., 2019; Stern-Ginossar et al., 2012; Weekes et al., 2014). In addition to protein-coding genes, HCMV also produces 23 miRNAs and 4 long non-coding RNAs (RNA2.7, RNA1.2, RNA4.9 and RNA5.0) whose roles in HCMV life cycle are poorly understood (Dhuruvasan et al., 2011; Gatherer et al., 2011; Zhang et al., 2007).

1.1.5. Laboratory strains

Despite having a wide range of tissue tropism, HCMV strains accumulate deletion and point mutations when propagated in cell culture (Stanton et al., 2010). Gene-disrupting mutations in a set of at least 26 genes are common, contributing to the high genome diversity within different HCMV strains (Sijmons et al., 2015a). For example, the large fragment of UL/b' has been replaced by inverted repeat from the left terminus of the HCMV genome in highly-passaged, laboratory-adapted strains AD169 and Towne (Cha et al., 1996; Chee et al., 1990). AD169 also carries frameshifts of RL5A, RL13 and UL131A, resulting in inactivation of these genes (Akter et al., 2003; Davison et al., 2003; Yu et al., 2002). Towne has mutations that disable RL13 and UL130. Sometimes UL1, UL36, UL40, UL42, UL43, US1 and US9 are mutated in heterogeneously maintained laboratory-propagated stains (Bradley et al., 2009; Dargan et al., 1997; Mocarski et al., 1997; Skaletskaya et al., 2001). Although minimally passaged in cell culture, HCMV strains Merlin and Toledo still have mutations in at least UL128 and RL13. Merlin UL128 is truncated by a single nucleotide substitution that introduces a premature termination (Dolan et al., 2004). Toledo UL128 mutation is induced by inversion of a region following

the UL segment (Davison et al., 2003). Toledo has an in-frame deletion in RL13, and after a small number of passages in vitro, Merlin generally develops a frameshift mutation in RL13 (Dargan et al., 2010). In comparison with the unpassaged clinical isolates, nearly all of the passaged strains have function-disrupting mutations in UL128, UL130, or UL131A, and most have mutations in at least one member of the RL11 gene family, such as RL13 (Akter et al., 2003; Dolan et al., 2004). Highly productive TB40/E is a low passage endotheliotropic strain that has frameshifted UL141, but usually have intact UL128, UL130 and UL131A (Sinzger et al., 2008).

It has been reported that HCMV strains cultured in fibroblasts have improved replication and release of progeny virus but attenuated virulence such as the ability to infect epithelial and endothelial cells (Revello and Gerna, 2010). Extensive study of the commonly mutated genes has suggested the reasons underlying these observations. RL13, for instance, is shown to efficiently repress HCMV replication in multiple cell types (Stanton et al., 2010). It has also been shown that loss of any one of three components, namely protein products of UL128, UL130, and UL131A, of the pentameric complex gH:gL:UL128:UL130:UL131A compromises attachment and replication efficiency in epithelial and endothelial cells (Hahn et al., 2004; Sinzger et al., 2008; Wang and Shenk, 2005). The major genetic difference between high passage and low passage strains lies in the ~15 kb UL/b' region, which leads to further attenuation of infectivity. Loss of the UL133-UL138 segment suppresses viral replication in hematopoietic progenitors and augments replication in endothelial cells (Grainger et al., 2010; Umashankar et al., 2011). A study in severe combined immunodeficiency (SCID) mice with human tissue implants demonstrate that AD169 has lost the ability to replicate *in vivo* (Wang et al., 2005).

1.1.6. Latency

Like other members of the herpesvirus family, one key characteristic of HCMV is its ability to establish latency. HCMV latency is associated with host cell type, with endothelial cells and myeloid cells are considered as sites for HCMV latency and persistent infection. *In vitro* studies suggest that aortic endothelial cells but not brain

microvascular endothelial cells support latent HCMV infection (Fish et al., 1998). Cells of the early myeloid lineage, such as $CD34^+$ hematopoietic progenitor cells and $CD14^+$ monocytes derived from $CD34^+$ cells have been shown to harbour latent HCMV *in vivo* (Sinclair and Sissons, 2006). In these cells, viral genome is maintained without production of infectious progeny. HCMV reactivation has been extensively studied in myeloid cell differentiation, a process in which $CD34^+$ hematopoietic stem cells differentiate into mature dendritic cells or macrophages (Poole et al., 2015; Reeves and Sinclair, 2013). Regulation of chromatin structure at the major immediate early promoter (MIEP) within myeloid cells is considered crucial to HCMV activation (Elder and Sinclair, 2019).

Prior studies have suggested that the HCMV genome resides as a circular episome in latently infected cells (Bolovan-Fritts et al., 1999; Slobedman and Mocarski, 1999). Other features of HCMV latency include the detectable expression of the latency-associated genes and the absence of global viral gene transcription (Elder and Sinclair, 2019; Slobedman et al., 2010). This set of latency-associated genes contains UL82 (pp71), UL138, glycoprotein UL144, chemokine receptor US28, latency-associated viral interleukin 10 (vIL10, UL111.5A), and latency unique natural antigen (LUNA, encoded by antisense UL81-82) (Goodrum et al., 2007). Some of these latency-associated transcripts are different isoforms of viral transcripts observed in lytic infection. For instance, UL111A encodes latency-associated viral interleukin 10 and its isoform found in lytic infection (Jenkins et al., 2004). Recent transcriptomic analysis with single-cell RNA sequencing on experimental and clinical samples has revealed that a broad spectrum of canonical viral lytic genes are expressed in latency, albeit at low expression level (Cheng et al., 2017; Shnayder et al., 2018).

1.1.7. Lytic replication cycle

A typical productive HCMV replication cycle, from infectious virions entering a host cell to new progeny virions leaving the cell, takes 48 to 96 hours to complete. In order to enter host cells, HCMV gB trimers and gH:gL heterodimer to bind host surface factors

such as platelet-derived growth factor, heparan sulfate, integrins, and epidermal growth factor receptor (EGFR) (Compton et al., 1993; Feire et al., 2004; Wang et al., 2003). Depending on the cell type, HCMV enters host cells either through direct fusion at the cell surface (fibroblasts) or endocytosis (epithelial and endothelial cells). Large tegument protein (UL48), a binding protein (UL47), and facilitate capsid trafficking to the nucleus and capsid uncoating (Bechtel and Shenk, 2002; Fuchs et al., 2002). Upon entry, HCMV genes are expressed in a temporally regulated cascade, starting with immediate-early (IE) genes, followed by early (E) genes, and finally the late (L) genes. Viral genes are transcribed by host RNA polymerase II and translated by host ribosomes.

By 1 hpi, viral genome has been deposited into host nucleus (Rosenke and Fortunato, 2004). In the nucleus, HCMV genome binds to nuclear domain 10 (ND10, also known as PML nuclear body) components, where promyelocytic leukemia protein (PML) and speckled protein 100 kDa (SP100), α-thalassemia/mental retardation X-linked (ATRX), and death-domain associated protein (DAXX) aggregate (Everett and Chelbi-Alix, 2007; Ishov and Maul, 1996). The heterodimer DAXX/ATRX mediates histone deacetylase (HDACs) and represses MIEP activity (Maul, 2008; Reeves, 2011; Sinclair, 2010). However, pre-released tegument proteins pp71 (UL82) and pUL69 locate to ND10 bodies and degrades DAXX, initiating the transcription of major IE genes, including IE1 (UL123) and IE2 (UL122) (Hensel et al., 1996; Sanchez et al., 1998). IE1 protein also regulates signal transducer and activator of transcription (STAT) signalling, interacts with DAXX and HDAC3, and disrupts ND10 bodies to overcome the chromatin repression of MIEP and other viral promoters (Lee et al., 2007; Maul, 2008; Nevels et al., 2011; Tavalai and Stamminger, 2011). IE2 is the main activator of the later E and L genes while IE1 act as a coactivator. IE2 transactivates promoters through direct interaction with cis repression sequence sites on viral DNA, initiating viral gene transcription together with RNA pol II and cell cycle-controlling kinases (Kapasi and Spector, 2008; Reeves et al., 2006).

E genes are indispensable for viral DNA synthesis. DNA synthesis initiates at the oriLyt site situated between the UL57 and UL69 genes at around 18 hpi (Anders et al., 1992; Yatim and Albert, 2011). The HCMV replisome consists of UL54-encoded DNA polymerase catalytic subunit, UL44-encoded polymerase processivity subunit, UL57-

encoded single-strand DNA binding protein, and heterotrimeric helicase-primase encoded by UL70, UL102 and UL105 (Erice, 1999; Kim and Ahn, 2010; Pari and Anders, 1993). Gene products of UL112-UL113 (pp34, pp43, pp50, pp84) direct the replisome to the viral genome via UL44 (Park et al., 2006). UL84 encodes a betaherpesvirus-specific protein (ppUL84) that together with IE2, bind to the oriLyt promoter and facilitate viral DNA replication initiation (Colletti et al., 2004; Sarisky and Hayward, 1996).

L gene products control capsid maturation, DNA packaging, virion maturation, and egress from the cell. Capsids are assembled in the nucleus with the products of UL86, UL46, UL85, and UL48A. Viral DNA is encapsidated by the terminase complex (UL89, UL56, UL51) through a channel formed by pUL104. Nuclear egress of the nucleocapsid is mediated by the nuclear egress complex (UL50 and UL53). Like other herpesvirus, virions undergo primary envelopment and de-envelopment before joining viral surface glycoproteins at cytoplasm and exit cells through exocytosis. (Mettenleiter, 2002; Varnum et al., 2004)

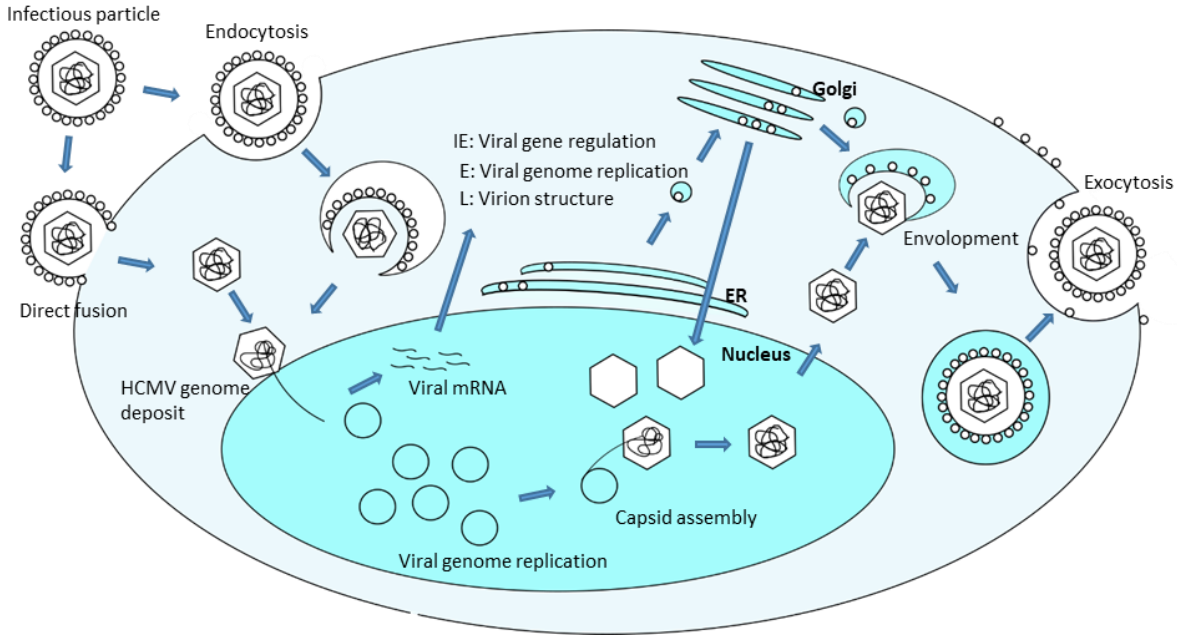

Figure 1.3. Lytic Cycle of HCMV Infection.
Infectious particles enter cells by either direct membrane fusion of endocytosis. Viral envelope uncoating occurs the same time as membrane fusion with the cell membrane or endosomal membrane, and tegument proteins and the

nucleocapsid released into the cytosol. The nucleocapsid is translocated towards the nucleus along the cytoskeleton, and the viral DNA is released into the cell nucleus. HCMV DNA often circulates via annealing of the terminal repeats. A regulated temporal cascade of gene expression is activated. Firstly immediate early (IE) genes, followed by early (E) genes, which initiate viral genome replication, and late (L) genes, which encode viral structural proteins. Capsid proteins translocate back to the nucleus and packaging of the nucleocapsid occurs. Acquisition of tegument proteins in the cytosol is followed by envelopment at viral assembly complex which contains components of the endoplasmic reticulum (ER), Golgi apparatus, and endosomal machinery. More tegument proteins and a viral envelope attach to the particles by budding into intracellular vesicles at the AC. Mature virions are released along with non-infectious dense bodies through exocytosis. Figure and figure legend are adapted from (Jean Beltran and Cristea, 2014).

Compared to IE-E-L viral gene classification, a new method to describe viral temporal classes has been proposed. Using an unbiased proteomics approach coupled with k-means clustering, 136 canonical and 14 non-canonical HCMV proteins were distributed into five classes (Tp1-Tp5) according to their temporal expression profile (Figure 1.4). Viral proteins that fall within the same group have similar expression pattern throughout infection. In this classification, Tp1 proteins have relative high expression early in infection, while Tp5 have highest expression only late in infection (Weekes et al., 2014).

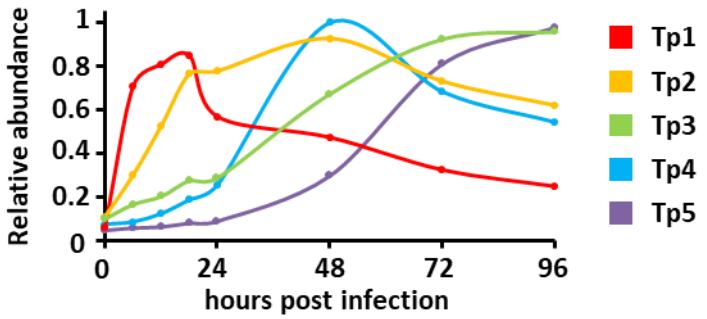

Figure 1.4. Temporal classes of HCMV gene expression.
Figure modified from (Weekes et al., 2014). HCMV proteins were clustered into 5 temporal classes using k-means method. The average relative expression of each Tp class protein are shown.

1.1.8. HCMV-associated diseases

Primary HCMV infection is generally asymptomatic in healthy immunocompetent individuals, but flu-like or mononucleosis-like symptoms have been reported in very rare cases (Sissons and Carmichael, 2002). Sporadic reactivation of HCMV from latency in differentiated myeloid cells has been associated with rare cases of cardiovascular disease (Simanek et al., 2011), Guillain-Barré syndrome (Orlikowski et al., 2011), and glioblastoma (Dey et al., 2015; Dziurzynski et al., 2012), although the oncogenic properties of HCMV are highly controversial. In contrast, HCMV causes life-threatening complications in immunocompromised, immunosuppressed and immunonaïve patients, in particular acquired immunodeficiency syndrome (AIDS) patients, transplant recipients, and neonates.

HCMV infection occurs in approximately 0.5% of live births, and around 10% of infections are symptomatic (Britt, 2018). Infants with congenital HCMV infection may suffer from rashes, jaundice, retinitis, hepatosplenomegaly, and microcephaly. They are at long term risk of mental retardation, vision loss, hearing impairment and seizures (Boppana et al., 2013).

HCMV affects both solid organ transplant recipients and hematopoietic stem cell transplant recipients. In general, HCMV is linked to a higher risk of graft rejection, as well as increased morbidity and mortality (Gandhi and Khanna, 2004). Patients can suffer from HCMV pneumonia, gastrointestinal disease, central nervous system disease, hepatitis, retinitis, in addition to CMV syndrome, which is characterised by fever and malaise as well as leukopenia, thrombocytopenia, elevated liver enzymes such as alanine aminotransferases and aspartate transaminase (Azevedo et al., 2015; Humar and Michaels, 2006; Ljungman et al., 2002).

1.1.9. Intervention

Several antiviral drugs have been clinically approved for the treatment of HCMV infections. Most target the viral DNA polymerase UL54 and are nucleotide analogues

such as ganciclovir, cidofovir, acyclovir, as well as pyrophosphate analogue foscarnet (Krishna et al., 2019). These drugs has been associated with serious dose-dependent cytotoxicity. The adversary effects are hematologic, causing neutropenia and thrombocytopenia, and nephrotoxic, leading to proximal tubular cell injury and acute renal failure (Upadhyayula and Michaels, 2013). In contrast, letermovir is the most recent drug to be approved for HCMV treatment. It associates with terminase complex UL56 subunit, which overcomes the drug resistance resulting from HCMV mutations in UL54 (Marty et al., 2017). However, cases of letermovir resistance have been reported (Cherrier et al., 2018).

1.2. Viral DNA Sensors for Herpesviruses and Viral Counteractions

1.2.1. Interferon

Interferons (IFN) are a family of secreted autocrine and paracrine proteins that regulate the antiviral immune response. There are three types of interferons. The type I IFN family is the largest of 3, comprised of 13 subtypes of IFNα and several single-gene products including IFNβ, IFNε, IFNκ, and IFNω in human (Stetson and Medzhitov, 2006). These cytokines are rapidly produced upon activation of pattern-recognition receptor (PRR). They stimulate the type I IFN receptor on infected and surrounding cells, through activation of Janus activated kinases (JAKs), tyrosine kinase 2 (TYK2) and JAK1. (Platanias, 2005). IFNα is mainly produced by plasmacytoid dendritic cells (pDCs) and macrophages while IFNβ is predominantly produced by non-immune cells, such as fibroblasts and epithelial cells.

Type II IFN consists of IFNγ only, predominantly produced by NK cells upon phosphorylation of STAT4. IFNγ binds to type II IFN receptor, which associates with JAK1 and JAK2 (Lee and Ashkar, 2018). The type III IFN family comprises IFNλ1 (interleukin-29, IL-29), IFNλ2 (IL-28A), IFNλ3 (IL-28B), and IFNλ4. In contrast to humans, in mice only *Ifnl2* and *Ifnl3* are functional; *Ifnl1* and *Ifnl4* are pseudogenes (Lasfar et al., 2006). Animal studies point out that IFNλ response is restricted mainly to mucosal epithelial tissues such as lung epithelial and intestinal epithelial cells. Similar to type I IFN, type III IFN

receptor associates with JAK1 and TYK2 (Wack et al., 2015). Activation of the JAK signalling cascade results in phosphorylation of STAT2 and STAT1, which form a complex with interferon regulatory factor 9 (IRF9), known as the IFN-stimulated gene factor 3 (ISGF3). Activated ISGF3 translocates to the nucleus and binds to IFN-stimulated response elements (ISREs) in DNA to initiate transcription of interferon-stimulated genes (ISGs). Type I and type II IFNs also signal through STAT1–STAT1 homodimers that bind to IFNγ-activated site (GAS) elements in some ISGs and induces their transcription (Platanias, 2005). The phosphoinositide 3-kinase (PI3K)–mammalian target of rapamycin (mTOR) pathway and multiple mitogen-activated protein kinase (MAPK) pathways are also downstream to type I interferon receptor (Ivashkiv and Donlin, 2014).

Of these interferons, IFNβ is the best-defined and most broadly expressed type I IFNs. Its role during viral infection has been broadly discussed. This thesis focuses on type I interferon, especially IFNβ since HCMV infection was studied in human fibroblasts in this project.

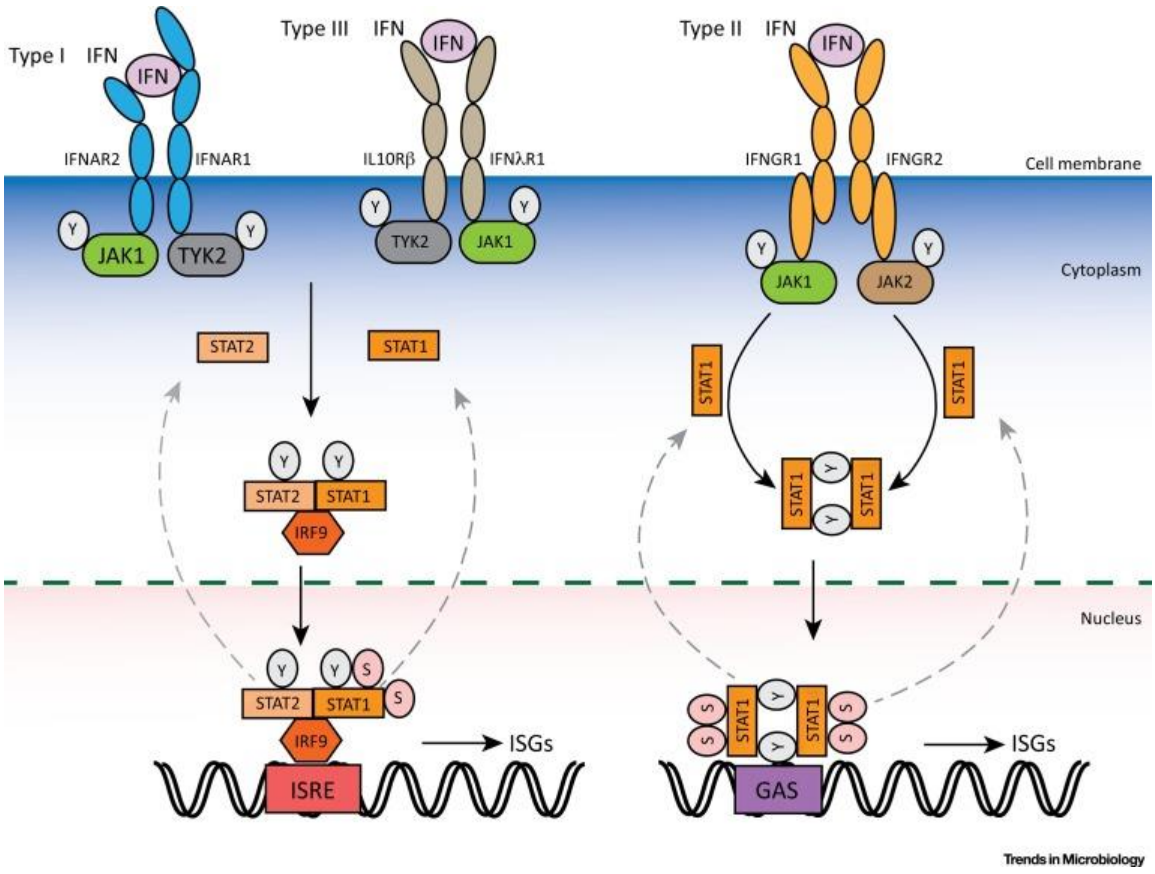

Figure 1.5. The IFN signalling pathways in regulating ISG transcription.
The three different classes of IFNs signal through their corresponding receptors, leading to phosphorylation of the associated JAKs. For type I and III IFNs, activated JAK1 and TYK2 recruit and phosphorylate STAT1 and STAT2. STAT1 and STAT2 then recruit IRF9 to form ISGF3. For type II IFNs, the phosphorylated JAK1 and JAK2 lead to activation and homodimerisation of STAT1. Both ISGF3 and STAT1 homodimers translocate to the nucleus for further phosphorylation at specific serine residues of STAT1, thereby achieving full activation. Consequently, ISGs are transcriptionally activated by binding of ISGF3 and STAT1 homodimers to ISREs and GAS promoter elements, respectively. Conversely, specific phosphatases in the nucleus dephosphorylate STAT1 and STAT2 to avoid excessive and detrimental IFN responses. Figure and figure legend are derived from (Wang et al., 2017).

1.2.2. Type I interferon production and signalling

Viral infection is detected by several PPRs in the cells. These sensors recognise viral DNA, RNA, or other non-nucleic-acid pathogen-associated molecular patterns (PAMPs) including the viral glycoproteins of HSV (Leoni et al., 2012) and the dUTPase of EBV (Ariza et al., 2009). The RNA helicases retinoic acid-inducible gene I (RIG-I) and melanoma differentiation-associated gene 5 (MDA5) are the major cytosolic RNA sensors (Goubau et al., 2013). A broad array of cytosolic DNA sensors detects cytosolic DNA, compared to self DNA that mainly locates in the nucleus and mitochondria. The antiviral roles of these sensors, particularly DNA sensors are discussed below.

Toll-Like Receptors (TLRs)

TLRs are a group of type I transmembrane proteins that use a domain containing leucine-rich-repeat to recognize PAMPs and activate host defence mechanisms against infections. (Kawai and Akira, 2006; West et al., 2006). Among the TLR family, endosome-residing TLR9 recognises unmethylated CpG-rich DNA that is frequently found in microbial genomes (Cornélie et al., 2004; Hemmi et al., 2000; Takeshita et al., 2001). There is also evidence showing that TLR9 also senses 2-deoxyribose sugar backbone of the viral DNA, indicating that viral sensing of TLR9 could be mostly sequence-independent (Haas et al., 2008). TLR9 is predominately expressed in endosomes of pDCs, B cells, and epithelial cells. Studies in pDC shows that TLR9 recruits myeloid differentiation primary response gene 88 (MyD88) to further activate downstream

nuclear factor kappa B (NFκB) and IRF7, leading to production of inflammatory cytokines and type I IFN (Sato et al., 2003).

Tlr9-/- mice exhibited increased viral titres following MCMV infection, probably due to impaired type I IFN and interleukin 12 production, as well as delayed NK cell activation (Krug et al., 2004a). Similarly, TLR9 mediates HSV-1 replication through early but not late type I IFN response in mice (Krug et al., 2004b; Rasmussen et al., 2007). HSV-2 DNA can be recognised by TLR9 and trigger IFNα production in mouse pDCs (Lund et al., 2003). Higher viral loads were also observed in *Tlr9*-/- mice infected with murine gammaherpesvirus 68 (MHV68), accompanied with elevated IFNα, IL-12, and IL-6 secretion (Guggemoos et al., 2008).

Other TLRs also sense viral components during infections. The endosomal receptors TLR3, 7, 8 sense either double-stranded or single-stranded RNA (Kawai and Akira, 2010) while cell membrane-bound TLR2 senses viral glycoproteins, such as HCMV envelope proteins B and H, upon viral contact with the cell surface (Boehme et al., 2006; Juckem et al., 2008).

RNA polymerase III (RNA Pol III)

RNA polymerase III is comprised of multiple enzyme subunits that transcribe small stable RNAs such as ribosomal 5S RNA (5S rRNA) and tRNA (Dieci et al., 2007), as well as EBV-encoded small RNA (EBER), viral products important for promoting growth and avoid apoptosis for EBV-transformed cells (Howe and Shu, 1989; Iwakiri and Takada, 2010). RNA Pol III was demonstrated to use AT-rich DNA and HSV-1 DNA as templates to produce 5' triphosphate RNA molecules that are subsequently recognized by the RIG-I RNA sensing mechanism (Chiu et al., 2009). However, RNA Pol III does not participate in early recognition of HSV-1 and an RNA pol III-independent sensing pathway was reported (Melchjorsen et al., 2010). On the other hand, RNA pol III inhibitor reduces IFNα production in human EBV-positive Burkitt's lymphoma Mutu III cell line in a dose-dependent manner, indicating a potential role in anti-EBV innate immunity (Ablasser et al., 2009). RNA pol III elicits a stimulator of IFN gene (STING)-independent pathway involving recognition of transcribed dsRNA from AT-rich DNA by RIG-I and IFN regulatory

factor 3 (IRF3) activation by TANK-binding kinase-1 (TBK1) (Ablasser et al., 2009; Chiu et al., 2009).

DNA-dependent activator of interferon (DAI)

DAI, also known as Z-form (left-handed helix, instead of the more common B-form right-handed helix) DNA/RNA-binding protein 1 (ZBP1), was initially described as an inducible gene in tumour stroma and activated macrophages by IFNγ. However, studies in the past two decades have recognized DAI as an innate sensor of viral infection that regulates cell death and antiviral inflammatory responses (Fu et al., 1999; Kuriakose and Kanneganti, 2018). Near the N-terminus, DAI encodes two Z-DNA-binding domains that bind to nucleic acids, which are critical for an innate immune sensor (Deigendesch et al., 2006). In 2007, Takaoka and colleagues identified DAI as a cytosolic DNA sensor that triggers innate immune responses against bacterial and viral infections. They found that to regulate HSV1 infection, DAI recognizes viral dsDNA, recruits TBK1, and induces type I IFN via IRF3 (Takaoka et al., 2007). Independent of viral DNA sensing, DAI can also suppress HSV1 through regulation of infected cell protein 0 (ICP0) promoter activity (Pham et al., 2013). Other than HSV1, DAI is shown to contribute to IFNβ induction during HCMV infection via STING signalling pathway, which controls HCMV replication (DeFilippis et al., 2010).

DAI harbours two receptor-interacting protein homotypic interaction motif (RHIM) domains, which can interact with RHIM domains of receptor-interacting serine/threonine protein kinases 1/3 (RIPK1 and RIPK3), which is required for NFκB activation during murine cytomegalovirus (MCMV) infection (Rebsamen et al., 2009). RIPK1/3 are involved in regulating signalling of necroptosis, a form of programmed cell death characterized by cell swelling and cell membrane rupture, which is considered a way to control infection (Nailwal and Chan, 2019). MCMV M45 protein, a viral inhibitor of RIPK activation, inhibits MCMV-induced necrosis by targeting DAI-RIPK3 complex with its RHIM domain (Upton et al., 2010). Taking advantage of mutant MCMV encoding M45 with mutated RHIM domain, viral transcription activated by immediate early protein IE3 was found to be essential for necroptosis triggered by MCMV (Sridharan et al., 2017).

Cyclic GMP-AMP synthase (cGAS)

cGAS belongs to the nucleotidyltransferase (NTase) family, which includes dsRNA binding 2'-5'-oligoadenylate synthase 1 (OAS1) and adenylate cyclase. Members of this family all have the ability to add nucleotides to substrates such as nucleic acids, proteins, and, antibiotics (Aravind and Koonin, 1999). Upon cytosolic DNA activation, cGAS-DNA complex dimerises and synthesises cyclic-GMP-AMP (cGAMP) from ATP and GTP. cGAMP then serves as a second messenger to STING (Ablasser et al., 2013; Gao et al., 2013b; Zhang et al., 2013). The ability of cGAS to detect viral infection has been investigated in cGas -/- mice and cGAS knockdown cell lines. Loss of cGAS impairs IFNβ production upon infection of DNA viruses, including HSV1 (Li et al., 2013b; Wu et al., 2013), vaccinia virus (VACV) (Schoggins et al., 2014), adenovirus (Lam et al., 2014), MHV68 (Schoggins et al., 2014), HCMV (Lio et al., 2016), and MCMV (Lio et al., 2016). cGAS can also detect HIV-1 after its genome has been reverse transcribed into DNA (Gao et al., 2013a).

DExD/H-box helicases

DExD/H-box helicases are a family of proteins that contain the conserved sequence of 4 amino acids, where the first and second are the negatively charged aspartate and glutamate, the third amino acid could be any, and the fourth could be either aspartate or the positively charged histidine. This motif is involved in activities such as ATP binding, ATP hydrolysis, and nucleic acid binding, and nucleic acid unwinding (Tanner and Linder, 2001). Several members of this family, namely, DEAD-box helicase 41 (DDX41), DEAH-box helicase 9 (DHX9), and DEAH-box helicase 36 (DHX36) are implicated with viral DNA sensing.

DDX41 binds to HSV1 DNA and recruits STING in the cytosol to induce type I interferon production in myeloid dendritic cells, bone marrow–derived myeloid dendritic cells, and human monocyte cell line (Zhang et al., 2011). DHX9 and DHX36 are identified as CpG DNA binding partners. In pDC, DHX9 is known to trigger tumour necrosis factor α (TNFα) and interleukin 6 (IL6) production and NFκB activation in response to CpG, while DHX36 is associated with IFNα production and IRF7 nuclear translocation. Their roles in DNA

virus infection has yet to be confirmed (Kim et al., 2010). Although DEAD-box helicase 3 (DDX3) contributes in DAI-dependent IFNβ production during HCMV infection, its role as HCMV DNA sensor was not examined, but it is rather identified as a phosphorylation substrate of TBK1 that conducts DAI sensing activation (Kim et al., 2010).

DNA-dependent protein kinase (DNA-PK)

DNA–PK is a nuclear serine/threonine protein kinase comprised of a catalytic subunit and a regulatory heterodimer Ku70/Ku80. The protein is well recorded as a DNA damage response protein contributing to nonhomologous end-joining (NHEJ) of DNA double-strand break repair, lymphocyte V(D)J recombination, chromatin structure modulation, and telomere maintenance (Smith and Jackson, 1999). In 2012, Ferguson et al discovered that in response to immunostimulatory DNA transfection or VACV infection, DNA-PK translocates to the cytosol, senses cytosolic DNA, recruits TBK1, and triggers type I interferon and antiviral cytokine production via IRF3 activation (Ferguson et al., 2012). On the other hand, VACV encoded C16 protein, interacts with DNA-PK, inhibiting DNA sensing, thus contributing to viral virulence (Peters et al., 2013).

Interferon-inducible protein 16 (IFI16)

IFI16 harbours a pyrin domain that interacts with other proteins, and two DNA-binding hematopoietic expression, interferon-inducible nature, and nuclear localization (HIN) domains (Unterholzner et al., 2010). IFI16 predominantly expresses in the nucleus, it recognises herpesviral DNA deposited to the nucleus, such as those of HSV1 (Li et al., 2012; Unterholzner et al., 2010), HCMV (Gariano et al., 2012; Li et al., 2012), EBV (Ansari et al., 2013), and KSHV (Kerur et al., 2011), and promote production of type I IFN and proinflammatory cytokine IL1β. Upon viral DNA activation, histone acetyltransferase p300 acetylates IFI16 and translocates it to the cytosol, where IFI16 activates signalling of IFN via interaction with STING (Unterholzner et al., 2010), and inflammasome via interaction with inflammasome adaptor protein apoptosis-associated speck-like protein containing a caspase recruitment domain (ASC) (Kerur et al., 2011).

IFI16 has prominent antiviral restriction function limiting virus replication. It can oligomerise into a filamentous structure along dsDNA (Morrone et al., 2014; Stratmann

et al., 2015), forming a platform to recruit PML, Sp100, ATRX, and cGAS, thus suppressing viral gene transcription and promoting IFN production (Diner et al., 2016; Merkl and Knipe, 2019). Additionally, an HCMV study has shown that the viral gene repressing function of IFI16 is associated with transcription factor special protein 1 (SP1) (Gariano et al., 2012).

Downstream of cytosolic sensors

Despite diverse methods to detect viral infection, the downstream signalling following these receptors include a few common molecules, including IRF3 and IRF7, which initiate IFNα/β gene transcription (Tamura et al., 2008). In some cases, NFκB and activator protein 1 (AP-1) participate in IFN production as cofactors (Honda et al., 2006). Upstream to the IRFs and NFκB, TBK1 and the inducible inhibitor of NFκB (IκB) kinase ε (IKKε) are responsible for phosphorylation of IRF3 and NFκB respectively (Miyahira et al., 2009). NFκB induces transcription of proinflammantory cytokines, mainly interleukin 1 (IL1) and TNFα (Lawrence, 2009). Alternatively, TLR9, DHX9, and DHX36 activate IRFs through MYD88 and tumour necrosis factor receptor-associated factor 6 (TRAF6) (Kim et al., 2010; Tamura et al., 2008). The adaptor mitochondrial antiviral signalling protein (MAVS) and STING are required for RIG-I and MDA5 to activate TBK1. Some DNA sensors, including cGAS, IFI16, and DDX41 also activate TBK1 through STING (Barber, 2015). Upon activation, STING move from ER to the ER-Golgi intermediate compartment (ERGIC) or Golgi apparatus, and this translocation is essential for IFN production (Ishikawa and Barber, 2011; Saitoh et al., 2009).

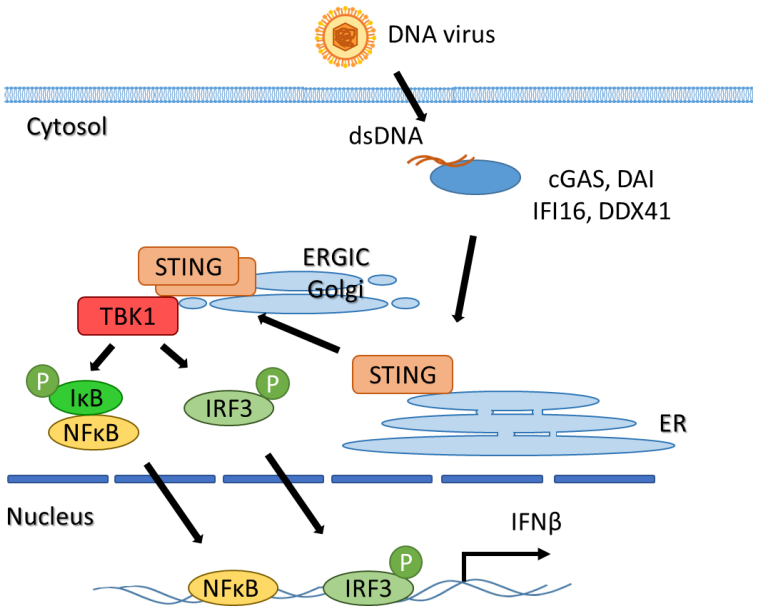

Figure 1.6. Type I interferon production signalling pathway triggered by dsDNA sensors.
Recognition of viral DNA by DNA sensors trigger STING dimerization and translocation to the ERGIC or Golgi apparatus. TBK1 and IRF3 are recruited and activated. Activation of STING also trigger activation of NFκB via TAK1, which is sometimes performed by IKKε instead of TBK1 (Balka et al., 2020). IRF3 and NFκB translocate to the nuclear and promote IFNβ transcription.

Evasion of host innate sensing

In order to successfully establish infection, disease-causing viruses need to adapt many strategies to evade multiple lines of host nucleic acid sensing pathways. Herpesviruses encode many viral proteins that target the sensors and signalling components of the IFN induction pathway. KSHV tegument protein ORF52 and HCMV tegument protein UL31 interact with nucleotide binding domain of cGAS, thus inhibiting viral DNA recognition (Huang et al., 2018; Wu et al., 2015). HSV1 tegument protein UL37 deaminates asparagine and glutamine residues in cGAS and inhibits its ability to synthesise cGAMP (Zhao et al., 2016). HSV1 endonuclease UL41 selectively degrades cGAS mRNA and decreases the presence of cGAS. IFI16 is another DNA sensor herpesviruses target. IFI16 was directed to proteasomal degradation by HSV1 tegument protein and E3 ubiquitin ligase ICP0 (Johnson et al., 2013; Orzalli et al., 2012). HCMV tegument protein UL83 binds to PYR domain of IFI16 and hinders the oligomerisation of IFI16 (Li et al., 2013a).

Besides antagonising the DNA sensors, herpesviruses also interfere with the downstream signalling molecules. HSV1 immediate early infected-cell protein 27 (ICP27) binds to the activated STING-TBK1 complex and inhibit IRF3 phosphorylation (Christensen et al., 2016). Similarly, MHV68 tegument protein open reading frame 11 (ORF11) interacts with the kinase domain of TBK1 and blocks IRF3 phosphorylation (Kang et al., 2014). HCMV tegument protein UL82 and MCMV m152 protein disrupt STING translocation from the ER to the Golgi compartment, thus blocking downstream signalling (Fu et al., 2017; Stempel et al., 2019). Virus encoded kinases, such as EBV BGLF4, VZV ORF47, HSV1 UL13, and MHV68 ORF36, can directly targets IRF3, but with different mechanisms. EBV BGLF4 interferes DNA binding activity of IRF3 (Wang et al., 2009); HSV1 UL13, and MHV68 ORF36 diminish association between IRF3 and the transcription activator CREB-binding protein (CBP) (Hwang et al., 2009); VZV ORF47 prevents IRF3 homodimerization and induction of IFN (Vandevenne et al., 2011).

1.3. Protein degradation in the cell

Cellular proteins are maintained in a dynamic state with the levels of proteins determined by rates of synthesis and degradation. Since proteins are the key effectors of biological process in cells, rapid protein degradation is one of the processes cells adapt in response to external stress such as nutrient deprivation, abnormal temperature, and chemical stimuli, or internal stress such as organelle dysregulation and intracellular infections (Dikic, 2017). In eukaryotic cells, the ubiquitin (Ub)–proteasome pathway and the lysosomal proteolysis are the two major pathways that regulates cellular protein degradation.

1.3.1. Ubiquitin-proteasome pathway

Between the two pathways, the ubiquitin-proteasome pathway is the major degradation system in the cell. This pathway uses ubiquitin to target proteins that are destined for degradation through proteasome. Ubiquitination is a series of enzymatic

actions that conjugates a chain of poly-ubiquitin to the protein substrate. Within the cascade, the ubiquitin-activating enzyme E1 and the ubiquitin-conjugating enzyme E2 prepare Ub for conjugation, while the ubiquitin ligase enzyme E3 transfer Ub onto specific target proteins (Lecker et al., 2006). Depending on the structure, E3 enzymes belong to the really interesting gene (RING) family, the homology to HPV E6 protein associated protein (E6AP) C terminus (HECT) domain family, or the RING-between-RING (RBR) family (Metzger et al., 2014). Ubiquitinated proteins are then hydrolysed by ATP-dependent proteasomes, which are found in the nucleus and the cytosol of all cells (Voges et al., 1999). Proteasomes consist of two major complexes: a catalytic core particle (CP, or 20S proteasome) and one or two regulatory particle (RP, or 19S particle) attached to core particle terminals. Subunits of RP recognise and cleave Ub tag of target proteins while subunits of CP catalyse proteolysis of substrate proteins, generating small peptides, which are subsequently hydrolysed into amino acids by peptidases (Tanaka, 2009).

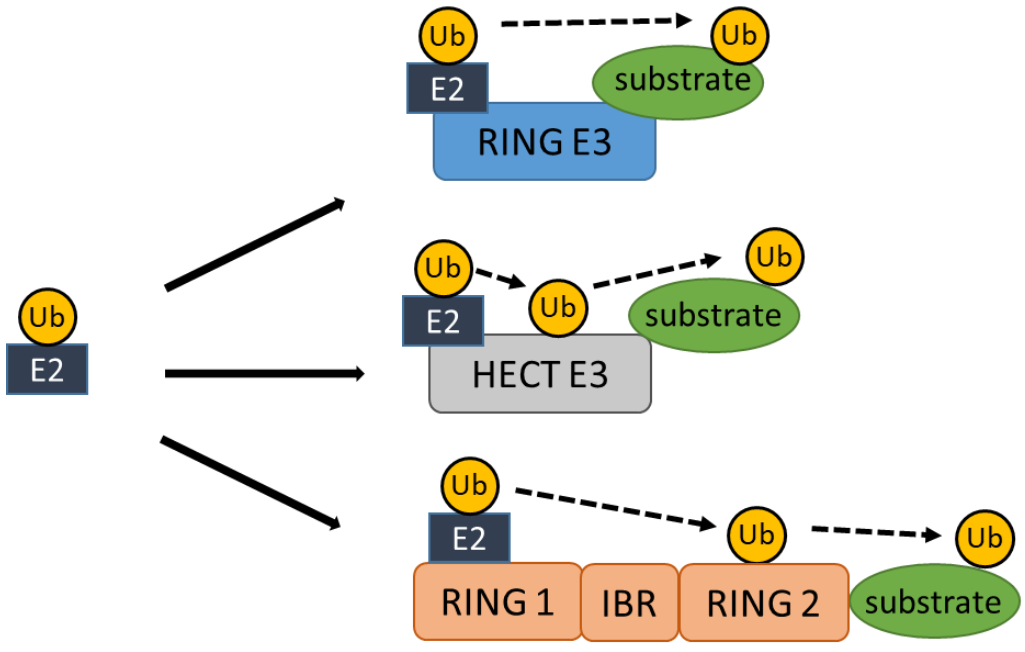

Figure 1.7. Classification and mechanism of E3 ligases.
E3 ligases are grouped into three classes according to their structural organisation. (Top) The RING E3 ligase has one RING domain and transfers ubiquitin from an E2 ligase to the substrate. (Middle) The HECT E3 ligase first transfer Ub to a cysteine residue of the HECT domain, then to the substrate. (Bottom) Ub is first transferred

from E2 to the RING domain of the RBR E3 ligase that does not bind the E2, then to the substrate.

E3 Ligases

E3 ligases play an essential role in substrate targeting by binding directly to the substrate and interacting with E2-Ub (Figure 1.7). In the case for HECT E3 ligases, ubiquitin is transferred from a cysteine active site in E2 to a cysteine residue of the HECT domain, which is subsequently transferred to a lysine residue of the substrate (Huibregtse et al., 1995). RBR domain of RBR E3 ligases contains two proposed RING domains separated by a conserved sequence called the in-between-ring (IBR) domain. One of the RING domain is responsible to E2 binding while substrates of RBR E3 ligases receive Ub from a catalytic cysteine site in the other RING domain, similar to HECT E3 ligases (Wenzel et al., 2011). RING E3 ligases carry out Ub transfer directly from E2 to substrates, without prior Ub conjugation to E3 (Deshaies and Joazeiro, 2009).

RING E3 ligases

RING E3 ligases are the most abundant type of ubiquitin E3 ligases, with ~600 identified in humans. They contain either RING domain, which coordinates two Zn^{2+} ions and helix folds to binds E2, or RING-like U-box, which adopts the same RING fold without zinc (Metzger et al., 2014). RING E3 ligases can function as monomers (i.e. immune signal-regulating Casitas B-lineage lymphoma proto-oncogene-b [Cbl-b]) (Lutz-Nicoladoni et al., 2015), homodimers (i.e. HIV-1 core protein-targeting tripartite motif containing 5 alpha [TRIM5α]), heterodimers (i.e. p53-regulating murine double minute 2 [MDM2]-murine double minute X [MDMX]) (Shadfan et al., 2012), or protein complexes consisting of multiple subunits (i.e. Cullin RING E3 ligases [CRL] and anaphase-promoting complex subunits [ANAPC]) (Castro et al., 2005; Petroski and Deshaies, 2005). RING E3 ligases have been implicated in immune signalling. For instance, RING E3 ligases tripartite motif-containing protein 32 (TRIM32) and TRIM56 have been shown to ubiquitinate NFκB essential modulator (NEMO) and subsequently activate NFκB kinase β subunit (IKKβ), leading to NFκB activation (Fang et al., 2017).

Cullin RING E3 Ligases

The largest subset of RING E3 ligases functioning as a protein complex are known as CRL. They are recognised to be responsible for around 20% of ubiquitin-dependent protein degradation in cells (Soucy et al., 2009). All CRLs contain a cullin protein (CUL1, 2, 3, 4A/B, 5, or 7) serving as scaffold, a RING domain-containing protein (named RING-box 1/2 [RBX1/2] or regulator of cullin 1/2 [ROC1/2]) that catalyses Ub transfer, and one or more adaptor protein(s) that bridge(s) substrate receptors and CULs. RBX1 is associated with most CULs except CUL5, which associates with RBX2 (Kamura et al., 2004). The complexity of adaptors and substrate receptors interacting with cullin proteins reflect the great capacity of CRL in protein degradation, with over 200 associating substrate receptors having been identified (Petroski and Deshaies, 2005). However, cullin proteins interact with a specific adaptor protein and substrate receptors containing specific protein domain. CUL1 and CUL7 use S phase kinase-associated protein 1 (SKP1) as adaptor, which binds to substrate receptors containing F-box (first described in cyclin F). CUL2 and CUL5 use Elongin B/C heterodimer as adaptor, with interacts with suppressor of cytokine signalling (SOCS) box proteins. CUL4A/B use DNA damage-binding protein 1 (DDB1) as adaptor, which binds to DDB1- and CUL4-associated factor (DCAF) proteins. And finally, the adaptors that bridges between CUL3 and substrates is BTB (bric-a-brac-tramtrack-broad complex) proteins, without substrate receptors. CUL9 can directly bind its own subtract, such as the inhibitor of apoptosis protein survivin (Li et al., 2014; Lydeard et al., 2013; Petroski and Deshaies, 2005; Skaar et al., 2013).

HECT E3 ligase

There are 28 HECT-containing E3 ligases reported so far. They can be classified into three subfamilies based on their N-terminal domain structure: the neuronal precursor cell-expressed developmentally downregulated 4 (NEDD4) family, the HECT and regulator of chromatin condensation 1 like domains (RLD)-containing (HERC), and the “others” (Sluimer and Distel, 2018; Wang et al., 2020). The NEDD4 family members all contain an N-terminal single Ca^{2+}-binding C2 domain followed by several WW domains responsible for substrate recognition. Depending on their binding partners, HECT E3 ligases have various functions. For example, NEDD4-like E3 ligase NEDD4L triggers ubiquitination and

proteasomal degradation of dishevelled (Dvl) protein, the central component of wingless (wnt) signalling in embryo development and tissue homeostasis (Ding et al., 2013). Upon T cell activation, c-Jun N-terminal kinases (JNK) phosphorylates and activates E3 ubiquitin-protein ligase Itchy homolog (ITCH), which then ubiquitinates transcription factors AP-1 and c-Jun, and leads to their degradation (Fang et al., 2002; Gao et al., 2004). HERC family is characterised by the presence of RLD domain, which acts as guanine nucleotide-releasing factor for small GTPase in membrane trafficking (Sánchez-Tena et al., 2016). HERC2 protein ubiquitinates the Xeroderma pigmentosum complementation group A (XPA) protein and promotes nucleotide excision repair (NER) pathway (Kang et al., 2010). One member of the "other" HECT E3 ligase, HECT, UBA and WWE domain containing 1 (HUWE1), naturally targets the tumour suppressor p53 for degradation (Chen et al., 2005), and is found overexpressed in sever types of tumour (Adhikary et al., 2005).

RBR E3 ligase

Fourteen RBRs are identified in humans so far, but only Parkin 2 (PARK2), human homolog of Ariadne (HHARI), and the heterotrimeric linear ubiquitin chain assembly complex (LUBAC) have been well studied. Mutation of PARK2 is responsible for autosomal recessive juvenile Parkinsonism (Kitada et al., 1998). It regulates mitochondrial clearance by targeting mitochondrial membrane proteins (Jin and Youle, 2012). HHARI interacts with the eukaryotic mRNA cap binding protein, translation initiation factor 4E homologous protein (4EHP) and leads to its polyubiquitination, therefore affecting protein translation (Tan et al., 2003). LUBAC contains three hetero subunits, two of which have RBR domain but only HOIL1-interacting protein (HOIP, also known as RNF31) is catalytically active (Kirisako et al., 2006; Tokunaga et al., 2009). LUBAC is involved in tumour necrosis factor (TNF)-mediated NFκB activation by linear ubiquitination of NEMO (Spit et al., 2019). This linear Ub chain serves as a scaffold for the inhibitor of NFκB kinase (IKK) complex to gather. Transactivation of IKK β subunit (IKKβ) then phosphorylates IκB protein, leading to its degradation and the subsequent release of NFκB (Lawrence, 2009).

1.3.2. Viral interference of proteasome-mediated degradation

As obligate intracellular pathogens, viruses often reprogram host cellular processes to favour their infection and replication. A number of viral proteins are known to exploit the proteasomal degradation pathway and direct host proteins to destruction via proteasome. Inhibition of proteasome activities has been shown to impede replication of DNA viruses such as HSV1, HCMV, VCAV, hepatitis B virus, and adenovirus (Bandi et al., 2010; Delboy et al., 2008; Gupta et al., 2013; Satheshkumar et al., 2009; Tran et al., 2010b), which is suggestive of the necessity of virally-induced proteasome activities during a permissive infection. Proteasomal degradation mediates multiple stages of viral cycle starting from entry, as demonstrated in HSV1 and KSHV (Delboy and Nicola, 2011; Delboy et al., 2008; Greene et al., 2012), to virion egress, as demonstrated in HIV-1 (Meng and Lever, 2013).

Herpesviruses have evolved to evade host immunosurveillance and establish lifelong latency. One of the cellular mechanisms viruses exploit is the proteasome degradation machinery. Presentation of viral peptide major histocompatibility complex (MHC) allows T lymphocytes to eliminate infected cells. To subvert this, some viral proteins, such as EBV nuclear antigen 1 (EBNA1), and KSHV latency-associated nuclear antigen 1 (LANA1) contain different repeat motifs that interfere with host proteasomal processing (Bennett et al., 2005; Kwun et al., 2007). HCMV US2 and US11 effectively target MHC class I and class II molecules in endoplasmic reticulum (ER) for proteasomal degradation (Wiertz et al., 1996a; Wiertz et al., 1996b).

Innate immunity includes a cascade of signal transduction during viral infection, resulting in transcription of antiviral genes via activation of transcription factors such as AP-1, NFκB, and IRF. A gammaherpesvirus, murid herpesvirus 4 (MuHV 4) encodes latency associated protein ORF73, which recruits a CRL5 complex and leads to degradation of NFκB subunits (Rodrigues et al., 2009). VZV ORF61, a protein containing a RING E3 ubiquitin ligase domain, binds and ubiquitinates phosphorylated IRF3, leading to its proteasome-mediated degradation (Zhu et al., 2011). In response to interferon treatment, PML NBs aggregate in the nucleus and components of them, such as SP100, DAXX, microrchidia CW-type zinc finger 3 (MORC3), have proven or potential antiviral

functions (Everett and Chelbi-Alix, 2007). The HSV-1 ICP0 protein harbours a RING E3 ubiquitin ligase domain that targets PML. A similar function can be performed by MHV68 ORF75c, despite the requirement of PML SUMOylation prior to this ubiquitination (Sewatanon and Ling, 2013). HCMV targets STING and STAT2 for proteasomal degradation, which dampens interferon production and interferon response respectively (Kim et al., 2017; Le et al., 2008).

In addition to immune pathways, viruses also regulate other cellular process through proteasomes. One example is HCMV UL21a-induced degradation of anaphase-promoting complex (APC) subunits, a cellular E3 ubiquitin ligase that regulates multiple cell cycle regulatory proteins, and favours viral DNA replication (Fehr et al., 2012). Oncogenic HPV E6 protein hijacks HECT E3 ligase E6AP, resulting in ubiquitination and degradation of p53 (Howley, 2006).

1.3.3. Lysosomal proteolysis

Lysosomes are single lipid bilayer membrane organelles containing acid hydrolases that aim to break down macromolecules such as proteins, DNA, RNA, polysaccharides, and lipids (Luzio et al., 2007). They are characterised to have a relative low pH to allow hydrolases to function; this low pH is maintained by vacuolar ATPase (V-ATPase), which deliver protons into lysosomes and endosomes (Maxson and Grinstein, 2014). Lysosomal membrane proteins (LMPs) are associated with acidification of the lysosomal lumen, membrane fusion, and substrate transportation, thus also essential to lysosomal function. The most abundant LMPs are lysosome-associated membrane proteins (LAMP1 & LAMP2) and tetraspanin (CD63) (Eskelinen et al., 2003). Despite their intracellular catabolic role, there is growing evidence indicating that lysosomes also have roles in membrane repair, nutrient metabolism, protein secretion, and pathogen defence (Settembre et al., 2013). Defective lysosome functions can lead to a variety of diseases, most of them are neurodegenerative, including Parkinson's, Alzheimer's, and Huntington's diseases, as well as cancer, cardiac disease, and infections (Levine and Kroemer, 2008; Maxfield, 2014). Lysosomes are involved in two digestive processes,

namely endocytosis (pinocytosis, phagocytosis, and receptor-mediated endocytosis) and autophagy, each has distinctive initiation features but both end with lysosomal fusion and destruction of content inside the vesicle.

Endocytosis-lysosome degradation

Endocytosis describes a general process where invagination of the plasma membrane internalises substances such as fluid, receptor-ligand complexes, membrane proteins, nutrients, cell debris, as well as some bacteria and viruses inside a cell (Huotari and Helenius, 2011). There are various mechanisms of internalisation, which can be categorised by the involvement of the vesicle coating protein clathrin and the fission GTPase dynamin (Thottacherry et al., 2019). Subsequent to internalisation, protein cargos are mostly transported to early endosome, where they are sorted for recycling back to the plasma membrane, sending to the trans-Golgi network, or lysosomal degradation (Jovic et al., 2010). Ubiquitination of the protein cargo is recognised by endosomal sorting complex for transport (ESCRT) machinery to allow sorting to the lysosomal degradation pathway (Raiborg and Stenmark, 2009). Downstream of the pathway, intralumenal vesicles encasing the protein cargo form inside early endosome at the perinuclear region. Early endosome thus matures into late endosome, also known as multivesicular bodies (MVB) (Huotari and Helenius, 2011). Lysosome interacts with late endosome in an initial transient (kiss-and-run) fashion, but eventually full fusion occurs and components inside intralumenal vesicles are exposed to lysosomal hydrolysis (Luzio et al., 2007). Lysosomal trafficking and fusion are controlled by membrane-associated Rab GTPases (i.e. RAB5 and RAB7) and N-ethylmaleimide-sensitive attachment protein (SNAP) receptor (SNARE) proteins (Luzio et al., 2014).

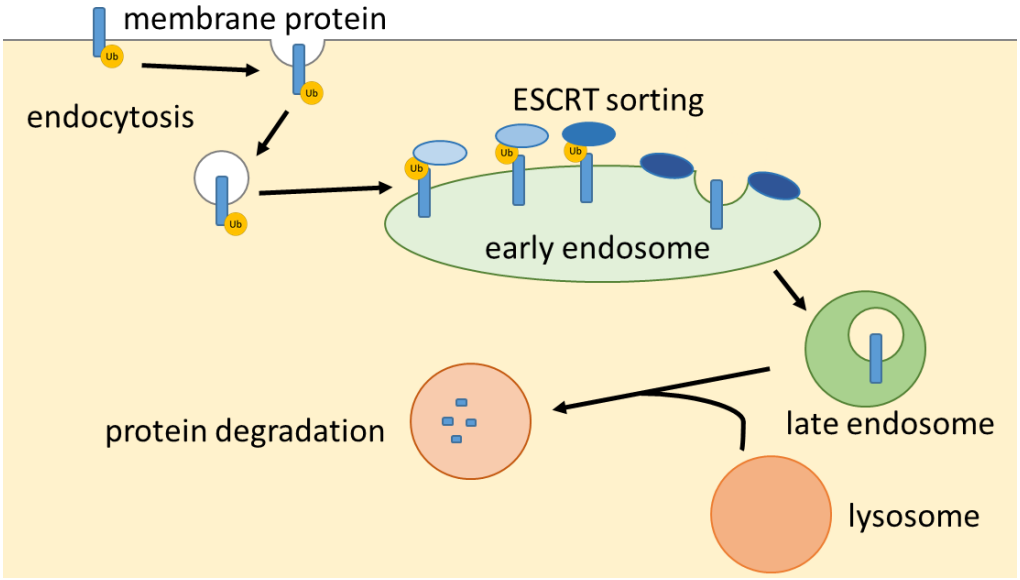

Figure 1.8. Protein degradation via endocytosis.
Ubiquitinated membrane protein is internalised through endocytosis (most commonly receptor-mediated endocytosis) and transferred to the early endosome. The ubiquitin tag is sequentially associated with endosomal sorting complex required for transport (ESCRT) protein complexes ESCRT-0, I, and II. Ubiquitin is removed by endosome-associated deubiquitinating enzyme recruited by ESCRT-III. The ub-free membrane protein is eventually encased as the luminal vesicles of the endosome through the activity of ESCRT-III. Luminal vesicles marks the maturation of early endosome into late endosome, which subsequently fuses with lysosome. The proteases inside lysosome break down the membrane protein.

Autophagy-lysosome pathway

While membrane proteins are degraded via the endosome-lysosome system, intracellular proteins can reach the lysosome through autophagy, a catabolic process where proteins, damaged organelles, or intracellular pathogens are engulfed by a double-membrane structure (autophagosome), which eventually fuse with the lysosome for degradation. Macroautophagy, the best well studied form of autophagy, initiates with activation of unc-51-like autophagy activating kinase 1 (ULK1) complex, followed by the recruitment of the class III phosphatidylinositol 3-kinase complex I (PI3KC3–C1) (Hurley and Young, 2017). Subunits of PI3K-C1, Beclin 1 (BECN1) and phosphatidylinositol 3-kinase vacuolar protein sorting-associated protein 34 (VPS34) contribute to the formation of an isolated membrane known as a phagophore, derived

from the endomembrane system (Simonsen and Tooze, 2009). The serine/threonine kinase mTOR inhibits ULK1 activation, thus is an important regulator of autophagy (Kim and Guan, 2015). Two autophagy-specific systems of ubiquitin-like proteins control the early events of autophagosome formation (Shpilka et al., 2012). One conjugates autophagy protein 12 (ATG12) to ATG5, which then associate with ATG16L1. The other (ATG7 and ATG3) conjugates a phosphatidylethanolamine (PE) to the light chain 3 (LC3), turning cytosolic LC3-I into lipidated LC3-II (Nakatogawa, 2013). Lipidated LC3-II commonly serves as a marker for autophagosome formation as it is embedded within the lumen of the autophagosome (Kabeya et al., 2000). Both events cause the phagophore to curve while extending, enclosing targets for degradation in either random or selective manner. An example of selective autophagy is observed with autophagy receptor p62 (sequestosome 1, SQSTM1), which function as a bridge between polyubiquitinated protein aggregate and LC3-II (Bjørkøy et al., 2005). Finally, the closed pharophore forms autophagosome, fuses with a lysosome, and the luminal contents are degraded (Tong et al., 2010).

The autophagic and endocytic pathways intersect when autophagosomes fuse with late endosomes, forming an amphisome (Tooze et al., 2014). This convergence of autophagosome and endocytic pathways is verified by early electron microscopy studies (Eskelinen et al., 2011). Amiphisomes eventually fuse with lysosomes, forming autolysosomes and contents within are hydrolysed. The process is mediated by small Rab GTPase proteins and SNAREs, which are the common regulators of fusion between lysosomes and late endosomes (Ganley et al., 2011).

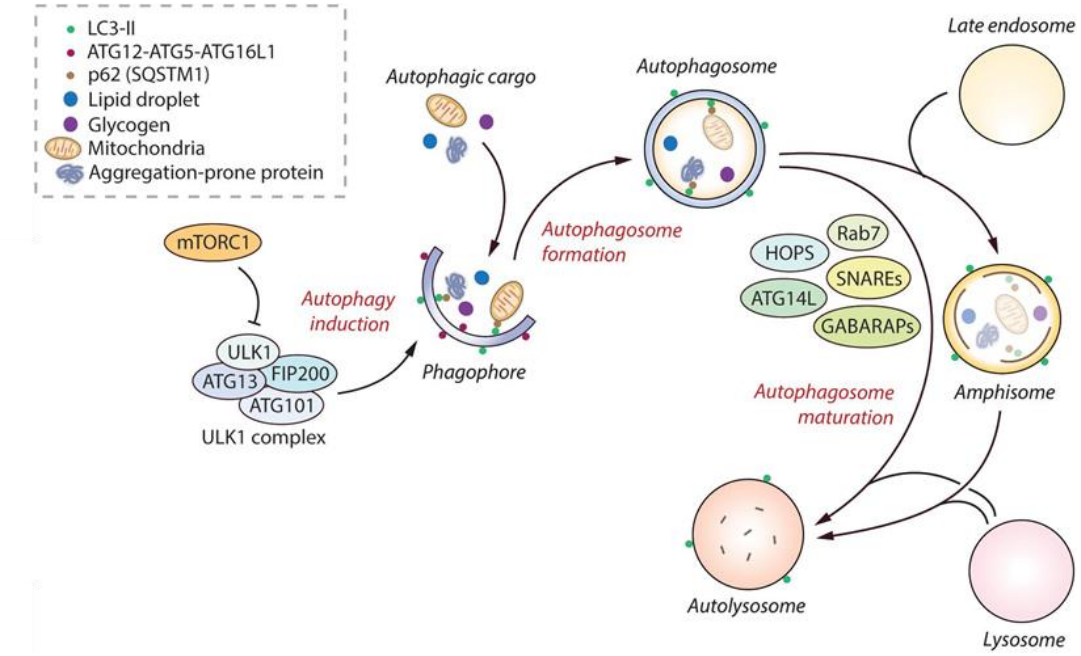

Figure 1.9. Overview of autophagy.
Autophagy initiates by the formation of phagophore that expands and engulfs autophagic cargo to form autophagosome. Mature autolysosomes form by directly fusion with the lysosome. In some cases, late endosomes fuse with autophagosome and form amohisomes, which are then fused with lysosomes. The classical regulator of autophagy is mTORC1, which negatively regulates autophagy by inhibiting the ULK1 complex. Autophagosome maturation in the late stage of autophagy is governed by various factors including SNAREs, HOPS complex, Rab7, GABARAPs, and ATG14L, amongst others. Figure and figure legend adapted from (Palhegyi et al., 2019).

1.3.4. Viral subversion of lysosomal degradation

Viral subversion of endocytosis pathways

Although direct fusion between virus envelope and plasma membrane is an established method for viral entry, most viruses, including non-enveloped ones, take advantage of endocytosis mechanisms to enter a host cell. Subsequent to binding of viral surface glycoprotein to cell surface receptor, induction of such as receptor tyrosine kinases (RTKs) and integrins results in endocytic internalisation of the viral particle (Mercer and Helenius, 2012). Clathrin-mediated endocytosis is the most common mechanism for virus to enter through endocytosis. This mechanism is utilised by many viruses, such as vesicular stomatitis virus (VSV) (Sun et al., 2005), influenza A virus (Suzuki et al., 2005),

HCMV (Compton et al., 1993; Halary et al., 2002), adenovirus 2 (Wickham et al., 1993), and Vaccinia virus (Husain and Moss, 2005). KSHV (Valiya Veettil et al., 2010), respiratory syncytial virus (RSV) (Krzyzaniak et al., 2013), and Ebolavirus (Chandran et al., 2005) can enter cell through phagocytosis, with the endocytic pathway mediated by actin and Rho GTPases (Sobhy, 2017). To evade lysosomal destruction of viral particles, engulfed viruses often disrupt endosome membrane to release capsid or other viral contents to the cytosol. Enveloped viruses can achieve this by carrying out membrane fusion, resulting from conformational changes of viral glycoprotein induced by low pH, proteolytic cleavage by cathepsins, or redox reactions (Harrison, 2005). On the other hand, processed structural proteins of non-enveloped viruses break free from endosomes by either sequestering the hydrophilic head of lipid molecules or inserting inside the hydrophobic layers, resulting in membrane disruption or pore formation respectively (Agosto et al., 2006; Brabec et al., 2005; Hinz and Galla, 2005; Seth, 1994).

Viral subversion of autophagy

Autophagy is generally described as a cell innate defence against viral infection through directly engulfing viral particles invading the cell. Other antiviral actions carried out by autophagy have been reported. Ubiquitinated capsid proteins of Togaviruses, Sindbis virus and Chikungunya virus, as well as non-structural Tat protein of human immunodeficiency virus type 1 (HIV1) are recognised by p62/SQSTM1 and targeted for selective autophagy (Judith et al., 2013; Orvedahl et al., 2010; Sagnier et al., 2015). Autophagy also promotes MHC I molecules presentation of HSV-1 glycoprotein gB and MHC class II presentation of EBV-encoded latent protein EBNA1, promoting clearance of the virus by T lymphocytes (English et al., 2009; Paludan et al., 2005). However, Herpesviruses have co-evolved with the host and successfully subvert autophagy.

A crosstalk between innate viral sensing and autophagy was reported in HSV-1 infection. Early induction could be observed during early infection of HSV1, prior to de novo viral protein expression (McFarlane et al., 2011; Tallóczy et al., 2006). Myeloid differentiation primary response protein (MyD88), downstream of TLR2 and TLR9 activation, was required for this early activation of autophagy during HSV-1 infection (Cai et al., 2013; Siracusano et al., 2016). Inhibition of this autophagosome activation impaired viral

replication (Siracusano et al., 2016). Upon HSV-1 infection, BECN1 binds to cytosolic viral DNA sensor cGAS, and this interaction inhibits cGAMP and type I IFN production (Liang et al., 2014). As HSV1 lytic cycle progresses, autophagy was inhibited through interaction of viral neurovirulence protein ICP34.5 with BECN1, as well as US11 with a protein kinase (PKR) upstream to BECN1 activation (Lussignol et al., 2013; Orvedahl et al., 2007; Tallóczy et al., 2002). Autophagy adaptor p62/SQSTM1 and mitophagy adaptor optineurin for proteasomal degradation, which are targeted by HSV1 viral protein ICP0 for proteasomal degradation, mediate ISG56 production and viral replication (Waisner and Kalamvoki, 2019). However, blocking the autophagic pathway via targeting ATG5 did not significantly alter the replication of HSV1 (Alexander et al., 2007).

Early autophagosome induction was also observed in HCMV infection. Shortly after HCMV enters the infected fibroblast, HCMV DNA triggers lipidation of LC3 and autophagosome formation (Chaumorcel et al., 2012; McFarlane et al., 2011). This is later inhibited by two BECN1-binding viral proteins, TRS1 and IRS1 (Chaumorcel et al., 2012; Mouna et al., 2016). However, autophagy is considered essential to HCMV viral assembly. Even though autophagy does not affect viral gene expression, it is involved in cytoplasmic envelopment of HCMV viral particles (Taisne et al., 2019; Zimmermann et al., 2020). This proviral role of autophagosome formation is also observed in EBV-infected cells. Upon lytic reactivation, EBV lytic transactivator Rta and Zta induce formation LC3-positive vesicles in the cytosol (Hung et al., 2014; Nowag et al., 2014). This accumulation results from inhibition of fusion between autophagosome and lysosome, and this is important for EBV lytic gene expression and replication (Granato et al., 2014).

Viral manipulation of lysosomes

While most herpesvirus have evolved ways to subvert complete autophagy, MCMV harnesses the degradative power of autophagy. MCMV M45 protein targets NEMO of NFκB, directing it to autophagosome and promote its degradation (Fliss et al., 2012). Since NFκB promotes expression of proinflammatory cytokines, this viral exploitation implies an effective method of MCMV to combat antiviral inflammatory response. One way HCMV evades host immunosurveillance is by down-regulating natural killer cell

ligands through lysosomes. HCMV US20 targets natural killer group 2D ligand (NKG2DL) MHC class-I chain-related proteins A (MICA) for degradation in lysosomes (Fielding et al., 2014; Fielding et al., 2017). Natural cytotoxicity receptor NKp30 ligand B7-H6 is depleted by viral gene US18 and US20 through lysosomes (Charpak-Amikam et al., 2017; Fielding et al., 2017). Given these ligands are cell surface membrane proteins, their degradation likely takes the endocytosis-lysosome pathway.

1.4. DNA repair

The DNA integrity in the cells is constantly challenged from both endogenous and exogenous sources, and eukaryotic cells have adapted elaborate pathways to maintain genetic stability. For a single nucleotide error, base excision repair enzymes remove damaged bases, mismatch repair proteins recognize wrong base incorporation errors, and nucleotide excision repair machinery removes bulky DNA adducts. For double strand breaks (DSB), cells repair the DNA backbone via homologous recombination (HR) and non-homologous end joining (NHEJ). Cells activate multiple signalling pathways, collectively known as the DNA damage response (DDR), to deal with complex DNA lesions. DNA-PK, ataxia telangiectasia-mutated (ATM), and ATM and Rad3-related (ATR) are the three major kinases involved in DDR signalling transduction. (Sirbu and Cortez, 2013)

When DNA damage occurs, ATM and ATR phosphorylate H2AX, a variant of the histone 2A protein family, producing γH2AX (Dickey et al., 2009; Fernandez-Capetillo et al., 2004). Together with ATM-activated the mediator of DNA damage checkpoint protein 1 (MDC1), γH2AX-MDC1 serves as a scaffold to recruit DNA repair proteins. For example, RING ubiquitin ligases RING finger 8 (RNF8) and RNF168, as well as an E2 enzyme ubiquitin-conjugating enzyme 13 (UBC13), are recruited to ubquitinate histones at double strand break (Al-Hakim et al., 2010). Ubiquitylation at the DSB sites then promote the aggregation of the DSB repair proteins breast cancer 1 (BRCA1) and p53 binding protein 1 (TP53BP1), which directs HR or NEJH respectively (Davalos et al., 2004; Tibbetts et al., 2000).

In the presence of DNA damage, the cell cycle undergoes arrest. ATR activates downstream checkpoint kinase 1 (CHK1), ATM activates kinase CHK2, which both then phosphorylates p53, releasing it from its repressing binding factor mouse double minute 2 homolog (MDM2) (Matsuoka et al., 2000; Maya et al., 2001; Shieh et al., 2000). p53 subsequently induces a number of genes, including p21, a cyclin-dependent kinase inhibitor, and suppresses Cyclin E/ cyclin-dependent kinase 2 (CDK2) kinase activity, resulting in G1 arrest (Macleod et al., 1995). CHK2 activation also phosphorylates S-phase inducer phosphatase cell division control protein 25 homolog A (CDC25A) and causes cell division control protein 2 homolog A (CDC2A) to be ubiquitinated and degraded. CDC25A therefore cannot remove inhibitory phosphorylation from CDK2, and this hinders Cyclin A/CDK2 and Cyclin E/CDK2 function in S phase progression (Bartek and Lukas, 2001; Xiao et al., 2003). In a similar fashion, another phosphatase CDC25C is targeted by activated CHK1 and CHK2, leading to Cyclin B1/CDK1 inactivation, and eventually causes G2 arrest (Abraham, 2001; Peng et al., 1997).

1.4.1. DNA repair and herpesviruses

Growing evidence has shown that herpesviruses have evolved to selectively activate or deactivate pathways in DDR to benefit their own replication. HSV-1, for instance, requires ATM activation to initiate viral replication. However, ATM activation is not required for HSV-2 replication (Shirata et al., 2005). Activated ATM then phosphorylates multiple downstream targets including Nijmegen breakage syndrome 1 (NBS1), CHK2, and p53. ATM activation also causes DSB repair protein MRE11, RAD50, NBS1 to accumulate at HSV replication sites, forming a MRN complex that is crucial for HSV-1 replication (Lilley et al., 2005; Shirata et al., 2005). Another study also demonstrates that HR repair proteins such as replication protein A (RPA), RAD51, and NBS1 that participate in the host DDR are recruited at ND10 region, in association with ssDNA binding protein UL29 and viral replication protein UL42 (Wilkinson and Weller, 2004). On the other hand, ICP0 E3 ligase, an important factor for HSV lytic reactivation, promotes the degradation of RNF8 and RNF168 to prevent full ATM activation, thus promotes viral transcription, replication, and progeny production (Chaurushiya et al., 2012; Lilley et al., 2010).

As an oncogenic herpesvirus, it has been well accepted that EBV induces genome instability to promote tumorigenesis (Gruhne et al., 2009a; Gruhne et al., 2009b; Kamranvar et al., 2007). During latency, EBNA1 promotes the generation of reactive oxygen species that cause DNA damage, EBNA3C disrupts CDK-Rb-E2F pathways, and latent membrane protein 1 (LMP1) inhibits CHK2 through ATM down-regulation (Chen et al., 2008; Nikitin et al., 2010; Parker et al., 2000). All of these reduce host DNA repair and introduce genome lesions. However, following reactivation, an ATM-dependent DDR is induced, and MRN complex is recruited at the replication site (Kudoh et al., 2005). Similar to HSV-1, HR proteins such as RPA, RAD51 and RAD52 are recruited to the viral replication site, in association with EBV polymerase processivity factor early antigen diffuse component (EA-D, encoded by BMRF1) and ssDNA binding protein BALF2 during viral replication (Kudoh et al., 2009). Although DNA repair mechanisms are activated, cell cycle is still bypassed during lytic cycle. Mechanically, EBV IE lytic transactivator Zta recruits functional CUL2- and CUL5-RING ligases that rapidly promote p53 ubiquitylation and proteasome-mediated degradation. The absence of p53 thereby promotes cell proliferation (Sato et al., 2009a; Sato et al., 2009b). Zta has also been shown to bind directly to TP53BP1, which is required for optimal virus replication (Bailey et al., 2009).

HCMV viral proteins have also been found to modulate cellular DNA repair factors. Early during infection, IE1 induces p53 accumulation at the post-transcriptional level. IE1 also activates ATM, resulting in p53 activation and therefore cell cycle arrest (Castillo et al., 2005; Gaspar and Shenk, 2006; Shen et al., 1997). NBS1 is also activated at early times post-infection (Luo et al., 2007). Growing evidence has led to the conclusion that ATM activation, regardless of the magnitude of ATM phosphorylation, is required for efficient HCMV replication (Gaspar and Shenk, 2006; Li et al., 2011; Luo et al., 2007; Shen et al., 1997). During 24 hpi and 48hpi, viral DNA replication reaches to its peak, γH2AX, p53 and MRN complex are recruited to the viral replication site (Bryant et al., 2009; Haince et al., 2008). One study has pointed out UL35 associates with deubiquitinase USP7 as well as with components of the CUL4-DCAF1 E3 ubiquitin ligase complex to increase H2AX levels, leading to cell cycle arrest (Salsman et al., 2012). In later time points during infection, CHK2 function is inhibited by HCMV through mislocalising it to the virus

assembly point in the cytosol, where CHK2 is colocalised with virion structural proteins (Gaspar and Shenk, 2006).

Like all other kinase signalling cascades, DDR is regulated in a temporal and spatial manner. High resolution analysis that can allow the investigation of protein interaction within small time frames is required to further understand the interwoven relationship between herpesviruses and host DNA repair mechanism.

1.4.2. Helicase-like transcription factor (HLTF)

HLTF, also known as SWI/SNF-related matrix-associated actin-dependent regulator of chromatin subfamily A member 3 (SMARCA3) participates in error-free post-replication DNA damage tolerance, allowing damaged DNA to continue to replicate. HLTF has a RING domain close to its C-terminus that allows it to serve as a ubiquitin E3 ligase for polyubiquitination of chromatin-bound proliferating cell nuclear antigen (PCNA) (Motegi et al., 2008; Unk et al., 2008) (Figure 1.10A). HLTF also has double-stranded DNA translocase activity that can regress replication fork-like structures (Achar et al., 2011; Blastyák et al., 2010). A study also demonstrates that in an ATP-independent manner, HLTF facilitates DNA strand invasion and the formation of a D-loop structure, which pairs the nascent DNA and the 3’ end of the invading strand that can be used by a polymerase for further DNA extension (Burkovics et al., 2014). The N-terminus of HLTF harbours a DNA-binding HIP116 Rad5p N-terminal (HIRAN) that specifically interact with 3’ ssDNA of the nascent leading strand (Akter et al., 2003; Dhont et al., 2016; Kile et al., 2015).

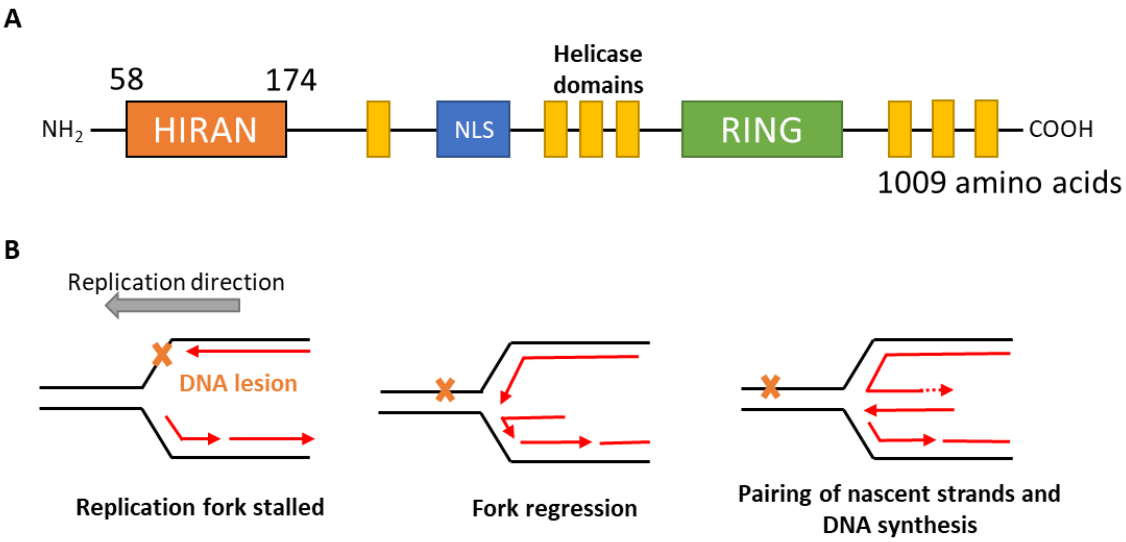

Figure 1.10. Structure and DNA repair mechanism of HLTF.
(A) Domain organisation of HLTF protein. Closed to the N-terminus, HLTF bears a DNA-binding HIP116, Rad5p, N-terminal (HIRAN) domain. Seven helicase domains span across HLTF. HLTF also contain a nuclear localisation signal (NLS) site within two helicase domains and a RING domain near the C-terminus that ubiquitinates PCNA. Full-length HLTF consists of 1009 amino acid. Amino acids 58-174 are identified as HIRAN domain (Hashimoto et al., 2017). (B) Mechanism of HLTF DNA repair, adapted from (Kile et al., 2015). On sensing a DNA leision, HLTF unwind helixes of replicated DNA segments, regression the fork. HIRAN domain of HLTF binds to ssDNA of leading strand to the lagging strand synthesised from undamaged host template.

HLTF can be found in brain, heart, kidney, liver, lung, pancreas, placenta and skeletal muscle tissues (Ding et al., 1996; Gong et al., 1997)). Its expression is generally low in colon cancer, gastric cancer and cervical adenocarcinoma, and a truncated HLTF lacking the RING domain can be found in head and neck cancers (Dhont et al., 2016). HLTF has also been shown to activate expression of cellular genes, such as human plasminogen activator inhibitor-1 and β-globin, through regulating their promoter activities (Ding et al., 1996; Mahajan and Weissman, 2002).

In 2016, two independent studies both demonstrated that HLTF was directed by HIV viral protein R (Vpr) to degradation via the CUL4-DDB1-DCAF1 complex (Hrecka et al., 2016; Lahouassa et al., 2016). In this E3 ligase complex, CUL4 serves as the platform, DDB1 is the adaptor for the actual E3 ligase DCAF1. Even though HLTF has been shown

to be important for G2/M transition in mouse cells (Helmer et al., 2013a; Helmer et al., 2013b), Vpr-mediated down-regulation of HLTF isn't involved in Vpr-induced G2 cell cycle arrest (Hrecka et al., 2016; Lahouassa et al., 2016). Plus, HLTF doesn't affect HIV replication in macrophage (Lahouassa et al., 2016). In other words, the function of HLTF in virus infection remains a mystery.

1.5. Multiplexed proteomic analysis screening of host protein degradation during early HCMV infection

To actively search for host proteins targeted for degradation during early HCMV infection, the lab developed a systematic method taking advantage of tandem mass tag (TMT)-based multiplexed proteomic analysis (Figure 1.11) before I stated my PhD project. TMT labelling allows analysis of multiple samples in a single mass spectrometry experiment. The first screen, "inhibitor screen", adapted the protease inhibitor MG132 and the lysosome inhibitor Leupeptin (Figure 1.11A). It measured protein abundance throughout early infection in the presence or absence of inhibitors and identified proteins whose down-regulation was aborted with treatment of inhibitors. "Rescue ratio" was obtained by comparing protein abundance during HCMV infection ± inhibitor with protein abundance during mock infection ± inhibitor to assess the effect of inhibitor. The method of significance A was used to estimate the p-value that each ratio was significantly different to 1 (Cox and Mann, 2008). Values were calculated and corrected for multiple hypothesis testing using the method of Benjamini-Hochberg in Perseus version 1.5.1.6 (Cox and Mann, 2008).

The second screen was designed to circumvent the off-target effects of these inhibitors by coupling the approaches of TMT labelling and pulsed stable isotope labelling by amino acids in cell culture (SILAC). Different SILAC media were applied to cells pre- and post-infection (Figure 1.11B). Protein synthesis and degradation could thus be traced by quantifying peptides labelled with different SILAC isotopes. Experiments were done over 6h and 18h of infections. With respect to protein concentration, protein degradation typically follows first order kinetics whereas protein synthesis is a zero-order process.

The rate of protein decline in mock- and HCMV-infected samples was therefore estimated using exponential regression in Excel and the formula: [relative protein abundance] (t) = $e^{Kdeg \cdot t}$ where Kdeg is the rate constant for degradation, and should be negative for degraded proteins. A degradation ratio was calculated by r_{deg} = $Kdeg_{HCMV}/Kdeg_{mock}$. In cases where $Kdeg_{mock}$ was greater than 0, a fold change (FC_{CMV}) in protein abundance in the HCMV-infected sample at 6 or 18 hpi was instead used, defined by $FC_{HCMV} = e^{-Kdeg(CMV) \cdot t}$. P-values of r_{deg} ($Kdeg_{mock} < 0$)and FC_{CMV} ($Kdeg_{mock} > 0$) were estimated and corrected for multiple hypothesis testing using the method of Benjamini-Hochberg (Benjamini and Hochberg, 1995). A protein was considered down-regulated if $Kdeg_{HCMV}/Kdeg_{mock} > 1.5$ ($Kdeg_{mock} < 0$) or $FC_{HCMV} > 1.5$ ($Kdeg_{mock} > 0$).

The third screen examined transcriptional regulation and protein level changes during early HCMV infection. Here samples collected for proteomic analysis were simultaneously collected for RNA-sequencing (Figure 1.11C). Protein fold change ($FC_{protein}$) was obtained by comparing the protein abundance during HCMV infection with the protein abundance during mock infection at 24 and 72 hpi The RNA sequencing experiment was performed in biological triplicate at 0, 24 and 72 h after infection. Mean was calculated for normalised reads per kilobase million (RPKM) values for each time point (0, 24, 72 h). RNA fold change (FC_{RNA}) at 24h was calculated from mean $RPKM_{24h}$/mean $RPKM_{0h}$. A similar value was calculated for 72 h data. The k-means method was used to cluster proteins into 7 classes based on the similarity of kinetic protein/RNA expression profiles. One of the cluster was enriched in proteins known to be degraded during HCMV infection, including the NK-activating ligand CD112/nectin cell adhesion molecule 2 (NECTIN2) (reviewed in Weekes et al., 2014).

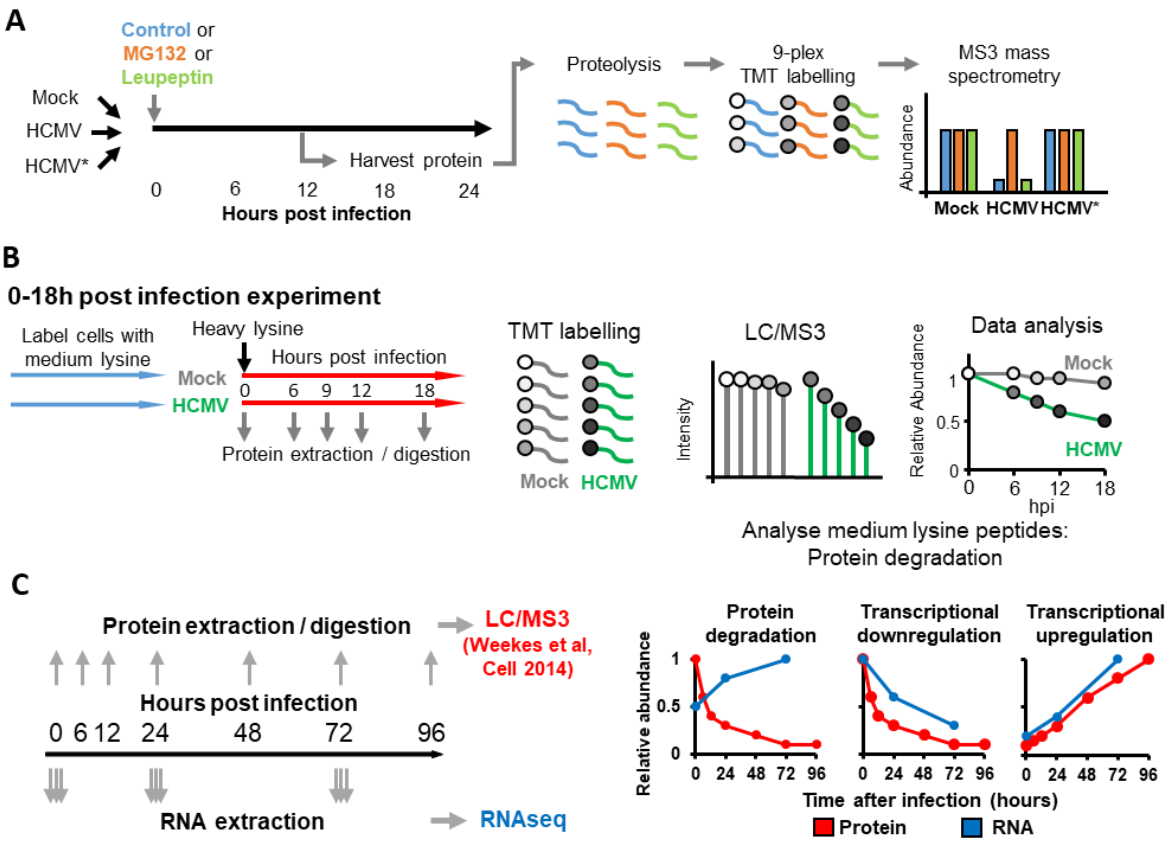

Figure 1.11. Quantitative proteomic/transcriptomic methods identify host factors degraded by HCMV.
Schematics (A) inhibitor screen, (B) pSILAC analysis, and (C) RNA/protein screen.

1.5.1. Protein with E3 ligase domain was targeted for degradation during HCMV infection

With high confidence, 35 proteins were identified to be rapidly degraded during HCMV infection. They sufficed at least two of the three screening criteria: (1) significantly rescued by MG132 at 12, 18, or 24 hours post infection (MG132 "rescue ratio" was >1.5 and $p<0.01$) in the first inhibitor screen (appendix table 1); (2) significant faster degradation rate over 6 h or 8 h HCMV infection compared to mock infection (r_{deg} or FC_{CMV} with $p<0.05$) in the second pSILAC screen (appendix table 2); (3) A protein was considered degraded at 24 hpi or 72 hpi if its protein fold down-regulation by HCMV >1.5 ($p<0.05$) and RNA fold upregulation>1 (appendix table 3).

Several host proteins on that shortlist are reported HCMV restriction factors, such as MORC3, SP100 ANAPCs. This suggested that other proteins on this list might have antiviral functions. I applied DAVID software (Huang da et al., 2009) to determine which pathways were enriched among degraded proteins from the three screens. "Ubiquitin-mediated proteolysis" was the only significantly enriched pathway (p=0.03) within the "high-confidence" shortlist, and included 6 ubiquitin E3 ligases (ANAPC1, ANAPC4, ANAPC5, NEDD4L, TRAF6, ITCH). A comprehensive search of all 35 "high-confidence" proteins for E3 ligase activity identified one additional E3 ligase, HLTF. Degradation of ANAPCs, NEDD4L, TRAF6, and ITCH during HCMV infection has been described previously (Koshizuka et al., 2018; Koshizuka et al., 2016; Kumari et al., 2017; Weekes et al., 2014). HLTF was chosen as the follow-up target since its HCMV-mediated degradation has not yet been reported.

1.5.2. HLTF was identified to be degraded via proteasome during HCMV infection

HLTF was one of the targets that fit all the screen criteria. It was rescued by MG132; its degradation rate was faster during HCMV infection, and the down-regulation was post-transcriptional (Figure 1.12). This suggested that HLTF might play a key functional role in early viral infection, possibly being degraded by the virus to evade antiviral restriction.

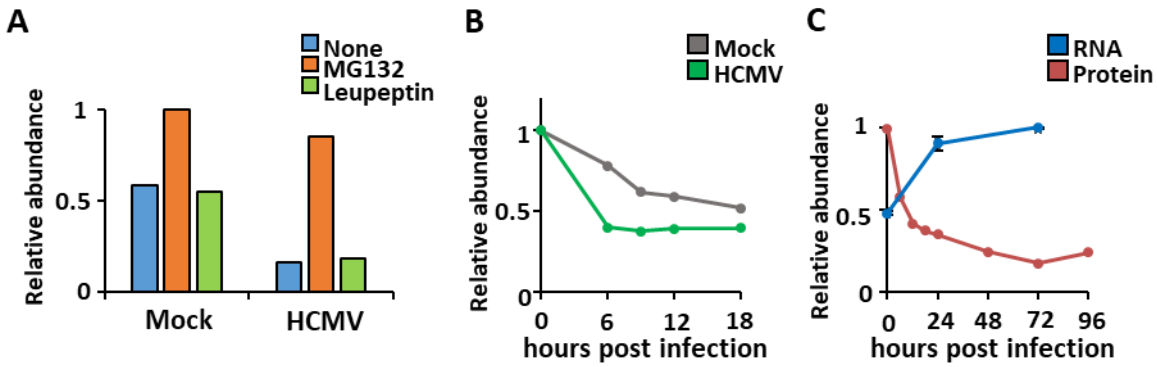

Figure 1.12. HLTF was identified as one of the top "hits" to be degraded by HCMV.
HLTF results from (A) inhibitor screen, (B) pSILAC analysis, and (C) RNA/protein screen are shown here.

1.5.3. Hypothesis

HLTF was found rapidly degraded during early HCMV infection. I postulated that HCMV deliberately targeted HLTF for proteasomal degradation and that HLTF had unexplored antiviral potentials that hindered HCMV replication.

1.5.4. Aims of this project

1. Elucidate the mechanism of HLTF degradation (Chapter 3).

2. Explore the roles of HLTF in HCMV infection (Chapter 4).

3. Refine the protein degradation screen with inhibitors with higher specificity (Chapter 5).

Chapter 2. Materials and Methods

2.1. Molecular Biology

2.1.1. DNA Preparation

E. coli cells containing plasmid to propagate were cultured in Luria-Bertani (LB) broth (10 g/l peptone, 5 g/l yeast extract, 10 g/l NaCl, autoclaved) for 16 h at 37 ˚C with constant agitation before being pelleted with centrifugation at 5000 xg, 10 min, room temperature (RT). DNA plasmids were extracted with Plasmid Mini Kit (QIAGEN) according to instructions from the manufacturer. Briefly, cells were lysed in alkaline solution containing RNase A and subsequently naturalized with acetic acid. Plasmid DNA released from cells was then collected in DNA-binding columns, washed with ethanol-containing solution, and eluted with sterile double-distilled water (ddH_2O). HCMV bacterial artificial chromosome plasmid (BACmid, provided by Dr. Richard Stanton, School of Medicine, University of Cardiff) was prepared using Plasmid Midi Kit (QIAGEN), with which the eluted DNA was additionally precipitated with isopropanol, washed with ethanol-containing washing buffer, and air-dried before dissolved in sterile ddH_2O.

2.1.2. Molecular Cloning

Restriction enzyme cloning

In order to make plasmid constructs expressing small hairpin RNA (shRNA), two oligonucleotides (Table 2.1) were annealed with each other by heating up to 95°C for 30 sec to remove secondary structure and then cooling down to room temperature. The resulting product has sticky ends of *BamHI* and *EcoRI* (New England Biolabs), and was ligated with shRNA lentiviral vector pHRSIREN (from Professor Paul Lehner, CIMR, University of Cambridge) digested with the two restriction enzymes. Vectors were treated with shrimp alkaline phosphatase (New England Biolabs) at 37 °C for an hour and ligation was performed using T4 ligase (Thermo) at 4 °C for 16 h.

Plasmid Transformation

The resulting products were then transform into Alpha-select silver efficiency complement *E. coli* cells (Bioline) that have *endA* and *recA1* mutations to increase plasmid yield and minimize DNA recombination respectively.

Gateway cloning

Temperate phages integrate genomes into the bacterial host chromosome during the lysogenic phase with site-specific recombination reactions (Landy, 1989). In these integrative recombinations, DNA with specific sequences on the phage (*att*P) and bacterial chromosomes (*att*B) are recombinase substrates, resulting in products containing specific sites (left and right, *att*L and *att*R). V5-tagged UL145 expressing lentiviral plasmid was constructed with the Gateway recombination cloning system (Thermo) (Figure 2.1), which is developed with the site-specific recombination reactions from bacteriophage λ.

*Att*B site-flanked V5-tagged UL145 DNA was generated with polymerase chain reaction (PCR) using UL145 expressing plasmid as the template (provided by Professor Gavin Wilkinson, University of Cardiff as part of a library of recombinant adenovirus expression vectors containing coding sequences for a large subset of HCMV proteins), primers (Table 2.1), and PfuUltra II Fusion HS DNA Polymerase (Agilent). The thermocycle programme was performed as below:

Activation 95 °C for 2 min

Denature 95 °C for 20 sec

Annealing 60 °C for 20 sec

Elongation 72 °C for 30 sec

Return to the denature step for 24 repeats

Extra elongation 72 °C for 3 min

DNA products were then isolated by agarose gel electrophoresis and gel extraction with QIAquick Gel Extraction Kit (QIAGEN).

BP recombination reaction was performed with *att*B-flanked UL145-V5 DNA, pDONR223 entry vector (containing *att*P-flanked *ccdB* and spectinomycin resistance gene). BP

Clonase enzyme mix (containing integrase from bacteriophage λ and *E. coli* integration host factor protein) in Tris-EDTA buffer (TE, pH 8.0) overnight (O/N) at room RT. The recombination product was transformed into *cddB* sensitive *E. coli*, and those transformed with UL145 containing plasmid survived selection on spectinomycin selection LB agar plates. pDONR223-UL145-V5 was propagated with mini prep (subsection 2.1.1).

LR recombination reaction was performed with pDONOR223-UL145-V5, lentiviral vector pHAGE (containing attR-flanked *ccdB* and puromycin resistance gene), and LR clonase enzyme mix (integrase and excisionase from bacteriophage λ and *E. coli* Integration host factor protein) in TE (pH 8.0) O/N at RT.

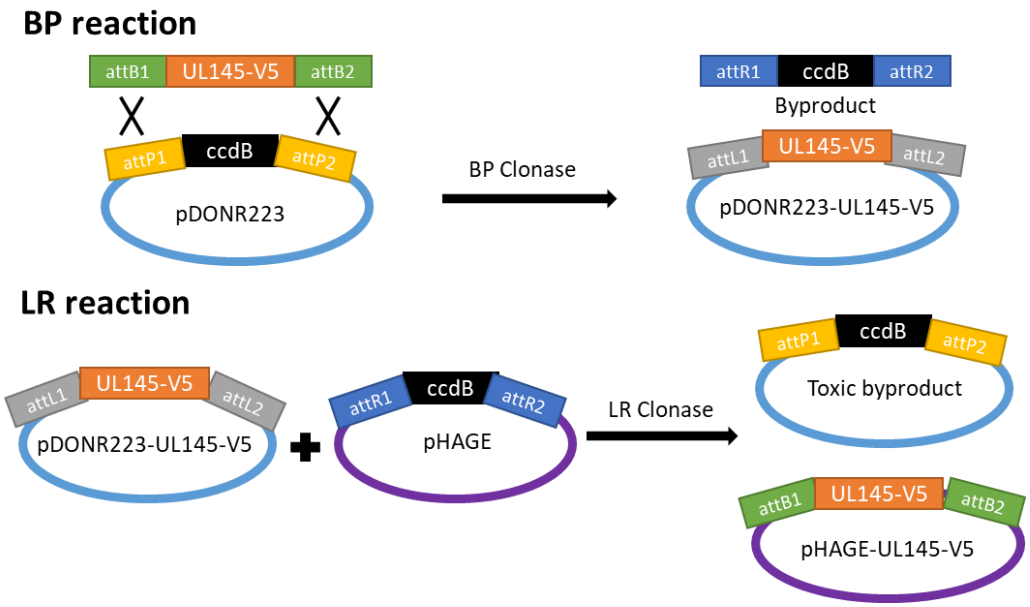

Figure 2.1. Generating UL145-V5 expressing plasmid with Gateway system. Schematics of BP (top panel) and LR (bottom) reactions from Gateway recombination cloning system.

Using the same method, full length and N-terminal deletion HLTF overexpression plasmids were generated with primers described in Table 2.1 and pCDNA3-HLTF as the template (provided by Dr. Edward Greenwood, CIMR).

Sequencing

Confirmation of insert sequence was performed with Sanger sequencing from the service of Genewiz (Takeley, Essex, UK) using the primers in Table 2.1.

Table 2.1. Oligonucleotides used in molecular cloning.

Name	Sequence (5' to 3')
Control shRNA 1 - top	gatccGTTATAGGCTCGCAAAAGGTTCAAGAGACCTTTTGCGAGCCTATAACTTTTTTg
Control shRNA 1 - bottom	aattcAAAAAAGTTATAGGCTCGCAAAAGGTCTCTTGAACCTTTTGCGAGCCTATAACg
Control shRNA 2 - Top	gatccGGCATATAACTATTTAGGTATTTCAAGAGAATACCTAAATAGTTATATGCCTTTTTTg
Control shRNA 2 - bottom	aattcAAAAAAGGCATATAACTATTTAGGTATTCTCTTGAAATACCTAAATAGTTATATGCCg
HLTF shRNA 1- top	gatccGCAGGTGGAGTTGGTTTGAATTTCAAGAGAATTCAAACCAACTCCACCTGCTTTTTTg
HLTF shRNA 1 - bottom	aattcAAAAAAGCAGGTGGAGTTGGTTTGAATTCTCTTGAAATTCAAACCAACTCCACCTGCg
HLTF shRNA 2 - top	gatccTGTGGTTGGACTACGCTATTATTCAAGAGATAATAGCGTAGTCCAACCACATTTTTTg
HLTF shRNA 2 - bottom	aattcAAAAAATGTGGTTGGACTACGCTATTATCTCTTGAATAATAGCGTAGTCCAACCACAg
Gateway expression control primer - forward	GGGGACAAGTTTGTACAAAAAAGCAGGCTCCCAGGCGAGAACGTGTGCGTGGACAAGCGAGCAGCATACGAACCCAGCTTTCTTGTACAAAGTGGTCCCC
Gateway expression control primer - reverse	GGGGACCACTTTGTACAAGAAAGCTGGGTTCGTATGCTGCTCGCTTGTCCACGCACACGTTCTCGCCTGGGAGCCTGCTTTTTTGTACAAACTTGTCCCC
UL145-V5 expression - forward	GGGGACAAGTTTGTACAAAAAAGCAGCTGAAGACACCGGGACCGATC

UL145-V5 expression - reverse	GGGGACCACTTTGTACAAGAAAGCTGGGTTTACGTAGAATCAAGACCT AGGAGC
HLTF full length expression- forward	ggggacaagtttgtacaaaaaagcaggctATGTCCTGGATGTTCAAGAG
HLTF full length expression reverse	ggggaccactttgtacaagaaagctgggtTTAAGCGTAATCTGGAACATCGTATG GGTAAGAACCTAAGTCAATTAATGTTCTGATTTCAT
HLTF N-terminal deletion expression forward	ggggacaagtttgtacaaaaaagcaggctATGGTAGATTCCGTTTTATTTGGAA
HLTF N-terminal deletion expression reverse	Same as HLTF full length expression reverse
U6 promoter (pHRSIREN sequencing)	GGGCAGGAAGAGGGCCTAT
SFFV promoter (pHAGE sequencing, forward primer)	CGCGCCAGTCCTCCGATTG
pHAGE sequencing, reverse primer	GCTTCGGCCAGTAACGTTA

2.1.3. Reverse transcription quantitative polymerase chain reaction (RT-qPCR)

Total RNA extraction

Total RNA of cells was extracted with RNeasy Mini Kit (Qiagen) according to manufacturer's instruction. Briefly, cells were lysed with RNA lysis buffer containing high concentration of chaotropic salt. Nucleic acids were precipitated with ethanol and RNA binds to silica-based column. RNA was collected with elution of RNase-free H_2O after the column had been washed with ethanol-containing solution for three times.

Reverse transcription (RT)

Complementary DNA was synthesized using GoScript Reverse Transcriptase (Promega) according to manufacturer's instruction. RNA with secondary structure resolved under 5 min at 70°C was annealed with random hexamers (0.5 μg per μg of RNA) on ice. The resulting primed RNA was then mixed with 5X reaction buffer, $MgCl_2$ (to final concentration of 2 mM), nucleotide mix (final concentration 0.5 mM each dNTP), RNasin ribonuclease inhibitor (20 units), and reverse transcriptase. First strand complementary DNA (cDNA) was then synthesised at 42°C for an hour. Finally, the reverse transcriptase was inactivated at 70 °C for 15 min.

Quantitative polymerase chain reaction (qPCR)

Quantitative PCR was performed with TaqMan assays (Thermo) to measure the relative mRNA abundance of interferon (IFN) β and GAPDH. Diluted cDNA was mixed with 2X TaqMan universal PCR master mix, and TaqMan probe specific for target gene. The thermal programme was performed with 7500 Real-Time PCR machine (Thermo) as below:

Activation 95 °C for 10 min

Denature 95 °C for 15 sec

Annealing and elongation 60 °C for 1 min

Return to the denature step for 39 repeats

For qPCR assays targeting genes other than IFNβ, SYBR green assay was performed. DNA samples were mixed with 2X Fast SYBR Green Master Mix (Thermo) and respective primers (Table 2.2). The thermocycle programme was performed as mentioned above, plus a melt curve analysis to validate that the amplified DNA segment was homogeneous. The thermal programme of melt curve analysis was carried out as below:

Denature 95 °C 10 sec

Annealing 60 °C 1 min

Melting 60 °C to 95 °C at the rate of 0.05 °C/sec

Hold 95 °C 15 sec

Cool down to RT

Table 2.2. Primer sequence used for SYBR green qPCR.

Primer name	Sequence 5' to 3'
UL145 - Forward	CCCATCATGCGTCGTATCAC
UL145 - Reverse	CCGACTGATCTAGCCTACGG
GAPDH - Forward	AGGGCTGCTTTTAACTCTGGT
GAPDH - Reverse	CCCCACTTGATTTTGGAGGGA
gB - Forward	CTGCGTGATATGAACGTGAAGG
gB - Reverse	ACTGCACGTACGAGCTGTTGG
Genomic GAPDH - Forward	CCTCTGACTTCAACAGCGACAC-
Genomic GAPDH - Reverse	TGTCATACCAGGAAATGAGCTTGA
MIEP - Forward	TGGGACTTTCCTACTTGG
MIEP - Reverse	CCAGGCGATCTGACGGTT
OriLyt – Forward 1	GGGGAGTGTCTACAGGGCTA
OriLyt – Reverse 1	GTCAGGGGTCACGTGAGAAG
OriLyt – Forward 2	ACACCATCGAATGTGGCGAT
OriLyt – Reverse 2	ACCAGGAAAGCTGTCTACGC
OriLyt – Forward 3	TTCCACTAGAGGCGGTCAGT
OriLyt – Reverse 3	GAGCGGTAATTTTCCACCGC
Human globin β promoter (HGBP)- Forward 1	TAAGCCAGTGCCAGAAGAGC
HGBP – Reverse 1	GATGGCTCTGCCCTGACTTT
HGBP- Forward 2	CCAGAAGAGCCAAGGACAGG
HGBP – Reverse 2	GCTCCTGGGAGTAGATTGGC
HGBP- Forward 3	TCCAACTCCTAAGCCAGTGC
HGBP – Reverse 3	GTGATGACAGCCGTACCTGT

Genomic GAPDH – Forward (ChIP)	CAATTCCCCATCTCAGTCGT
Genomic GAPDH – Reverse (ChIP)	CAATTCCCCATCTCAGTCGT

2.1.4. Stable cell generation with lentiviral transduction

Lentiviral plasmid and lentiviral helper plasmids (VSVG [envelope], TAT1B [viral transactivator], MGPM2 [group-specific antigen and polymerase], CMV-Rev1B [regulator of virion proteins expression]) were transfected into simian virus 40 (SV40) large T antigen transformed human embryonic kidney cells (HEK293T) using TransIT-293 transfecting reagent (Mirus) to pack lentiviruses, which subsequently transduced plasmid containing target genes into human telomerase reverse transcriptase immortalized foreskin fibroblast (HFFF-TERT) or HEK293T. Transduced cells were selected with puromycin (hygromysin for pHRSIREN transduced cells) for 2 weeks before experiments.

2.1.5. Small interference RNA (siRNA) Knockdown

HEK293T cells were transfected with a pool of CUL4A siRNAs (L-012610-00, Dharmafect) or a pool of non-targeting siRNAs (D-001810-10, Dharmafect) with DHARMAfect 1 Transfection Reagent (T-2001, Dharmafect) giving a final siRNA concentration of 25 nM. Cellular lysates were harvested 48 h post transfection for Western blot.

2.1.6. Western blot

Whole cell lysis

Trypsinised cells were neutralized with complete DMEM, washed with phosphate-buffered saline (PBS: 137 mM NaCl, 2.7 mM KCl, 8 mM Na_2HPO_4, and 2 mM KH_2PO_4) once, lysed in radioimmunoprecipitation assay (RIPA) buffer (10X concentrate from Cell

Signaling Technology) supplemented with complete EDTA-free protease inhibitors (Roche), homogenized by sonication (Diagenode Bioruptor), and centrifuged at 12000 xg for 10 min at 4 °C to obtain soluble protein extracts. Protein concentration was determined using a microplate bicinchoninic acid (BCA) assay kit (Thermo).

Trichloroacetic acid (TCA) precipitation

For cell lysates processed with 6M guanidine, undigested protein was precipitated with ProteoExtract Protein Precipitation Kit (Merck) according to the manufacturer's instruction. Briefly, protein sample was mixed and incubated with TCA-containing solution for an hour at -20 °C. Protein pallet was collected with centrifugation for 10 min at 10,000 xg, 4 °C, washed with ice-cold acetone three times, and air dried by Speed vac. Protein lysate was reconstitute with 2% sodium dodecyl sulphate (SDS) solution (2% SDS, 63 mM Tris pH 6.8).

SDS-polyacrylamide gel electrophoresis (SDS-PAGE)

Fifty micrograms of protein lysates were mixed with 6X protein loading dye (0.375 M Tris pH 6.8, 12% SDS, 60% glycerol, 0.6M dithiothreitol [DTT], and 0.06% bromophenol blue), denatured at 95 °C for 10 min, and loaded onto 4–20% acrylamide precast gel (Bio-Rad). Gel electrophoresis was performed under 100 V in running buffer (25 mM Tris, 190 mM glycine, 0.1% SDS) until proteins were separated as indicated by protein molecular weight marker (Bio-Rad).

Immunoblot

Separated proteins were then transferred from a gel to a polyvinylidene fluoride (PVDF) membrane (0.45 µm pore) in cold transfer buffer (25 mM Tris, 190 mM glycine, 20% methanol) under 350 mA of electricity for 90 min. The resulting membrane was incubated in blocking buffer (4% skim milk in PBS) at room temperature for an hour and cut into strips accordingly. The membrane was washed briefly with washing buffer (20 mM Tris pH 7.5, 150 mM NaCl, 0.1% Tween-20) and then probed with antibody against HLTF (1:1000, rabbit polyclonal, Abcam), HCMV IE1/2 (1:1000, mouse monoclonal [CH160], Abcam), V5 (1:1000, mouse monoclonal [R960-25], Thermo), or GAPDH

(1:10000, mouse monoclonal [686613], R&D Systems) at 4 °C for 16 hours. Blots were subsequently washed at room temperature 6 times for 10 min each to remove unbound antibodies. A secondary probing was done using near-infrared fluorescent antibodies (1:10000, LI-COR) against mouse or rabbit immunoglobin at room temperature for an hour. Afterwards, blots were then again washed 6 times for 10 min each before visualization on Odyssey Imaging Systems (LI-COR). Western blot images were processed through the software Image Studio Lite (LI-COR).

2.1.7. Firefly luciferase reporter assay

In 96-well opaque plates, 293T cells were transfected with reporter plasmid (pGL3-pIFNβ-Luc, provided by Professor Geoff Smith [University of Cambridge]; pGL4-NFκB-Luc2, purchased from Promega; pGL3-ISRE-Luc; Provided by Dr. Ceri Fielding [Cardiff University]) and internal control plasmid pHAGE-GFP (provided by Professor Paul Lehner [University of Cambridge]) using TransIT-293 transfecting reagent (Mirus). Two days post-transfection, cells were treated with relevant stimuli (Sendai virus, tumour necrosis factor α, interferon α) to induce promoter activities. Six hours post induction, cell culture was replenished with fresh SF DMDM and cells were lysed with Bright-Glo Luciferase Assay plus substrate (Promega) in to a final concentration of 30%. Luminescence and GFP fluorescence was read with microplate reader (Tecan SPARK) after incubation at RT for 5 min. Cell-free SF DMEM was used as blank, and readings from these wells were used for noise subtraction.

2.1.8. Chromatin immunoprecipitation assay

Sample preparation

Chromatin immunoprecipitation (ChIP) assays were performed with Imprint Chromatin Immunoprecipitation Kit (Sigma) according to manufacturer's instruction. Infected cells were washed once with PBS, resuspended in PBS, mixed with fresh formaldehyde at a final concentration of 1%, and incubated at RT for 5 min. Glycine was added to a final concentration of 125 mM to quench formaldehyde. The mixture was incubated at RT for

5 min. After medium removal and ice-cold PBS wash, cell nuclei were extracted with Nuclei Preparation Buffer lysis (200 µL/10^6 cells), vigorously vortexed, and centrifuged (180 xg, 5 min, 4 °C). Cell nuclei were then lysed with shearing buffer (100 µL/10^6 cells) containing protease inhibitor cocktail (PIC) (10 µL PIC/1 ml Shearing Buffer), incubated on ice for 10 min with occasional vortex. DNA was sheared by water-cooled sonication (Diagenode Bioruptor), with 40 cycles of "on" 30 sec and "off" 30 sec.

Protein/DNA Immunoprecipitation

Diluted clarified supernatant was incubated with relevant diluted (10 µg/ml, 1ml/10^6 cells) antibody (αHLTF rabbit polyclonal [Abcam], αhistone H3 rabbit polyclonal [Abcam], rabbit IgG [Sigma]), in provided strip well O/N at 4 °C with constant rocking. After immunoprecipitation, the wells were washed with IP Wash Buffer for 6 times and Tris-EDTA Buffer once.

De-crosslinking

The wells were then incubated with DNA Release Buffer containing Proteinase K (1ml Proteinase K/40 ml DNA Release Buffer) at 65 °C for 15 min. Reversing Solution was then added for a further incubation of 90 min at 65 °C to de-crosslink protein-DNA complex.

DNA Purification

DNA purification was performed with the provided DNA-binding silica-based column and ethanol-containing wash buffer. The resulting DNA samples were eluted with Elution Solution.

2.1.9. Co-immunoprecipitation

Cells were lysed on ice in mammalian cell lysis buffer (MCLB) (50 mM Tris pH 7.5, 300 mM NaCl, 0.5 % [v/v] NP-40, 1 M DTT) supplemented with complete EDTA-free protease inhibitors (Roche). Samples were tumbled for 15 min at 4 °C on a tube roller, then centrifuged at 16,100 x g for 15 min at 4 °C. Protein concentration was determined with BCA assay kit (Thermo).

V5 beads immunopreciptation

Bead slurry made up of monoclonal anti-V5 conjugated agarose resin (Thermo) in MCLB was incubated with the cell lysate for 3 h at 4 °C on a rotating mixer. Thirty µl of 50% (v/v) bead slurry was added per mg of protein lysate. Beads were subsequently washed with ice-cold MCLB 7 times, followed by 7 ice-cold PBS (pH 7.4) washes. Washes were performed in Pierce Spin Columns (Thermo) placed in a vacuum manifold (Promega). Protein bound to the beads was eluted in 250 µg/ml V5 peptide (Thermo) in PBS at 37 °C for 30 min with constant shaking.

HLTF immuniprecipitation

Cell lysate was incubated with anti-HLTF (2.5 ug per mg of lysate, rabbit polyclonal, Abcam) O/N at 4 °C in a rotating mixer (Stuart). The antibody bound HLTF complexes were then immunoprecipitated with protein A-Sepharose beads (Thermo) for 2 h at 4 °C on a rotating mixer. Beads were subsequently washed with ice-cold MCLB and PBS 7 times each in Pierce Spin Columns (Thermo) placed in a vacuum manifold (Promega). After washes, the immunoprecipitated complexes were eluted in 2% SDS solution at 95°C for 5 minutes to detach the complexes from the beads. Eluted protein samples were subjected to immunoblot analysis (subsection 2.1.6) or proteomic mass spectrometry analysis (section 2.4.).

2.2. Cell Biology

2.2.1. Cell lines and cell culture

All cells (HFFF-TERT, 293T) were cultured with complete DMEM supplemented with 10% foetal calf serum (Gibco), 100 U/ml penicillin, and 100 µg/ml streptomycin (Sigma) in humid incubators with 5% CO_2 at 37 °C. To make cell stocks, low-passage cells were resuspended in freezing buffer (10% dimethyl sulfoxide [DMSO] in foetal calf serum) and placed into a 4 °C isopropanol-containing freezing container (Mr. Frosty, Thermo), which was then stored at -70 °C.

2.2.2. Immunofluorescence Microscopy

HFFF-TERT cells were seeded on a sterile coverslip O/N to allow cells to adhere to the glass surface. Cells were subsequently infected with HCMV for 24 h and treated with 10 μM MG132 on coverslips for 12 h prior to harvest. Harvested cells were then cross-linked with fixation buffer (Biolegend), permeabilised with ice-cold methanol, and blocked with Human TruStain FcX (Biolegend). Two primary antibodies were used: rabbit anti-HLTF (ab17984, Abcam) and mouse anti-V5 (MA5-15253, Thermo). Secondary antibodies were anti-mouse Alexa Fluor 488 (4408S, Cell Signaling) and anti-rabbit Alexa Fluor 647 (A31573, Thermo). Cell nuclei were stained with 4',6-diamidino-2-phenylindole (DAPI) (Cell Signaling). Stained cells were mounted with ProLong Gold antifade mountant (Thermo). Fluorescence was observed using a confocal microscope (Zeiss LSM 710). Images were processed with Zeiss Zen software (Blue edition, version 2.3).

2.2.3. Flow Cytometry

Cell fluorescence analysis

Cell fluorescence, either from fluorescent proteins or proteins stained with fluorescent dye, was analysed with FACSCalibur cell analyser (BD Biosciences) and CellQuest PRO software (BD Biosciences). LSRFortessa cell analyser (BD Biosciences) and FACS DIVA software (BD Biosciences) were used for near-infrared fluorescent protein 713 (iRFP713) reading. Samples were fixed with fixation buffer (Biolegend) and adjusted to an approximate cell concentration of 5 x 10^5 cells/ml before subjecting to cell analysers.

Cell sorting

Infected cells were trypsinised, pelleted and resuspended in DMEM to reach approximate cell concentration of 10^6 cells/ml. Cells were sorted into infected and uninfected populations according to GFP intensity with FACSMelody cell sorter (BD Biosciences). Flow speed were adjusted so that more than 80% of the cells could be processed.

Data analysis and presentation

Raw data (FSC files) collected from analysers are processed with FLOWJO software (version 10, BD biosciences).

2.2.4. Enzyme-linked immunosorbent assay (ELISA)

96-well-based ELISA assay

Interferon beta released into cell culture medium was measured with a human IFNβ ELISA Kit (PBL Assay Science) according to manufacturer's instructions. Briefly, diluted cell culture supernatant was mixed with a buffer containing biotinylated secondary antibody, and incubated in assay well coated with IFNβ antibody for 2 h with constant rocking. After aspiration and washing three times, streptavidin conjugated horseradish peroxidase (HRP) was added to the well, and incubated for 30 min with constant rocking. Tetramethyl-benzidine (TMB) is the substrate, which was added to the well after it was washed thoroughly. This incubation was performed in the dark without agitation for 30 min. Finally, the reaction was terminated with stop solution and the absorbance at 450 nm was determined using a microplate reader (Tecan Spark) within 5 min after the addition of the stop solution. By plotting the standard curve, which was serial dilution of recombinant human IFNβ expressed in mammalian cells, the IFNβ concentration in the supernatant can be calculated.

Multiplex Bead-based ELISA assay

Supernatant of infected cells was analysed with Legendplex multiplex ELISA kit (Biolegend) to measure 13 human proteins, including interferons (α, β, γ, λ1 and λ2/3), interleukins (1β, 6, 8, 10, 12), TNFα, interferon-inducible protein 10 (IP-10, CXCL10) and granulocyte macrophage colony-stimulating factor (GM-CSF). Beads are differentiated by size and internal fluorescence intensities. Each bead is conjugated with a specific antibody on its surface and serves as the capture bead for that particular analyte. When a selected panel of capture beads is mixed and incubated with a sample containing target analytes specific to the capture antibodies, each analyte will bind to its specific capture beads. After washing, a biotinylated detection antibody cocktail is added, and

each detection antibody in the cocktail will bind to its specific analyte bound on the capture beads, thus forming capture bead-analyte-detection antibody sandwiches. Streptavidin-phycoerythrin (SA-PE) is subsequently added, which will bind to the biotinylated detection antibodies, providing fluorescent signal intensities in proportion to the amount of bound analytes. Beads sizes and their FITC and PE intensities were measured with FACSCalibur cell analyser (BD Biosciences) and data were processed with Legendplex software (Biolegend).

2.3. Virology

2.3.1. Viruses

All HCMV strains used in this project can be found in Table 2.3. RCMV 1111 strain was provided by Dr. Peter Tomasec (School of Medicine, Cardiff University), all the other strains were generated and provided by Dr. Richard Stanton (School of Medicine, Cardiff University).

Table 2.3.Complete list of HCMV used in this project

Virus name	Identifier	Mutations
WT Merlin	RCMV 1111	Mutated RL13 and UL128
ΔUL145 Merlin	RCMV 1814	Mutated in RL13 and UL128; UL145 deletion
WT Merlin UL36-GFP	RCMV 2582	Mutated in RL13 and UL128; UL36-P2A (self-cleaving peptide derived from foot-and-mouth disease virus)-GFP
ΔUL145 Merlin UL36-GFP	RCMV 2590	Mutated in RL13 and UL128; UL36-P2A-GFP; UL145 deletion
WT Merlin UL36-GFP Tet-on UL128	RCMV 2270	Mutated in RL13 and UL128; tetracyclin-regulated RL13 and UL128; UL36-P2A-GFP

ΔUL145 Merlin UL36-GFP Tet-on UL128	RCMV 2571	Mutated in RL13 and UL128; tetracyclin-regulated RL13 and UL128; UL36-P2A-GFP; UL145 deletion
WT Merlin UL145-V5	Not assigned	Mutated in RL13 and UL128; UL145-V5
WT AD169-GFP	RCMV288	UL/b' deletion; mutated RL5A, RL13, UL36 and UL131A; UL32-GFP

Sendai virus was (ATCC VR-907) purchased from ATCC and used after it was thawed, aliquoted, and stored at -70 °C.

2.3.2. Virus infection

HCMV

Virus stock was diluted with 37 °C serum-free (SF) Dulbecco's modified Eagle medium (DMEM, Sigma) according to the desired multiplicity of infection (MOI) and added directly to the cells. Cells were incubated at 37 °C with 5% CO_2 and constant rocking for 2 h before substituting virus-containing DMEM into complete DMEM.

Sendai virus

For Sendai virus (ATCC VR-907) infection, virus was diluted in 1:40 with SF-DMEM, and the viral mix was added to the cell (30 µl for a 96-well plate well). Cells were incubated at 37 °C with 5% CO_2 and constant rocking for 2 h before substituting viral mix into complete DMEM.

2.3.3. Viral production

HFFF-TERT cells were infected with a low-passage stock of HCMV Merlin strain at approximately MOI 0.01 for 14 days or until plaques were clearly visible to cover 70% of the cell lawn. During infection, cells underwent routine media changes every 2-3 days to

sustain cell viability and viral production. Virus-containing media was concentrated through high-speed centrifugation at 10,000 rpm (Beckman Coulter JAL-16.25 rotor, approximately 10,000 xg) at 35 °C for 2 h. Centrifuge brakes were turned off to avoid virion rupture and disruption of pallet formation. Virions were then resuspended in small volume of complete DMEM and aliquots were frozen at -70 °C.

2.3.4. Virus titration

Titration of non-GFP viruses

Intracellular staining of HCMV IE1/2 was used to determine virus titre. Virus stocks were serially diluted by 4-fold 4 times and used to infect HFF-TERT cells. Forty-eight hours post infection, cells were detached with trypsin, neutralized with complete DMEM and briefly washed once with PBS. Then, cells were fixed with fixation buffer (Biolegend) at 4 °C for 30 min, and permeabilised with ice-cold methanol on ice for 15 min. To remove non-specific binding of antibodies, permeable cells were treated with human TruStain FcX Fc receptor blocking solution (Biolegend) at 4 °C for 30 min. Subsequently, cells were incubated with antibody targeting HCMV IE1/2 (1:1000, mouse monoclonal [6F8.2], Millipore) at 4 °C for 30 min, followed by a PBS wash before labelling with anti-Mouse IgG conjugated with Alexa Fluor 647 (1:5000, Thermo). After another PBS wash, cells were subjected to fluorescence-activated cell sorting analysis using FACSCalibur (BD Biosciences) to determine the percentage of IE1/2 positive cells. The number of IE1/2 positive cells represented the number of HCMV infected cells, which was adapted to calculated plaque forming unit (PFU) in the viral stocks.

The Poisson distribution was used to predict the percentage of cells receiving a given number of infectious particles at different multiplicities of infection (MOI) (Condit, 2013). As applied to virus infections, the Poisson distribution can be written as:

$$P(k) = \frac{e^{-m}m^{k}}{k!}$$

In this equation, *P(k)* is the probability that a cell is infected with *k* infectious particles and *m* equals MOI.

According to the Poisson distribution, observation of 33% of infected cells implies more than 95% of these cells received only 1 virion. Therefore, dilutions with less than 33% infection population were used to estimate the input virion assuming all the infected cells are IE1/2 positive and 1 PFU equals 1 IE1/2 producing unit. The average of estimated virion amount from different dilutions was used as titre. An example is shown in Figure 2.2. 1:1024 and 1:4096 resulted in an infection population of less than 33% (5.1% and 0.84% respectively) and the average titres from these two dilutions was used to estimate the HCMV stock titre.

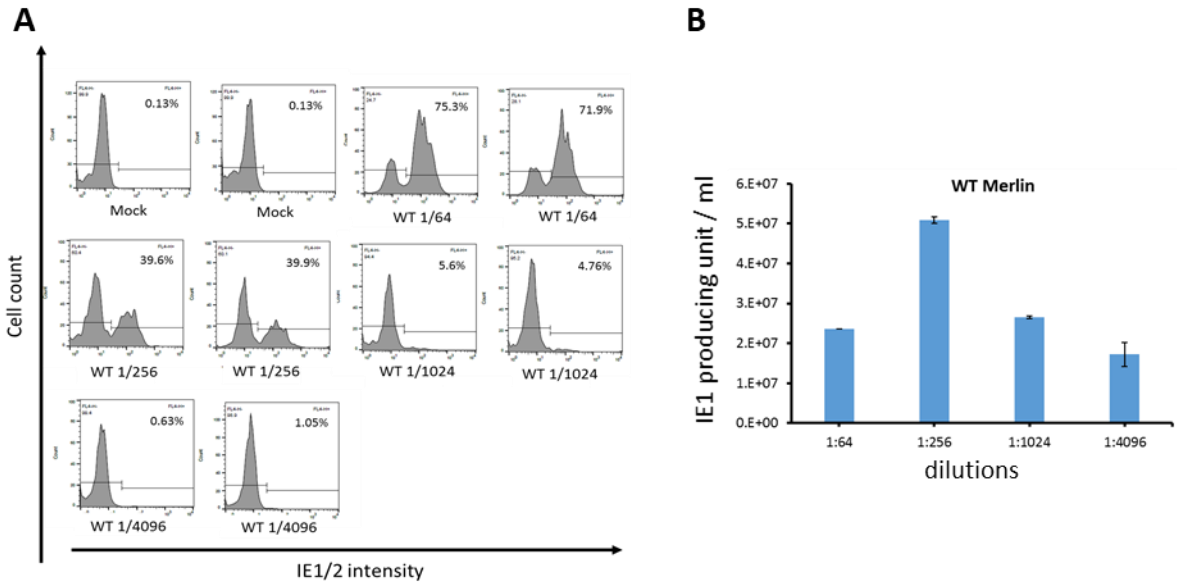

Figure 2.2. Example of a WT Merlin HCMV titration with intracellular IE1/2 staining.
(A) Histogram of IE1/2 intensity of wild-type (WT) Merlin HCMV serial dilution infection. Each infection was performed in biological duplicate. The percentage of IE1/2 positive cells were indicated on the top right corner of the graph. (B) The bar graphs representing the virus titre calculated in each dilution. The error bars represent the standard deviation between the two duplicates. Average of 1:1024 and 1:4096 results was used as the titre of the tested virus.

Titration of GFP viruses

For GFP tagged viruses, the percentage of GFP positive cells were quantified with FACSCalibur as percentage of HCMV infected cells directly instead of IE1/2 intracellular staining.

2.3.5. Viral DNA Replication Assay

Cells were infected with Merlin HCMV at the indicated MOI. At multiple time points post infection, infected cells were rinsed with PBS for 3 times to remove extracellular DNA and harvested using trypsin. Genomic DNA of these cells were extracted using DNeasy Blood & Tissue Kits (QIAGEN) according to instructions from manufacturer. The extraction principle is to lyse cells by vortex in the presence of detergent and protease. Nucleic acid was then precipitated with ethanol and collected with DNA binding columns. Finally, DNA was dissolved in sterilized ddH_2O after washing with ethanol-containing buffers. Extracted DNA was then analysed targeting viral gB gene and human genomic GAPDH with SYPR green qPCR described in subsection 2.1.3.

2.3.6. Virus Growth Curve Analysis

HFFF-TERT cells were infected with wild type or UL145-deleted GFP-encoded Merlin HCMV at MOI of 1. Cells were incubated with serum free DMEM for 24 h prior to infection. For a T25 experiment, $1x10^6$ cells are seeded and viral mix were replaced with 2 ml complete DMEM, supernatant was collected daily and stored at -70°C. Virus titre was determined as previously described. In some experiments, spare viral mix was collected and tittered together with supernatant as “day 0”.

2.4. Proteomics

2.4.1. Whole Cell Lysate Protein Digestion

Cells were washed with PBS once, typrsinised, neutralised with complete DMEM, pelleted, and lysed with 200 µl lysis buffer (6M Guanidine/50 mM HEPES pH 8.5) per T25 flask. Cells were then sonicated for 2.5 min at constant 4°C cooling with Bioruptor Pico (Diagenode), and cell debris was removed by centrifuging at 21,000 xg for 10 min at 4°C. To reduce protein, DTT was added and samples were incubated for 20 min at room temperature. Cysteine residues of protein were alkylated with 14 mM iodoacetamide

(IAA) and incubated 20 min at room temperature in the dark. Excess IAA was quenched with DTT for 15 min. Protein samples were then digested with LysC protease at a 1:100 protease-to-protein ratio for 3 h at room temperature after Guanidine concentration was lowered to 1.5M with 200 mM HEPES (pH 8.5). Guanidine concentration was further lowered to 0.5M and Trypsin was then added at a 1:100 protease-to-protein ratio followed by overnight incubation at 37 °C with constant shaking. Trypsin was quenched with 5% formic acid. Samples were then centrifuged at 21,000 xg for 10 min at at 4°C to remove undigested protein. Peptides were subjected to octadecyl carbon chain (C18) solid-phase extraction (SPE, Sep-Pak, Waters) and dried with speed-vac (Thermo).

For small-scale peptide extraction, instead of Sep-Pak, an in-house SPE column called StageTips were made with 200 µl pipette tips and tiny disks made of C18 bound beads embedded in a Teflon mesh (Thermo) (Rappsilber et al., 2007).

2.4.2. Peptide Labelling with Tandem Mass Tags (TMT)

Desalted peptides were dissolved in 200 mM HEPES (pH 8.5) and peptide concentration was measured by microBCA kit (Thermo). TMT reagents (0.8 mg) were dissolved in 43 µl anhydrous acetonitrile to make stocks and 3 µl was added to 25 µg of peptides at a final acetonitrile concentration of 30% (v/v). Following incubation at room temperature for 1 hr, the reaction was quenched with 0.3% (v/v) hydroxylamine. Equal amount of TMT-labelled samples were combined and subjected to C18 SPE and dried with speed-vac before subjected to mass spectrometer.

2.4.3. Stable isotope labeling by amino acids in cell culture (SILAC)

Specific isotopes of L-Lysine-dihydrochloride and L-Arginine-hydrochloride were added into DMEM without arginine or lysine (DMEM for SILAC, Thermo), supplemented with 10% dialysed FCS (Thermo), 100 U/ml penicillin (Sigma), 100 µg/ml streptomycin (Sigma), and 280 mg/l L-proline (Sigma). Excess proline was added to prevent arginine-to-proline and affecting arginine concentration. Before adding to SILAC medium, dialysed FCS was spun at 4000 rpm 10 min room temperature and subsequently filtered through a 0.45

um filter to remove insoluble proteins. “Heavy” SILAC medium was supplemented with 151.3 mg/l $^{13}C^{15}N_2$-lysine and 88 mg/l $^{13}C_6{}^{15}N_4$-arginine (CK Isotopes Limited); “medium” SILAC medium was supplemented with 148.7 mg/l $^{2}H_4$-lysine and 86.5mg/l $^{13}C_6$-arginine (CK Isotopes Limited); “light” SILAC medium contained natural 146 mg/l lysine and 84 mg/l arginine (Sigma). Cells were grown for seven passages in respective SILAC medium before experiments.

2.4.4. Offline high pH reversed phase fractionation (HpRP)

Liquid chromatography (LC) is a technique that separates different components within a mixture using a column which allows components to diffuse across at different rates. In reversed-phase high-performance LC (HPLC), a high pressure pump generates a constant flow of solvent called mobile phase that passes through a column containing absorbent silica particles coated with hydrophobic alkyl chains that interacts with peptides, called stationary phase. An autosampler introduces the sample into the mobile phase before entering the stationary phase in HPLC. Ultrahigh performance liquid chromatography (UHPLC) uses particles with diameter less than 2 µm to increase separation efficiency.

In order to increase sample resolution on mass spectrometer, TMT-labelled peptides were subjected to HpRP fractionation using an Ultimate 3000 rapid separation (RS) nano UHPLC system (Thermo) and 12 fractions were generated. The system is equipped with a Kinetex Evo C18 column (Phenomenex) that has 2.1 mm in internal diameter (ID) and 25 cm in length, is filled with C18 bound silica particles (stable at pH 1-12) with diameter of 1.7 µm. Mobile phase was made up of HPLC grade H_2O, acetonitrile, and ammonium formate (pH 10). The concentration of ammonium formate was maintained at 20 mM while concentration of acetonitrile gradually increased along the fractionation elution programme. Starting from 2.7% (v/v), acetonitrile concentration increased to 21% in the first 10 minutes, to 36% after 24 min 15 sec of elution, then to 51% after 33 min of elution. The acetonitrile concentration was subsequently increased to and maintained at 90% for 10 min to wash the column. The flow rate was 400 ml/min and the elution was performed at 45°C. UV absorbance was monitored at 280 nm and fractions were

collected into 96 well microplates using the integrated fraction collector. Fractions were recombined orthogonally in a checkerboard fashion, combining alternate wells from each column of the plate into a single fraction, and commencing combination of adjacent fractions in alternating rows. Wells were excluded prior to the start or after the cessation of elution of peptide-rich fractions, as identified from the UV trace. This resulted into two sets of 12 combined fractions, which were dried in a vacuum centrifuge and resuspended in 10 ml solvent (4% acetonitrile and 5% formic acid) prior to LC-MS3.

2.4.5. Liquid chromatography coupled with multi-stage mass spectrometry (LC-MS3)

At the LC stage, sample went through Ultimate 3000 RSLC nano UHPLC, which is equipped with a 300 µm ID x 5 mm Acclaim PepMap µ-Precolumn (Thermo) and a 75 µm ID x 50 cm 2.1 µm particle Acclaim PepMap RSLC analytical column (Thermo).

Loading solvent was 0.1% formic acid and analytical solvent contained HPLC grade H_2O, acetonitrile, and formic acid. Samples were loaded at 5 ml/min for 5 min in loading solvent before beginning the analytical gradient. Formic acid concentration was maintained at 0.1% during the analytical gradient while concentration of acetonitrile gradually increased. All separations were carried out at 55°C.

Mass spectrometry data were acquired using Orbitrap Lumos mass spectrometer (Thermo), which uses electrospray to charge peptides into positively-charged ions for analysis. An Orbitrap is an ion trap mass analyser that consists of two outer electrodes that form a barrel and a spindle like electrode in the middle (Figure 2.3). The electrodes create electromagnetic fields that cause ions to oscillate around the central electrode. During oscillation, each ion's motion induces a current in the outer electrodes due to electrostatic attraction, allowing detection of the oscillation frequency using Fourier Transform, which decomposes the induced current value over time into sine(*sin*) and cosine(*cos*) components over frequencies. The oscillation frequency is inversely proportional to square root of m/z:

$$T = \frac{1}{\omega} = k\sqrt{\frac{m}{z}}$$

In this equation, T is the period of oscillation, ω is the frequency, m is the mass of the ion, z is the charge of the ion, and k is a constant proportional to the potential difference between the central and the outer electrodes. Different ions oscillate at different frequencies, resulting in their separation. (Scigelova et al., 2011; Zubarev and Makarov, 2013)

Besides an Orbitrap, the system has quadrupole mass filters, which select ions with specific *m*/*z* with 4 rod-shape electrodes, and a collision-induced dissociation chamber, where fast moving ions collide with neutral gas and fragment into b- (contain N-terminus) and y- (contain C-terminus) type ions (Figure 2.3). Together both compartments allow an Orbitrap Lumos to perform tandem mass spectrometry (MS/MS, or MS2), which is pivotal for peptide sequence identification. For TMT experiments, an MS3 analysis was followed after MS2, in which MS2 ions were selected for higher energy collisional dissociation (HCD) and small *m*/*z* fragment reporter ions from TMT tags were quantified.

TMT-based analysis used a MultiNotch MS3-based method (McAlister et al., 2014). MS1 scans were surveyed between 380-1500 Thompsons (Th, a unit of *m*/*z*), with mass resolving power (resolution) of 120,000, automatic gain control (AGC) target of $2x10^5$, and maximum injection time of 50 ms. Ions that had the counts of $5x10^3$ counts and above triggered MS2 analysis, with Quadrupole isolation at an isolation width of 0.7 Th, normalised collision energy (NCE) set to 35% for CID fragmentation, $1.5x10^4$ AGC target, and 120 ms maximum injection time. The top 6 MS2 ions were selected for HCD fragmentation (NCE 65%) in MS3. MS3 resolution was 60,000, with an AGC target of $1x10^5$ and a maximum accumulation time of 150 ms. The entire MS/MS/MS cycle had a target time of 3 sec. Dynamic exclusion was set to +/- 10 ppm for 70 sec.

LC-MS2 was used to analyse SILAC samples. The parameters were slightly different to TMT experiments. MS1 scans read 300-1500 Th, with resolution of 120,000, AGC target $4x10^5$, and maximum injection time of 50 ms. MS2 fragmentation was trigged on precursors $5x10^4$ counts and above. Quadrupole isolation at an isolation width of *m*/*z* 1.6, HCD fragmentation (NCE 35) with fragment ions scanning in the Orbitrap from *m/z*

110, $5x10^4$ AGC target, 60 ms maximum injection time. Dynamic exclusion was set to +/- 10 ppm for 60 sec.

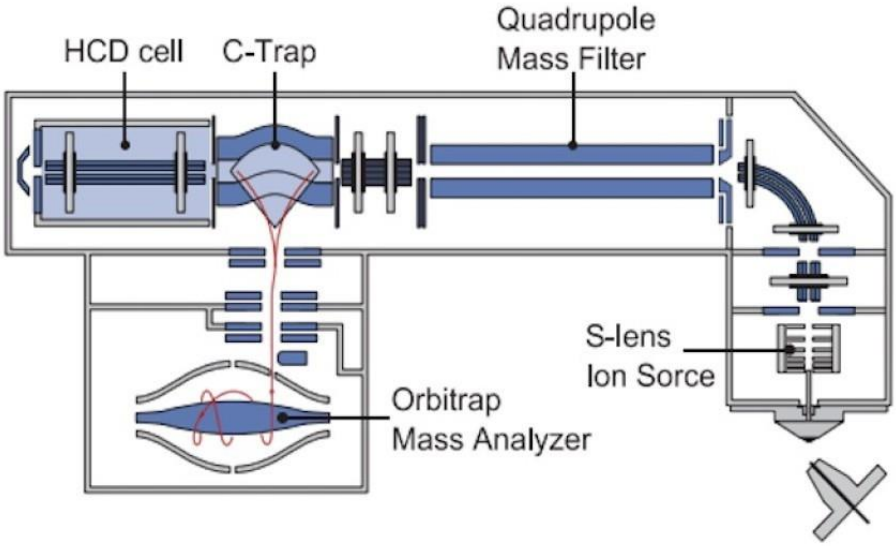

Figure 2.3. Schematic of a quadrupole coupled Obitrap LC-MS2.
Image is derived from Thermos website for Q Executive MS. Electrospray (bottom right) charged peptides. S-lens focuses charged ions. Quadrupole selects ions with specific m/z. C-trap retains ions before entering Orbitrap. HCD cell breaks down peptide ions for MS2 or MS3 analysis. Orbitrap measure m/z through oscillating frequency.

2.4.6. Protein quantification data analysis

Peptide identification

The SEQUEST algorithm is a search programme that compares tandem mass spectra of peptides against peptide sequences from a sequence database. The correlation score is given to identify the possible peptide sequence of tandem mass spectra of peptides (Eng et al., 1994). Mass spectra were processed using ‘‘MassPike’’, which is a SEQUEST-based software for quantitative proteomics, developed by Professor Steven Gygi and colleagues at Harvard Medical School. The data format mzXML is a format that allows open storage and exchange of mass spectroscopy data. In MassPike, MS spectra were converted to mzXML format using an extractor built upon Thermo Fisher’s RAW File Reader library (version 4.0.26). The standard mzXML format has been augmented during

extraction and conversion, with additional customisations that are specific to ion trap and Orbitrap mass spectrometry and essential for TMT quantitation. These customisations consider ion injection times for each scan, Fourier Transform-derived baseline and noise values calculated for every Orbitrap scan, isolation widths for each scan type, scan event numbers, and elapsed scan times.

Acquired mass spectra were searched against a combined protein sequence database that includes human proteins, HCMV proteins, and possible protein contaminants that might be introduced to samples. Human protein database was acquired from the human Uniprot database (Downloaded on 26th January, 2017). The HCMV protein database was assembled from the HCMV strain Merlin Uniprot database, noncanonical human cytomegalovirus ORFs described by Stern-Ginossar *et. al.* (Stern-Ginossar et al., 2012), a six-frame translation of HCMV strain Merlin filtered to include all potential ORFs of ≥8 residues (delimited by stop-stop rather than requiring ATG-stop). A database comprised of common contaminants included nonhuman protein such as bovine serum albumin and porcine trypsin, and annotated human protein contaminants such as keratins. Searches were performed using a 20 ppm precursor ion tolerance. Fragment ion tolerance was set to 1.0 Th.

Modifications were set to account for mass shifts caused by IAA treatment, TMT labelling, and SILAC labelling. IAA treatment induces carbamidomethylation of cysteine residues and increases peptide mass by 57.02146 Dalton (Da). TMT labelling adds 229.162932 Da to lysine residues and peptide N-termini. In SILAC labelling, “heavy” lysine increases mass by 8.01420 Da, “heavy” arginine by 10.00827 Da, “medium” lysine by 4.02511 Da, and “medium” arginine by 6.02013 Da. Oxidation of methionine residues (15.99492 Da) was also considered even for the absent of H_2O_2 or other strong oxidants in our experiments.

Peptide identification was executed in the order of the ranks using cross-correlation score (XCorr), as the correctness of peptide spectral matches (PSMs) decreased along the ranks. A target-decoy strategy was employed to ensure the quality of peptide identification (Elias and Gygi, 2007). A decoy database was generated by reversing the sequence of the composite protein database mentioned above. When identification of

a reverse sequence peptide occurred, it was predicted that another peptide had already been falsely identified. Peptide identification terminated before the total false discovery rate reached 2% (presumably 1% from identification of reverse sequence peptide and 1% from peptides that were truly falsely identified). Correct and incorrect spectral matches were distinguished from one another using linear discriminant analysis based on several parameters including XCorr (number of matching peaks in MS2 scan) of the top possible peptide, the XCorr difference between top and second possible peptide (ΔCn), precursor mass error (derived from the difference between predicted MS1 reading and the obtained reading), and the charge state.

Protein assembly

Protein assembly was performed by principles of parsimony to produce the smallest set of proteins necessary to account for all observed peptides, meaning in cases of redundancy, shared peptides were assigned to the protein sequence with the most matching peptides.

Protein quant

Following fragmentation, each TMT tag produces reporter ions with specific mass, which were surveyed in low m/z area of the MS3 spectrum. The maximum intensity nearest to the theoretical m/z of each reporter ion was used. Proteins were quantified by summing TMT reporter ion counts across all matching peptide-spectral matches. If a TMT experiment uses *n* (number) types of TMT tags, more than *n-1* TMT channels missing and/or a combined signal-to noise ratio of less than *25n* across all TMT reporter ions are considered poor quality of MS3 spectra. PSMs with poor or no MS3 spectra were excluded from quantitation. Protein quantitation values were exported for further analysis in Excel.

For SILAC analysis, quantitation was performed at the MS1 level by comparing the intensities of the precursor ions that were differently labelled by different SILAC medium.

2.4.7. Fold Change Significance Statistics

The data analysis of protein expression fold change included calculation of the significance of the fold change. Significance was calculated with PERSEUS software (Max Planck Institute of Biochemistry), using its Significance A/Significance B function. The significance A algorithm determines a standard deviation (SD) of a group of fold changes and calculates a p-value for each fold change based on this SD. The more the fold change deviates from the mean of this group according to SD, the lower significance A value this fold change has. For example, if 8000 proteins are quantified, 8000 fold changes (FCs) respective to a treatment are calculated. The significance algorithm first determines the standard deviation of FCs from all up-regulated proteins (FC>1) and the standard deviation of FCs from all down-regulated proteins (FC<1).The significance p-value of a given fold change is assigned according to how this fold change deviates from 1 (FC=1, no change).

Proteins with higher ion intensity are considered better quantified and the p-value are more significant. Significance B includes intensity as part of the p-value calculation, and splits ratio values into groups of 350 proteins according to their intensity. The SD / significance calculation is then performed within each group. All Significance A and B values are subsequently adjusted for multiple hypothesis testing using the method of Benjamini-Hochberg (Benjamini and Hochberg, 1995).

2.4.8. Pathway Analysis

The database for annotation, visualisation and integrated discovery (DAVID, version 6.8 http://david.ncifcrf.gov/) was used to determine pathway enrichment (Huang da et al., 2009). A given cluster was searched against a background of all proteins quantified within the relevant experiment, using default settings provided by this website.

2.4.9. Amino acid sequence alignment and secondary structure prediction

Amino acid sequence alignment of UL145 orthologues in primate cytomegaloviruses was derived using Clustal Omega (http://www.ebi.ac.uk/Tools/msa/clustalo/).

Secondary structure predictions were performed with Jpred 4 (http://www.compbio.dundee.ac.uk/jpred/)

2.4.10. Gene clustering

Hierarchical clustering was performed using Cluster 3.0 (http://bonsai.hgc.jp/~mdehoon/software/cluster/). The clustering results are visualized with Java TreeView (http://jtreeview.sourceforge.net/).

2.5. Statistics

For flow cytometry, ELISA and most of qPCR experiments, data were derived from duplicates and standard deviation (SD) was calculated to show the variability of measurements. For luciferase reporter assays and 4 qPCR experiments (Figs 4.2A, 4.6, 4.8A, 4.12) where n>2, standard error of the mean (SEM) was calculated to show how far the sample mean of the data is likely to be from the true population mean. Statistical analyses of proteomic experiments are described in subsection 2.4.7. For comparative studies in Chapter 5, linear trend lines (y-intercept was set to zero) and correlation coefficients (r^2) were generated by Excel.

Chapter 3. HLTF degradation mechanism during HCMV infection

HLTF was identified as one of the top targets for HCMV degradation in our proteomics screen. The first part of this project was to investigate how HCMV directs HLTF for proteasomal degradation during early infection. Study of the degradation mechanism will provide insights into how HCMV orchestrates host factors during infection and help to identify ways to counteract HLTF downregulation during infection. Results in this chapter showed that HLTF was targeted by HCMV UL145 protein for proteasomal degradation via cullin 4 (CUL4) E3 ligase.

3.1. Verification of HLTF proteasomal degradation

First, the results from proteomic experiments were validated with conventional molecular biology method Western blot. HFFF-TERT cells were infected with Merlin HCMV and harvested at 12, 24, 48 hours post infection (hpi). Twelve hours before each harvest, normal cell culture medium was replaced with complete DMEM with 10 μM MG132. Along the infection time course, HLTF was downregulated starting at 12 hpi, and its protein level remained low at 24 hpi and 48 hpi. (Figure 3.1 A&B) At 12 hpi, it was clear that MG132 blocked HLTF down-regulation. However, HCMV-mediated down-regulation of HLTF was far less prominent at 24 and 48 hpi, possibly because HLTF had a rather fast degradation rate during mock infection. During the course of HCMV infection, HLTF protein gradually decreased during mock infection (light blue bars Figure 3.1B), but this decrease was not observed under MG132 treatment (dark blue bars Figure 3.1B). The immunoblot results correlated with the previous proteomic MG132 inhibitor screen performed by Dr. Katie Nightingale (Figure 3.1C). In these TMT based experiments, MG132 rescued HCMV-mediated down-regulation of HLTF at 12, 24, and 48 hpi. Since the experiments were performed separately, degradation of HLTF over time in mock infection could not be observed.

During HCMV infection, 12 h of MG132 treatment resulted in different amounts of HLTF protein rescued at 24 and 48 hpi. One of the reasons could be the HLTF transcriptional

regulation during HCMV infection observed in the RNA sequencing. HLTF RNA level increased by 2 fold from 12 hpi to 24 hpi, and remained increased at 72 hpi (Figure 1.12C), this could be contributing to why there was more HLTF protein rescued at 48 hpi than at 24 hpi.

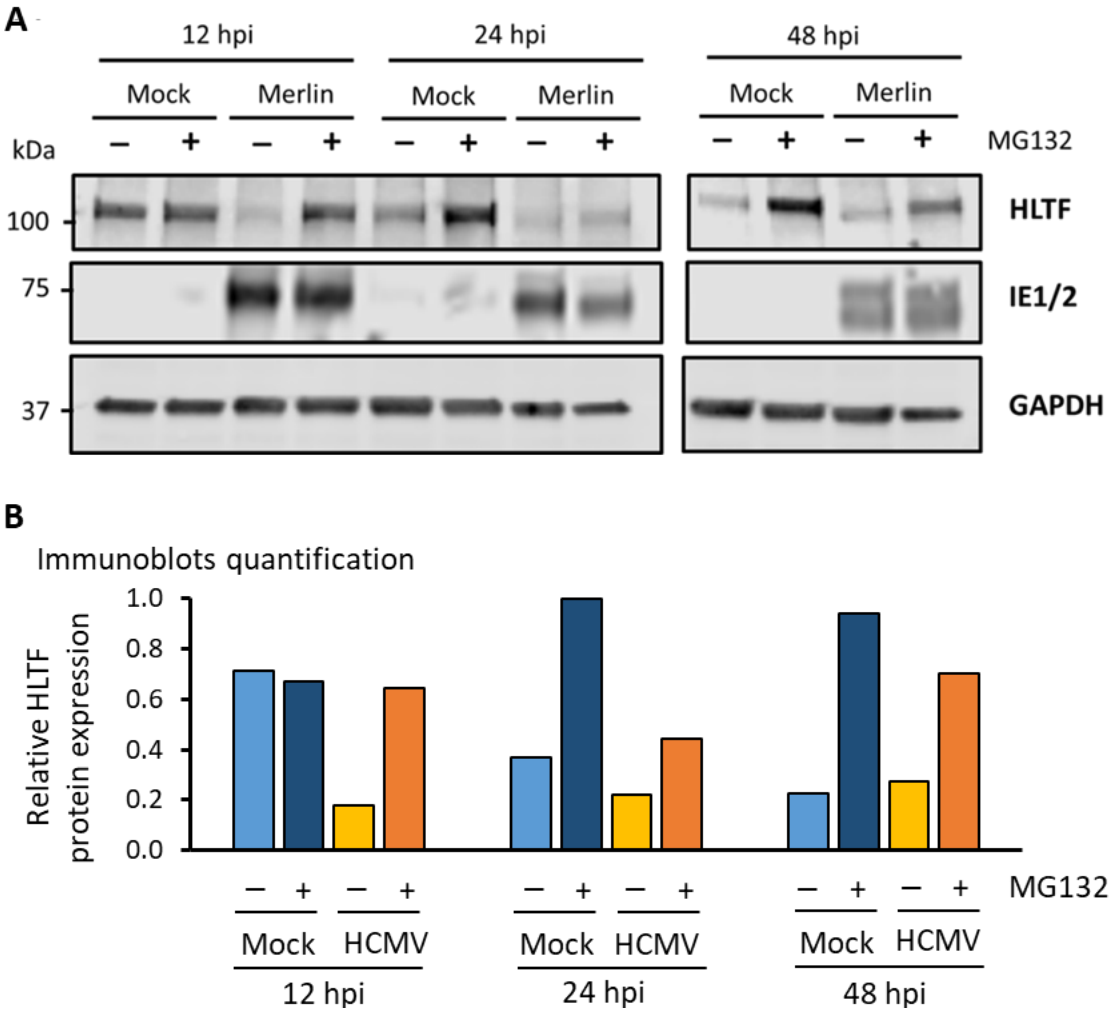

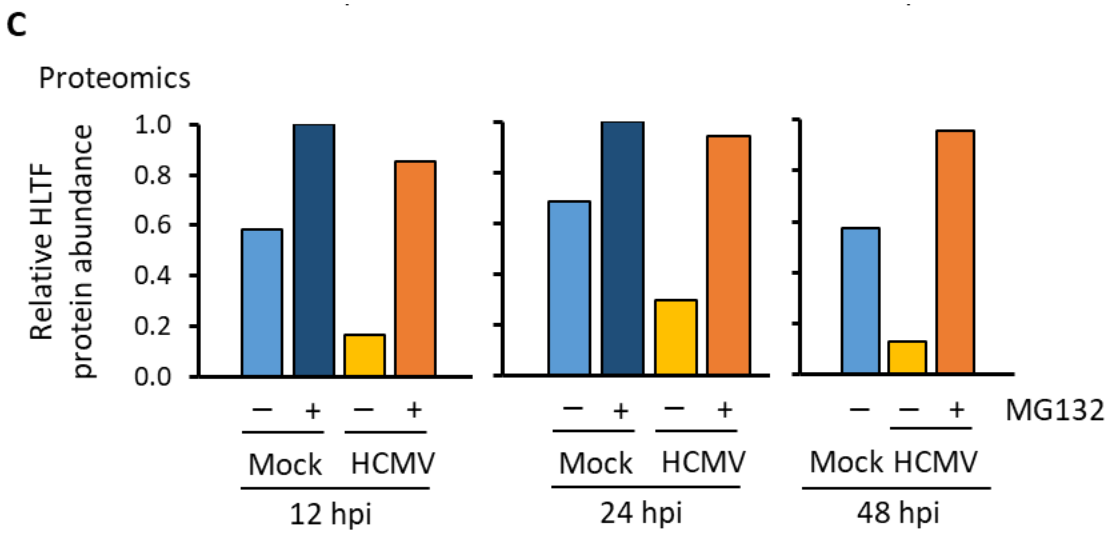

Figure 3.1. HLTF expression during HCMV infection under MG132 treatment.
(A) Western blot analysis of HLTF expression within 48 hours of Merlin HCMV infection. MOI was 5 for this experiment. IE1/2 expression indicated HCMV infection while GAPDH was stained as a loading control. (B) Western blot signal quantification was performed by measuring the median fluorescence intensity of HLTF and normalised by that of internal control GAPDH. Relative HLTF was calculated according to the highest HLTF/GAPDH value, in this case mock infection with MG132 at 24 hpi. (C) TMT-based proteomic analysis of HLTF during HCMV infection with MG132 described in subsection 1.5.2. HFFF-TERT cells were incubated with dexamethasone-containing serum free DMEM for 24 h. Cells were subsequently infected with Merlin strain HCMV at MOI of 10 for 12, 24, and 48 h. Twelve hours prior to harvest, infected cells were treated with 10 µM MG132 until harvest.

3.2. Identification of UL145 as the viral factor regulating HLTF degradation

Next, I wished to find out whether HLTF down-regulation was specifically caused by viral factors. If HLTF down-regulation results from expression of an HCMV protein, it could suggest that HCMV deliberately decreased HLTF expression and that HLTF degradation was not a cellular response to HCMV infection. In this section, UL145 of UL/b' region was identified to be sufficient and essential for HLTF degradation.

3.2.1. Block deletion virus

HCMV encodes over 170 proteins and it is difficult to check the effect of each viral protein one by one. Therefore, I took advantage of the lab-adapted AD169 strain, which bears a block mutation in the UL/b' region. As shown in Figure 3.2, AD169 infection did not lead to HLTF down-regulation, implying that viral protein that was responsible for HLTF degradation was encoded within UL/b' region. Moreover, expression of HLTF was higher in AD169-infected cells in comparison with uninfected cells at both 24 and 72 hpi. This indicated that one of the factors encoded by the UL/b' segment (or one of the other factors mutated in the AD169 compared to Merlin genome) led to degradation of HLTF. Furthermore, given the increased level of HLTF expression during infection with AD169 virus compared to Merlin, it is possible that viral infection in the absence of an antagonist encoded within UL/b' actually induced HLTF expression.

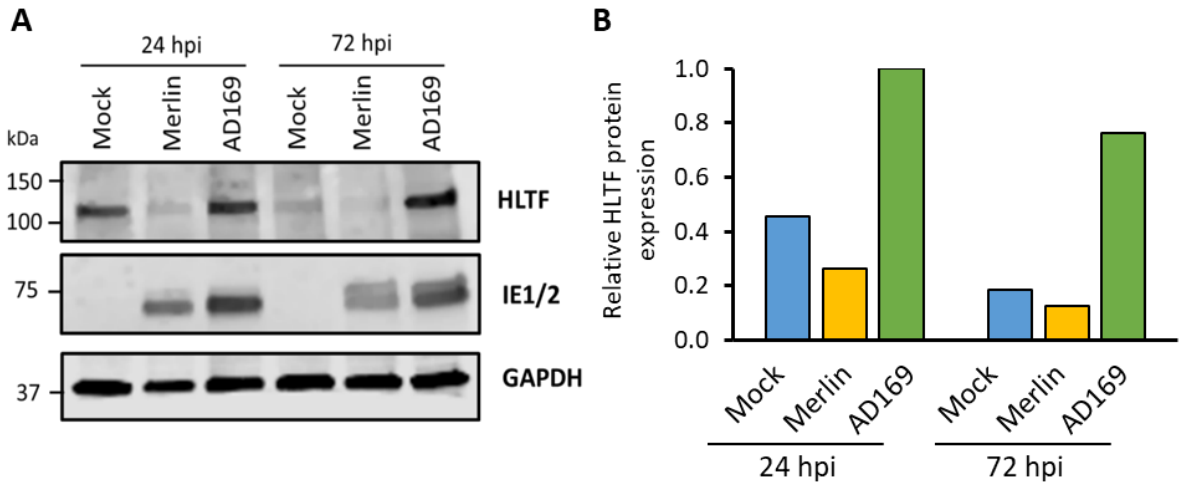

Figure 3.2. Immunoblots of Merlin- or AD169-infected HFFF-TERT.
(A) Western blot analysis of HLTF expression when HFFF-TERT were infected with Merlin or AD169 at MOI = 5 for 24 and 72 hr. E1/2 expression is HCMV infection indicator while GAPDH served as loading control. (B) Western blot signal quantification was performed by measuring the median fluorescence intensity of HLTF and normalised by that of internal control GAPDH. Relative HLTF was calculated according to the highest HLTF/GAPDH value, in this case AD169 infection at 24 hpi.

3.2.2. Single gene deletion virus

To determine which individual proteins target HLTF for degradation, a library of HCMV mutants with deletions of single canonical genes in UL/b' was generated by our collaborators at Cardiff University. Dr. Peter Tomasec infected the cells and collected the infected cells into guanidine lysis buffer. I carried out trichloroacetic acid (TCA) precipitation to concentrate the protein, and immunoblot to test the effects of single gene deletion on HLTF degradation. Only deletion of UL145 rescued expression of HLTF (Figure 3.3A). Overexpression of a C-terminally V5-tagged UL145 (UL145-V5) was sufficient to downregulate HLTF, and expression of HLTF protein was rescued by MG132. Together both experiments showed that UL145 was necessary and sufficient to down-regulate HLTF. MG132 also increased expression of UL145 protein, which suggested that UL145 was naturally degraded (Figure 3.3B). However, UL145 synthesis was more significant compared to degradation so overall UL145 protein accumulated along the infection time course (Figure 4.2 D).

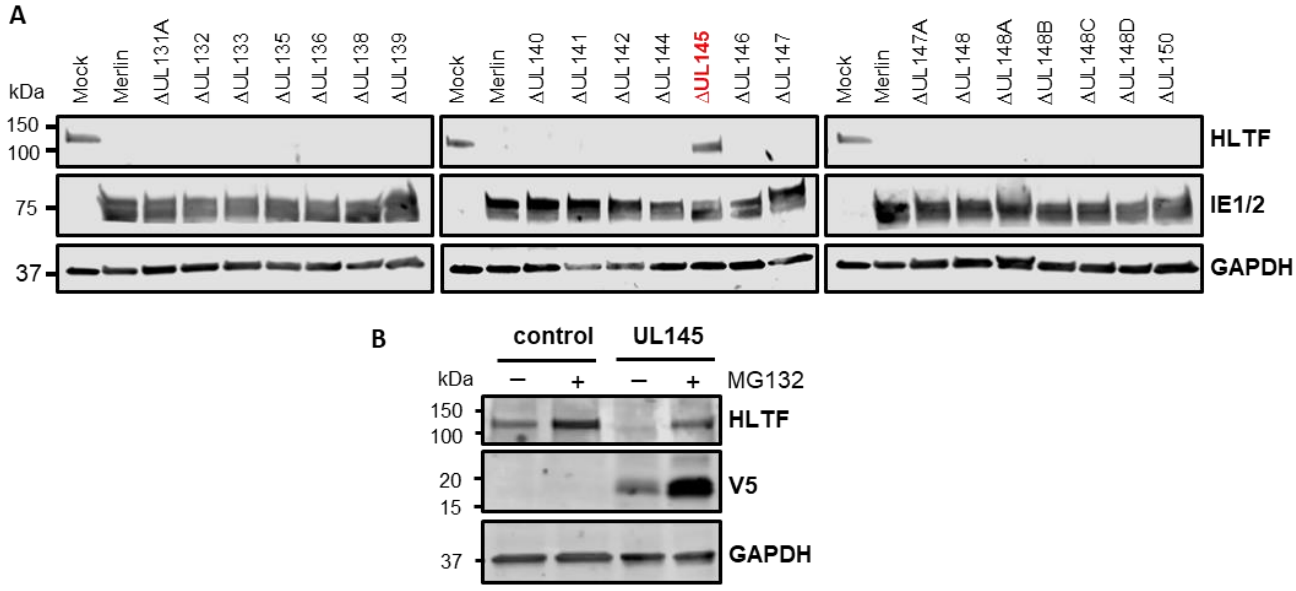

Figure 3.3. UL145 was necessary and sufficient to down-regulate HLTF.
(A) HFFF cells were infected with Merlin strain HCMV with UL/b' single gene deletion at MOI of 5 for 72 h. Cell lysates were subjected to Western blot analysis probing HLTF, IE1/2, and GAPDH. (B) HFFF-TERT cells stably overexpressing UL145 were treated with 10 µM MG132 for 12 h. Immunoblots probing HLTF, UL145-V5, and GAPDH (internal control) was carried out.

To visualise this finding using another approach, HFFF-TERT cells were infected with Merlin HCMV bearing V5 tagged to UL145 C-terminus. Cells were subjected to immunoflourescent confocal microscopy probing V5 and HLTF. As shown in Figure 3.4, cells expressing UL145 had drastically decreased HLTF expression compared to those without. UL145 was only detected in the nuclei of cells and HLTF was predominantly expressed in the nucleus. HLTF also formed perinuclear speckles in the uninfected cells (Figure 3.4).

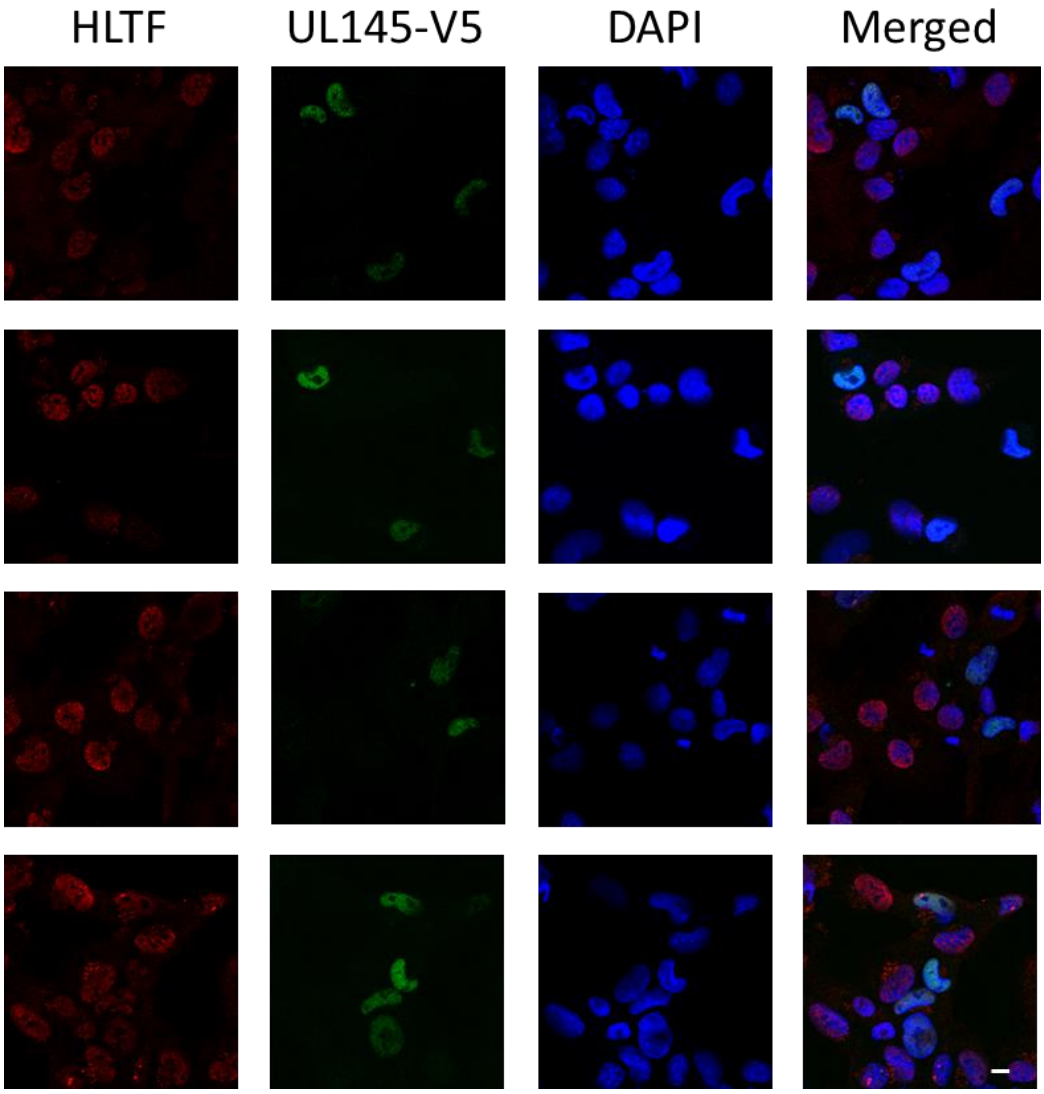

Figure 3.4. Immunofluorescent confocal microscopy analysis of HCMV infected HFFF-TERT cells.

HFFF-TERT cells were infected with recombinant Merlin strain HCMV with a C-terminal UL145 V5 tag at MOI of 0.1. Cells were harvested 24 h post infection and subjected to immunofluorescent staining probing HLTF and V5. Cell nuclei were stained with DAPI. Stained cells were observed under a confocal microscope. The scale bar in the bottom right figure is 10 µm.

3.3. UL145-induced HLTF degradation via cullin 4A E3 ligase

Since UL145 was identified as the main contributor to HLTF degradation, it was important to elucidate the mechanism of HLTF proteasomal degradation induced by UL145. Studying the degradation pathway might enable discovery of druggable targets if HLTF had antiviral functions. In summary, we found that UL145 recruited cullin 4A E3 ligase to tag HLTF with ubiquitin, which led to destruction of HLTF via the proteasome.

3.3.1. UL145 was associated with Cul4A and DDB1

To identify cellular factors interacting with UL145, I performed a SILAC immunoprecipitation in HFFF-TERT stably expressing UL145-V5 with Dr. Katie Nightingale. I labelled HFFF-TERT stably expressing UL145-V5 with “medium” SILAC medium and HFFF-TERT stably expressing Gateway vector control with “light” SILAC medium. We carried out co-immunoprecipitation experiment to immunoprecipitate UL145-V5 and its associated proteins from UL145-expressing cells using anti-V5 agarose beads. Mass spectrometry was performed by Dr. Robin Antrobus from CIMR proteomics core and proteomic data were analysed by Dr. Nightingale. Results showed that cullin 4 RING E3 ligase complex subunits such as CUL4A, DDB1 were abundantly associated with UL145 (Figure 3.5). However, HLTF was not identified in this IP.

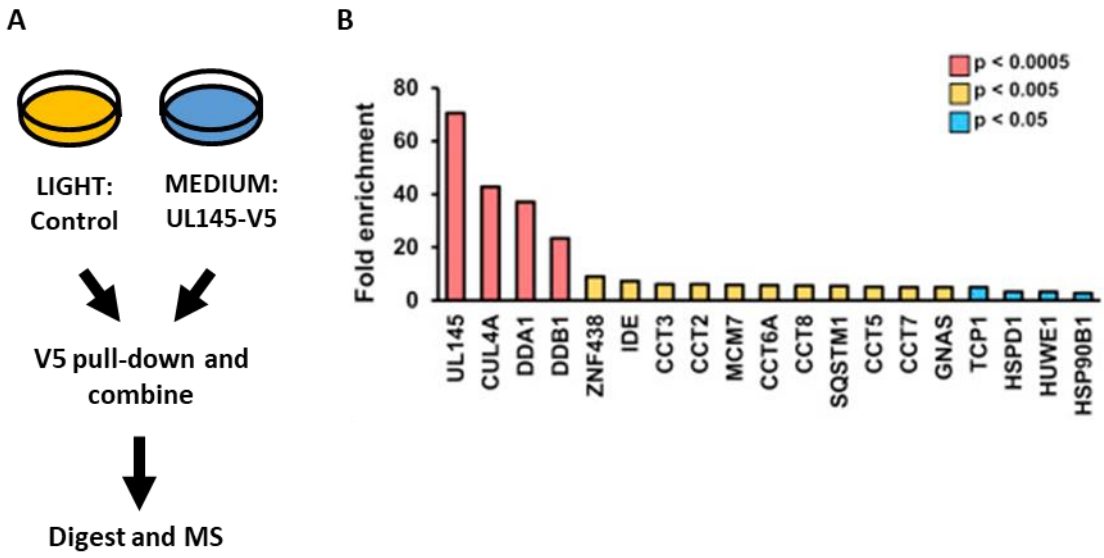

Figure 3.5. SILAC IP identified proteins associated with UL145 in HFFF-TERT cells
(A) Schematic diagram of the experimental procedure. (B) The fold enrichment of each protein immunoprecipitated with UL145-V5 is shown. P values were estimated using significance A algorithm, then corrected for Benjamini-Hochberg's multiple hypothesis testing method. Proteins enriched with $p < 0.05$ are shown in the graph.

3.3.2. UL145 might be weakly associated with HLTF

To identify proteins associated with HLTF in the presence of UL145, I attempted to overexpress HLTF and UL145 with lentiviral transduction and then immunoprecipitated HLTF. I cloned full-length HLTF with a C-terminal hemagglutinin (HA) tag into a lentiviral expression vector and transduced it into HFFF-TERT cells. After selection, cells were subjected to RT-qPCR and Western blot analysis. Transduction of HLTF resulted in more than 40 fold increase in HLTF transcripts (Figure 3.6A), however the increase in HLTF protein expression was minimal (Figure 3.6B&C). MG132 did not substantially increase HLTF protein expression compared to DMSO alone, suggesting that the failure of overexpression might have occurred at the translation level as compared to the transcriptional or post-translational levels.

I started a collaboration with Dr. Jinwoo Ahn from Department of Structural Biology at the University of Pittsburgh, whose group solved the structural interaction of how HIV1

Vpr recruits HLTF to the CRL4-DCAF1 E3 ligase (Zhou et al., 2017). Dr. Ahn advised me to express an N-terminus deletion of HLTF to minimise miss-folding of HLTF during ectopic expression of HLTF. I cloned a segment of HLTF sequence carrying 1-54 amino acid deletion (amino acids 58-174 are the HLTF DNA binding HIRAN domain, Figure 1.10A) into a lentiviral expression vector and transduced it into HFFF-TERT cells. After selection, cells were subjected to immunoblot analysis. Despite this, cells transduced with the N-terminal HLTF deletion plasmid did not express more HLTF protein (Figure 3.6 D&E).

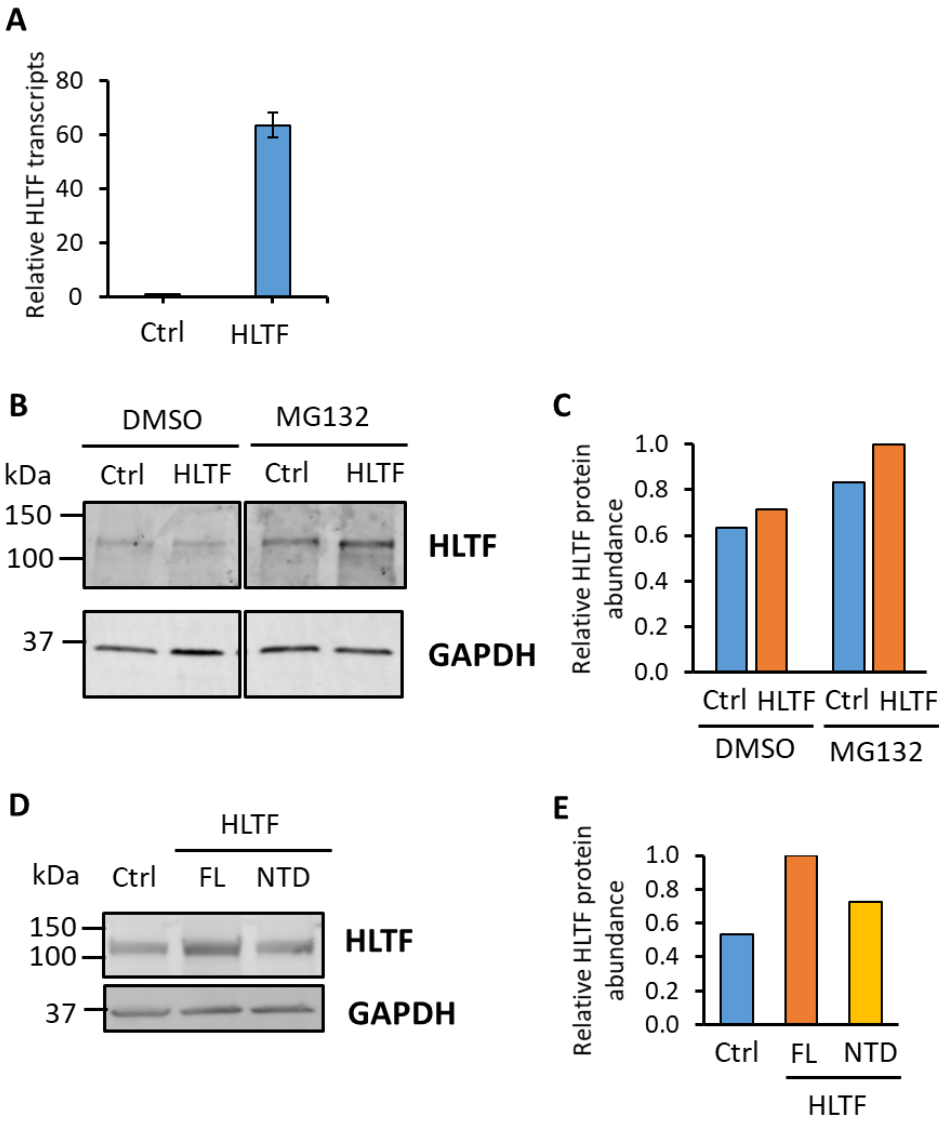

Figure 3.6. Attempts of HLTF overexpression.
(A) RT-qPCR analysis of HLTF transcripts in HFFF-TERT-HLTF cell line compared to its control (Crtl). GAPDH was used as internal control. Error bars show standard

deviation (SD) for technical duplicates. (B) HFFF-TERT-HLTF and its control were treated with 10 μM MG132 or DMSO control. Cells were harvested 12 h after treatment for Western blot analysis probing HLTF. GAPDH was used as internal control. (C) Immunoblot quantitation of median HLTF signal intensity after it was normalised to GAPDH. (D) Western blot analysis of HFFF-TERT transduced to full length (FL) or N terminus deletion (NTD) HLTF. GAPDH was used as internal loading control. (E) Relative HLTF quantification of immunoblots showed in (D). Overexpressing full-length and N-terminal deletion HLTF-HA with lentiviral transduction was attempted twice each. Representative results from 2 experiments are shown.

Overexpressing HA-tagged HLTF was not successful. In order to study the proteins associate with HLTF in the presence of UL145, I performed a SILAC IP with cells stably expressing UL145 and treated with MG132 and immunoprecipitating endogenous HLTF. MG132 treatment was in place to make sure the amount of HLTF immunoprepicitated was sufficient for analysis. HLTF and its associated proteins were immuniprecipitated from SILAC labelled cell lysates. Analysis of these proteins from HFFF-TERT cells and 293T cells was performed. Figure 3.7 revealed proteins that had higher affinity with HLTF in UL145-expressing cells compared in control cells. In 293T cells, where endogenous HLTF expression is higher (Figure 3.7D), UL145 was observed to be associated with HLTF. However, this interaction was not observed in HFFF-TERT. Furthermore, none of the proteins identified from either IP was associated with the ubiquitin conjugation system and therefore these SILAC experiments did not add to the understanding of how UL145 degrades HLTF during HCMV infection. DAVID analysis of the proteins associated with HLTF in both immunoprecipitations revealed that HLTF bound to different sets of proteins in the presence of UL145 in HFFF-TERT and 293T cells. HLTF was associated with nucleosome and ribosomal proteins in 293T cells while HLTF bound to poly(A) RNA binding proteins in HFFF-TERT cells (Table 3.1). These might either indicate subtleties of differentially expressed proteins in each cell type, or could theoretically indicate differences of HLTF protein function. However, since UL145 induces HLTF degradation and this analysis was performed with MG132 treatment, interpretation of this part of the results is more complex.

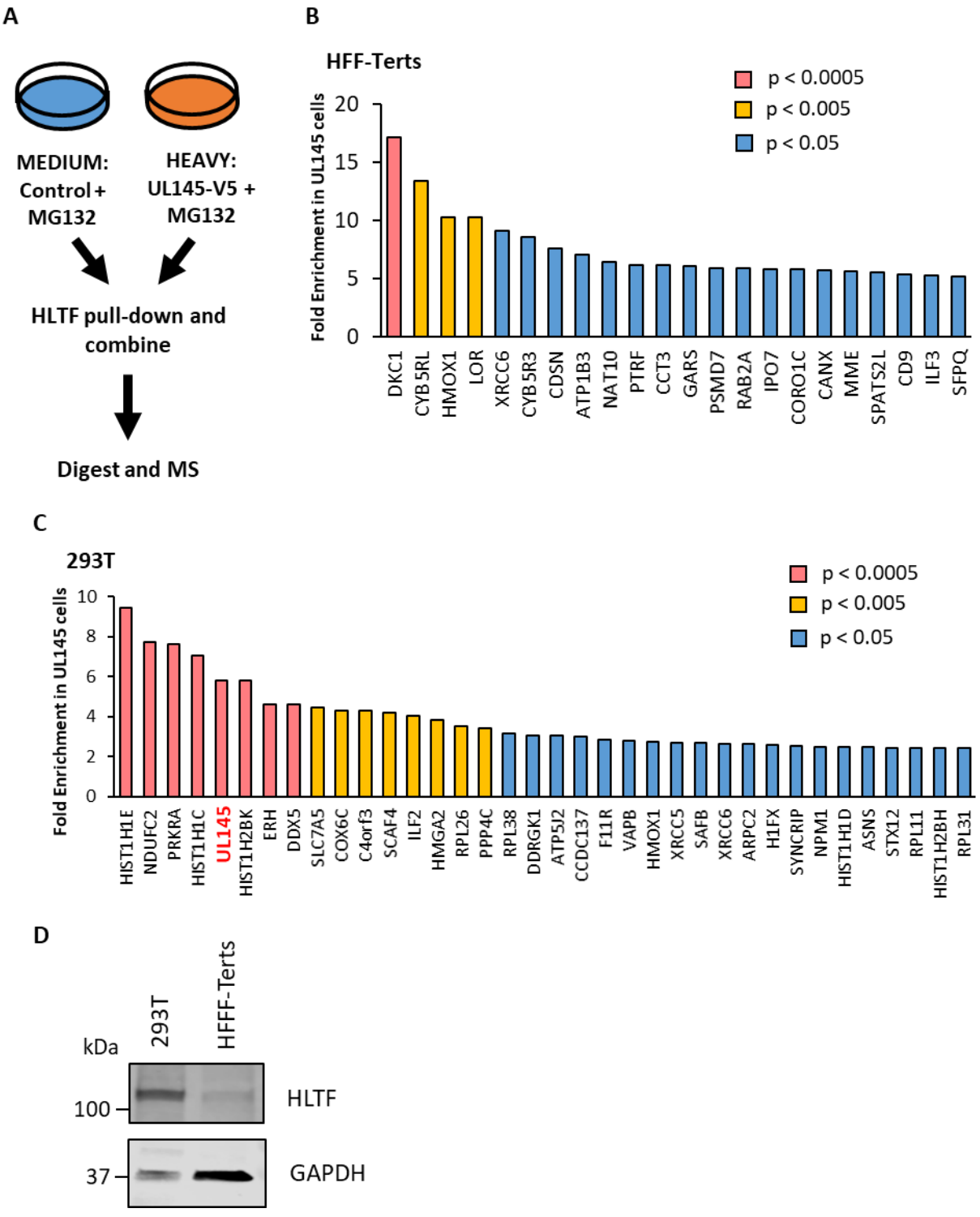

Figure 3.7. SILAC IP identified protein associated with HLTF in MG132-treated UL145 expressing HFFF-TERT and 293T cells.

(A) Schematic diagram of the experimental procedure. (B)(C) The fold enrichment of each protein immunoprecipitated with HLTF in (B) HFFF-TERT cells and (C) 293T cells is shown. P values were estimated using significance A values, then corrected for multiple hypothesis testing. Proteins enriched with $p < 0.05$ are shown in the graph. (D) Immunoblot of 293T and HFFF-TERT cell lysates probing endogenous HLTF.

Table 3.1. DAVID analysis of pathway enrichment among proteins identified by SILAC IP immunoprecipitating endogenous HLTF in MG132-treated UL145 cells. A given cluster identified in was always searched against a background of all human proteins from Uniprot database. Benjamini-Hochberg adjusted p values are shown for each pathway.

Pathway	Benjamini p value
Proteins associated with HLTF in MG132-treated UL145 expressing HFFF-TERT	
poly(A) RNA binding	0.0028
isopeptide bond	0.0051
Proteins associated with HLTF in MG132-treated UL145 expressing 293T	
nucleosome assembly	6.30E-10
chromosome	3.60E-09
cytosolic large ribosomal subunit	0.0005
5'-deoxyribose-5-phosphate lyase activity	0.0023

To attempt to further validate the direct association of HLTF and UL145 as observed in 293T SILAC IP, HLTF and its associated proteins under the influence of UL145 were immunoprecipitated from MG132 treated 293T cells stably expressing UL145 and subjected to Western blot. As shown in Figure 3.8, even though abundant HLTF protein was immunoprecipitated, UL145 was not seen to be interacting with HLTF. Conventional IP failed to detect the interaction of HLTF and UL145, which could only be detected using mass spectrometry.

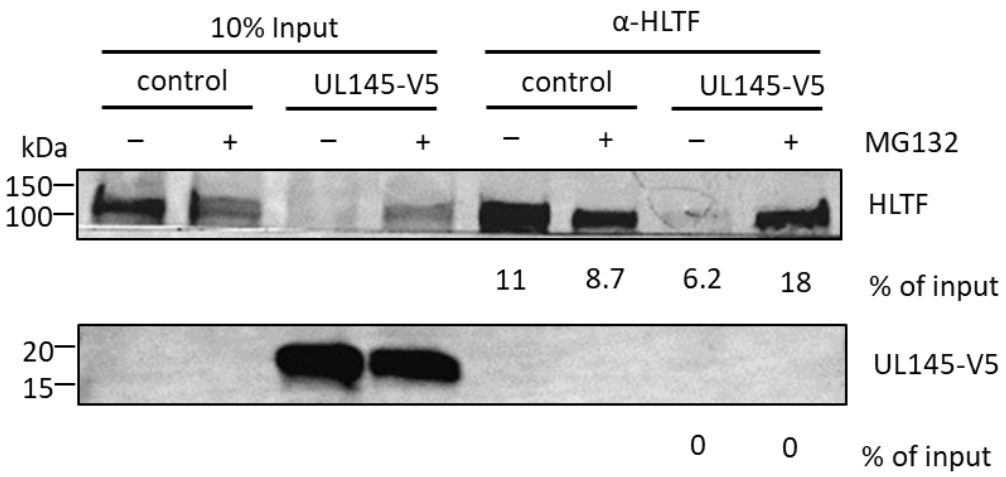

Figure 3.8. Conventional IP showed that UL145 is not strongly associated with HLTF.

293T cells stably expressing UL145 were treated with 10 μM MG132 for 12 h before lysis with RIPA buffer. HLTF and associated proteins were immunoprecipitated with anti-HLTF rabbit polyclonal antibody, and analysed with SDS-PAGE and Western blot. Percentage of input protein immunoprecipitated by anti-HLTF antibody was calculated according to the median band intensity of the corresponding 10% input.

3.3.3. CUL4A was responsible for UL145-induced HLTF degradation

Small interfering RNA (siRNA) specific for CUL4A was transfected into UL145 overexpressing 293T cells to validate the involvement of CUL4A in UL145-mediated HLTF degradation. Dr. Katie Nightingale transfected a pool of CUL4A siRNAs or a pool of non-targeting siRNAs into 293T cells overexpressing UL145-V5 or vector control and collected resulting cell lysates 48 h post transfection. I performed Western Blot analysis probing HLTF, CUL4A, and UL145-V5. As shown in Figure 3.9, knocking down CUL4A partially rescued HLTF downregulation, suggesting that UL145 directed CUL4A to target HLTF. This suggested that other mechanisms might be involved in UL145-mediated HLTF degradation.

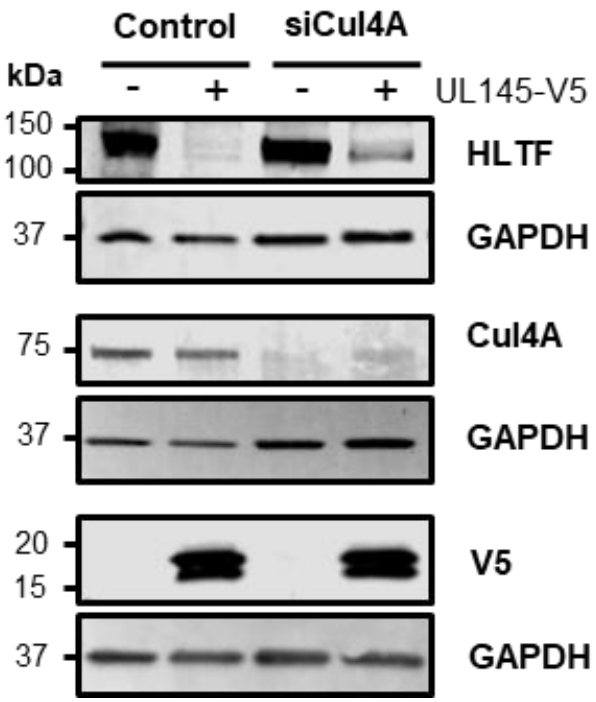

Figure 3.9. siRNA treatment of CUL4A disrupted UL145-mediated HLTF degradation.
Immunoblot showing HCMV UL145 downregulates HLTF in a CUL4A-dependent manner. 293T cells stably expressing UL145-V5 or vector control were treated with control siRNA, or siRNA against CUL4A for 48 h. Representative results from 2 experiments are shown.

3.3.4. UL145 harbours a potential DDB1 binding domain

UL145 has no homologues in murine cytomegaloviruses, but in several other primate cytomegaloviruses, homologues can be found. Alignment of amino acid sequences of these homologues revealed high degree of similarity, in a clustered order correlated to the phylogenetic order of the hosts (Figure 3.10). Professor Andrew Davison (MRC-University of Glasgow Centre for Virus Research) performed secondary structure predictions on these UL145 proteins. Four helixes were predicted to be conserved among UL145 protein from different strain of CMV, suggesting that they could be important in HLTF degradation. Structural analysis of CUL4-DDB1-DCAF E3 ligase complex revealed substrate binding receptor DCAF proteins interact with DDB1 through an α-helix, which was identified in other DDB1 interacting viral proteins such as simian virus V protein 5 (SV5) and the hepatitis B virus X protein (HBx) (Li et al., 2010). Recently,

the conserved α-helix in UL145 was found crucial for DDB1 binding (Le-Trilling et al., 2020).

Figure 3.10. Amino acid sequence alignment of UL145 homologs in primate cytomegaloviruses.
(A) Amino acid sequences of UL145 from two low passage HCMV strains (Merlin and Toledo) were clustered and compared with other primate CMV species including Panine herpesvirus 2 (also known as Chimpanzee cytomegalovirus [CCMV]), Simian cytomegalovirus (SCCMV) and Rhesus cytomegalovirus (RhCMV). Fully conserved residues are in red font. Sequence alignment was derived using Clustal Omega (B) Secondary structure predictions by Jpred 4. H, helical regions; E, extended regions.

3.4. Discussion

3.4.1. Viral exploitation of CUL4 E3 Ligase

HIV1 has been reported to reprogram the CUL4 E3 ligase complex to facilitate viral replication. HIV1 encodes an accessory protein Vpr that hijacks CRL4 E3 ubiquitin ligase complex to degrade several DNA repair proteins, such as uracil-DNA glycosylase 2 (UNG2) (Bouhamdan et al., 1996), structure-specific endonuclease MUS81 (Laguette et al., 2014), and HLTF (Hrecka et al., 2016; Lahouassa et al., 2016). Although its role in HIV1 restriction has not been fully explored, studies have shown that they are related to HIV1 genome replication (Yan et al., 2018; Yan et al., 2019). For the case of HIV-1 Vpr, the viral protein bridges the target substrate and a common CUL4 substrate receptor, DDB1 and CUL4-associated factor 1 (DCAF1). CUL4A and CUL4B are Interchangeable for HIV Vpr action through the CRL4 Complex (Sharifi et al., 2014). CUL4B could also be contributing to UL145-mediated HLTF degradation.

Other viral protein such as SV5, which induces rapid turnover of STAT1 and STAT2 (Didcock et al., 1999; Ulane and Horvath, 2002), and HBx (Leupin et al., 2005), interact with DDB1 mimicking DCAF. Structural analysis reveals that these viral proteins harbour an α-helical motif, which shares structure but not sequence homology with a α-helix found in the DCAFs (Li et al., 2010). The same helix domain is found in UL145, which might be the mechanism via which UL145 exploits the CRL4 E3 ligase complex to degrade HLTF.

3.4.2. UL145 exploitation of CUL4A E3 ligase

Here HLTF was suggested to be directed to be proteasomally degraded by UL145, but the interaction was not observed with conventional immunoprecipitation of endogenous HLTF and Western blot. A recent publication discovered that UL145 targets STAT2. UL145 directly binds to STAT2 and loads it onto CUL4 complex, serving as a bridge between STAT2 and DDB1 (Le-Trilling et al., 2020). The paper also identified a conserved helix in UL145 (Figure 3.10) resembling the DCAF helix domain that binds to DDB1 (Le-Trilling et al., 2020). My current model for UL145-induced HLTF degradation is depicted as Figure 3.11. In this model, CUL4A serves as the scaffold, DDB1 is the adaptor protein, and UL145 acts as substrate receptor that captures HLTF. RBX1 is the E3 ligase that transfer ubiquitin from E2 to HLTF. However, I lacked convincing evidence to show that UL145 was bound to HLTF during degradation. There might be mechanisms other than CRL4 that participated in HLTF degradation. For instance, deubiquitylating enzyme ubiquitin-specific protease 7 (USP7) is found responsible to HLTF protein stability in adenocarcinomic human alveolar basal epithelial A549 cells (Qing et al., 2011). There might be an undiscovered correlation between UL145 and USP7. Further discussion on this point can be found in subsection 6.3.1.

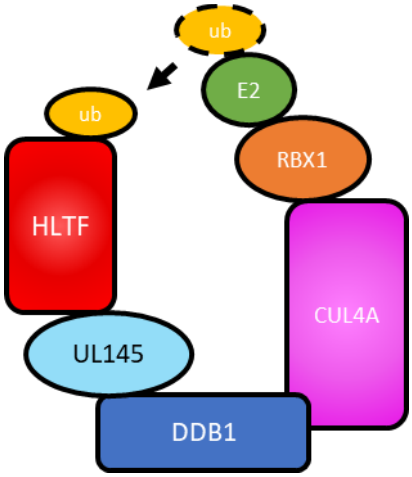

Figure 3.11.Model for UL145-mediated HLTF ubiquination.

Chapter 4. Function of HLTF during HCMV infection

Human cytomegalovirus (HCMV) has been reported to degrade host factors to create a suitable intracellular environment for replication. For example, HCMV immediate-early protein IE1 targets nuclear domain (ND10) component SP100 for degradation to antagonise acetylation of histones associated with the HCMV major IE promoter (MIEP), thus promoting viral gene transcription (Kim et al., 2011). Another HCMV immediate-early protein IE2 induces stimulator of interferon genes (STING) degradation and reduces interferon (IFN) β production (Kim et al., 2017). Helicase–like transcription factor (HLTF) was rapidly degraded by HCMV viral protein UL145, suggesting that UL145 may need to degrade HLTF to facilitate HCMV replication. One of the aims of this project was to explore the roles of HLTF during early HCMV infection. Here the function of both UL145 and HLTF in HCMV infection were investigated.

4.1. HLTF had antiviral restriction ability during early HCMV infection

To investigate how depletion of HLTF affects HCMV infection, Dr. Katie Nightingale adapted an assay previously deployed to examine the role of ND10 components in HCMV restriction (Tavalai et al., 2011) (Figure 4.1A). To identify HCMV-infected cells, Dr. Richard Stanton (Cardiff University) cloned enhanced GFP (EGFP) as a C-terminal fusion with the immediate-early gene UL36, with a self-cleaving porcine teschovirus-1 2A (P2A) peptide releasing the reporter GFP following synthesis. Immediate early protein UL36 was chosen because it was the 4th most abundantly expressed viral proteins within the first 6 h of infection, after IE1, IE2 and UL135. Dr. Richard Stanton performed a series of experiments with UL36-P2A GFP virus and found out that the insertion of GFP did not impede UL36 function to block Fas-mediated apoptosis (Nightingale et al., 2018). I generated HFFF-TERT cells stably expressing short hairpin RNA (shRNA) to knockdown HLTF (Figure 4.1B). SP100 acts to restrict HCMV infection and was selected as a positive control (Adler et al., 2011). SP100 depletion consistently enhanced HCMV UL36-GFP

expression in four independent experiments (Figure 4.1C). At low MOI, knockdown of HLTF significantly increased the efficiency of virus infection (Figure 4.1C). This effect was highly dependent on the viral dose (Figure 4.1D). At MOI of 0.1, the infection rate difference between shRNA cells and shControl cells was no longer detectable, suggesting that the antiviral activity of SP100 and HLTF was efficiently overcome (Figure 4.1D). The enhancement of HCMV infection at low MOI was confirmed using five independently derived clustered regularly interspaced short palindromic repeats (CRISPR)/Cas9 knockdown lines for both SP100 and HLTF (cell lines generated by Dr. Ben Ravenhill, Alice Fletcher-Etherington, and Lior Soday from the lab). Expression of SP100 and HLTF was substantially reduced in these cells, and HCMV infection was correspondingly significantly enhanced in these cells (Figure 4.1E&F). This suggested that HLTF might act to inhibit the efficiency of early HCMV infection at a low MOI infection, similar to that of the recognized HCMV restriction factor SP100. However, viral restriction provided by HLTF was not dose-dependent. For instance, HLTF knockout efficiency in polyclonal CRISPR/Cas9 cell line 1 was better than cell line 3, but cell line 3 was slightly more susceptible to HCMV infection compared to cell line 1 (Figure 4.1E&F).

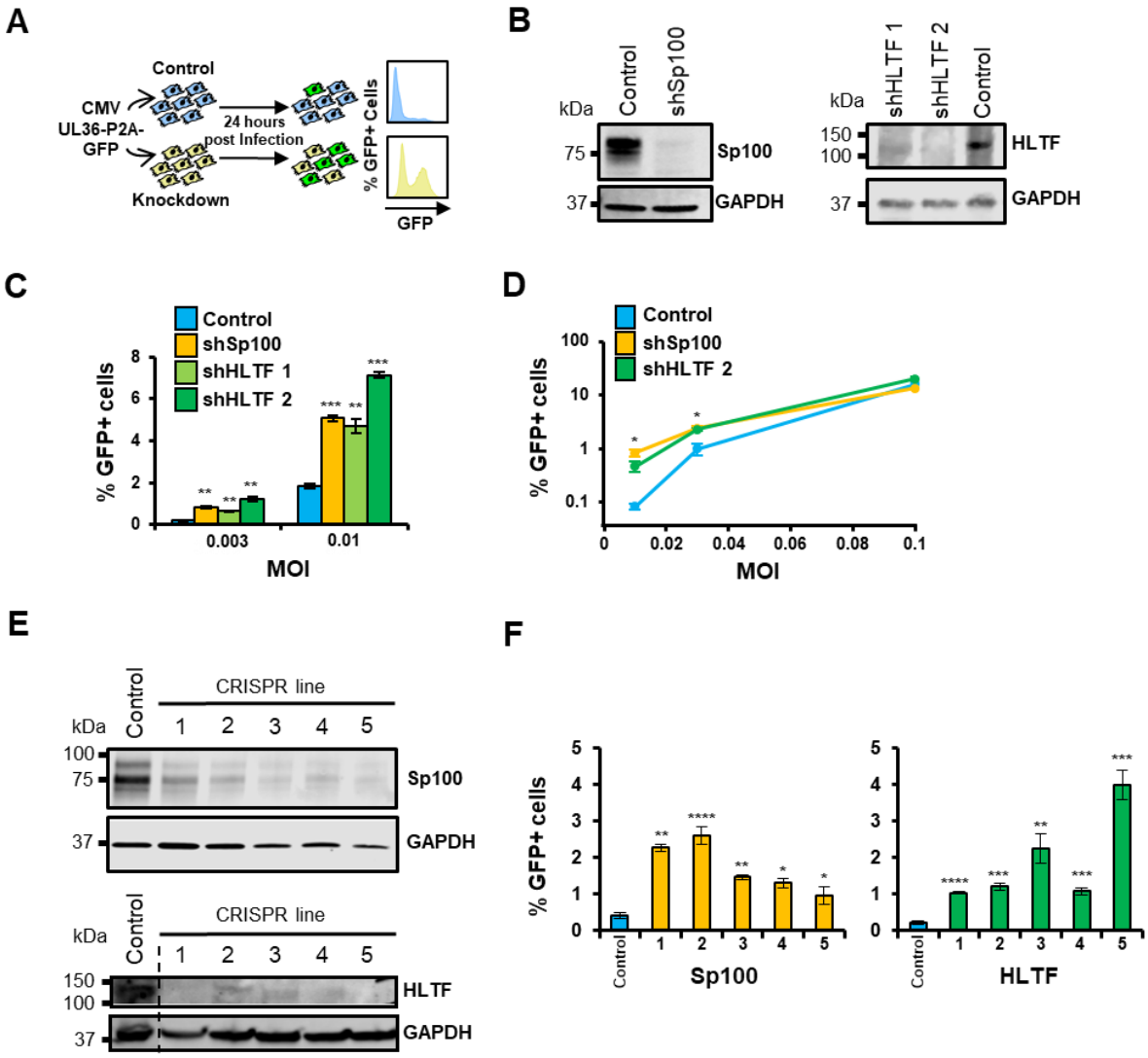

Figure 4.1. HLTF restricts early HCMV infection.

(A) Schematic of the restriction assay. shRNA or CRISPR/Cas9 was used to stably knock down HFFF-TERT for a putative restriction factor or control. Cells were infected at low MOI with UL36-P2A-GFP virus, and the percentage of GFP+ cells determined at 24 h. (B) Stable expression of shRNA targeting all Sp100 isoforms and HLTF were confirmed with immunoblot. (C) HLTF restricts early HCMV infection. Application of the restriction assay at low moi (0.003 and 0.01) to HFFF-TERT independently transduced with two different shHLTF vectors suggested that HLTF restricted infection at least as potently as Sp100. p-values were estimated using a two-tailed t-test (n=3). **p<0.005, ***p<0.0005. (D) In four independent experiments, flow cytometry was used to determine the percentage of GFP-expressing shSP100 cells in comparison to shControl cells after 24 h of infection, conducted with a range of MOI. Representative results from one experiment are shown. Values shown are mean +/- standard error of the mean (SEM). p-values for a difference between shSp100 or shHLTF and control cells were estimated using a

two-tailed t-test (n=3). *p<0.05 (for both Sp100 and HLTF where indicated). (E) Five independent polyclonal CRISPR/Cas9 Sp100 and HLTF HFFF-TERT cell lines were generated, each employing integrated gRNAs with different target sequences within a given gene. Control cells expressing non-targeting gRNAs were generated in a similar manner. (F) Infection at MOI of 0.01 identified a substantial increase in viral replication in knock-down compared to control cells. P values were estimated using a two-tailed Student's t-test (n=3). *p<0.05, **p<0.005, ***p<0.0005, ****p<0.00005.

4.2. Characterisation of UL145

HLTF was targeted by the undercharacterised viral protein UL145. It was therefore crucial to explore the function of UL145 in HCMV infection. UL145 locates in the highly variable UL/b' region. The adjacent genes UL144 and UL146 have high sequence variability and are considered genetic mutation hotspots of HCMV (Lurain et al., 1999; Sijmons et al., 2015b). Despite the physical proximity to these highly variable regions, analysis of UL145 from different clinical HCMV isolates and laboratory strains showed that UL145 is highly conserved, sharing over 95% sequence identity (Sun et al., 2007). The function of many UL/b' genes has been proposed and tested through experimentation. For example, UL144 encodes a structural homologue of tumour necrosis factor (TNF) receptor and regulates B and T lymphocyte attenuator (BTLA) (Benedict et al., 1999; Šedý et al., 2013). UL146, encodes viral C-X-C motif chemokine ligand 1 (CXCL1) that serve as neutrophil attractant and is able to induce calcium mobilization and degranulation in neutrophils (Heo et al., 2015; Lüttichau, 2010; Penfold et al., 1999). However, the function of UL145 had not been explored.

4.2.1. Temporal expression of UL145 during HCMV infection

UL145 was identified as an immediate early gene in an analysis of infection of HCMV clinical strain MOLD (Raftery et al., 2009). As for HCMV's MIEP, the promoter of UL145 gene is active without the requirement for expression of other HCMV proteins, and UL145 protein enhances MIEP activity (Raftery et al., 2009). This finding coincides with my qPCR analysis of UL145 during the first 24h of HCMV infection, in which a

considerable amount of UL145 transcript was detected at 6 hpi (Figure 4.2A). In the previous pulsed SILAC experiment, SILAC medium containing "heavy" isotopes was added upon HCMV infection, and protein synthesis could be quantified by measuring proteins labelled with these heavy isotopes (Figure 1.11B). Protein analysis with SILAC labelled HCMV infection lysate showed that these UL145 mRNA were translated into detectable UL145 protein (Figure 4.2B, performed by Dr. Katie Nightingale). TMT based proteomics analysis of a complete lytic cycle (Figure 4.2D, (Weekes et al., 2014)) and corresponding RNA sequencing of samples from the same collection (Figure 4.2C, performed by Dr. Michael Weekes and Dr. Peter Tomasec [University of Cardiff]) revealed that UL145 continued to increase throughout HCMV lytic progression.

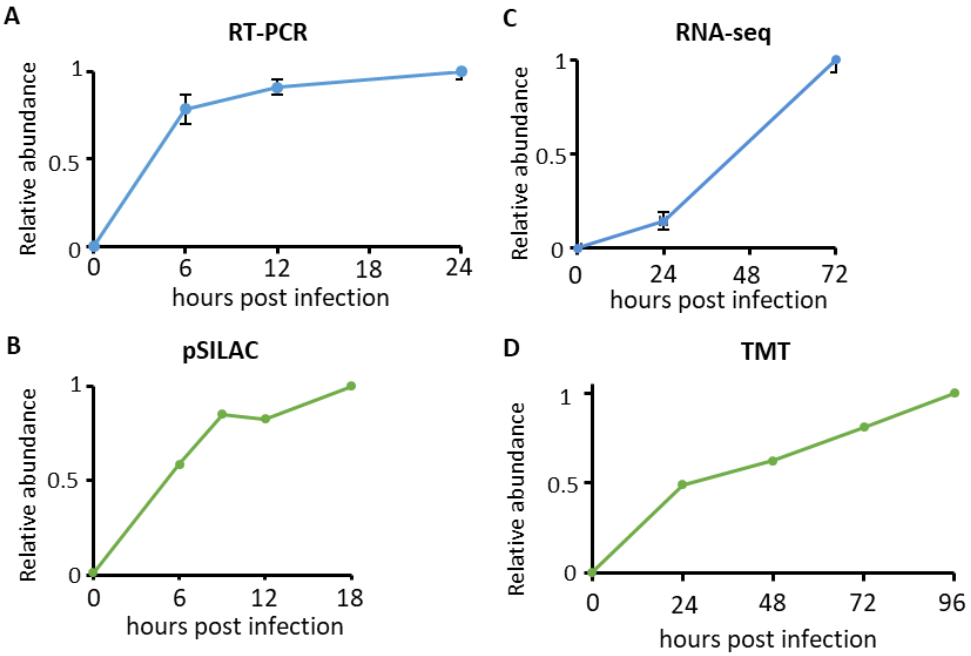

Figure 4.2. Temporal expression of UL145 during HCMV infection.
(A) HFFF-TERT cells were infected with Merlin strain HCMV at MOI of 1 for indicated time interval and then subjected to RT-PCR. Error bars show SEM for technical quadruplicates. (B) SILAC label revealed viral protein UL145 synthesis with in the first 18 hours of HCMV infection (MOI=5) in HFFF-TERT. (C) (D) HFFF cells were infected with Merlin strain HCMV at MOI of 10 and harvested at indicated time points for (C) RNA-sequencing and (D) TMT-based proteomics analysis.

4.2.2. Global proteome analysis of UL145 deletion virus

In order to understand the function of UL145 in HCMV infection, in an initial experiment, Dr. Katie Nightingale compared the protein changes in wild-type and ΔUL145 HCMV infections via proteomic analysis (Figure 4.3) with infection lysates produced by Dr. Peter Tomasac (University of Cardiff). HFFF cells were infected with Merlin strain WT or ΔUL145 HCMV at MOI of 10 for 72 h, and ratios comparing protein abundance during wild-type and ΔUL145 HCMV infection were calculated to monitor proteins changes related to UL145 deletion. As expected, UL145 deletion "rescued" HLTF down-regulation. Besides HLTF, deletion of the UL145 gene rescued expression of another DNA repair protein, the tumour protein p53 binding protein 1 (TP53BP1) (Callen et al., 2013), suggesting that UL145 may have wider roles in modulating the DNA-damage response. Notably, this data suggested that UL145 modulated expression of several interferon-inducible proteins, including SP100, viral RNA sensor 2'-5'-oligoadenylate synthetase OAS2 and OAS3, and GTP-binding protein MX2. IFN signalling mediated STAT2 and HIV-1 restriction factor SAM and HD domain containing deoxynucleoside triphosphate triphosphohydrolase 1 (SAMHD1) (Laguette et al., 2011) were also rescued by UL145 deletion, suggesting that UL145 may be important for antiviral activities.

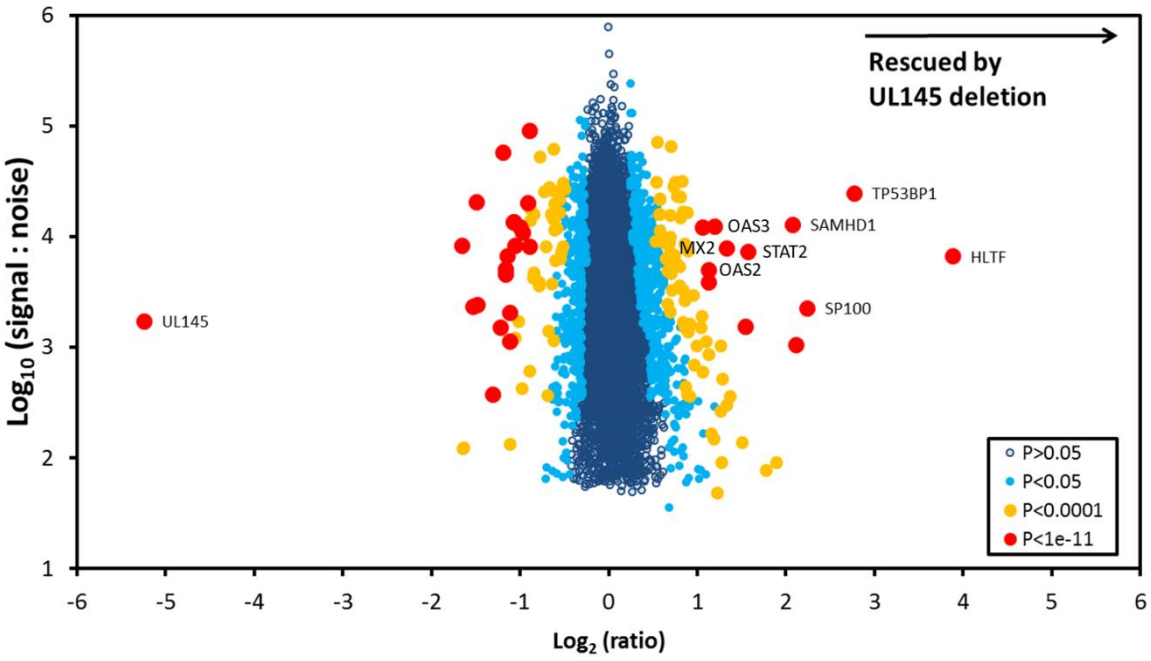

Figure 4.3. Protein expression fold change induced by UL145 deletion.
HFFF cells were infected with Merlin strain WT and ΔUL145 HCMV at MOI of 10 for 72 h. The x-axis represents the fold change of protein expression in ΔUL145 virus infection compared to wild-type Merlin infection in log 2 scale. The y-axis represents the intensity of the protein detected, which is the average of signal to noise, in log 10 scale. The colour of the dots represents the significance B of the fold change (Benjamini-Hochberg-corrected p-value). Proteins that were rescued by UL145 deletion are shown on the right side of the graph.

4.2.3. Proteomic analysis on UL145 effects of HCMV lytic progression

From this initial data, I performed a follow up analysis on how UL145 deletion affected HCMV proteins. Viral protein expression in ΔUL145 infection was compared to wild-type Merlin infection to calculate fold change. As shown in Figure 4.4, all of the viral proteins identified to have significant decreased when UL145 was deleted were Tp5 proteins (subsection 1.1.7), suggesting that the role of UL145 might be to inhibit the expression of true late genes. HLTF is part of the post-replication DNA repair machinery and the protein most substantially “rescued” upon infection with UL145 deletion virus compared to Merlin strain WT HCMV. It is possible that HLTF affects viral DNA replication and thus regulates true late viral gene expression.

The proposed functions of viral proteins that were down-regulated more than 2 fold in UL145 deletion is summarised in Table 4.1. UL145 expression modulated expression of virion structural proteins and viral factors that are associated with capsid trafficking and envelopment. Therefore, it could be inferred that UL145 might regulate the expression of these late genes and may therefore influence viral progeny production.

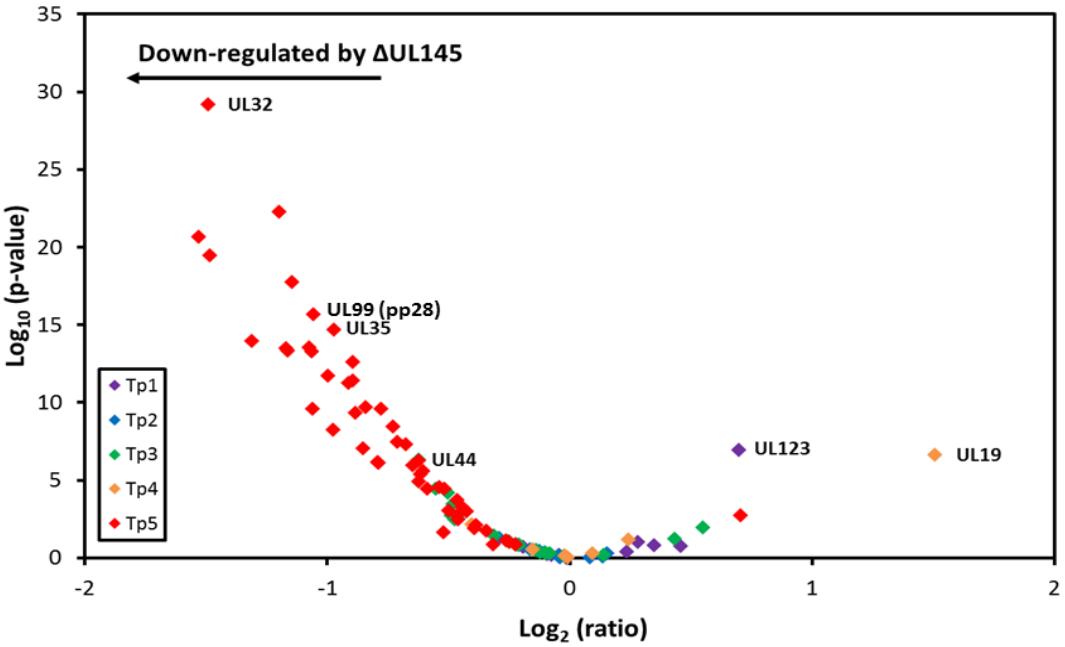

Figure 4.4. Volcano plot of Tp-classfied viral protein fold change and its fold change significance in ΔUL145 virus infection.
The x-axis represents the fold change of viral protein expression in ΔUL145 virus infection compared to wild-type Merlin infection in Log 2 scale. The y-axis represents the significance of the fold change (p-value) in log 10 scale. The colour of each dot indicates the Tp class of viral proteins.

Table 4.1. Viral proteins that were down-regulated due to UL145 deletion.
The name, Tp class, Tr class (classifications from (Weekes et al., 2014)), and the proposed function (derived from (Mocarski et al., 2013)) of viral proteins that were down-regulated by more than 2 fold.

Viral Protein	Tp Class	Tr Class	Proposed Function
UL53	Tp5	Tr5	Nuclear egress
UL32	Tp5	Tr5	Nucleocapsid-proximal stabilization protein
UL33	Tp5	Tr5	Virion envelope
UL147	Tp5	Tr5	Putative chemokine
UL83	Tp5	Tr5	Major tegument; suppresses interferon response
UL46	Tp5	Tr5	Capsid triplex component 1; interacts with UL85
UL100	Tp5	Tr5	8-transmembrane ptoein; virion envelope gp; role in envelopment
UL74	Tp5	Tr5	Virion envelope gP; delivery and release of virions
UL85	Tp5	Tr5	Capsid triplex component 2; interacts with TRI1/UL46
UL94	Tp5	Tr5	Tegument, Secondary envelopment in association with pp28
UL99	Tp5	Tr5	Myristylated tegument for secondary envelopment

4.2.4. HCMV titration in HLTF CRISPR cell lines

The foundation for comparative studies between WT and ΔUL145 was virus titration. The two viruses had to be titred together and further experiments were performed with this information to ensure that comparable amounts of infectious virions were added to WT and ΔUL145 infections. In the previous restriction assay, depletion of HLTF resulted in increased HCMV infection (Figure 4.1). On the other hand, ΔUL145 failed to degrade HLTF as WT HCMV did (Figure 3.3). I suspected that the endogenous HLTF that ΔUL145

HCMV failed to degrade might lead to underestimation of ΔUL145 virus titre in WT HFFF-TERT infection. Therefore, titrations of two separate batches of WT and ΔUL145 HCMV were performed in WT and monoclonal HLTF CRISPR knock-out HFFF-TERT cells.

If HLTF affected ΔUL145 titration, I should observe lower titre ratio comparing WT to ΔUL145 (WT/ΔUL145). However, titre ratios generated in different cells were similar in two biological duplicates (Table 4.2). Results from both batches revealed that titration in monoclonal HLTF CRISPR knock-out HFFF-TERT cells was not substantially different from titration in WT HFFF-TERT cells. Therefore, titration results using WT HFFF-TERT cells were used in experiments and further WT and ΔUL145 HCMV titration was performed only in WT HFFF-TERT cells.

Table 4.2. HCMV titration in WT and HLTF CRISPR cell lines
Two batches of Merlin strain WT and ΔUL145 HCMV containing UL36-P2A-GFP were titred in in WT and monoclonal HLTF CRISPR knock-out HFFF-TERT cells with methods described in subsection 2.3.4. Results and the titre ratio of WT/ΔUL145 in the same type of cells are listed here.

Batch 1			
Virus titre (PFU/ml)	WT	ΔUL145	Titre ratio WT/ΔUL145
Titration in WT HFFF-TERT	2.14×10^7	1.15×10^7	1.86
Titration in HLTF CRISPR HFFF-TERT (1B1)	1.73×10^7	7.52×10^6	2.30
Batch 2			
Virus titre (PFU/ml)	WT	ΔUL145	Titre ratio WT/ΔUL145
Titration in WT HFFF-TERT	1.99×10^7	6×10^7	0.332
Titration in HLTF CRISPR HFFF-TERT (5B1)	1.68×10^7	5.1×10^7	0.329

4.2.5. UL145 and HCMV replication

The decrease of late HCMV proteins in UL145 deletion hinted that UL145 might impair virus replication, especially at later stage of virion packaging since many viral structural

proteins were affected. The infectivity of ΔUL145 in comparison with WT HCMV was analysed with growth curve analysis. HFFF-TERT cells were infected with GFP-encoded ΔUL145 or its WT control at MOI of 1. Supernatant were collected at multiple time points and the virus concentration of each collection was measured altogether by infecting HFFF-TERT cells in 24-well plates and FACS determination of infected GFP positive cells (Figure 4.5A).

Four independent experiments were carried out, with biological duplicates (A and B) being set up each time. Infectious particles were detected 3 days post infection. As shown in Figure 4.5B results were not consistent. In 6/8 (75%) times, ΔUL145 produced fewer infectious particles at the first measured time point after the completion of a lytic cycle (day 4 in the first experiment [top left], and day 5 in the other three). This low virion production of the first lytic cycle was also observed with WT HCMV, but only 1/8 (12.5%, third experiment [bottom left]). However, at day 7 or 8 post infection, all ΔUL145 infections produced as many infectious particles as WT infections. This suggested that UL145 was not an essential viral gene in HCMV replication and UL145 might possibly affect the first cycle of viral replication, although the effect was not evident after a day or two.

I took a number of steps to make sure I had infected cells with comparable titres of WT and ΔUL145 viruses. After the first growth curve experiment, I thought that the effect of UL145 deletion on HCMV replication might be subtle and it was crucial to have similar amount of virions for the infections. Even though the viruses used in the experiment had been titred at least twice, separate flasks of cells were generated for parallel infection and harvested on day 2 post infection starting from experiment 2. In experiment 3 and 4, a proportion of the infection mix was saved and stored with the supernatant collections and titred together. There were always less than 12% difference on the input virion, which did not change my interpretation of the results.

A

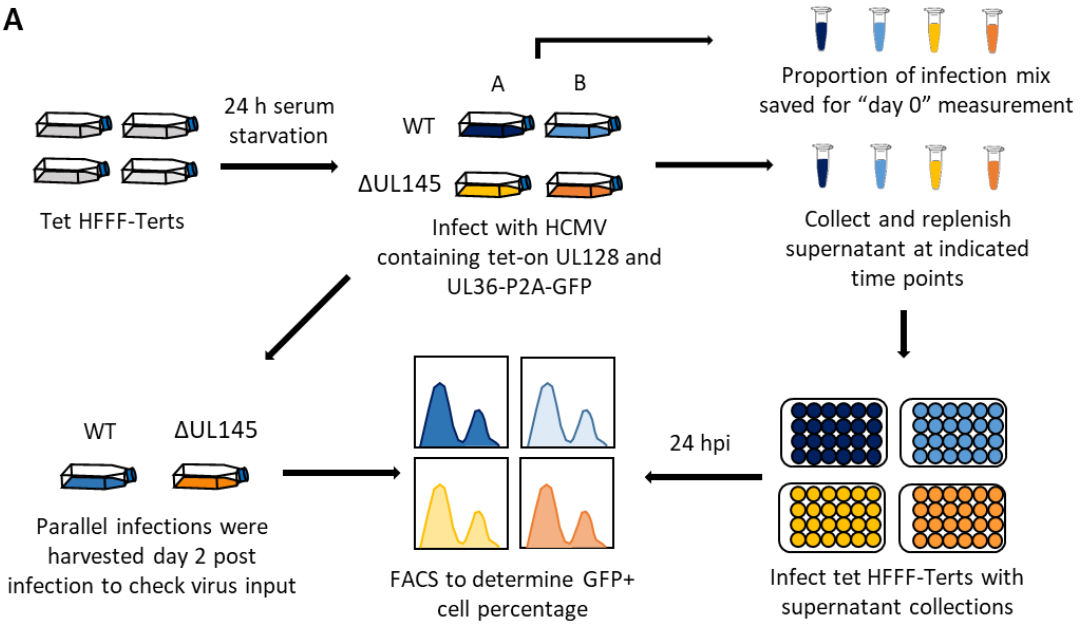

B

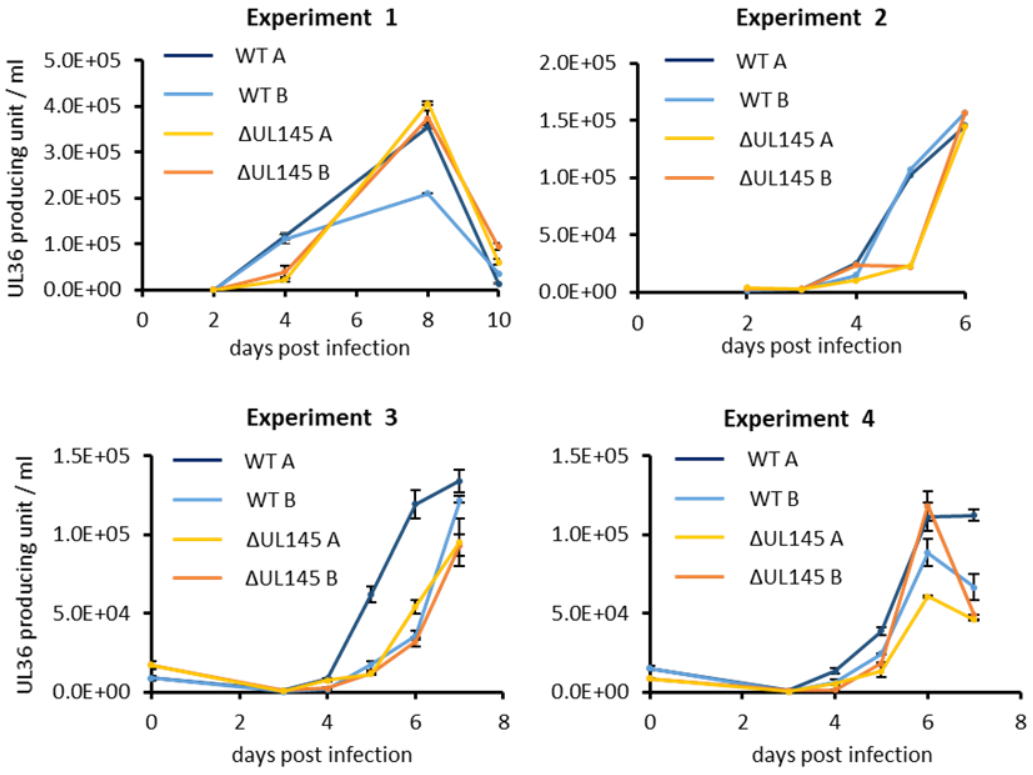

C

Percentage of infection	WT	ΔUL145
Experiment 2	21.0%	32.6%
Experiment 3	45.5%	34.0%
Experiment 4	37.0%	37.6%

Figure 4.5. Growth curve analysis of ΔUL145 HCMV compared to WT.
(A) Schematic of the growth curve assay. HFFF-TERT cells stably expressing tetracycline (tet) were incubated with serum-free DMEM for 24 h to induce a reversible cell cycle arrest prior to infection with HCMV-GFP at MOI of 1. The Merlin strain viruses encoded tet-regulated (tet-on) UL128 and UL36-P2A-GFP. Supernatants from the infected cells were collected and replenished at indicated time points. Virus titration of the supernatant and the viral mix was performed in 24-well plates seeded with HFFF-TERT-tet cells. Percentage of GFP positive cells reflected the percentage of infected cells which was used to calculate virus titre. (B) Results of four independent growth curve analysis are shown here, each analysis was performed in biological duplicate. In the latter two analyses (experiments 3&4), a portion of infection mix was stored and titred together with the supernatant collections to show that the amount of input viruses was comparable. Error bars show SD for technical duplicates in virus titration. In the second experiment (experiment 2), technical duplicates were not included and therefore no error bar is shown. (C) Percentages of GFP positive cells were measure in parallel at day 2 post infection for experiments 2, 3&4.

4.2.6. Viral DNA replication

The preliminary proteomics analysis of ΔUL145 HCMV suggested that UL145 downregulated two post DNA replication repair proteins, HLTF and TP53BP1. It was therefore possible that UL145 had an important modulatory role in viral DNA replication. To test this, HFFF-TERT cells were infected with ΔUL145 and its WT control at two different MOIs and HCMV DNA copy number was measured. The amount of HCMV gB in DNA samples was compared with a HCMV BACmid to calculate viral DNA copy number using SYBR green qPCR. I validated my assay by performing a serial dilution of BACmid to test HCMV gB primers over a range of dilutions. This method can accurately detect copy numbers within the range of 10-10,000,000 (Figure 4.6A). As shown in Figure 4.6 B&C, viral DNA of ΔUL145 replicated at a rate not substantially different from WT, producing three times more viral DNA at 3 days post infection. This result implied that the potential, albeit inconsistently observed regression in virus production in the first lytic cycle observed in ΔUL145 was not caused by a defect in viral DNA replication. Interestingly, after 36 hpi, DNA replication rates seemed to be comparable between the two viruses, as the DNA replication curves were nearly parallel at both MOIs, suggesting UL145 functioned before 36 hpi.

A further experiment with shHLTF HFFF-TERT cell lines and ΔUL145 HCMV revealed that genome replication of ΔUL145 was not affected by HLTF. Knocking down HLTF with shRNA did not have unidirectional effect on ΔUL145 DNA replication. shHLTF2-expression cells exhibited improved knockdown efficiency compared to shHLTF1 cells (Figure 4.1B) and facilitated ΔUL145 genome replication, while ΔUL145 produced less viral DNA in shHLTF1 compared to both control cells (Figure 4.7).

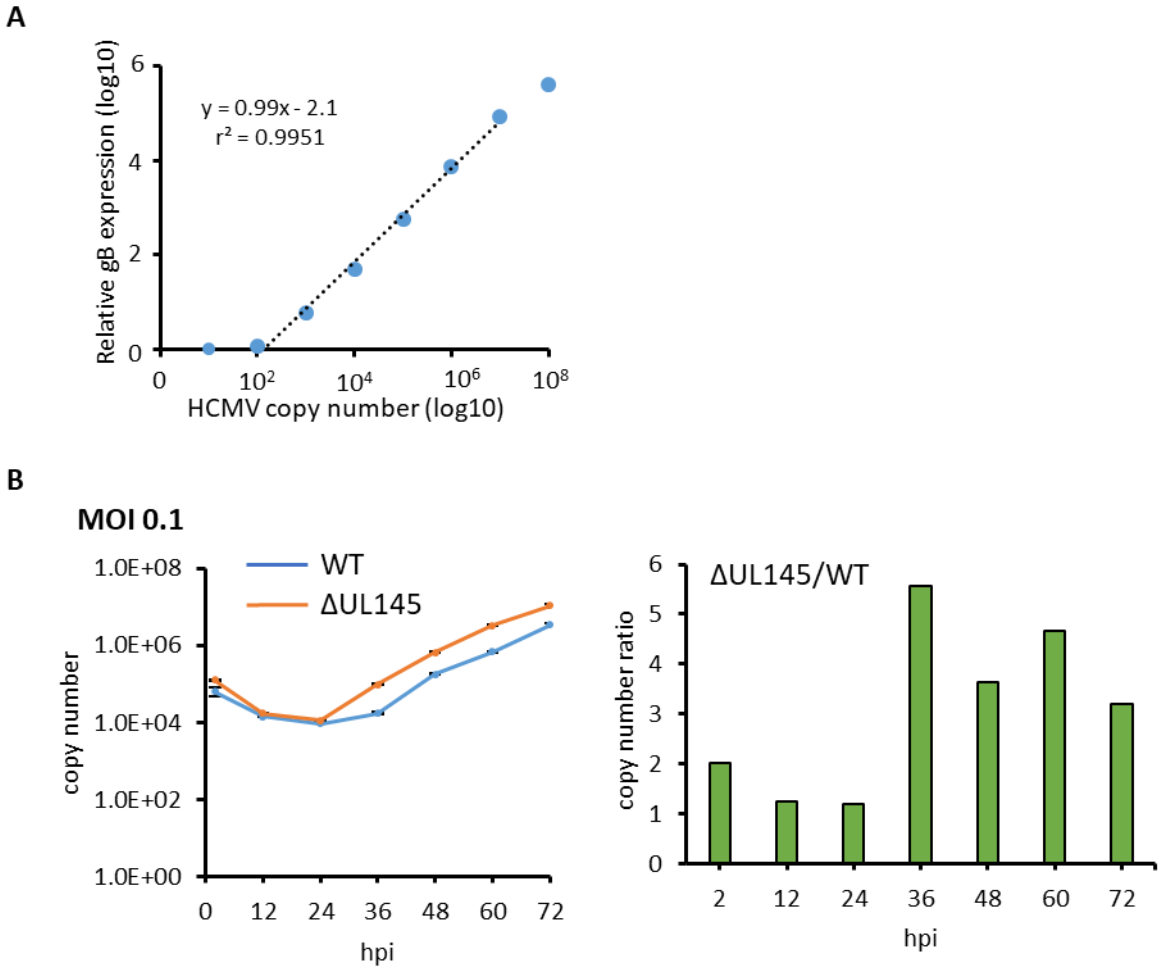

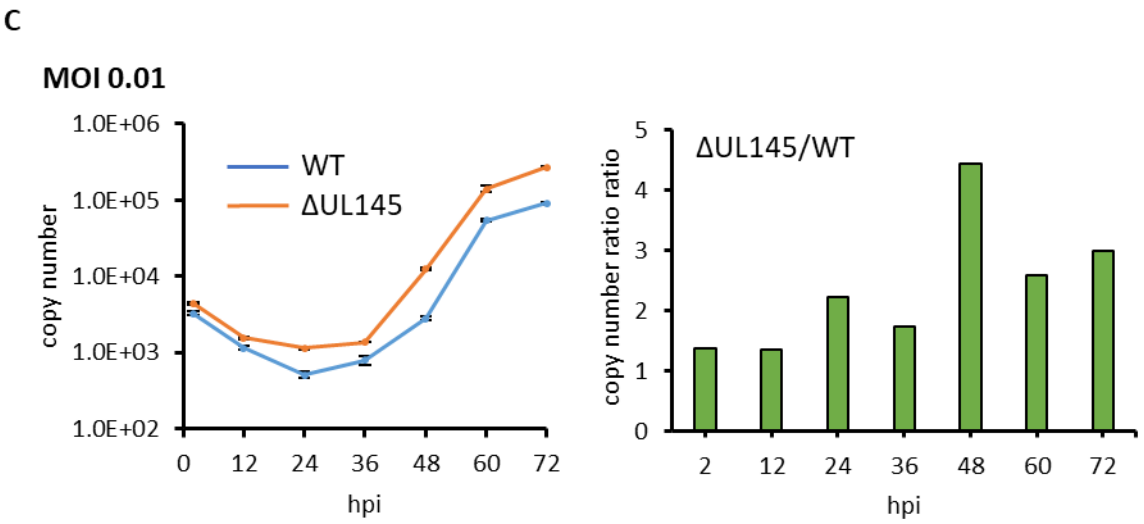

Figure 4.6. Viral DNA replication assay suggested that the rate of replication of ΔUL145 HCMV and WT viral DNA was similar.
(A) HCMV BACmid was serially diluted by 10 fold according to its copy number. The conversion from DNA concentration to HCMV copy number was calculated using an online calculator to determine the number of copies of a template (http://cels.uri.edu/gsc/cndna.html) with the BACmid size (243,724bp). The relative gB expression, in Log 10 scale, was normalized with the lowest gB expression (10 copies of HCMV). (B&C) HFFF-TERT cells were infected with WT and ΔUL145 HCMV (Merlin non-GFP viruses) at MOI of (B) 0.1 and (C) 0.01. Total DNA of infected cells was extracted and HCMV gB DNA fragments in each sample collection were measured with SYBR green qPCR. Genomic GAPDH was used as internal loading control for qPCR. HCMV copy number was calculated with HCMV BACmid as standard. Viral DNA replication curve is shown in log 10 scale on the left and the viral DNA ratio between ΔUL145 and WT is shown on the right. Error bars show SEM for technical triplicates.

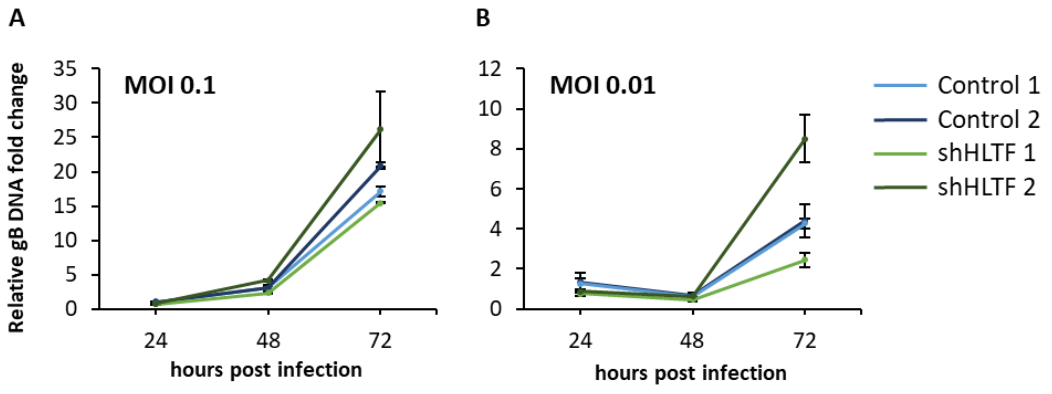

Figure 4.7. Viral DNA replication assay of ΔUL145 in shHLTF cells.
HFFF-TERT cells stably expressing shRNA targeting HLTF were infected WT with and ΔUL145 HCMV (Merlin non-GFP viruses) at MOI of (A) 0.1 and (B) 0.01. Total

DNA of infected cells was extracted and HCMV gB DNA fragments in each sample collection were measured with SYBR green qPCR. Genomic GAPDH was used as internal loading control for qPCR. Fold change were calculated against ΔCt value of control 1 at 24 hpi. Error bars show SD for biological duplicates of infection.

Overall, UL145 is expressed during the earliest phases of HCMV infection. Deletion of UL145 did not substantially affect HCMV viral DNA replication, suggesting that restriction by HLTF might occur at a different level. Further work including repeats of the experiments shown in Figure 4.6 and Figure 4.7 is required to validate these conclusions.

4.3. Interferon regulation by UL145 and HLTF

Several interferon inducible proteins, such as SP100, OAS2, OAS3, MX2, were rescued by UL145 deletion (Figure 4.3), suggesting UL145 might decrease interferon production during HCMV infection. It is possible that UL145 degraded HLTF to attenuate type I interferon production and promoted viral infection as seen in the previous restriction assay with HLTF knockdown and knockout cells Figure 4.1. To test this hypothesis, the ability of ΔUL145 to induce IFNβ was explored compared to WT HCMV, and the involvement of HLTF was investigated with HLTF knockdown or knockout cell lines. This part of the project is still ongoing and will need more work as discussed in the later section of this chapter and chapter 6.

4.3.1. Kinetics of IFNβ induction during HCMV infection

The type I IFN response to HCMV infection is complicated, with various mechanisms triggering IFNβ transcription. In particular, TLR2 and CD14 detect viral glycoprotein gB and gH (Boehme et al., 2006; Compton et al., 2003); cGAS, TLR9, IFI16, and ZBP1 detect viral dsDNA (DeFilippis et al., 2010; Li et al., 2013a; Paijo et al., 2016). On the other hand, there are multiple counteractions deployed by the virus to subvert IFNβ activation. HCMV tegument protein UL83 (pp65) exerts multifaceted regulation on IFNβ. Both IRF3 and NFκB, two main effectors of IFNβ transcription, has been reported to be targeted

by UL83 (Abate et al., 2004; Browne and Shenk, 2003). Moreover, UL83 binds to IFI16 and cGAS, and directly supresses their detection of HCMV DNA (Biolatti et al., 2018; Li et al., 2013a). Another tegument protein, UL82 (pp71), negatively affects IFNβ induction by disrupting STING translocalisation, an essential step for IRF3 activation (Fu et al., 2017). STING is affected by glycoprotein US9 as well, inhibiting IRF3-medicated IFNβ activation (Choi et al., 2018). In addition, IE2 is considered the master suppressor of IFNβ induction. It has been shown to keep NFκB from binding to the IFN-β promoter 16378994, and direct STING to proteosomal degradation (Kim et al., 2017).

Using Merlin WT GFP virus, I found that IFNβ transcription was found being induced at early time points of infection, and then dampened at later time points (Figure 4.8A). The drop of IFNβ protein production experienced a delay compared to transcripts (Figure 4.2B). At 24 hpi, IFNβ protein remained high when transcription activity had already fallen. Two reasons may contribute to this. First and mostly, IFNβ protein has much longer half-life of 16 h (Harari et al., 2015), in respect to a shorter half-life of 4 h observed with IFNβ mRNA (Abe et al., 2012). Secondly, the rate HFFF cells taking up IFNβ protein may also affect the amount of available for ELISA measurement.

In different experiments, I detected peak IFNβ transcription at different time points. A more rapid peak IFNβ response was observed in the experiments shown in Figure 4.9 and Figure 4.13, with induction already dampened by 12 hpi. Therefore, it is crucial to consider the time of sample harvest when analysing IFNβ induction during HCMV infection carefully. In a single experiment, infection with AD169 strain HCMV, the observed increase in IFNβ mRNA was more substantial that observed with Merlin strain HCMV (Figure 4.9 compared to Figure 4.8). More biological replicates should be included in order to fully characterise how IFNβ mRNA and protein are regulated during HCMV infection, with different strains. However, this optimisation experiments were performed as a result of less-than-convincing data resulting from other IFNβ experiments, which might be one of the reasons I have not yet generated convincing and reproducible results to explain how UL145 and HLTF regulate IFNβ induction.

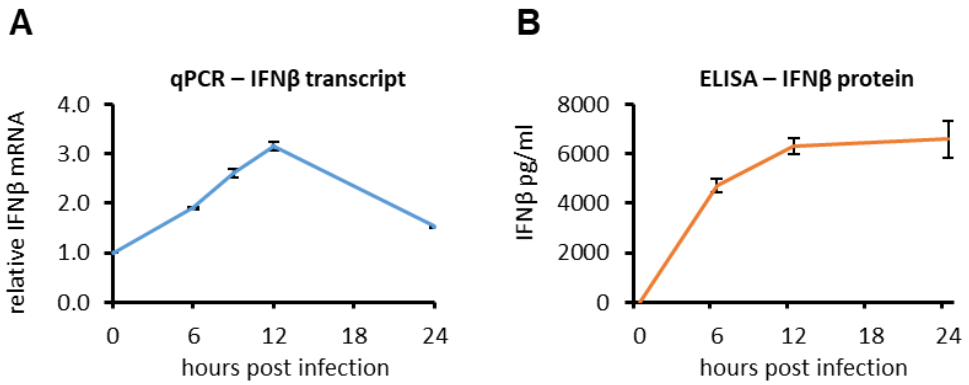

Figure 4.8. IFNβ induction time dependent kinetics during HCMV lytic cycle.
HFFF-TERT cells were infected with Merlin WT HCMV-GFP (Merlin with tet-on UL128) at MOI of 1. (A) Infected cells were collected at multiple time points as indicated, and subjected to RT-qPCR (Taqman) probing IFNβ using GAPDH as internal control. Fold change was calculated setting time 0 collection as 1. Error bars show SEM of technical triplicates. (B) In a separate experiment, supernatant of infected cells were collected and processed with IFNβ ELISA measurement. Measurement of time 0 was presumed as null. Error bars show SD of technical duplicates.

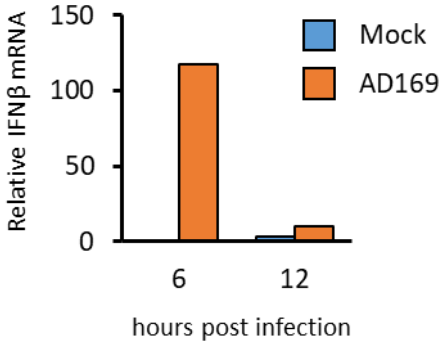

Figure 4.9. IFNβ transcriptional induction by AD169 at 6 and 12 hpi.
HFFF-TERT cells were infected with AD169 strain HCMV-GFP at MOI of 5 for 6 and 12 hours. RT-qPCR (Taqman) probing IFNβ using GAPDH as internal control was performed setting mRNA abundance of mock infection at 6 hpi as 1.

4.3.2. UL145 may modulate IFNβ induction

HFFF-TERT cells were infected with WT and ΔUL145 HCMV-GFP viruses at two different MOIs. Supernatants from infected cells were harvested at 24 hpi and IFNβ concentration was measured by ELISA. Infection at a higher MOI triggered greater IFNβ production

during infection by both viruses. However, ΔUL145 did not induce significantly more IFNβ production compared to WT (Figure 4.10A). In a separate experiment, supernatant and cell lysates were collected at the same time 24 hpi. RT-qPCR showed that ΔUL145 induced significantly more IFNβ transcripts, however, this increase was not translated into more IFNβ protein (Figure 4.10B). This may suggest that ΔUL145 did not constitutively induce more IFNβ in the first 24 hour of infection.

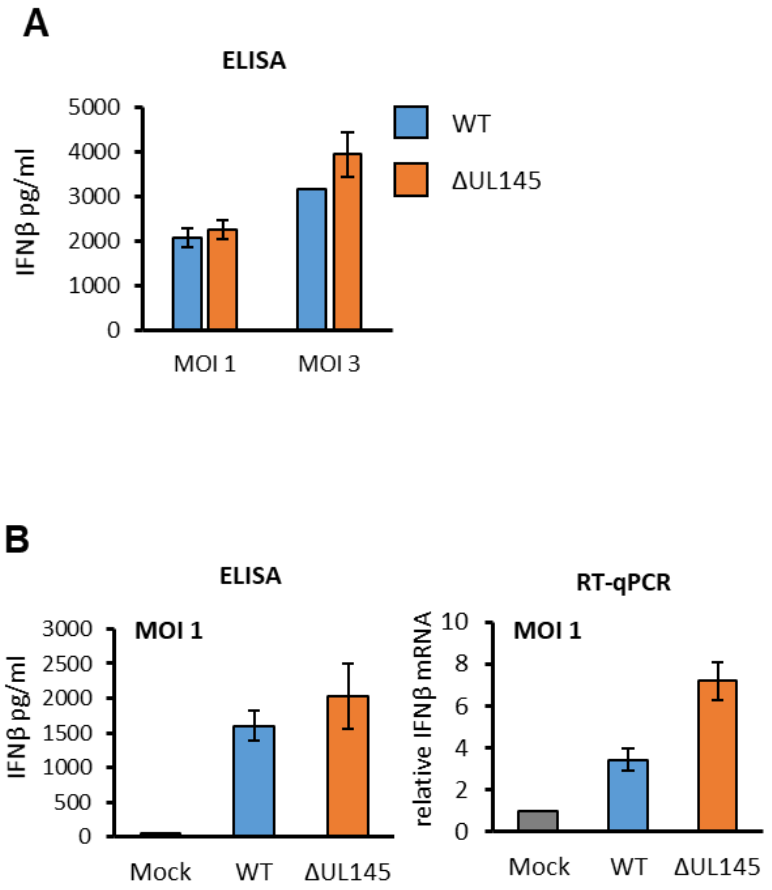

Figure 4.10. ΔUL145 HCMV induced more IFNβ transcripts but not IFNβ protein at 24 hpi.
(A) HFFF-TERT cells were infected with WT and ΔUL145 HCMV-GFP viruses (Merlin without tet-on UL128) at MOI 1 or 3. Supernatant was harvested 24 hpi and IFNβ protein was detected with ELISA. Error bars show SD of two biological replicates. (B) HFFF-TERT cells were infected with WT and ΔUL145 HCMV-GFP viruses at MOI of 1 for 24h. IFNβ protein was measured from supernatant while IFNβ mRNA was measured with Taqman qPCR, with GAPDH as internal control. Error bars show SD of two technical duplicates

The fact that the HLTF restriction assay was MOI dependent prompted me to examine whether ΔUL145 Merlin strain HCMV induced less IFNβ than WT at low MOI. Given that measuring low concentration of IFNβ with ELISA could create larger observational error, I resorted to analysing IFNβ transcripts using RT-qPCR with FACS sorted cells with infection at MOI of 0.03. HCMV-GFP viruses allowed me to isolate infected population and uninfected populations at 22 hpi according to their GFP expression. Isolated cells were washed once with PBS and lysed at 24 hpi to extract total RNA (Figure 4.11A). At 24 hpi, WT virus hardly induced more IFNβ in infected cells compared to uninfected cells. ΔUL145 on the other hand induced 6 times more IFNβ transcripts in infected cell compared to uninfected cells at 24 hpi. The difference of IFNβ transcripts induced by two viruses was statistically significant. Additionally, the bystander uninfected cells in ΔUL145 infection produced around half (50.1%) of IFNβ transcripts compared to the bystander uninfected cells in WT infection. (Figure 4.11B)

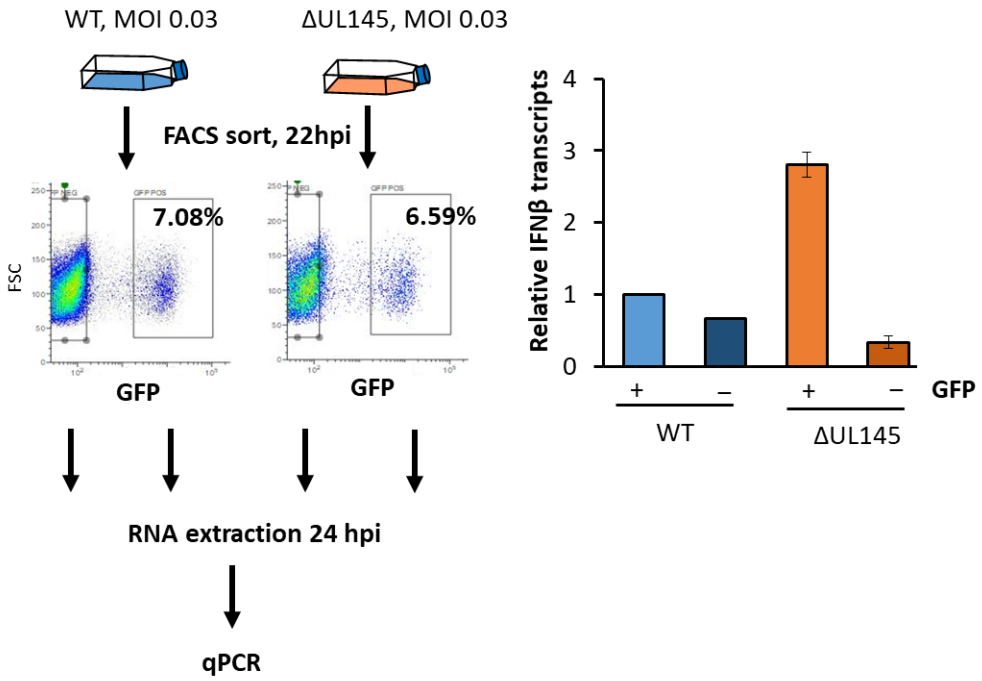

Figure 4.11. Low MOI ΔUL145 infection had increased IFNβ induction at 24 hpi.
(A) Schematic of the FACS sorting of HCMV infection at low MOI. HFFF-TERT cells were infected with WT HCMV-GFP (Merlin with tet-on UL128) at MOI of 0.03 for

22 hours. Infected cells were concentrated at 10^6 cells/ml and sorted using FACSMelody as shown in the gates above. Total RNA from the sorted cells was extracted at 24 hpi for RT-qPCR (B) Reverse transcription and Taq-man qPCR were performed to probe IFNβ with GAPDH as internal control. Error bars show SD of technical duplicates.

A repeat was attempted with three MOIs (0.3, 0.1, 0.03) of each virus. However, I underestimated the time to sort enough infected cells for RNA extraction and RT-qPCR. By the time the cells were lysed for RNA extraction, it was around 30 hpi. As shown in Figure 4.12, IFNβ induction could not be observed in any infection condition. From this experiment, it was difficult to tell whether UL145 deletion had impact on IFNβ induction compared to WT HCMV.

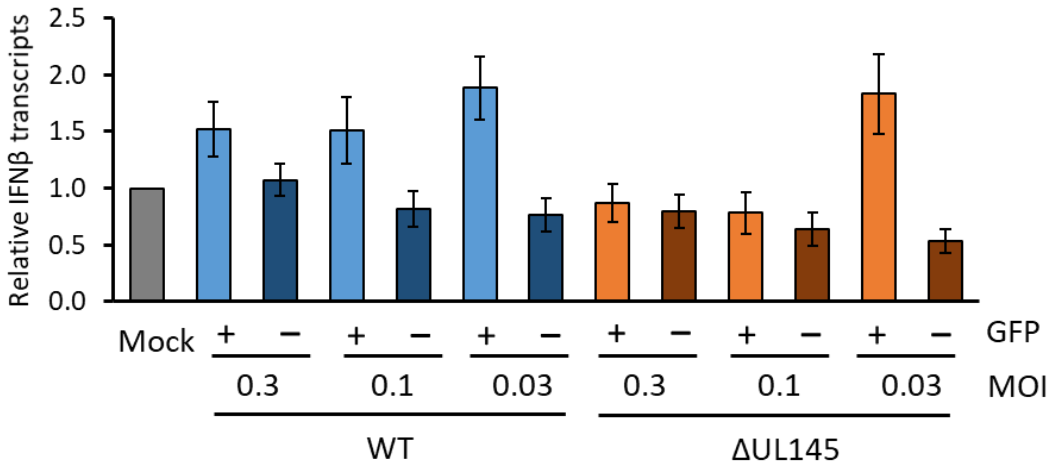

Figure 4.12. RT-qPCR analysis of IFNβ transcripts in WT and ΔUL145 at three different MOIs.
HFFF-TERT cells were infected with WT HCMV-GFP (Merlin with tet-on UL128) at MOI of 0.3, 0.1, or 0.03 for 22 hours. Infected cells were concentrated at 10^6 cells/ml and sorted. Sorted cells were lysed at 30 hpi and subjected to RT-qPCR probing IFNβ with GAPDH as internal control. Error bars show SEM of technical triplicates.

4.3.3. HLTF may regulate in IFNβ induction

One of the main aims of this project was to characterise the function of HLTF during HCMV infection. To investigate whether HLTF regulates IFNβ induction, HFFF-TERT shHLTF cell lines were infected with WT HCMV and IFNβ qPCR was perform with RNA collections at 3, 6, 12 hpi. The results were not straightforward. In the control shRNA cells, IFNβ gradually increased from 3 hpi to 6 hpi, and this induction was dampened at 12 hpi. When HLTF was knocked down, HCMV triggered IFNβ production at 3 and 12 hpi, but not 6 hpi. This pattern was observed in both HLTF knock down cell lines. (Figure 4.13)

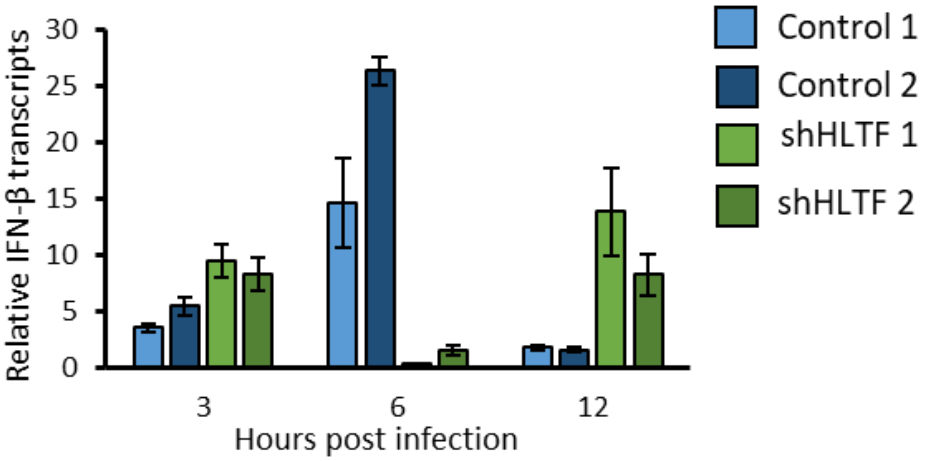

Figure 4.13. IFNβ transcript analysis in shHLTF cells.
HFFF-TERT shHLTF cell lines were infected with Merlin WT HCMV (non-GFP) at MOI of 1. Mock infection was also performed alongside. Infected cells were harvested at 3, 6, and 12 hpi for RT-qPCR (Taqman) measuring IFNβ transcripts, using GAPDH as internal control. Here IFNβ fold change against corresponding mock infection is graphed. Error bar show SD of technical duplicates.

An enzyme-linked immunosorbent assay (ELISA) assay was followed to examine whether this abnormal IFNβ mRNA induction pattern translated into IFNβ protein. Two monoclonal CRISPR knocked out HLTF cells were included together with their control counterparts. These genetically modified cells were infected with WT and ΔUL145 HCMV, and IFNβ production was measured with ELISA 24 hpi. Initially, supernatant collected

was subjected to multiplex beads-based ELISA. However, this method resulted in high variation in technical duplicates, in particular because of the simultaneous quantification of different cytokines (Figure 4.14A). Thus, the same collection of supernatant was analysed again with a highly sensitive 96-well-based ELISA kit. WT and ΔUL145 HCMV induced similar levels of IFNβ in all cell lines, similar to what had been observed in Figure 4.10. As shown in Figure 4.14B, HCMV induced much less IFNβ in CRISPR HLTF cells compared to control cells. This suggested that the decreased IFNβ transcription at 6 hpi resulted in less IFNβ protein production.

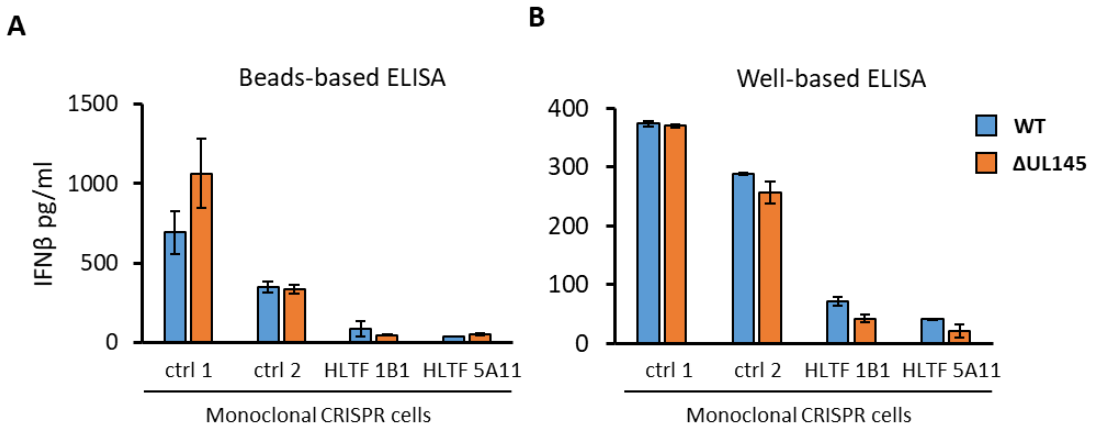

Figure 4.14. ELISA assay of WT and ΔUL145 HCMV infection in HLTF knock out cells.
CRISPR HFFF-TERT cells were infected with WT and ΔUL145 HCMV (non-GFP) at MOI of 1. Supernatant of infected cells was collected at 24 hpi and processed through IFNβ ELISA. Error bars show SEM of technical duplicates. Single clone CRISPR cells were generated by serially diluting polyclonal CRISPR cells and antibiotic selection by Dr. Ben Ravenhill, Alice Fletcher-Etherington, and Lior Soday from the lab. IFNβ ELISAs were performed with (A) multiplexed bead-based ELISA kit and (B) well-based IFNβ ELISA kits.

4.3.4. No evidence for HLTF participation in IFN induction and signalling pathways

In order to explore further the role of HLTF in IFN induction and signalling pathways, reporter assays with IFNβ promoter (pIFNβ), NFκB responsive element, and interferon stimulated responsive element (ISRE) were performed in 293T cells. Luciferase reporter

plasmids each contained one of the response elements driving a firefly luciferase gene. Plasmids were co-transfected with one of the shHLTF plasmids mentioned in Figure 4.1B into 293T cells. Forty-eight hours post transfection, cells were treated with the stimulus of the corresponding responsive element for 6 h. The IFNβ promoter was activated with Sendai virus infection, NFκB responsive element was activated with TNFα, and ISRE was activated with human interferon alpha (IFNα). Promoter activity was measured by luciferase production.

In an experiment performed in biological triplicate, SeV infection induced varied levels of IFNβ transcription within shHLTF and control cells, making it difficult to interpret whether knocking down HLTF in this context modulated SeV-mediated IFNβ activation (Figure 4.15A).Figure 4.15B shows that knocking HLTF gene did not substantially modulate NFκB activation by TNFα (Figure 4.15B). In addition, HLTF did not apparently participate in interferon stimulated gene activation via ISRE (Figure 4.15C).

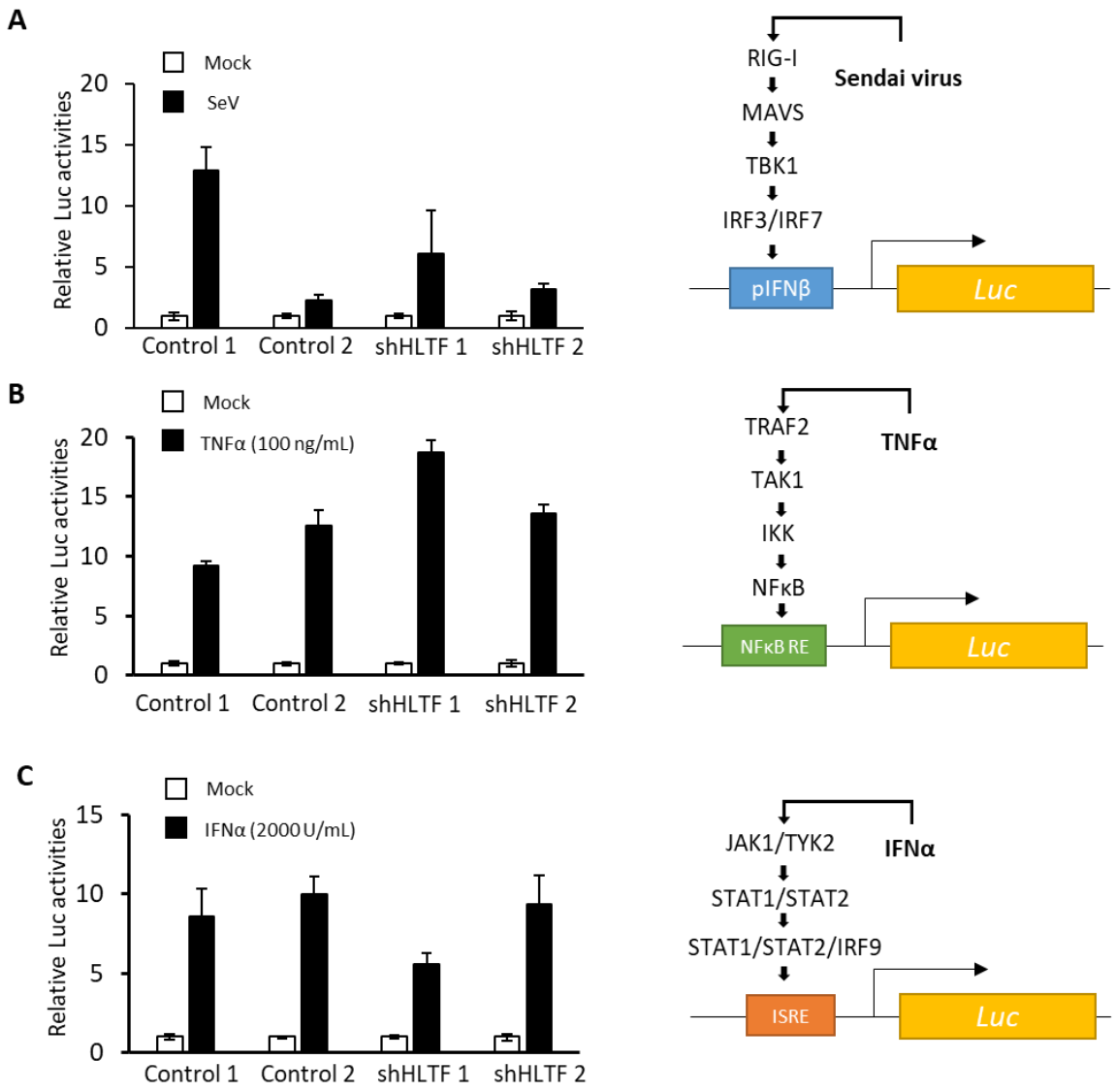

Figure 4.15. Luciferase reporter assay with cells transfected with shHLTF and treated different stimuli.

293T cells were transfected with reporter plasmid, and GFP expressing plasmid was also transfected as a transfection internal control in a 96-well using liposomal transfection reagent (Mirus). Forty-eight hour post transfection, cells were infected with Sendai virus (SeV) for 6 hours, followed cell lysis and luciferase substrate incubation. Luminescence reading was normalised with GFP fluorescence reading to calculate relative luciferase activity. Similar experiments were performed with (B) TNFα-induced NFκB reporter plasmid and (C) IFNα induced interferon stimulated responsive element (ISRE) reporter plasmid. Error bars show SEM of biological triplicates.

Besides the mitochondrial RIG-I viral sensing pathway, Sendai virus also activates IFN transcription through endosomal TLR7/8 (Xagorari and Chlichlia, 2008). Because of my

concerns that liposomal transfection reagents might interfer with Sendai virus-mediated pIFNβ activation, I established 293T cell lines that stably expressed shHLTF for reporter assays. In transduced cell lines, SeV activated similar level of pIFNβ activity in all 4 cell lines, suggested knocking down HLTF did not affect SeV-mediated pIFNβ induction (Figure 4.16A).

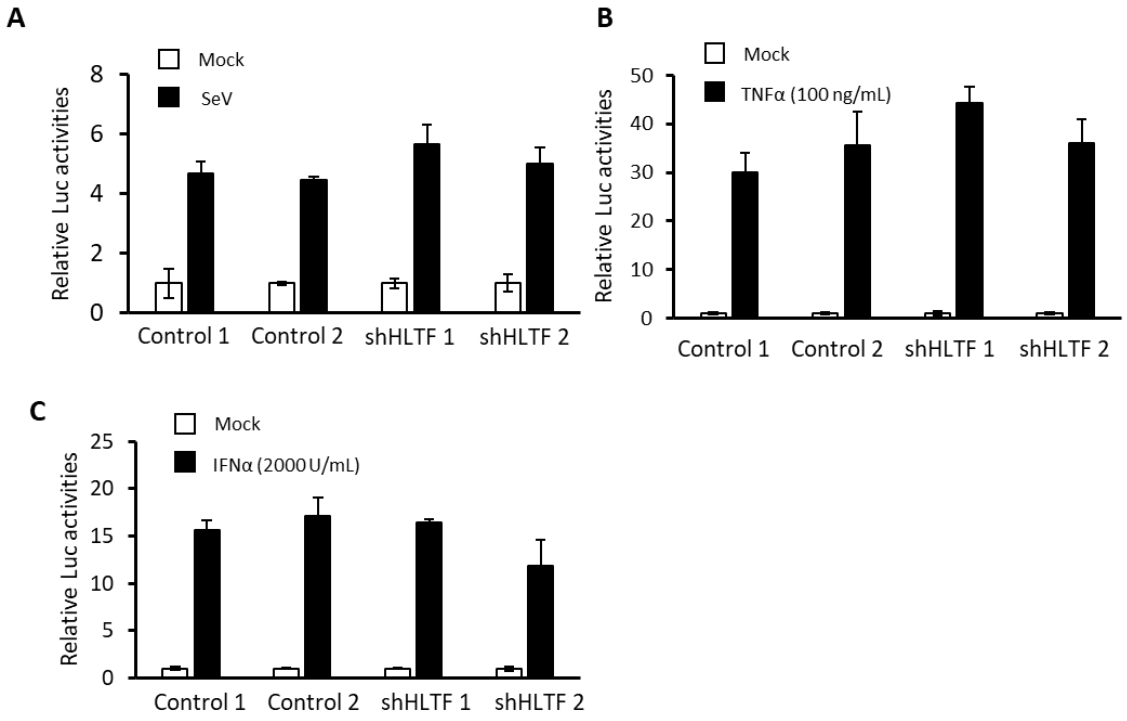

Figure 4.16. Luciferase reporter assay with cells transduced with shHLTF and treated different stimuli.

293T cells stably expressing shHLTF were transfected with luciferase expressing plasmid driven by IFNβ promoter, which contains binding sites for activated IRF3 and NFκB, and GFP expressing plasmid as transfection internal control in a 96-well. Forty-eight hpur post transfection, cells were incubated with stimuli-containing DMEM for 6 hours, followed cell lysis and luciferase substrate incubation. Luminescence reading was normalised with GFP fluorescence reading to calculate relative luciferase activity. Error bars show SEM of biological triplicates.

4.3.5. HLTF bound to HCMV DNA and cellular DNA

Since HLTF harbours a DNA binding domain that binds to SERPINE1 and HIV1 promoters and the SV40 enhancer (Ding et al., 1996; Sheridan et al., 1995), I postulated that HLTF might serve as a viral DNA sensor detecting HCMV DNA triggering relevant kinases for IFNβ induction signalling. To test whether HLTF selectively binds to HCMV DNA, chromatin immunoprecipitation (ChIP) assay was performed in HFFF-TERT cells infected with ΔUL145 for 6 hours, the time prior to HCMV DNA replication, and 72 hours, the time for a complete lytic cycle, to analyse DNA fragment associated with HLTF.

Several ChIP conditioning experiments were carried out with HFFF-TERT cell lysates to optimise the length of formaldehyde crosslink time, the length of sonication, and the repeats of washes. Ideally, after crosslink and sonication, sizes of fragmented DNA would be around 1 kb. I tested formaldehyde crosslink for 10 min and 60 min, in combination of sonication cycles of 20, 40, 60, and 80 (30 sec on and 30 sec off in each cycle). When cell lysates were incubated with formaldehyde for 60 min, not even 40 min of sonication (80 cycles) fragmented DNA. A 10-min formaldehyde crosslink, followed by 40 cycles of sonication was chosen as most of the fragmented DNA molecules under this condition had the size around 1 kb (Figure 4.17A).

To optimise washing conditions, sonicated DNA from HFFF-TERT was incubated with anti-RNA pol III antibody (positive control), which associates with DNA binding RNA pol III, or mouse IgG (negative control), which does not specifically bind to any protein. Here I was attempting to find a washing condition that allowed DNA to be detected for anti-RNA pol III precipitants but not IgG precipitants. Six washes with the washing buffer supplied by the manufacturer was compared with 12 washes. Twelve washes were too rigorous as no DNA could be detected in anti-RNA pol III precipitants and thus 6 washes were chosen (Figure 4.17B).

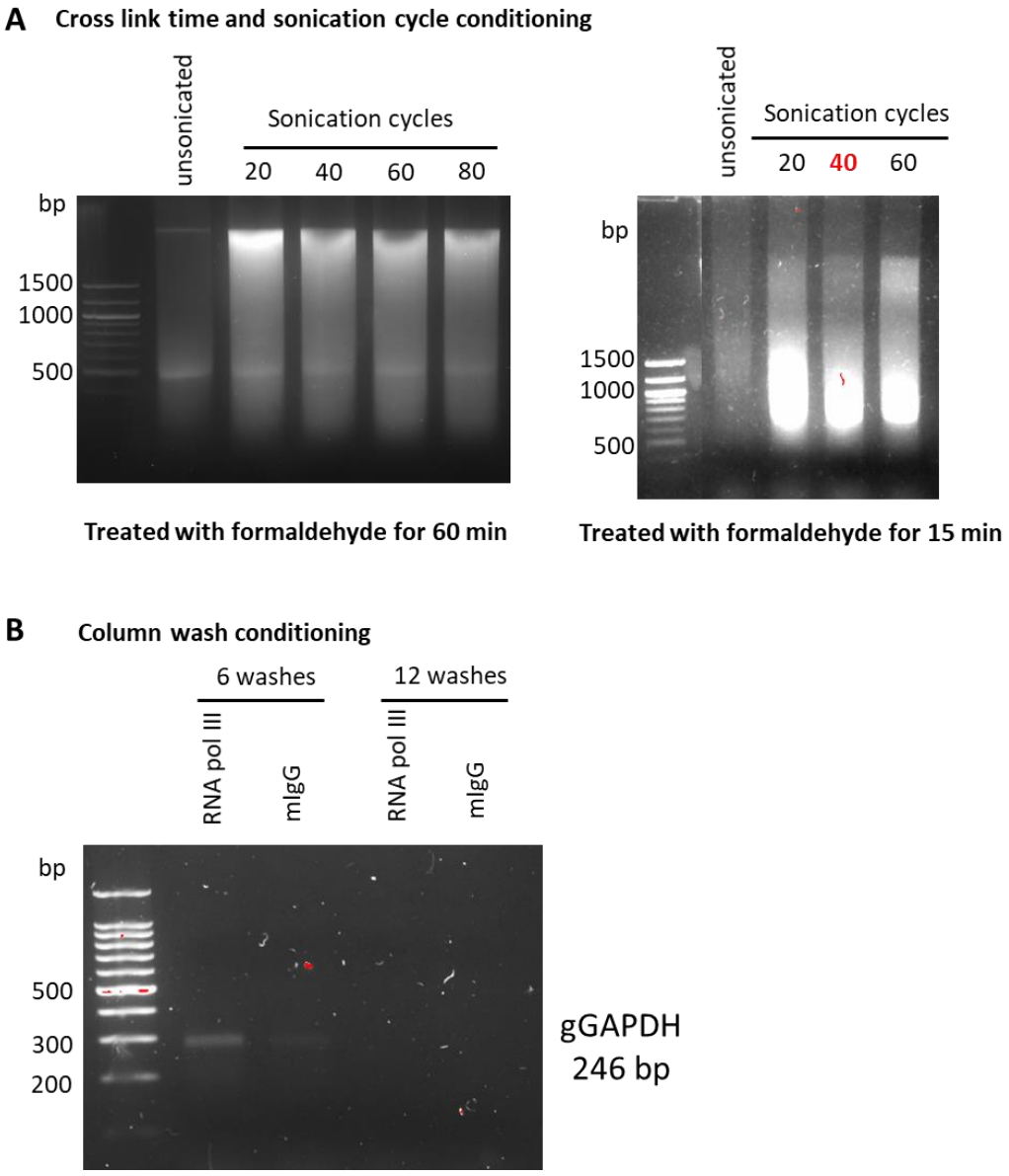

Figure 4.17. ChIP conditioning for crosslink, sonication, and wash steps.
Conditioning experiments were performed with components from the Imprint ChIP kit (Sigma). (A) 1 X 10^6 HFFF-TERT cells were incubated with 1% (v/v) formaldehyde for 10 or 60 min at room temperature. Glycine was added to a final concentration of 125 mM to quench formaldehyde after crosslink. Cell nuclei were extracted with Nuclei Preparation buffer and then lysed with shearing buffer. DNA was sheared by water-cooled sonication (Diagenode Bioruptor), with various cycles of 30 sec "on" and 30 sec "off". 0.2 M NaCl Solution was then added for an incubation of 90 min at 65 °C to de-crosslink protein-DNA complex. DNA were extracted with a silica-based column and the resulting DNA was subjected to gel electrophoresis with SYBR green dye-containing 1% agarose gel in Tris-acetate-EDTA (TAE) buffer. DNA signal was visualised under UV light. (B) Sonicated cell lysates were incubated with mouse anti-RNA pol III antibody or a control mouse IgG (mIgG) at 4°C overnight in an antibody binding well. Supernatant was remove after immunoprecipitation and the well was washed with washing buffer for 6 or

12 times. 0.2 M NaCl Solution was then added for an incubation of 90 min at 65 °C to de-crosslink protein-DNA complex. Precipitant DNA were extracted with a silica-based column. DNA samples were analysed with PCR probing human genomic GAPDH. Resulting DNA samples were subjected to gel electrophoresis with SYBR green dye-containing 1% agarose gel in TAE buffer and visualisation under UV light.

After optimisation, an initial attempt at an experimental ChIP assay was performed and the resulting DNA samples were analysed using SYPR green QPCR. Histone H3 antibody was used IP positive control and rabbit IgG (rIgG) was used as negative control. Histone H3 unselectively binds to all DNA and control rabbit IgG does not specifically bind to any protein. Precipitant lysates were probed for HCMV major immediate early promoter (MIEP) and origin of lytic replication (oriLyt) as HCMV DNA fragments. Primers targeting human globin β promoter (HGBP) was used as HLTF DNA binding positive control (Mahajan and Weissman, 2002) while genomic GAPDH (gGAPDH) was designed as a negative control. The SYBR green melting curve analysis on the end PCR products indicated that multiple amplicon products were detected for oriLyt and HGBP, suggesting that PCR conditions for these primers were not optimised and non-specific primer binding occurred. Thus, I designed two new primers for oriLyt and HGBP, and tested them with different annealing temperature. One of the new primers were selected to replace the original (marked in red), and the annealing temperature was adjusted to 56 °C (Figure 4.18).

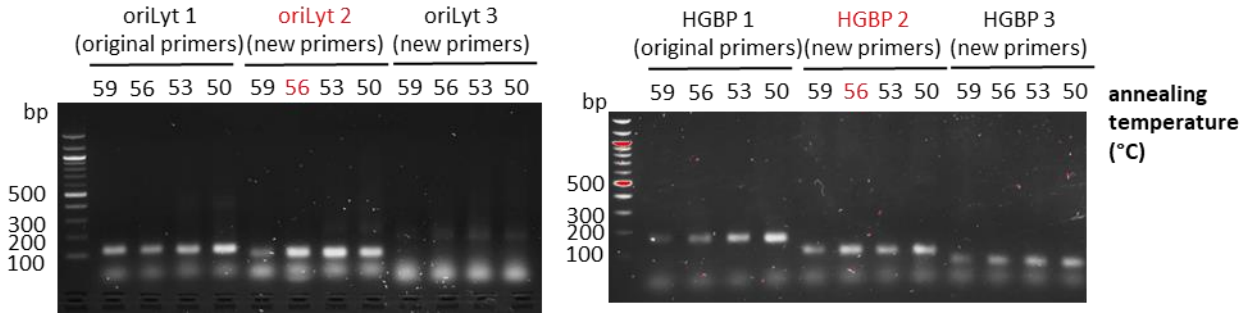

Figure 4.18. PCR conditioning for oriLyt and HGBP.
HFFF-TERT cells were infected with Merlin WT HCMV at MOI of 1 for 72 h. Total DNA of the cells were extracted with QIAamp DNA blood mini kit (QIAGEN). PCR analysis was performed with different primers and annealing temperatures as

indicated. Resulting DNA samples were subjected to gel electrophoresis with SYBR green dye-containing 1% agarose gel in TAE buffer and visualisation under UV light.

With new sets of primers and optimised annealing temperature, I performed the second ChIP assay. The amount of specific DNA fragment associated with a given antibody was adjusted according to the total DNA input of the immunoprecipitation. Whether HLTF bound to a certain DNA fragment was determined in comparison with that DNA fragment precipitated with rabbit IgG, which theoretically should be none. Histone H3 precipitation was designed to serve as a positive control, being anticipated to immunoprecipitate viral and cellular DNA, compared to rIgG immuniprecipitation. Overall, histone H3 did not precipitate much more DNA compared to rIgG control, especially at 6 hpi. Therefore, technical error easily led to statistical insignificance, as demonstrated with HGBP and gGAPDH QPCR analysis of 6 hpi lysates. A better positive control antibody could be used to improve this assay. Nonetheless, HLTF still bound to significant amounts of oriLyt and HGBP DNA compared to IgG at 6 hpi. At 72 hpi, both HLTF and histone H3 associated with a higher percentage of viral DNA, possibly because there were more viral DNA in the nucleus at the late stage of HCMV infection. Besides viral DNA, HLTF was also found associated with cellular DNA, including gGAPDH, which was designed to serve as negative control. One possible conclusion of this experiment was that HLTF bound to viral and cellular DNA non-selectively, similarly to histone H3. Overall, however, time constraints and COVID-related lockdown precluded further optimisation of this experiment in order to yield further biological replicates and further optimised data.

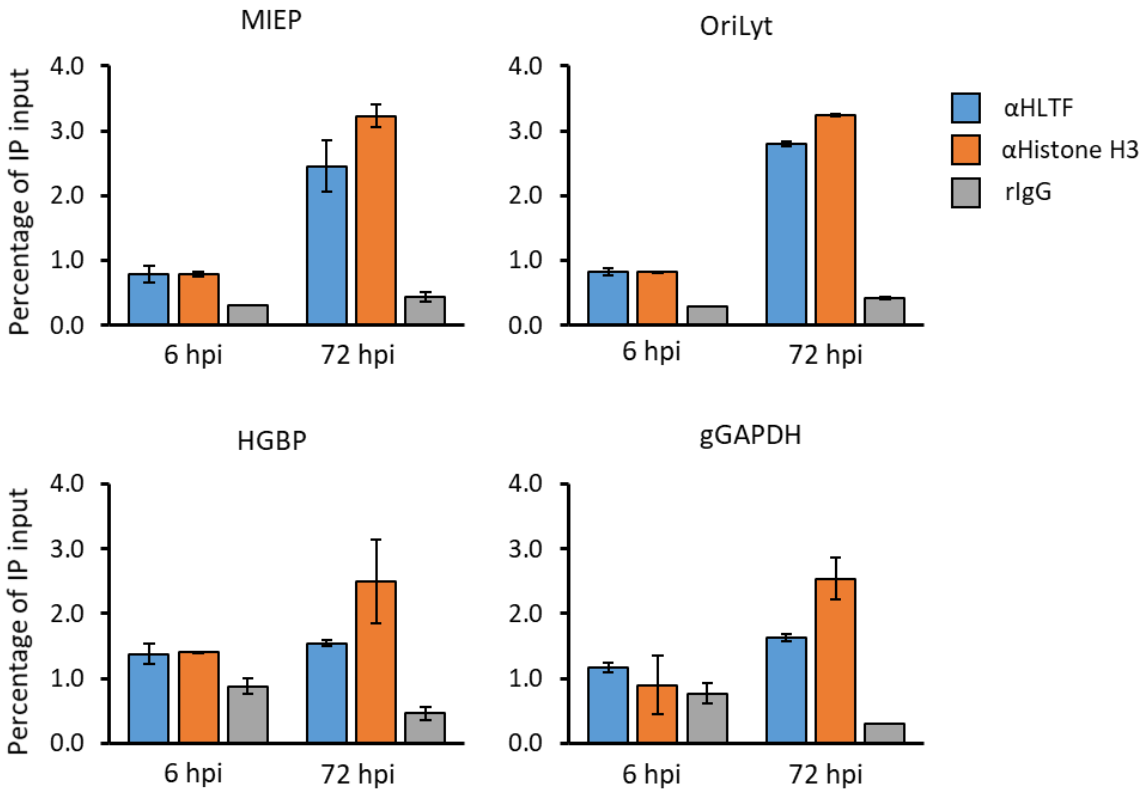

Figure 4.19. ChIP assay of HLTF binding DNA during ΔUL145 infection.
Cell cycle synchronised HFFF-TERT were infected with Merlin ΔUL145 at MOI of 5, cell lysates were harvested at 6 and 24 hpi with sonication. Immunoprecipitation were performed with rabbit polyclonal anti-HLTF antibody, mouse anti-histone H3 antibody, and rabbit IgG. Protein associated DNA were extracted and DNA fragments of MIEP, OriLyt, HGBP, gGAPDH were measured with SYBR green qPCR, in comparison with DNA extraction 20% of IP lysate. Error bars show SD of two technical duplicates of qPCR.

4.4. Quantitative proteomics revealed ΔUL145 infection kinetics

4.4.1. UL145 effects on interferon production over time

A conclusion of the previous ΔUL145 proteomic analysis was that UL145 might modulate IFNβ expression at 72 hpi (Figure 4.3). Increased IFNβ protein production was not detected at 24 hpi with ELISA even though IFNβ transcription had increased in RT-qPCR analysis (Figure 4.10). These results suggested that it was important to perform a detailed analysis on UL145 regulation of IFN and IFN-stimulated proteins over time. Thus, a TMT-based proteomics analysis of WT and ΔUL145 time course was carried out (Figure

4.20). In this 3-h mass spectrometry experiment, 2334 proteins were identified and quantified, including 64 HCMV proteins.

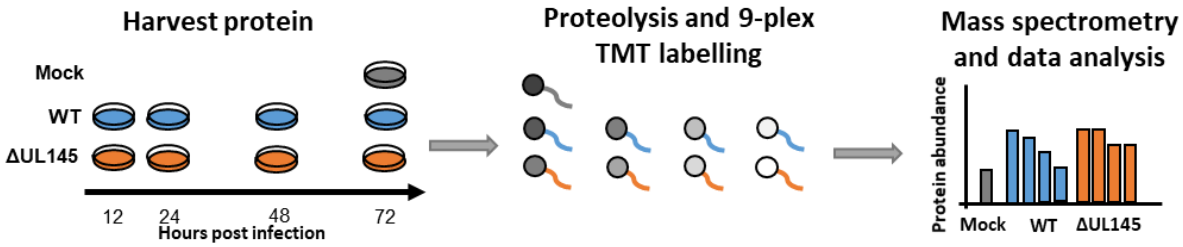

Figure 4.20. Schematic of a TMT based MS experiment analysing WT and ΔUL145 over time.
HFFF-TERT cells were infected with Merlin strain WT and ΔUL145 HCMV-GFP (with tet-on UL128) at MOI of 5. Prior to infection, cells were treated with dexamethasone-containing serum free medium for 24 h. Cells lysates were harvested at the indicated time points and digested into peptides with trypsin and LysC prior to TMT labelling. Digested peptides were subjected to a 3-h MS3 proteomics analysis.

Fold change comparing protein abundance in WT and ΔUL145 infections at each time point was calculated. Proteins that were up-regulated upon UL145 deletion, (i.e. proteins decreased by UL145 expression), are shifted to the right side of the graph, while proteins that were down-regulated by UL145 deletion, (i.e. the proteins increased by UL145 expression), are shifted to the left (Figure 4.21). Most of the interferon-related proteins that were previously identified to be affected by UL145 deletion, such as SP100, OAS2, and MX2, were not quantified in this single-shot experiment most likely reflecting the relative abundance of these proteins in comparison to other cellular proteins. More proteins would be anticipated to be quantified by an analysis of fractionated peptide samples.

At 12 and 24 hpi, most of the proteins significantly up- or down-regulated by UL145 deletion ($p<10^{-10}$) were HCMV proteins (13/28 at 12 hpi and 7/14 at 24 hpi). Host proteins modulated at these time points including CUL5, unc-80 protein homolog

(UNC80), cilia- and flagella-associated protein 100 (CP100), NADH dehydrogenase (ubiquinone) 1 beta subcomplex subunit 4 (NDUB4), and NADH dehydrogenase (ubiquinone) 1 alpha subcomplex subunit 2 (NDUA2) have not previously been found to be regulated by interferon. However, at 48 and 72 hpi, interferon-induced protein with tetratricopeptide repeats (IFIT) 2 and 3 were found to be rescued by UL145 deletion (Figure 4.21), consistent with the previous data (Figure 4.3). Hierarchical clustering of fold change comparing protein abundance in WT and ΔUL145 infections at each time point identified more interferon inducible proteins, including IFIT1, ubiquitin-like interferon stimulated gene 15 (ISG15), and E3 ubiquitin-protein ligase DTX3L that were upregulated in cells infected with the UL145 deletion virus (Figure 4.22). A closer look at the expression patterns of these proteins characterised a distinctive feature of ΔUL145. In WT infection all four proteins peaked at 12 or 24 hpi, then the protein expression gradually decreased. In ΔUL145 infection, expression of IFIT proteins peaked at 24 hpi, and their decline was slower compared to WT. ISG15 displayed a delayed peak at 48 hpi instead at 24 hpi (Figure 4.23). Interferon regulates expression of these proteins. The expression profiles observed here suggested a possible trend of higher IFNβ at 48 and 72 hpi in ΔUL145 infection. However that this would need at least two more biological repeats to determine if there was a genuine statistically significant change.

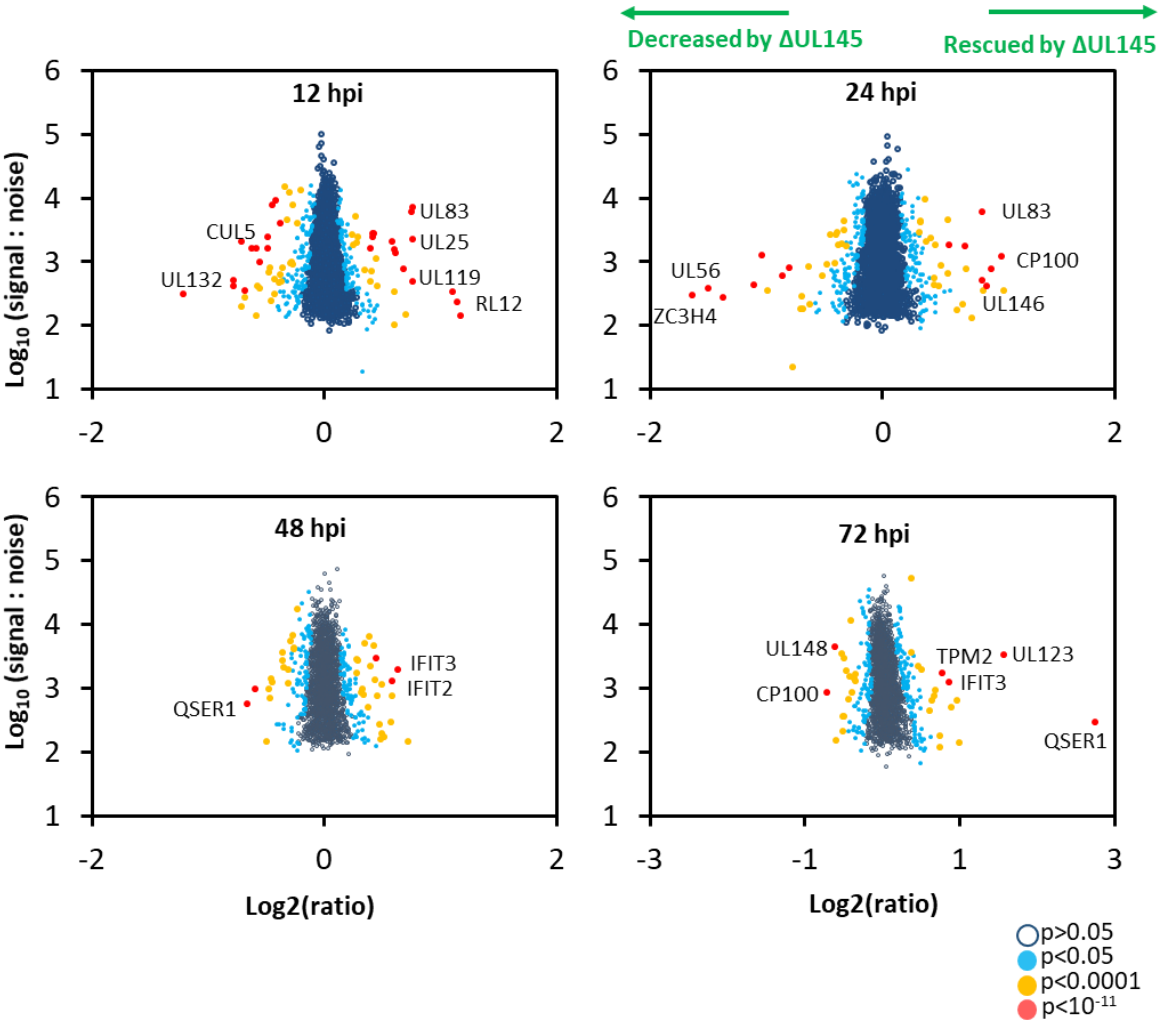

Figure 4.21. Scatter plots showing proteins up- and down-regulated during ΔUL145 infection compared to WT.

The x-axis represents the fold change of protein expression in ΔUL145 virus infection compared to WT infection in log 2 scale. The y-axis represents the average intensity of the protein detected, which is the sum of signal to noise, in log 10 scale. The colour of the dots represents the significance B of the fold change (estimated using a Benjamini-Hochberg-corrected p-value). Proteins that were up-regulated by UL145 deletion are shown on the right side of the graph while those which were down-regulated were shown on the left side. Protein names of some of those which were significantly regulated were mark next to the corresponding dots.

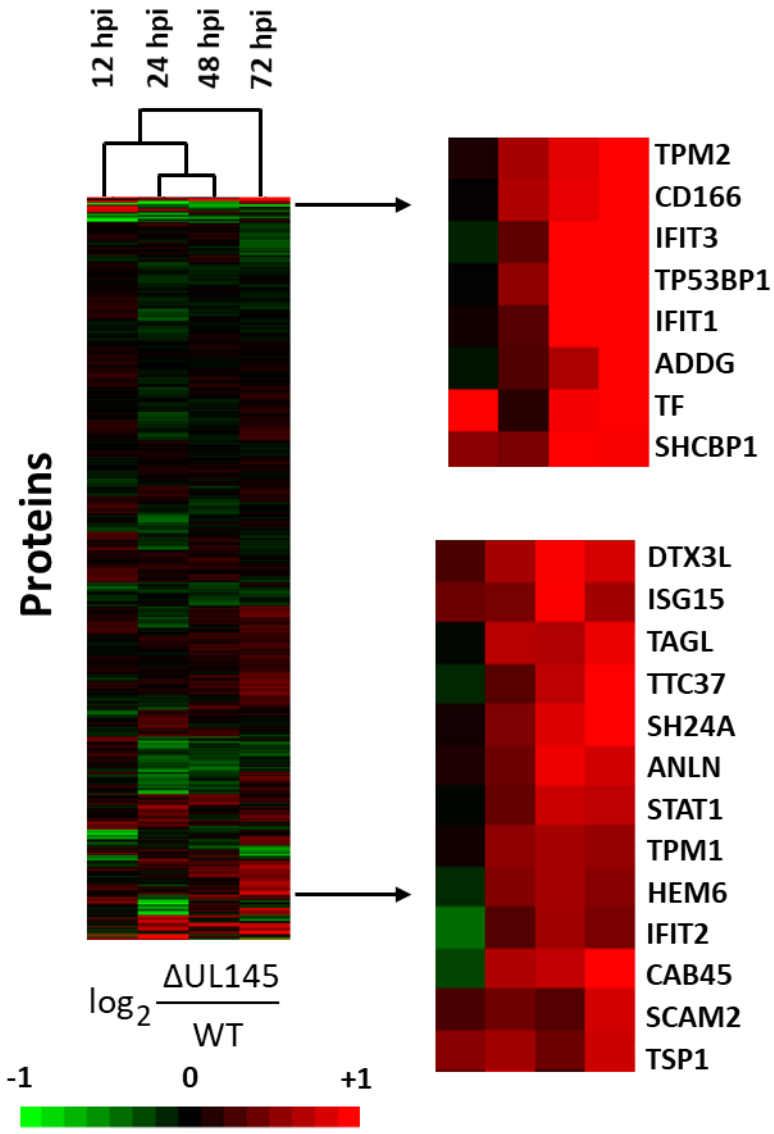

Figure 4.22. Hieratical clustering of fold change over time between WT and ΔUL145.

Hierarchical clustering of proteins quantified in WT and ΔUL145 time course according the fold change of protein abundance in ΔUL145 infection compared to WT. Two subclusters of proteins with increasing fold change are shown on the right.

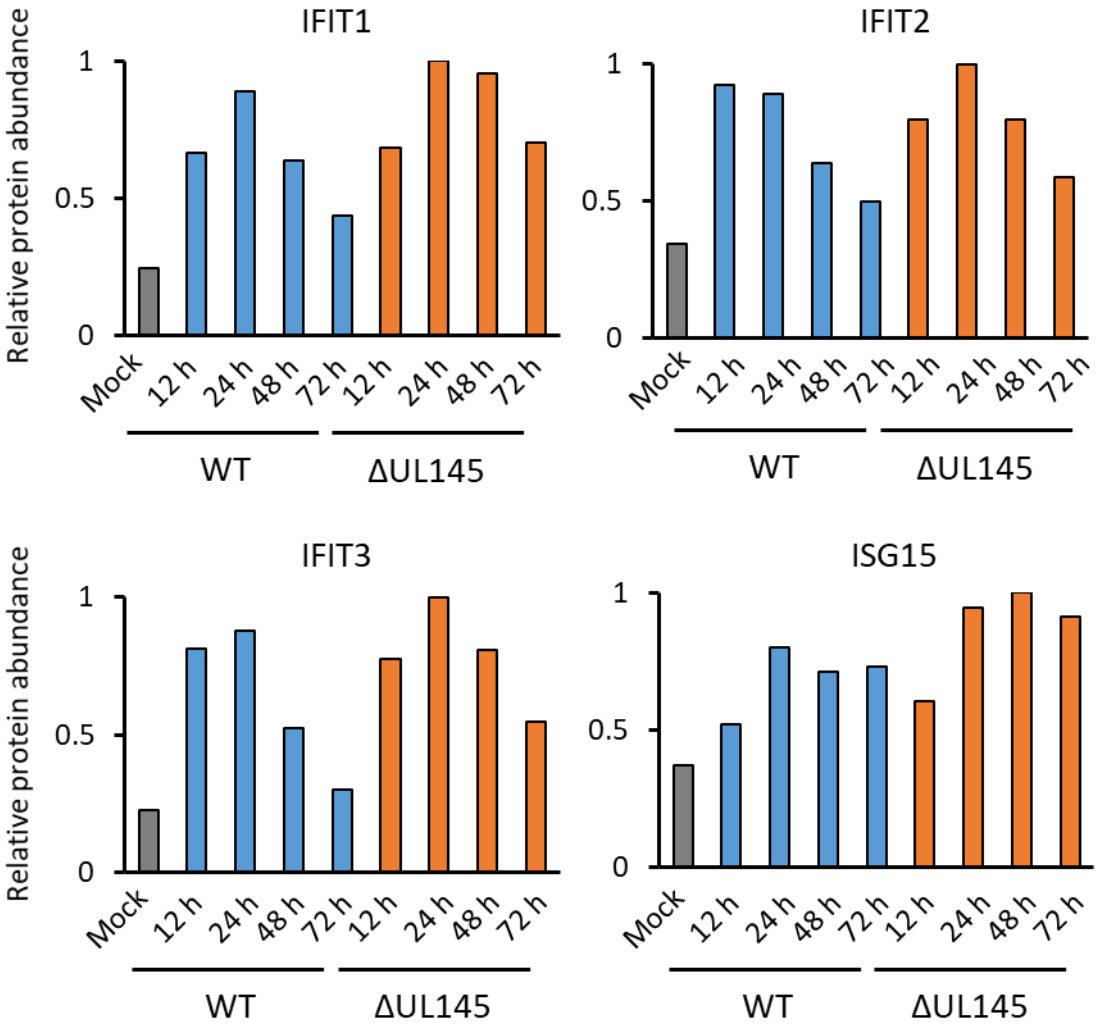

Figure 4.23. Protein abundance of interferon inducible proteins IFIT1, IFIT2, IFIT3, and ISG15 during WT and ΔUL145 infection.
The relative protein abundance of 4 interferon inducible proteins measured in TMT based proteomics analysis of WT and ΔUL145 infection at 12, 24, 48, and 72 hpi. The highest reading of each protein was set as 1.

4.4.2. Possible UL145 kinetic regulation of viral proteins

In Figure 4.24, many viral proteins significantly dysregulated by UL145 deletion at 12 and 24 hpi were HCMV Tp5 proteins (13 Tp5 proteins at 12 hpi, 7 Tp5 proteins at 24 hpi, with fold change significance $p<10^{-10}$). In a previous comparison of viral protein expression in WT and ΔUL145 infection at 72 hpi, 11 viral proteins were down-regulated more than 2

fold (Figure 4.4), and were enriched in Tp5-class proteins. In my repeat temporal analysis, 6 of the same proteins were quantified, but none of these were down-regulated by UL145 deletion at 72 hpi, weakening the hypothesis that UL145 may regulate HCMV late gene expression via its effect on HLTF.

At 12 and 24 hpi, all viral proteins were significantly up-regulated ($p<10^{-20}$) by UL145 deletion, including UL83, UL25, and UL94 were classified as Tp5 proteins (Figure 4.24). Their up- or down-regulation was not observed at later time points at 48 and 72 hpi. For instance, tegument protein UL94 was up-regulated by 1.5 fold at 12 hpi, but its expression in ΔUL145 infection seemed unchanged compared to WT infection at 24, 48, and 72 hpi. These proteins are structural tegument proteins that express at the highest levels at late stage (~72 h) HCMV infection. Their up-regulation at 12 hpi might merely have reflected more input virions in ΔUL145 infection compared to WT or UL145-mediated viral structural protein degradation. One way to have confirmed or refuted this hypothesis would have been to have measured expression of the viral protein the virus titration was based on, UL36 by proteomics. However, UL36 was not quantified in this 3-h MS analysis. WT and ΔUL145 viruses used in this experiment had GFP tagged to UL36, and GFP was used as infection indicator. Another possibility would have been to have performed simultaneous infections in T25 flasks to measure the % infection contemporaneously with the experiment. However, such additions would have used substantial additional amounts of limited stocks of virus, and the titrations had already been performed extensively.

Nonetheless, in this experiment, UL145 deletion did not modulate the expression of UL83, UL25, and UL94 at 72 hpi. By comparison, UL83 and UL94 were identified to be down-regulated by more than 2-fold during ΔUL145 infection previously (Figure 4.4). Further interpretation of this data would require several further biological repeat experiments to address whether the changes found in Figure 4.4 or 4.21 were more likely to represent reality.

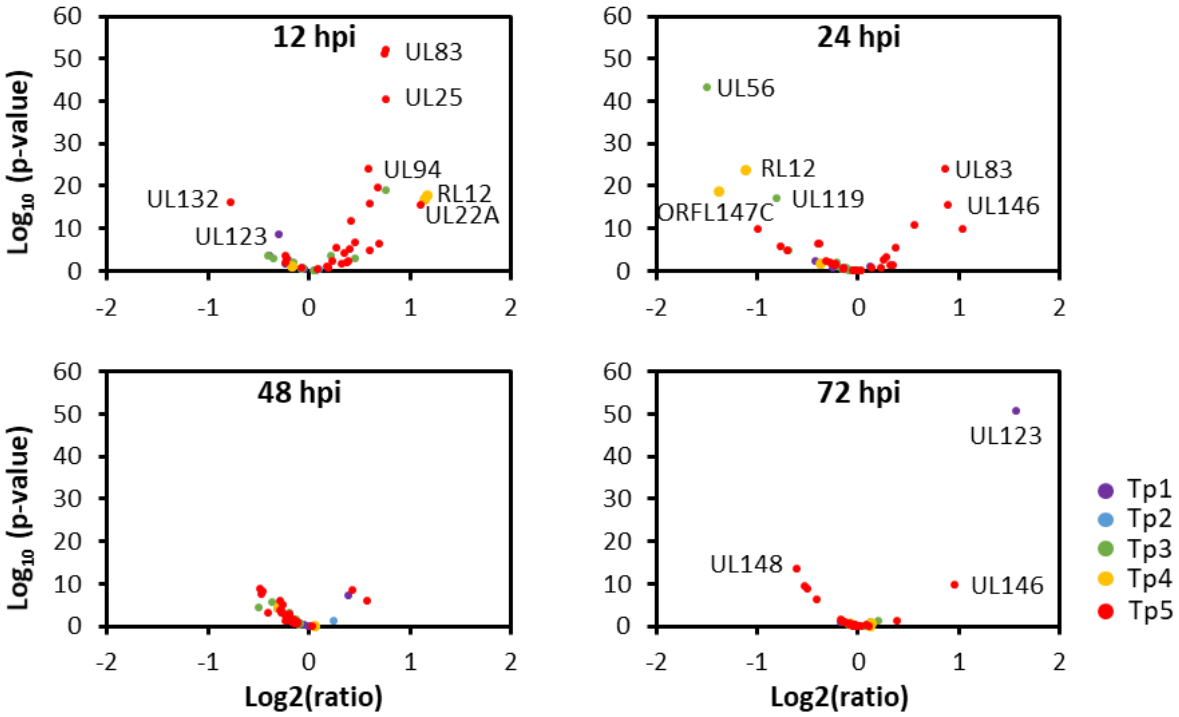

Figure 4.24. Volcano plots of Tp-classfied viral protein fold change and significance in ΔUL145 virus infection at multiple time points.
The x-axis represents the fold change of viral protein expression in ΔUL145 virus infection compared to wild-type Merlin infection in Log 2 scale. The y-axis represents the significance of the fold change (p-value) in log 10 scale. The colour of each dot indicates the Tp class of viral proteins.

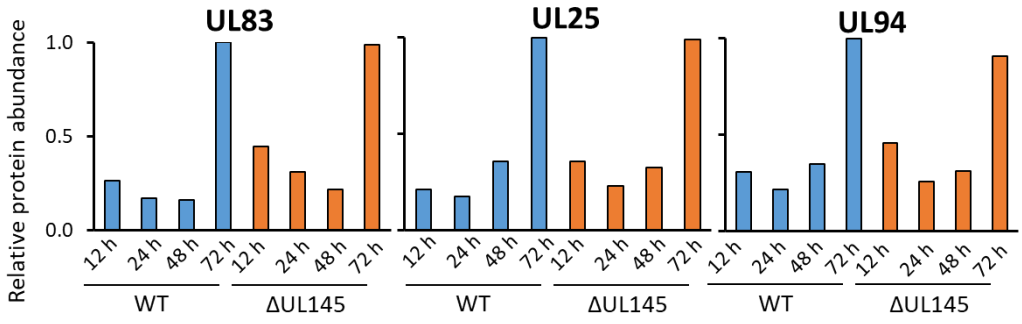

Figure 4.25. Protein abundance of viral tegument proteins UL83, UL25, and UL94 during WT and ΔUL145 infection.
The relative protein abundance of Tp5 tegument proteins UL83 (phosphoprotein 65, pp65), UL25 (phosphoprotein 85, pp85), and UL94 (cytoplasmic envelopment protein 2) measured in TMT based proteomics analysis of WT and ΔUL145 infection at 12, 24, 48, and 72 hpi. The highest reading of each protein was set as 1.

The previous comparision between WT and ΔUL145 infection was performed at MOI 10, and my repeat experiment performed with MOI of 5. To examine whether the discrepancy in viral protein regulation mentioned above was MOI dependent, I conducted a comparative analysis comparing fold changes derived from comparing protein abundance during WT and ΔUL145 infection at 72 hpi in both experiments. However, as shown in Figure 4.26, my 3-h MS analysis did not quantify many proteins that were dysregulated because of UL145 deletion. Proteins that were down-regulated in ΔUL145 infection were all viral Tp5 proteins (marked in red rectangles). Therefore, it was hard to interpret the effect of using lower MOI. A further analysis of the fractionated samples would identify more proteins and might help identify the reason causing the difference between the two experiments. However, prior to performing fractionation, ideally several further biological repeats of this experiment would be conducted in 3h single-shot format to establish reliable data.

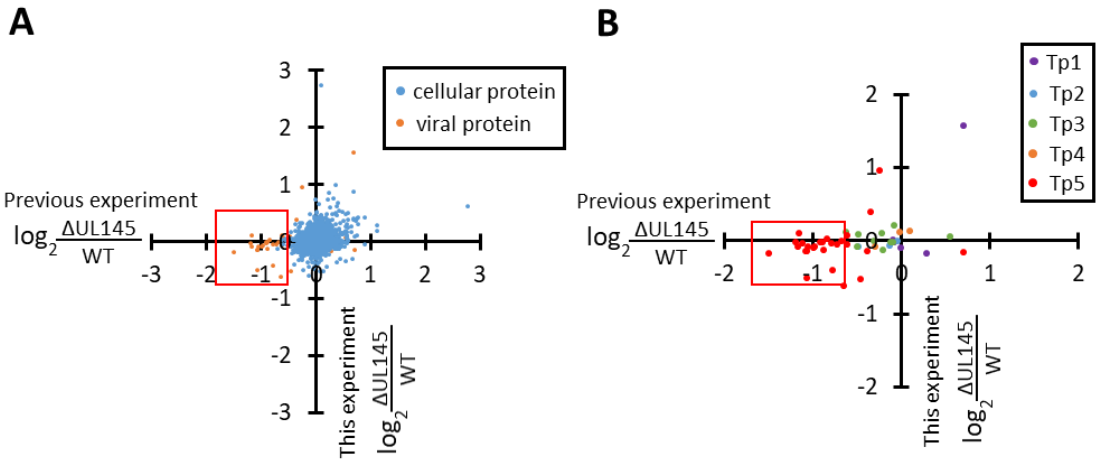

Figure 4.26. Comparative analysis between two MS experiments comparing WT and ΔUL145 infection.
Fold change derived from comparing protein abundance during WT and ΔUL145 infection at 72 hpi was used in this comparative analysis. X-axis represents the original WT vs. ΔUL145 experiment while y-axis represents my repeat experiment. (A) Cellular proteins and viral protein quantified in both experiments are shown here. Cellular proteins are in blue and viral proteins are in orange. (B) Fold change of viral proteins quantified in both experiments are plotted. Viral proteins were coloured according to their Tp classes.

4.5. Discussion

4.5.1. UL145 is not essential for HCMV replication

As a gene in the UL/b' region, UL145 is absent in certain laboratory adapted HCMV strains, such as AD169 and Towne, suggesting that UL145 is not required for HCMV to establish infection and replicate. UL145 has been shown to down-regulated DNA repair proteins HLTF and TP53BP1. From my preliminary data, I found that viral DNA replication was similar to DNA replication of WT virus during ΔUL145 infection, I observed some modulation of IFN induction in comparison to cells infected with WT virus, however changes needed further replicate experiments to be reliably interpretable. Results from growth curve analysis showed that deletion of UL145 did not consistently impair HCMV replication. Even when less infectious particle production was observed, the defect was shortly recovered as infection progressed. All of these results so far lead to the conclusion that UL145 is not essential for HCMV to replicate *in vitro*.

One potential explanation for a lack of restriction of spread of HCMV within fibroblasts by increased IFNβ secretion could be the high MOI used. HCMV encodes many viral effectors that attenuate IFNβ-triggered JAK-STAT signalling. For example, IE1 binds to STAT2 and disrupts the association of STAT2-IFN-stimulated gene factor 3 (ISGF3) complex and ISRE sites of ISG promoters (Huh et al., 2008; Paulus et al., 2006), therefore restricting ISG transcription. Another immediate early protein tandem repeats 1 (TRS1) directly binds to IFNβ-induced protein kinase R (PKR) and prevents the phosphorylation of the host eukaryotic translation initiation factor eIF-2α, thus inhibiting further ISG activation (Hakki et al., 2006; Vincent et al., 2017). It is therefore possible that the IFNβ induction regulation by UL145 deletion was not sufficient to counteract enough to downplay the overall attenuation of IFNβ signalling and was easily overcome with high virus titre infection.

Another interesting finding was the interplay between expression of UL145 and IE1, which is the only viral protein shown to be affected by UL145 deletion in both proteomic analysis. Previously UL145 protein was demonstrated to promote MIEP activity (Raftery et al., 2009), but here UL145 seemed to have positive effect on IE1 although not IE2

protein expression (Figure 4.27). IE1 showed significant slower decline in ΔUL145 infection, and the IE1 increase at 72 hpi was observed before (Figure 4.4). How UL145 regulates IE1 expression remains an open question. IE1 was not targeted for proteasomal degradation during the entire lytic cycle of HCMV, as indicated in our MG132 proteomics analysis, suggesting IE1 regulation by UL145 may be solely on a transcriptional level. To verify the direct effect of UL145 on IE1, ΔUL145 infection could be performed in UL145 overexpressing HFFF-TERT. If UL145 negatively regulates IE1 expression, there should be less IE1 transcripts in UL145 expressing cells compared to control HFFF-TERT.

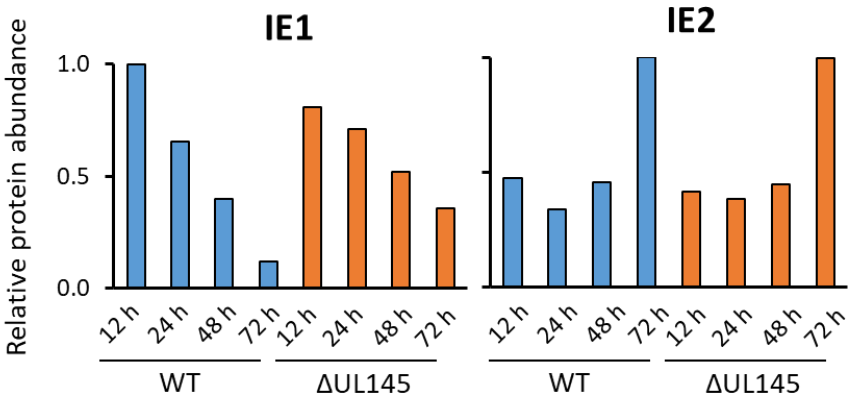

Figure 4.27. Protein abundance of viral immediate early proteins IE1 and IE2 during WT and ΔUL145 infection.
The relative protein abundance of immediate early proteins IE1 and IE2 measured in TMT based proteomics analysis of WT and ΔUL145 infection at 12, 24, 48, and 72 hpi. The highest reading of each protein was set as 1.

IE1 cooperates with IE2 to promote transcriptional activation of the viral early genes at low MOI infection (Gawn and Greaves, 2002; Greaves and Mocarski, 1998). Besides interfering JAK-STAT signalling as mentioned above, IE1 also antagonises apoptosis (Zhu et al., 1995), activates p53-related cell cycle arrest (Castillo et al., 2005) and ND10-related transcription silencing (Korioth et al., 1996; Sanchez and Spector, 2008). The experiment described in section 4.4 is a preliminary 3-hour analysis of unfractionated peptides. Further biological repeats of this sample are required, in order to generate a

kinetic analysis of ΔUL145 with higher resolution. If viral gene regulation, JAK-STAT signalling, cell cycle regulation, or anti-apoptosis emerges to be related to UL145, IE1 should also be taken into consideration.

4.5.2. A delayed, transient IFNβ transcription up-regulation was observed in ΔUL145 infection

In Figure 4.10 & Figure 4.11, more IFNβ transcripts were detected in ΔUL145 infection compared to WT at 24 hpi, when normally in WT infection IFNβ transcription had already been dampened. If this observation repeated in several more replicate experiments, it might suggest that UL145 deletion caused higher IFNβ transcriptional activity, or weaker suppression of IFNβ induction as discussed in subsection 4.3.1. If UL145 deletion led to higher transcriptional activity, higher IFNβ should be detected at 24 hpi, but this was not the case in the 2 independent ELISAs I performed, where ΔUL145 did not lead to more IFNβ secretion at 24 hpi (Figure 4.10). Overall from the present data, it is possible to speculate that UL145 might contribute to suppression of IFNβ induction before 24 hpi, although, again this requires further experiments to validate.

The IFNβ transcriptional up-regulation seen with UL145 deletion seemed to be short-lived and transient. As in Figure 4.12, the IFNβ induction seemed non-existent on RNA level at 30 hpi in both WT and ΔUL145 infection. And in Figure 4.23, the decline of these ISGs at 48 and 72hpi might correlate with the decrease of IFNβ at later time points. However, there is still the possibility that UL145 deletion resulted in higher IFNβ induction at later time points post 24 hpi. More work should be done to understand how UL145 regulates IFN induction over time, and future experimental plans are discussed in subsection 6.3.2.

4.5.3. Mechanism of HLTF in anti-HCMV interferon activation

How HLTF restricts early HCMV infection has yet to be fully elucidated, but current results have pointed to the possibility of differences in IFN induction. Studies with

shHLTF cell lines showed that loss of HLTF impaired IFNβ transcriptional induction at 6 hpi, and this regulation was limited to a very short time frame with WT virus inducing more IFNβ mRNA in shHLTF cells at 12 hpi (Figure 4.13). Nonetheless, the transcriptional regulation affected overall IFNβ production at 24 hpi (Figure 4.14), suggesting HLTF's role in IFNβ activation during early HCMV infection. However, these experiments have only been done once and will require repeating.

In Figure 4.14, gene knock out of HLTF by CRISPR seemed to impair IFNβ production. However, the lab established that there was significant biological variability between independent monoclonal CRISPR HFFF-TERT cell lines. Lior Soday from the Weekes lab established that out of 8 monoclonal control CRISPR cell lines, substantial differences in early GFP expression were observed in restriction assays (experimental design for these assays shown in Figure 4.1). Upon infection with Merlin-strain UL36-GFP HCMV (MOI 0.1, 24h), she observed up to 20-fold difference in the percentage of infection between control cell lines (0.2%-4%). In an attempt to validate results in Figure 4.14, Dr. Katie Nightingale found that the two monoclonal CRISPR control cell lines produced a significantly varied amount of IFNβ during HCMV infection. When infected two control CRISPR cell lines with Merlin HCMV (MOI 1, 24 h), one control cell line produced 97 pg/ml IFNβ, while the other CRISPR HLTF cell line secreted 1152 pg/ml IFNβ, suggesting that one of the CRISPR control cell line did not have an adequate antiviral response.

Several reasons may contribute to different infection outcome with different monoclonal CRISPR control cell lines. Off-target effects in CRISPR has been widely discussed (Zhang et al., 2015). It is possible that off target effects of the control CRISPR guide RNA may lead to suppression of certain antiviral genes. This off target effect may be augmented by stable overexpression of Cas9 (Zhang et al., 2015). Furthermore, to generate monoclonal CRISPR cell lines, an isolated cell has to be passaged for an extended long time, which might create more opportunities for CRISPR system to introduce mutations. Therefore, instead of monoclonal CRISPR cell lines, polyclonal CRISPR cells as demonstrated in Figure 4.1 might be more reliable, although there may be concerns about stability of knockdown in this situation. Alternatively, a CRISPR system with an inducible promoter driving Cas9 could be adapted, or Cas9 protein and gRNA could be introduced into cells by electroporation. Furthermore, having established

a system without ongoing expression of Cas9 and gRNA, inducible expression of the knocked-out gene could be established in independent knockout clones, facilitating comparison of cells expressing different levels of the gene of interest on a monogenic background.

HLTF has the preference of binding 3' ends of ssDNA (Kile et al., 2015), which are created with abundance during HCMV DNA replication. ChIP results also demonstrated that HLTF associated with viral DNA at 72 hpi, although unselectively (Figure 4.19). A series of reporter assays in Figure 4.15 suggested that HLTF was not part of IFNβ induction signalling pathway downstream of viral sensing. Therefore, HLTF is likely to be detecting HCMV replicating DNA and triggering IFN response. Whether this contributes to the transient IFNβ up-regulation seen in ΔUL145 infection requires further investigation of ΔUL145 induction with shHLTF cells. Further experimental plans are discussed in subsection 6.3.2.

Chapter 5. Refining protein degradation screens

Previously, the lab had developed a systematic approach to actively search for human proteins that are degraded during HCMV early infection, which included proteomics and transcriptomic analysis (Section 1.5.). With high confidence, a shortlist of 35 host proteins enriched in antiviral restriction factors (host proteins with the ability to inhibit early viral infection), were identified. Harnessing the ability of the proteasome inhibitor MG132 and lysosome inhibitor Leupeptin, the previous inhibitor screen identified 53 proteins rescued by one drug or the other at 12 h post-infection, 8 of which were anti-HCMV restriction factors known to be degraded by HCMV. Due to documented off-target effects of MG132 and Leupeptin (Tsubuki et al., 1996; Yasuma et al., 1998), the application of these broad, non-selective, potent inhibitors helped us generate a comprehensive list of proteins targeted for degradation by HCMV, rather than elucidate the precise pathway of degradation of each protein during HCMV infection. I therefore investigated the effects of a selective protease inhibitor, Bortezomib, and two lysosome protease inhibitors E64 and CA-074, aiming to systematically determine the mechanism(s) of host protein degradation during HCMV infection.

5.1. Proteosomal degradation

This part of the project represents a collaborative work performed with Dr. Katie Nightingale and Lior Soday. Dr. Katie Nightingale performed the infection, treatment, and the sample collection. She also completed a preliminary 3-h mass spectrometry analysis to check the quality of the samples. I processed the samples with high pH-based peptide fractionation and enriched peptide samples for a 36-h mass spectrometry analysis by the CIMR proteomics core. Lior Soday processed the mass spectrometry RAW data into protein abundance signal:noise values and I carried out all of the subsequent detailed data analysis and interpretation.

MG132 is a peptide aldehyde that potently blocks the proteolytic activity of the 26S proteasome and thus has been widely used as an agent to disrupt proteasome activity (Kisselev and Goldberg, 2001). Peptide aldehydes are substrate analogues of the chymotrypsin-like domain of proteasomes as well as cysteine proteases such as cytosolic calpains and several lysosomal cathepsins (Chapman et al., 1997). Although 10-fold higher concentrations are required, MG132 inhibits cathepsins and calpains (Tsubuki et al., 1996), indicating that the proteins rescued by MG132 might be degraded via lysosome. Adding to the complexity, MG132 has been linked to ER-stress-induced autophagy (Bao et al., 2016; Wang et al., 2019). In order to identify proteins that are truly processed by proteasome, a proteasome inhibitor with higher selectively is required. The drug selected, Bortezomib, covalently binds to catalytic core of 26S proteasome with increased specificity, which is mediated by the boronate group of the drug (Groll et al., 2006). It is now in use for the treatment of multiple myeloma, and its use for the treatment of other malignancies is being explored (Kubiczkova et al., 2014).

5.1.1. Optimising Bortezomib concentration

Bortezomib has been used in human cell line experiments to inhibit proteasome activity, however, different studies have employed different concentrations, ranging from 0.1 µM to 20 µM (Chui et al., 2019; Price et al., 2011). Our first task was to find an appropriate Bortezomib concentration to match with MG132 in HFFF-TERT infection model. The ratio comparing protein abundance with and without inhibitor during HCMV infection was used to determine inhibitor efficacy. Ratios obtained from different concentrations of Bortezomib treatment were compared to those from 10 µM MG132 treatment, the condition employed in our previous study (Figure 1.11A). Here I was hoping to identify a pattern that had a linear correlation with a slope close to 1 and a relatively high correlation coefficient (r^2).

Three concentrations of Bortezomib were first tested: 50 nM, 150 nM, and 500 nM. For each protein, ratios of (HCMV with Bortezomib) / HCMV and (HCMV with MG132) / HCMV were compared to quantify the relative efficacy of protein rescue. The trend of

linear correlation and slope of the trend line both increased with increasing Bortezomib concentration (Figure 5.1). Three higher concentrations: 500nM, 1 µM, and 2 µM, were then tested. Similar trends were observed when Bortezomib concentration increased (Figure 5.2). These three higher concentrations all demonstrated high correlation coefficients, and the 2 µM Bortezomib treatment was chosen for further analysis and comparison with 10 µM MG132 because the trend line slope was the nearest to 1.

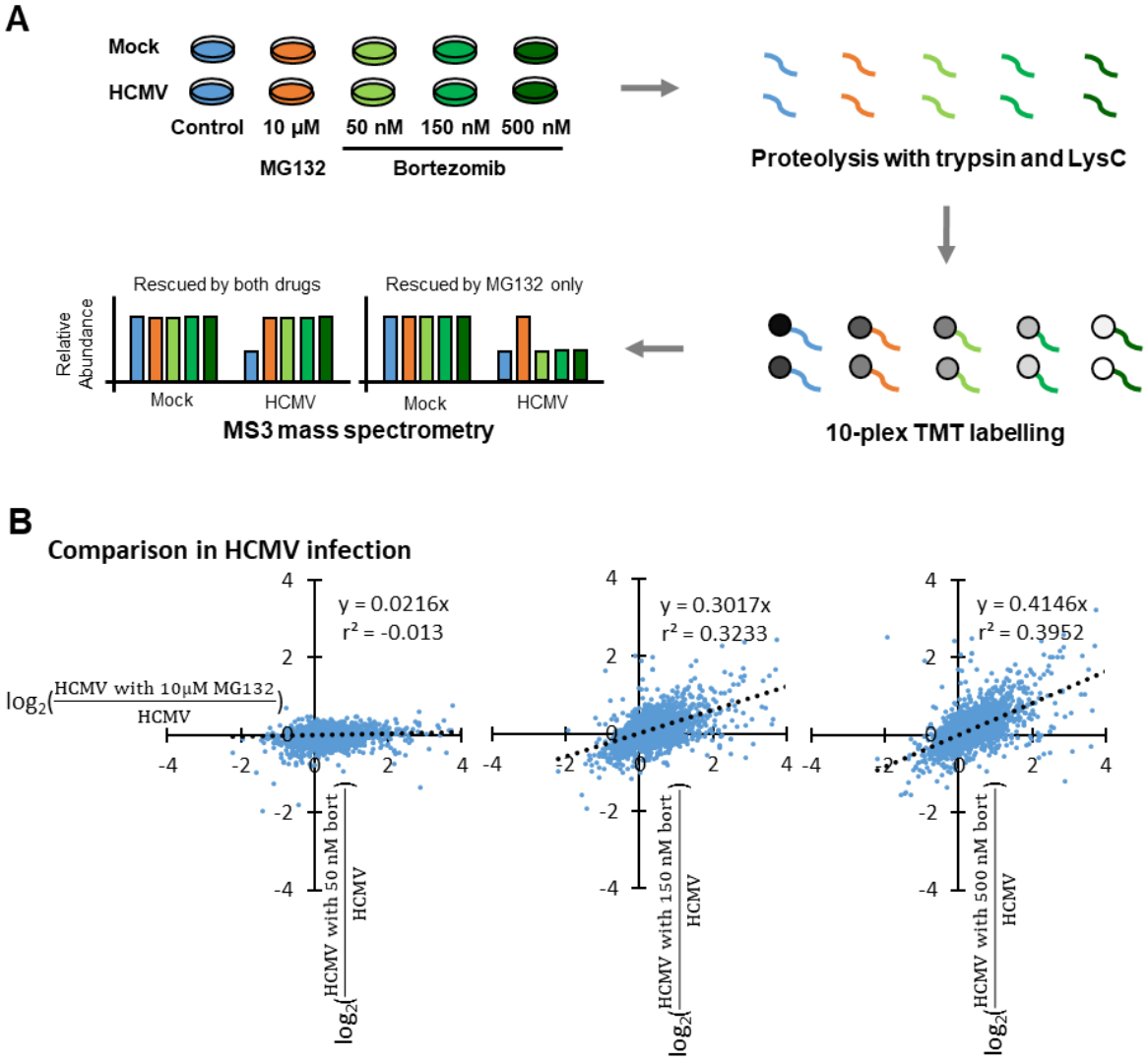

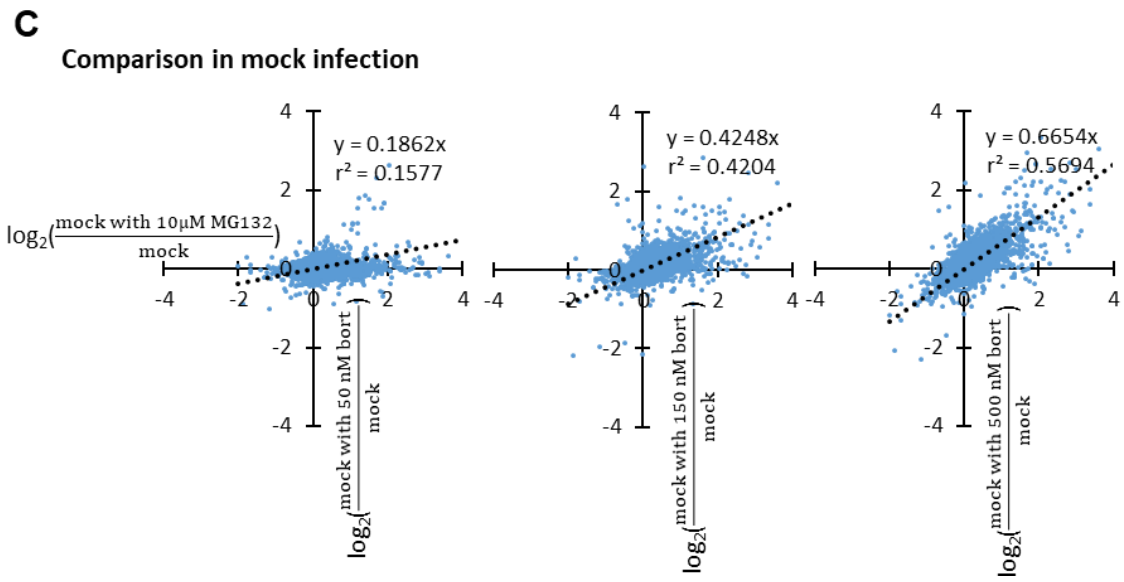

Figure 5.1. Optimisation of Bortezomib concentration by comparison with 10 μM MG132.

(A) Schematic of the experimental workflow. HFFF-TERT cells were infected with Merlin strain HCMV (MOI 5) or mock infected for 24 h. Cells were treated with 10 μM MG132, 50 nM, 150 nM or 500 nM Bortezomib 12 h prior to harvest. Whole cell lysates were digested into peptides, which were labelled with TMT reagents followed by MS3 mass spectrometry. (B&C) Log_2 (fold change of protein abundance) between the presence and the absence of proteasome inhibitor during (B) HCMV infection and (C) mock infection

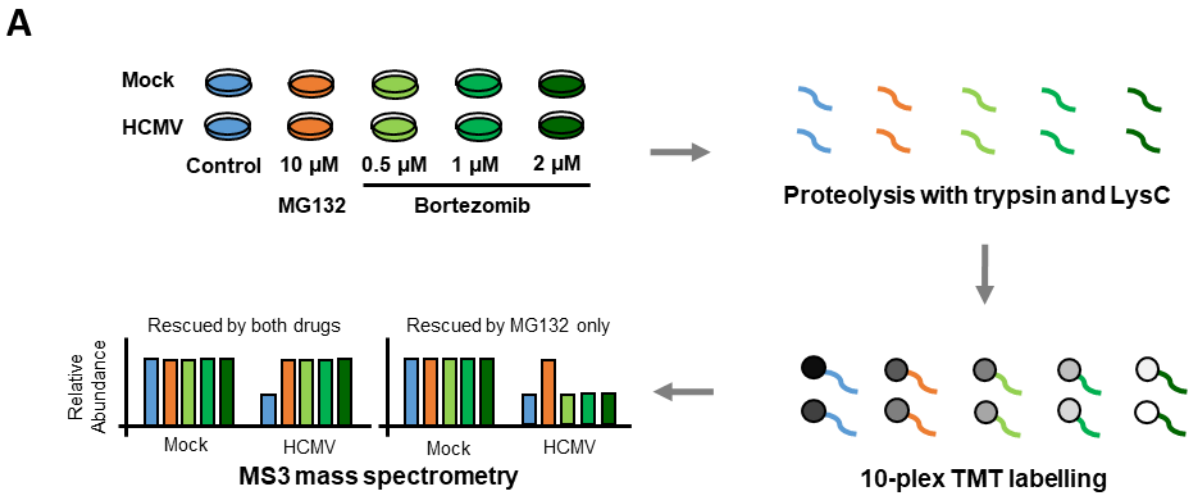

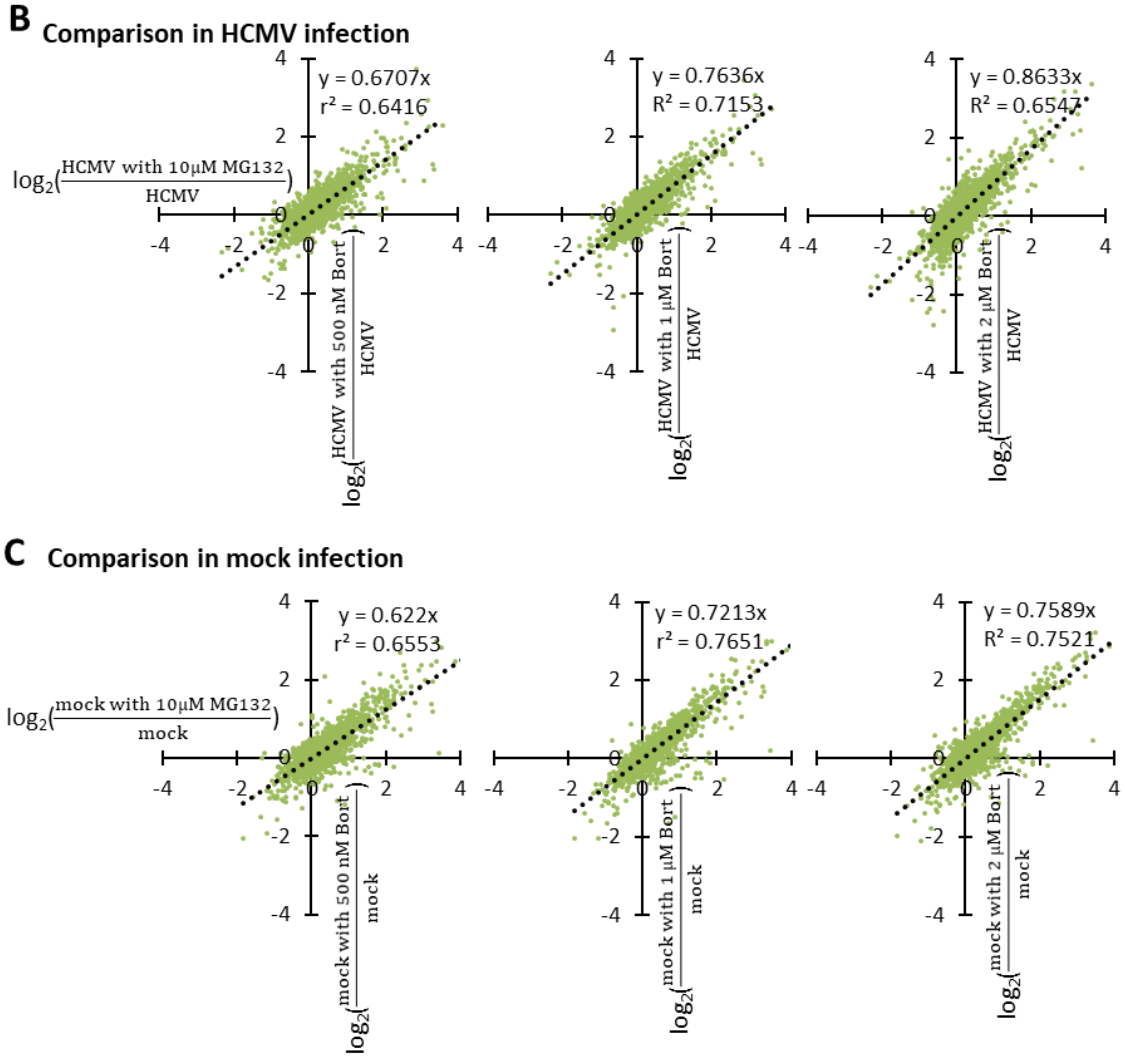

Figure 5.2. Second optimisation of Bortezomib concentration by comparison with 10 µM MG132

(A) Schematic of the experimental workflow. HFFF-TERT cells were infected with Merlin strain HCMV (MOI 5) or mock infected and simultaneously treated with 10 µM MG132, 500 nM, 1 µM or 2 µM Bortezomib. Whole cell lysates were digested into peptides, which were labelled with TMT reagents followed by MS3 mass spectrometry. (B&C) Log_2 (fold change of protein abundance) between the presence and the absence of proteasome inhibitor during (B) HCMV infection and (C) mock infection

5.1.2. Multiple host proteins are targeted for proteasomal degradation early during HCMV infection

To build a detailed mechanistic picture of host protein degradation early during HCMV infection, experimental samples including the 2 µM Bortezomib condition were

subjected to high pH-based peptide fractionation, and each fraction analysed by MS3-based mass spectrometry (Figure 5.1). Overall, 7192 host proteins were quantified, 145 of which were down-regulated >1.5-fold (with $p<0.01$) compared to mock infection. MG132 and Bortezomib 'rescue ratios' were calculated for each protein, obtained by comparing protein abundance during HCMV infection +/- inhibitor with protein abundance during mock infection +/- inhibitor (Figure 5.3). This ratio enabled us to identify proteins with increased expression under drug treatment more during infection compared to mock, rather than proteins with high turnover rate naturally.

Proteins rescued by both MG132 and Bortezomib

For simplicity and consistency with the previous study (Figure 1.11A), a ratio of 1.5-fold with $p<0.01$ was set as a cut-off to determine whether the proteins were rescued by each inhibitor. Under these criteria, 64/145 (44%) of proteins were considered to be rescued by either protease inhibitor, which is in line with our previous finding. More than half (34/64, Figure 5.3 red dots) of these proteins were rescued by both drugs (

Table 5.1). Notably, this group contains several HCMV restriction factors reported previously, such as nuclear domain 10 (ND10) components SP100, MORC3, DAXX, cell cycle regulating protein ANAPC1 (Figure 5.3B) (Schreiner and Wodrich, 2013; Sloan et al., 2016; Tavalai et al., 2011; Weekes et al., 2014). HLTF was also rescued by both MG132 and Bortezomib, validating the findings in section 3.1.

Proteins rescued by either MG132 and Bortezomib only

Thirty proteins were identified to be rescued by MG132 or Bortezomib only. Of proteins exhibiting a greater rescue ratio with Bortezomib compared to MG132 (Figure 5.3 purple dots), 8/9 (89%) exhibited MG132 rescue ratios >1.25 but <1.5 (examples in Figure 5.3 bottom panel & Figure 5.4,

Table 5.2), suggesting that nearly all proteins in this class were in fact rescued by both inhibitors. The one exception was LIM domain-containing protein AJUBA, whose MG132 rescue ratio was 1.16 in this data (Figure 5.3C bottom panel), but was 1.48 in our previous MG132 screen; these differences may reflect relatively poor quantitation by

only two or one peptides, respectively in the two experiments. In conclusion, no proteins were rescued by Bortezomib but not MG132, reflecting the selectivity of Bortezomib.

Twenty-one proteins exhibited a greater degree of rescue with MG132 compared to Bortezomib (Figure 5.3, yellow dots). Thirteen (62%) of them exhibited Bortezomib rescue ratios of >1.25 and <1.5, suggesting that many of this group of proteins may nevertheless be proteasomally degraded. These included the PDZ domain containing protein 11 (PDZD11) and transcriptional repressor BEN domain containing 3 (BEND3) (Figure 5.4, Table 5.3). In contrast, 8/21 proteins appeared genuinely to be selectively rescued by MG132 but not Bortezomib (Bortezomib rescue ratio <1.25), including the fibroblast growth factor receptor Golgi glycoprotein 1 (GLG1), E3 ligase neural precursor cell expressed, developmentally down-regulated 4 (NEDD4) and carbohydrate sulfotransferase 14 (CHST14) (Figure 5.3 middle panel, Table 5.3).

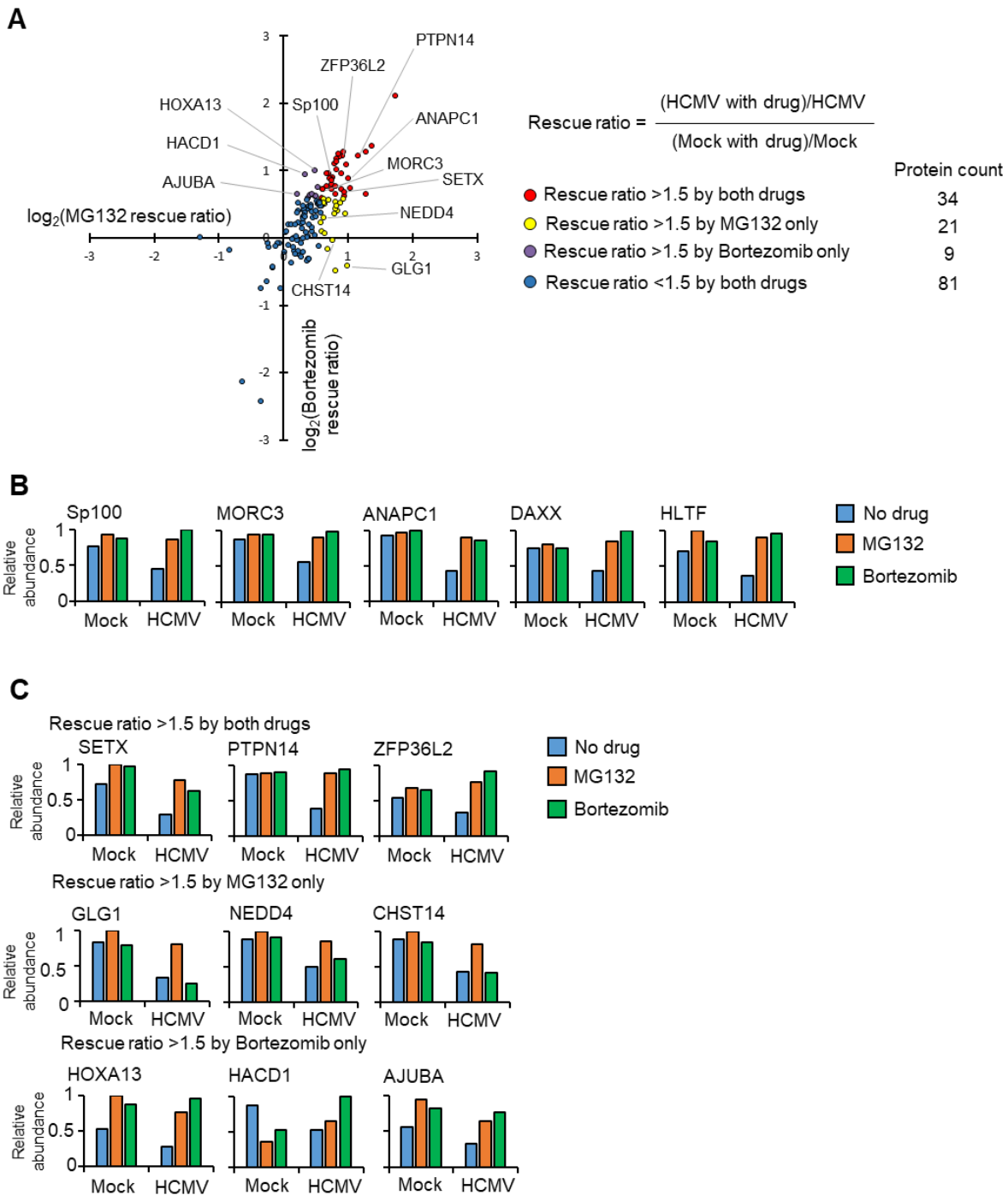

Figure 5.3. Identification of proteins targeted for degradation by HCMV using an inhibitor-based proteomic screen.

(A) Results of the inhibitor-based screen. All 145 proteins downregulated >1.5 fold are plotted, with down regulated proteins divided into 4 groups using rescue ratios of >1.5 as cut-offs. The table shows the number of proteins in each group. For rescue ratios, the denominator (mock with drug)/mock was limited to a minimum of 1 to prevent artificial ratio inflation. (B) Examples of positive controls from the existing literature that were validated in this screen. (C) Examples of degraded proteins rescued by both inhibitors (top panels), MG132 only (middle panels), or Bortezomib only (bottom panels).

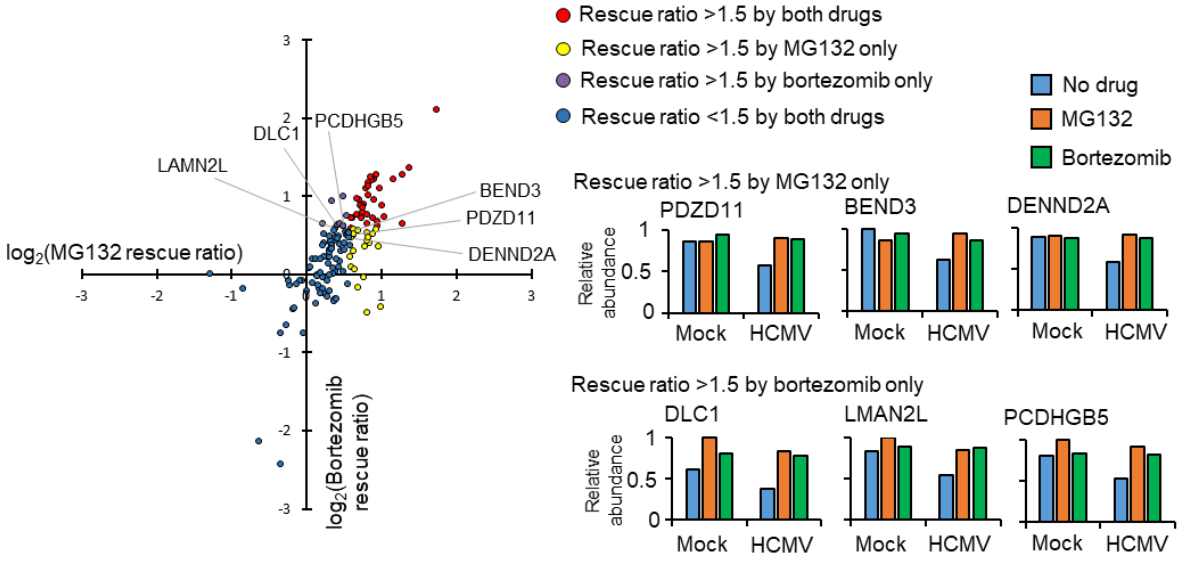

Figure 5.4. "Borderline" proteins rescued by both MG132 and Bortezomib identified.
Examples of proteins exhibiting rescue ratios >1.5 with only one of two inhibitors, but a rescue ratio between 1.25 – 1.5 fold with the other inhibitor.

Table 5.1. Host proteins rescued by both MG132 and Bortezomib.
Proteins with rescue ratio >1.5. The number of peptide quantified shows how well the proteins is quantified. Benjamini-Hochberg adjusted significance A values were used to estimate p values.

Protein Name	Peptides Quantified	MG132 rescue ratio	MG132 rescue ratio p-value	Bortezomib rescue ratio	Bortezomib rescue ratio p-value
CFLAR	1	3.34	1.50E-22	4.30	1.01E-21
MLKL	1	2.58	6.75E-15	2.58	2.24E-10
CITED2	3	2.43	2.37E-13	1.57	1.31E-03
FRMD6	5	2.42	2.83E-13	2.42	2.83E-09
PTPN14	4	2.23	2.48E-11	2.33	1.25E-08
CTGF	8	2.05	2.05E-09	1.67	3.16E-04
ANAPC1	5	2.00	5.29E-09	1.84	2.61E-05

SNX16	1	1.97	1.10E-08	2.13	2.64E-07
LAYN	2	1.93	2.78E-08	1.53	2.30E-03
SETX	4	1.92	3.29E-08	1.61	8.02E-04
HOXA11	1	1.90	5.85E-08	2.43	2.49E-09
ZFP36L2	5	1.88	9.61E-08	2.32	1.41E-08
ZMYND11	3	1.87	1.07E-07	1.94	5.36E-06
RPS6KA4	4	1.86	1.46E-07	1.65	4.37E-04
DAXX	4	1.83	2.94E-07	2.29	2.08E-08
FAM101B	2	1.81	4.01E-07	2.38	5.52E-09
RGL2	1	1.78	9.46E-07	2.01	1.71E-06
HLTF	7	1.77	1.09E-06	2.19	9.91E-08
TFAP4	1	1.77	1.15E-06	2.26	3.39E-08
STK32B	2	1.76	1.37E-06	1.70	2.16E-04
MEN1	3	1.75	1.53E-06	1.56	1.49E-03
ZBED1	3	1.73	2.48E-06	2.14	2.31E-07
MED20	1	1.70	5.12E-06	1.86	1.97E-05
TCEAL4	14	1.69	6.50E-06	1.83	3.08E-05
TADA1	1	1.68	7.24E-06	1.73	1.28E-04
RALGPS2	1	1.67	8.67E-06	1.81	4.19E-05
TOX	3	1.67	9.16E-06	1.64	4.74E-04
GLS-3	2	1.64	1.70E-05	1.83	2.78E-05
CCDC71L	2	1.63	2.37E-05	1.93	6.43E-06
RGCC	1	1.59	4.61E-05	1.71	1.88E-04

SP100	10	1.59	4.63E-05	1.95	4.88E-06
MORC3	6	1.52	1.96E-04	1.64	4.68E-04
CDC42EP3	4	1.52	2.09E-04	1.64	4.74E-04
ARHGAP35	21	1.51	2.38E-04	1.51	3.03E-03

Table 5.2. Host proteins with greater Bortezomib rescue ratio.
Proteins with Bortezomib rescue ratio >1.5 and MG132 rescue ratio <1.5 are listed here.

Protein Name	Peptides Quantified	MG132 rescue ratio	MG132 rescue ratio p-value	Bortezomib rescue ratio	Bortezomib rescue ratio p-value
SUGP2	14	1.45	8.64E-04	1.69	2.42E-04
RBPMS	13	1.41	1.66E-03	1.53	2.23E-03
PCDHGB5	3	1.41	1.85E-03	1.53	2.26E-03
HOXA13	1	1.41	1.89E-03	2.00	2.20E-06
NACC2	1	1.36	4.08E-03	1.57	1.28E-03
DLC1	6	1.33	7.53E-03	1.54	1.89E-03
LMAN2L	1	1.31	1.12E-02	1.51	3.23E-03
HACD1	1	1.26	2.38E-02	1.91	8.13E-06
AJUBA	2	1.16	1.01E-01	1.57	1.35E-03

Table 5.3. Host proteins with greater MG132 rescue ratio.
Proteins with MG132 rescue ratio >1.5 and Bortezomib rescue ratio <1.5 are listed here.

Protein Name	Peptides Quantified	MG132 rescue ratio	MG132 rescue ratio p-value	Bortezomib rescue ratio	Bortezomib rescue ratio p-value
DENND2A	2	1.54	1.34E-04	1.49	3.86E-03
FAM126A	1	1.91	4.15E-08	1.48	4.39E-03
ZNF668	1	1.62	2.67E-05	1.47	5.36E-03
NLGN2	1	1.75	1.74E-06	1.45	6.70E-03
PCDHGB2	2	1.85	1.97E-07	1.44	8.19E-03
PKNOX1	1	1.55	1.12E-04	1.43	8.36E-03
PDZD11	1	1.55	1.08E-04	1.42	1.01E-02
AHR	1	1.77	1.09E-06	1.39	1.46E-02
BEND3	4	1.51	2.77E-04	1.39	1.50E-02
PCDHGC3	2	1.76	1.31E-06	1.34	2.59E-02
DIMT1	1	1.78	7.75E-07	1.32	3.28E-02
RNF150	2	1.73	2.80E-06	1.28	5.49E-02
CNTNAP1	3	1.94	2.09E-08	1.28	5.66E-02
DAPK2	1	1.54	1.29E-04	1.22	1.02E-01
NEDD4	10	1.50	3.04E-04	1.16	1.86E-01
ADAMTS1	9	1.52	2.25E-04	1.07	4.44E-01
WWP2	1	1.56	9.93E-05	1.04	5.32E-01
CHST14	1	1.70	4.95E-06	0.98	8.38E-01
DKK3	3	1.61	3.27E-05	0.89	7.93E-01
GLG1	16	1.98	8.68E-09	0.75	2.81E-01

GLT8D1	6	1.75	1.76E-06	0.71	1.94E-01

5.1.3. Three proteins rescued by MG132 only were also rescued by Leupeptin

The reproducibility of results enabled me to interpret proteomics data better and reject poorly quantified data as discussed above. Since treatments of 500 nM and 1 µM Bortezomib had similar effects compared to 10 µM MG132, results from these conditions were used as biological replicates to assess the reproducibility of results from 2 µM Bortezomib. As shown in Figure 5.5, Bortezomib truly did not have effects on the down-regulation of GLG1, CHST14, and NEDD4 while MG132 rescued their down-regulation previously. A closer look along with our previous MG132/Leupeptin screen revealed that these were the proteins whose down-regulation was reversed by Leupeptin and were regarded as proteins degraded by lysosomes (Figure 5.5). Interesting, these proteins are membrane-associated, likely became parts of intracellular vesicles eventually fused with lysosomes, either through endocytosis and autophagy mechanisms, during early HCMV infection.

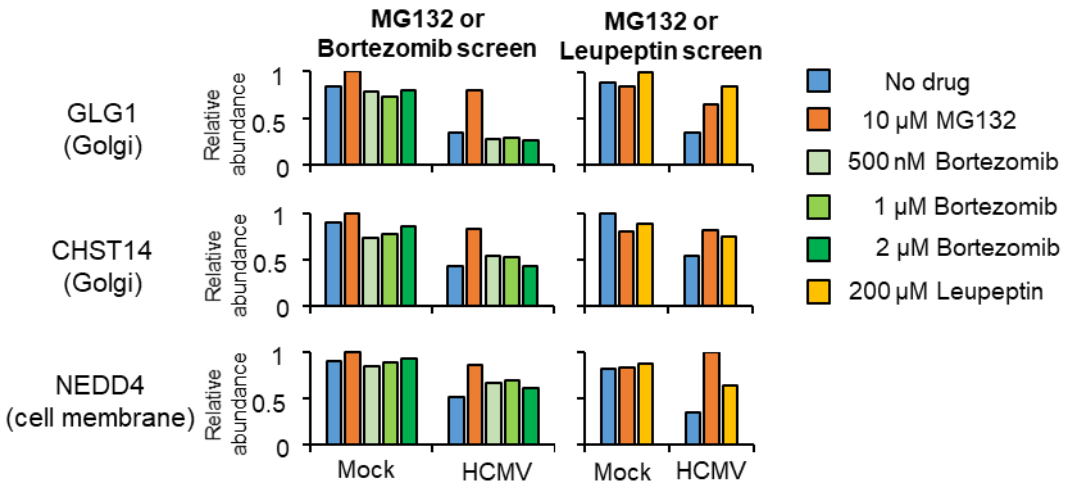

Figure 5.5. Proteins rescued by MG132 but not Bortezomib were also rescued by Leupeptin.
Results for GLG1, CHST14 and NEDD4, proteins selectively rescued by MG132 but not Bortezomib. The left hand panels show data from the complete

MG132/Bortezomib screen and the right hand panels show the MG132 (10 μM) /Leupeptin (200 μM) screen (12 hpi) from the previous investigation (Figure 1.11).

5.1.4. A shortlist of proteins degraded via proteasome during early HCMV infection

In the previous MG132/Leupeptin screen (Figure 1.11A), 46 proteins were identified to be proteasomally degraded within 12 h of HCMV infection (Appendix table 1). Of these 46 proteins, 24 exhibited increased degradation in HCMV-infected cells compared with mock infection in the pSILAC screen (Figure 1.11B). Additionally, 13/46 proteins belonged to the gene cluster that were down-regulated at protein level but not transcript in the RNA/protein screen (Figure 1.11C). 7 of these 13 proteins were also identified to be degraded during HCMV infection by pSILAC screen (Appendix table 4). Of the 46 proteins rescued by MG132 at 12 hpi, 30 proteins was validated by pSILAC screen, or RNA/protein screen, or both. These 30 proteins were searched against the MG132/Bortezomib screen generated in this section. Seventeen out of these 30 proteins were rescued by both MG132 and Bortezomib, with rescue ratios >1.25 and $p<0.01$ (Table 5.4). Other "hits" with unidentified roles in HCMV infection were mixed lineage kinase domain-like protein (MLKL), tyrosine-protein phosphatase non-receptor type 14 (PTPN14), ribosomal protein S6 kinase alpha-4 (RPS6KA4), Ras-specific guanine nucleotide-releasing factor 2 (RALGPS2), and Rho GTPase-activating protein 35 (ARHGAP35).

Table 5.4. Proteins identified to be proteasomally degraded during HCMV infection.

Four screens were developed to search for proteins that were degraded during HCMV infection via proteasome. The first screen, MG132/Leupeptin screen, selected proteins with MG132 rescue ratio >1.5 and p<0.01 at 12 hpi. The second screen selected proteins that had 50% higher degradation rate (Kdeg) during HCMV infection compared to mock (r_{deg} >1.5 if $Kdeg_{mock}$<0, FC_{HCMV}>1.5 if $Kdeg_{mock}$>0). The third screen defined a group of proteins that were downregulated at protein level. Fold changes of protein and RNA at 24 hpi are listed here. RNA FC= RNA abundance at 24 hpi/RNA abundance at mock infection. Protein FC=protein abundance at 24 hpi/protein abundance at mock infection. Rescue ratios from MG132 and Bortezomib treatments were explained in Figure 5.3. FC=fold change, N/A=not available because it was not quantified.

Screen	MG/Leu	pSILAC	RNA/Protein		MG/Bort	
Protein name	**MG132 rescue ratio**	**r_{deg} or FC_{HCMV}**	**RNA 24h FC**	**Protein 24h FC**	**MG132 rescue ratio**	**Bort rescue ratio**
MLKL	2.49	11.43	2.86	N/A	2.58	2.58
PTPN14	3.29	1.77	0.72	0.20	2.23	2.33
ANAPC1	3.43	10.60	2.60	0.20	2.00	1.84
RPS6KA4	2.34	2.43	0.77	0.61	1.86	1.65
HLTF	3.02	1.76	1.88	0.35	1.77	2.19
RALGPS2	2.85	5.69	1.03	N/A	1.67	1.81
SP100	2.11	3.40	1.54	0.56	1.59	1.95
MORC3	2.21	2.57	1.69	0.52	1.52	1.64
ARHGAP35	3.02	4.20	1.07	0.25	1.51	1.51
CNTNAP1	2.15	2.61	0.27	0.42	1.94	1.28
ARMC9	2.41	N/A	0.53	N/A	1.56	1.39
BEND3	2.14	N/A	14.93	0.47	1.51	1.39
LMAN2L	4.65	N/A	1.39	0.51	1.31	1.51
ANAPC4	2.56	5.32	1.78	N/A	1.47	1.42
ANAPC5	2.55	4.63	1.29	0.33	1.38	1.28

MAP3K2	2.05	N/A	1.56	0.32	1.33	1.37
NEDD4L	2.35	N/A	2.00	0.37	1.27	1.48

5.2. Lysosomal degradation

The work presented in this section was performed by myself. I designed and performed the experiments and prepared TMT-labelled peptides samples for a 3-h mass spectrometry analysis by the CIMR proteomics core. I subsequently carried out all the data analysis and interpretation.

Lysosomes generally contain several cysteine peptidases of the papain family, namely cathepsins B, H, L, and S (Turk et al., 2012). Leupeptin is a natural occurring lysosome inhibitor extracted from a strain of *Streptomyces exfoliates* that inhibits cysteine proteases as well as serine proteases, resulting in nonselective inhibition (Suda et al., 1972). In search of a selective cysteine protease inhibitor, E64 was discovered from another fungus *Aspergillus japonicas* (Kazunori Handa, 1978). E64 potently inhibits cathepsin B and cathepsin L in an irreversible manner (Towatari et al., 1991). CA-074 is the methyl ester derivative of E64 that was developed to selectively inhibit cathepsin B but not cathepsin L (Murata et al., 1991). They are used alongside with Leupeptin to identify proteins that are degraded via lysosomes during early HCMV infection in this project.

5.2.1. Optimising cathepsin inhibitor concentration

E64 and CA-074 have been used in cell-based experiments to restrict autophagy via cathepsin inhibition (Montaser et al., 2002; Zhang et al., 2006). To find the optimal concentration for our HFFF-TERT HCMV infection model, I tested three concentrations of E64 and CA-074 against 200 µM Leupeptin, the condition used in the previous MG132/Leupeptin screen (Figure 5.6).

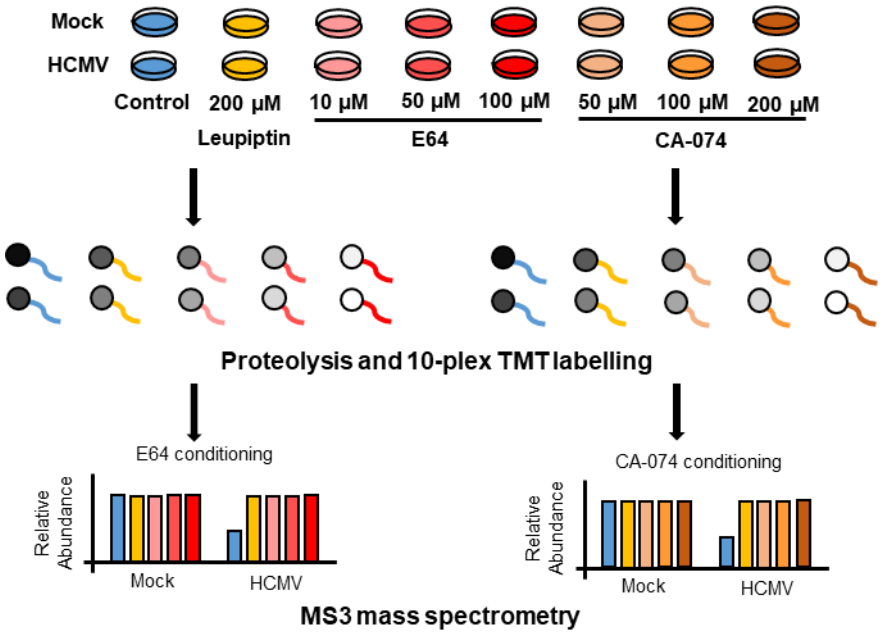

Figure 5.6. Schematic of optimisation of cathepsin inhibitor concentration. HFFF-TERT were infected with Merlin strain HCMV at MOI of 5. Cells were treated with serum-free DMEM for 24 h prior to infection. Inhibitors were added to the cells from the point of infection. Proteins were harvested 12 hpi and split into two groups for proteolysis and TMT labelling. Labelled peptides underwent a 3-h mass spectrometry and data analysis reveal how well each treatment performed compared to 200 µM Leupeptin.

A ratio comparing protein abundance with or without inhibitor treatment during HCMV infection was derived to monitor the efficacy of each concentration compared to 200 µM Leupeptin. Dot plots with linear trend lines were generated to estimate the correlation between treatments (Figure 5.7). All comparison showed positive correlation with r^2 values between 0.36-0.5, possibly because lysosome inhibitors did not influence the expression of many proteins during HCMV infection. Nevertheless, 100 µM E64 and 100 µM CA-074 were chosen because their comparison trend line had the slope closet to 1 with the highest r^2.

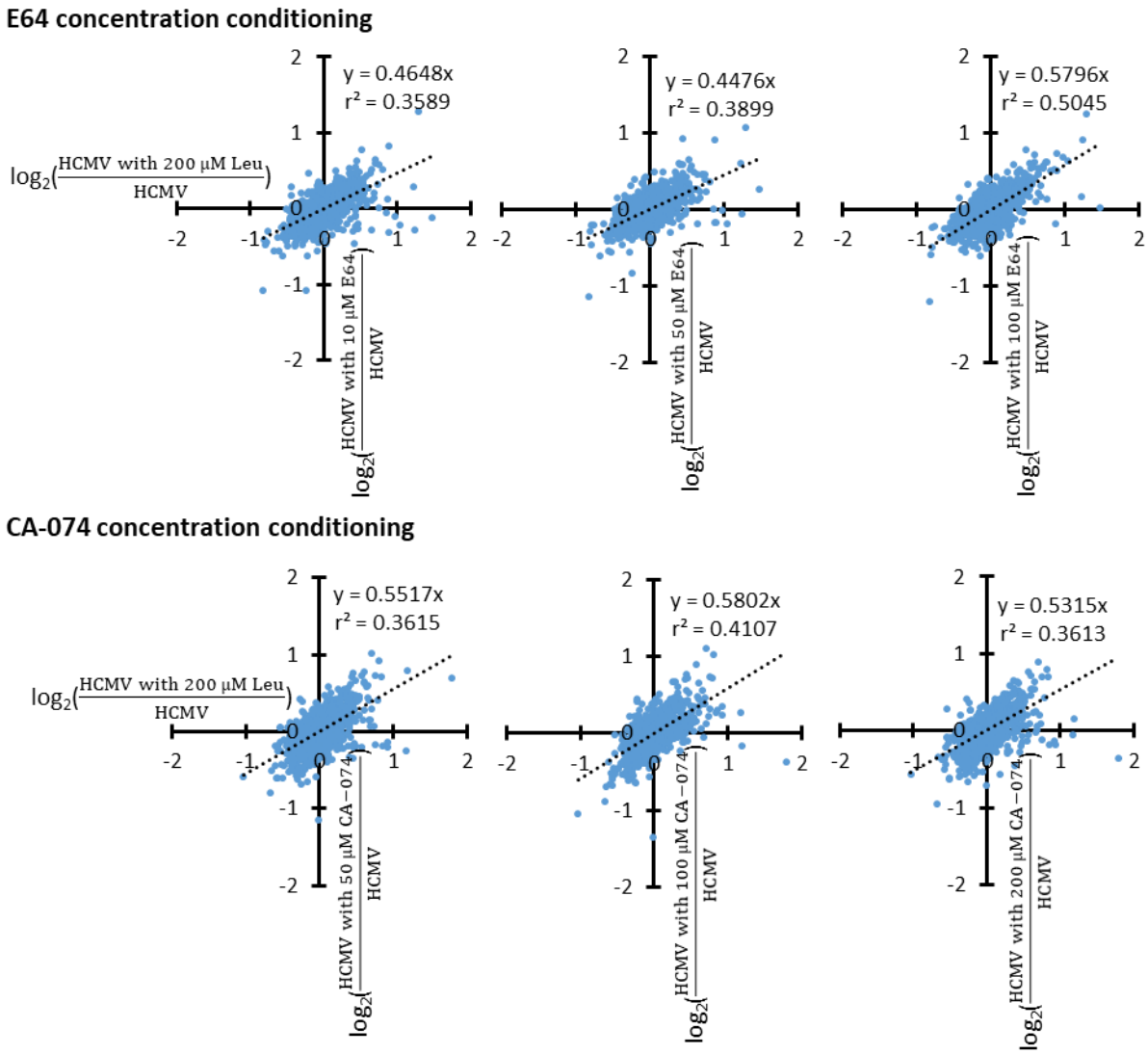

Figure 5.7. Optimisation of cathepsin inhibitor concentration.
Log_2 (fold change of protein abundance) between the presence and the absence of lysosome inhibitor during HCMV infection

5.2.2. Identification of proteins degraded via lysosome during HCMV infection

In order to search for proteins that were lysosomally degraded during HCMV infection, cells were treated with Leupeptin, CA-074, or E64 simultaneously with HCMV infection. Cells were harvested at 12 hpi and TMT-based mass spectrometry analysis was performed. Overall, 1676 proteins were quantified, including 2657 host proteins and 19 HCMV proteins.

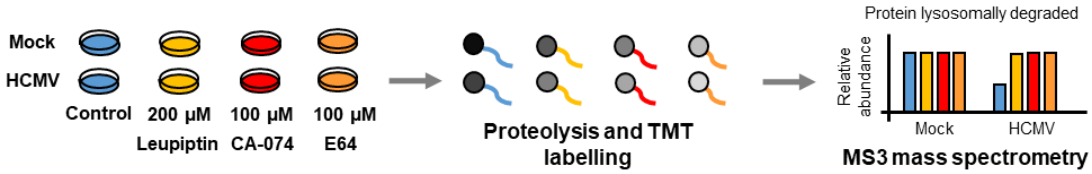

Figure 5.8. Schematic of the Leupeptin/cathepsin inhibitor screen.
Cell cycle synchronised HFFF-TERT were infected with HCMV (non-GFP) at MOI of 5 and treated with inhibitors simultaneously. Proteins were harvested 12 hpi for proteolysis and TMT labelling. Labelled peptides underwent a 3-h mass spectrometry analysis.

Efficacy of cathepsin inhibitors

The efficacy of each cathepsin inhibitor was compared again with 200 μM Leupeptin. Surprisingly, CA-074 performed just as well as Leupeptin, reaching a trend line slope nearly to 1 and relatively high r^2. Even though E64 also performed much better than the conditioning experiments, the trend line slope indicated that it was less effective compared to 200 μM Leupeptin and 100 μM CA-074 (Figure 5.9). Therefore, CA-074 was selected to screen proteins that were degraded via lysosome.

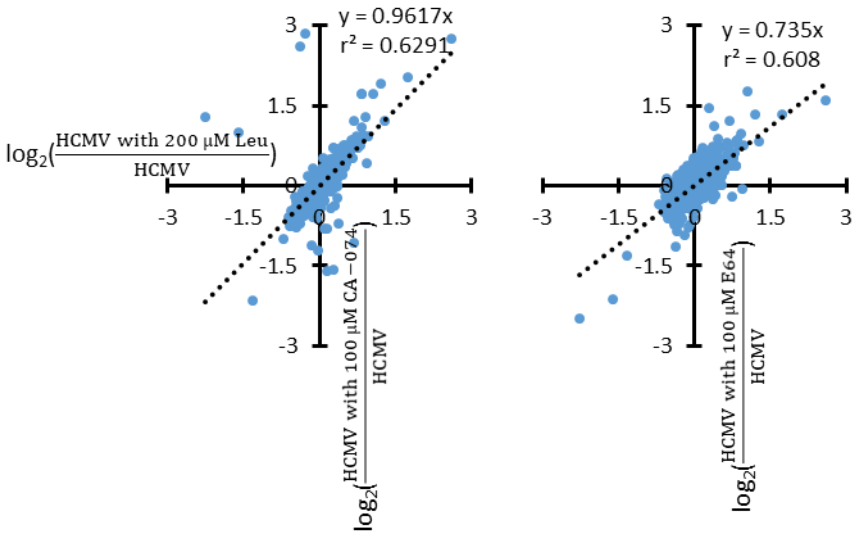

Figure 5.9. Efficacy of 100 µM CA-074 and E64 compared to 200 µM Leupeptin during HCMV infection.
Log_2(fold change of protein abundance) between the presence and the absence of lysosome inhibitor during HCMV infection. Trend lines were generated along with their slope and coefficient of correlation.

Finding proteins rescued by Leupeptin and CA-074

Among the 2657 host proteins quantified, 70 proteins were downregulated by HCMV infection at least by 30% with p-value <0.05. Rescue ratios of these proteins by Leupeptin and CA-074 were compared (Figure 5.10). 65/70 of these down-regulated proteins were not affected by either Leupeptin or CA-074. Four proteins had Leupeptin rescue ratio>1.25 (p<0.05), two were also rescued by CA-074 (rescue ratio>1.25, p<0.05). The downregulations of heterogeneous nuclear ribonucleoprotein U (HNRNPU) and RNA binding motif protein 4 (RBM4) were rescued by both Leupeptin and CA-074. The two nuclear proteins might be processed through autophagy.

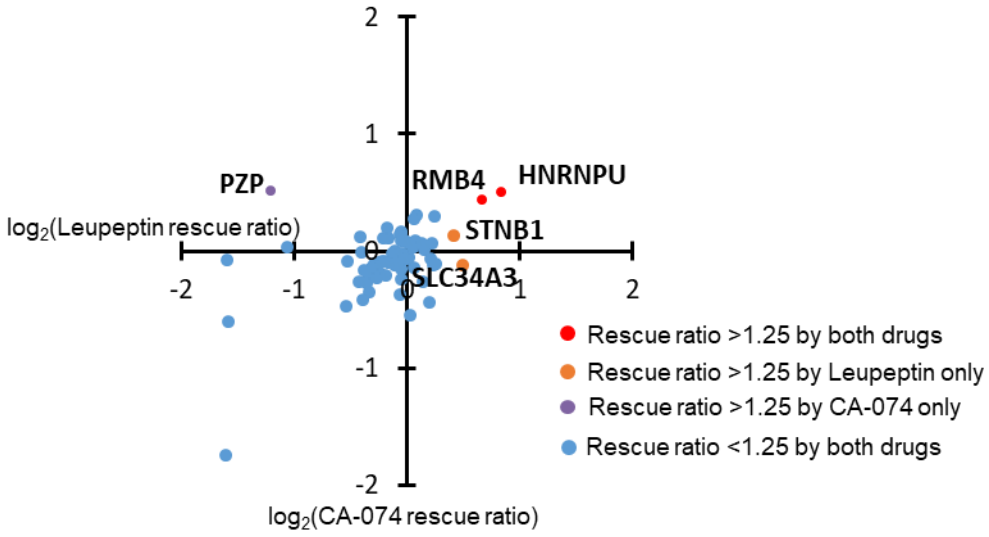

Figure 5.10. Identification of proteins targeted for lysosomal degradation by HCMV.
Results of crossing lysosomal inhibitor-based screens. All 70 proteins downregulated >1.3 fold are plotted, with down regulated proteins divided into 4 groups using rescue ratios of >1.25 as cut-offs (p<0.05). For each given protein, the Leupeptin rescue ratio (x-axis) are plotted against the CA-074 rescue ratio (y-axis) here.

5.2.3. Proteins previously identified to be lysosomally degraded

MG132/Leupeptin screen

In the previous MG132/Leupeptin screen, 12 proteins were identified to be rescued by Leupeptin at 12 hpi. All of them unfortunately were not quantified in this screen.

MG132/Bortezomib screen

GLG1, CHST14 and NEDD4 are membrane proteins suggested to be degraded via the lysosome (Figure 5.5). Unfortunately, they were not quantified in this experiment. In the previous 12 h MG132/Leupeptin screen (Figure 1.11A), 8033 proteins were quantified and 12 (0.15%) proteins were identified to be rescued by Leupeptin (rescue ratio>1.5 and $p<0.01$). In the current dataset performed with unfractionated peptide samples, a similar percentage (0.15%, 4/2657) of quantified proteins was identified to be rescue by Leupeptin (rescue ratio>1.25 and $p<0.05$). I would expect to identify ~12 proteins rescued by Leupeptin with fractionated peptide sample analysis and a smaller proportion would be expected to be rescued by CA-074. Upon fractionated analysis of an optimised experiment, it would be anticipated that the lysosomal degradation of GLG1, CHST14, or NEDD4 during HCMV infection would be validated.

5.3. Discussion

5.3.1. How to consider a rescue ratio significant?

In the MG132/Bortezomib screen, the fold change cut-off of 1.5 was adapted for both downregulation by HCMV, and rescue by either inhibitor, however it had the effect of excluding proteins with 'borderline' rescue ratios of >1.25 but <1.5. 39/81 proteins with MG132 and Bortezomib rescue ratios <1.5 exhibited rescue ratios for MG132 or Bortezomib or both that were nevertheless >1.25, suggesting that this group of proteins included some candidates that were downregulated by degradation. Therefore the p-value of a given rescue ratio estimated by significance A was taken into consideration

(subsection 2.4.7). The significance A algorithm calculates p values according to the distribution of all the rescue ratios measured in an experiment, fitting ratios to a normal distribution but with separate standard deviation estimates for ratios greater and less than 1 to account for global differences in protein up- or down-regulation. A rescue ratio of 1.5 would have a more significant p-value estimated by significance A value if the inhibitor induces fewer changes. For instance, in the MG132/Bortezomib screen, to achieve significance A $p<0.01$, the MG132 rescue ratio needed to be >1.32, in comparison to a Bortezomib rescue ratio of >1.42.

There are several other factors to help determine the confidence in a measurement. For example, one should always be cautious about when interpreting measurement derived from a single quantified peptide. Similar rationale is applied to the calculation of significance B p value, which adjusts significance A value according to the ion intensity measurement when there are >700 proteins identified (proteins are grouped into sets of 350 proteins based on ion intensity). As always, biological replicates boost the reliability of an experiment. Now the lab and I have generated 3 datasets detailing protein changes in MG132-treated HCMV infection at 12 hpi. Those proteins that have been routinely identified as targets of virus-mediated proteasomal degradation, including HLTF and PTPN14, are the top targets to investigate their roles in HCMV infection.

5.3.2. Proteasomal degradation is the major protein degradation pathway during HCMV infection

HCMV orchestrates the regulation of host gene expression to facilitate viral replication while evading immune defences. At 12 h of HCMV infection, 2-5% of host proteins were down-regulated for more than 1.5 fold (369/7688 in temporal analysis of HCMV-infected whole cell lysate published in (Weekes et al., 2014), 281/8034 in MG132/Leupeptin screen, and 146/7162 in MG132/Bortezomib screen). I was interested in proteins degraded at this time point because within 12 h of infection HCMV needs to circumvent intrinsic barriers such as cytosolic viral DNA sensor cGAS and viral transcription repressor SP100 to produce immediate early proteins and initiate viral replication.

MG132 is a less selective proteasomal inhibitor than Bortezomib, having previously been reported to inhibit lysosomal degradation pathways via inhibition of calpains and cathespsins (Kisselev and Goldberg, 2001), in addition to the proteasome. In the previous MG132/Leupeptin screen (Figure 1.11A), 75% (9/12) of proteins rescued by Leupeptin at 12 h of infection were also rescued by MG132. The usefulness of comparing this broad proteasomal/lysosomal inhibitor with the specific proteasomal inhibitor Bortezomib is the identification that 62-85% (using 1.25 or 1.5 as rescue ratio cut off respectively) of proteins rescued by MG132 were also rescued by Bortezomib, suggesting that the proteasome is the predominant route for early protein degradation during HCMV infection. Overall, of all downregulated proteins, 44% (64/145 using 1.5 as the cut-off)-59% (85/145 using 1.25 as the cut-off) were rescued by at least one of MG132 or Bortezomib. Previously Dr. Katie Nightingale calculated the median protein half-life of 58.4 h in uninfected fibroblasts with pulsed SILAC (Figure 1.11B). HCMV is characterised with a prolonged replication cycle (>72 h). It is possible that in order to downregulate certain proteins, HCMV must employ degradative pathways in order to achieve sufficiently rapid change in protein abundance.

Comparison of data from this study with the previous transcriptional analysis of host gene expression during infection (Figure 1.11C) suggested that 54% of the 81 proteins with MG132 and Bortezomib rescue ratios <1.5 were more than 1.5-fold transcriptionally downregulated, which would be expected to be a major mechanism of protein downregulation in the absence of degradation. In the previous RNA/protein screen (Figure 1.11C), 1%–5% of proteins were degraded and also had reduced mRNA levels, suggesting that multiple regulatory mechanisms may be employed by HCMV for effective control of certain targets. For example, gap junction alpha-1 protein (GJA1) has been reported to be degraded in the proteasome (Stanton et al., 2007). Even though the current MG132/Bortezomib screen did not identified GJA1 as a down-regulated protein, possibly because it was only quantified by a single peptide, previous MG132/Leupeptin and pSILAC screens confirmed that GJA1 was degraded during HCMV infection. The RNA-seq data suggested that GJA1 was also transcriptionally downregulated (Figure 5.11).

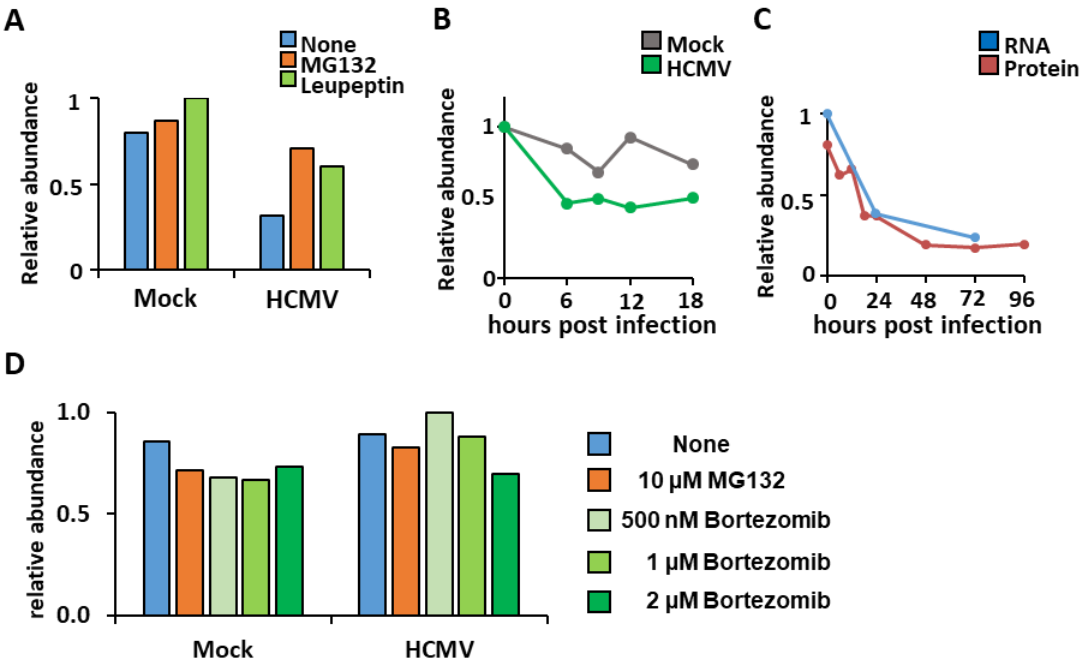

E

Screen	Quantified peptide
MG132/Leupeptin	9
pSILAC	5
RNA/Protein	11
MG132/Bortezomib	1

Figure 5.11. GJA1 results from 4 screens.
GJA1 results from (A) MG132/Leupeptin screen (Figure 1.11A), (B) pSILAC analysis (Figure 1.11B), (C) RNA/protein screen (Figure 1.11C), and (D) MG132/Bortezomib (Figure 5.2A) are shown here. (E) Numbers of peptides identified in each proteomic experiments are listed.

5.3.3. Lysosomal degradation during HCMV infection

Studies have shown that membrane proteins are targeted for lysosomal degradation during HCMV infection. HCMV latency-associated UL138 targets the multidrug resistance protein 1 (MRP1, ABCC1) for lysosomal degradation (Weekes et al., 2013). Four members of the US12 gene family contribute to the HCMV evasion from natural killer (NK) cells. For example, US18 and US20 concordantly target the membrane protein B7-H6 that serves as the infection alert molecule to NK cells for lysosomal degradation (Charpak-Amikam et al., 2017; Fielding et al., 2017). Besides degradation, HCMV also

sequesters plasma membrane proteins in the cytosol to evade NK cell immunosurveillance. For example, HCMV UL141 retains the poliovirus receptor in the endoplasmic reticulum, inhibiting cell-surface expression and preventing interaction with activating NK receptor DNAM-1 (Prod'homme et al., 2010; Tomasec et al., 2005; Weekes et al., 2014).

Data here identified that 8 proteins rescued by MG132 but not Bortezomib had a membrane origin. Certain proteins were exclusively degraded by a non-proteasomal route, including GLG1 and CHST14. Extension of these inhibitor studies to examining membrane-enriched samples, for example samples enriched for plasma membrane proteins (Weekes et al., 2013; Weekes et al., 2014) would therefore be of substantial interest, and may identify a distinct degradative route for proteins originating from these compartments. Autophagy delivers intracellular protein cargos to the lysosomes while integral membrane proteins reach lysosomes through endocytic pathway (Yang and Klionsky, 2010).

Besides disposal of protein aggregates and damaged organelles, lysosomal degradation pathways serve a much broader function, including the regulation of cell signalling, metabolism, pathogen clearance, and immune responses. For example, mammalian target of rapamycin complex 1 (mTORC1) kinase complex regulates lysosome activity in response to amino acid deprivation (Laplante and Sabatini, 2012). When levels of leucine and arginine are low, mTORC1 cannot dock on the lysosome membrane to be activated (Bar-Peled et al., 2012). Transcription factor EB (TFEB) is dephosphorylated and translocates to the nucleus where it functions as a master gene regulator of lysosome biogenesis (Hesketh G.G., 2018). Lysosomal regulation of the antiviral immune response has been established with autophagy. Toll/interleukin-1 receptor homology (TIR) domain containing adaptor molecule 1 (TRIF1) is an adaptor that associates with endosomal dsRNA toll-like receptor 3 (TLR3) and activates NFκB for the synthesis of inflammatory cytokines and interferon regulatory factors (IRFs) (Lee and Kim, 2007). TRIF is targeted by selective autophagy by the tripartite motif-containing protein 32 (TRIM32)-human T-cell leukemia virus 1 TAX1 protein (TAX1)-binding protein 1 (TAX1BP1) complex for degradation upon induction of poly(I:C) and LPS (Yang et al., 2017).

Chapter 6. Discussion

6.1. Identification of novel antiviral factor

Viruses need to resolve many restrictions imposed by host cells to replicate successfully. Before infectious particles enter cells, a panoply of factors are in place to hinder viral infection, with roles in sensing of pathogen-associated molecular pattern (PAMP), antiviral response through interferon (IFN) and the inflammasome via direct antiviral activity. As the paradigm of viral evasion and persistent infection, HCMV is an excellent model to study the host-pathogen interface and search for novel antiviral factors.

6.1.1. Proteasomally degraded proteins as antiviral factors

The previous and my current inhibitor screens were designed on the basis that HCMV targets antiviral factors for degradation via proteasome. Previously, employing three orthogonal proteomic screens 35 proteins were identified to be degraded during HCMV infection with high confidence (Appendix table 4). Of these 35 proteins, 9 proteins (MLKL, PTPN14, ANAPC1, RPS6KA4, HLTF, RALGPS2, SP100, MORC3, ARHGAP35) passed the selection of MG132/Bortezomib screen (using rescue ratio >1.5 and $p<0.01$ as selection criteria for both MG132 and Bortezomib). Three of them (ANAPC1, SP100, MORC3) are known anti-HCMV restriction factors (Kim et al., 2011; Sloan et al., 2016; Tran et al., 2010a). Although the mechanism of HLTF restricting HCMV infection is not fully elucidated, my results have suggested that HLTF may be restricting early HCMV infection by regulating type I IFN induction. Besides HLTF, the function of mixed lineage kinase domain-like protein (MLKL) was explored by Alice Fletcher-Etherington in the lab. HCMV tegument protein UL36 was found responsible for degradation of MLKL and this helps the subversion of necroptosis in infected cells (Fletcher-Etherington et al., 2020). With majority of the proteins on the list having antiviral roles, the remaining four proteins (PTPN14, RPS6KA4, RALGPS2, ARHGAP35) may have undiscovered antiviral potential, and should be investigated for this.

Interestingly, these proteins have been associated with regulation of cell growth and tumorigenesis. Non-receptor tyrosine phosphatase 14 (PTPN14) and Rho GTPase-activating protein 35 (ARHGAP35) both negatively regulate yes-associated protein 1 (YAP1) (Frank et al., 2018; Liu et al., 2013), which inhibits the nuclear retention of YAP and decreases the YAP-dependent cell growth and proliferation (Meng et al., 2016; Zhao et al., 2007). The YAP1 pathway has been shown to contribute to tumorigenesis of oncogenic herpesviruses including EBV and KSHV (He et al., 2017; Kang et al., 2018; Liu et al., 2015). Degradation of PTPN14 and ARHGAP35 might result in YAP1-mediated cell growth and proliferation. Function of Ras-specific guanine nucleotide-releasing factor 2 (RALGPS2) is poorly understood but it has been loosely implicated with cytoskeleton remodelling (Ceriani et al., 2007). Mitogen- and stress-activated kinase 2 (MSK2, RPS6KA4) is the downstream effector of extracellular signal-regulated kinases 1/2 (ERK1/2) and p38 mitogen-activated protein kinase (p38 MAPK) (Wiggin et al., 2002). Less apoptosis was observed in RPS6KA4 knockout mice when treated with epidermal growth factor or ultraviolet C radiation (Wiggin et al., 2002). Loss of RPS6KA4 might be a method HCMV has adapted to subvert apoptosis. Besides antagonising intrinsic and innate immune responses, HCMV reprograms numerous host pathways such as metabolic signalling pathways, programmed cell deaths, and cell cycle progression to create an optimal environment for viral replication. HCMV infection is known to arrest cells in the G0/G1 phase to allow viral gene expression (Fortunato et al., 2002; Salvant et al., 1998). Virally induced cell cycle arrest seems to contradict to what has already been proposed for the loss of PTPN14, ARHGAP35, or RALGPS2. Their roles in HCMV infection require further investigation.

6.1.2. Other strategies HCMV adapts to manipulate host factors

In addition to degradation of host proteins, HCMV also mislocalises host factors to achieve the optimal replication environment. For example, HCMV glycoprotein UL37 directly associates with IFN-inducible viperin resulting in translocation from the endoplasmic reticulum to the mitochondria. There fatty acid metabolism is inhibited, which benefits viral envelope acquisition and virion release, thus enhancing infection at late stage (Seo and Cresswell, 2013; Seo et al., 2011). In addition, HCMV modulates the

IFN induction pathway by misplacing host factors such as innate nuclear viral DNA sensor IFI16 and key adaptor protein STING (Dell'Oste et al., 2014; Fu et al., 2017). HCMV glycoprotein UL16 retains natural killer (NK) receptor NKG2D ligands in the endoplasmic reticulum (ER) and cis-Golgi apparatus while glycoprotein UL144 retains NK receptor DNAM-1 ligand poliovirus receptor in the ER, contributing to the evasion immunosurveillance and cytotoxicity imposed by NK cells (Dunn et al., 2003; Tomasec et al., 2005). By 24 h of HCMV infection, such sequestered proteins were downregulated >2-fold from the plasma membrane (PM) analysis but were not downregulated in whole cell lysates analysis (Weekes et al., 2014). Overall, this trend was observed for only 1.6% of PM proteins, suggesting that the predominant mechanism HCMV employs to downregulate proteins during the early phase of infection is proteasomal degradation.

6.2. Viral DNA sensors

Sensing viral DNA has been regarded as a key event during initiation of antiviral innate immune response. The recognition of viral dsDNA results in the activation of an array of signalling cascades that ultimately lead to the production of IFNs and pro-inflammatory cytokines. Besides the IFN induction discussed in Chapter 1, the inflammasome pathway contributes to the production and secretion of inflammatory cytokines interleukin (IL) 1β and IL18 (Guo et al., 2015). Absent in melanoma 2 (AIM2) is the main inflammasome sensor that detects intracellular DNA. AIM2 binds to viral DNA with pyrin and HIN-20 domain, which subsequently activates caspase-1, acting as the protease that cleaves pro-IL1β pro-IL18 into mature IL1β and IL18 (Lugrin and Martinon, 2018). Even though AIM2 inflammasome is triggered by MCMV infection (Rathinam et al., 2010), it is functionally attenuated in HCMV infection since IE2 protein inhibits transcription and induces degradation of the pro-IL1β (Botto et al., 2019). This coincided with the preliminary result of a beads-based ELISA assay (subsection 2.2.4) I performed with supernatant of HCMV-infected cells that IL1β was barely detected. Therefore, IFNβ production was the main readout when studying HLTF-mediated antiviral response.

6.2.1. Redundancy of viral DNA sensors

Although not yet convincing, my data showed that UL145 and HLTF might regulate IFNβ induction during HCMV infection. One potential explanation for the difficulties I encountered exploring the possibility of HLTF becoming a viral DNA sensor might be the functional redundancy among several reported receptors. IFI16, cyclic GMP-AMP synthase (cGAS), DNA-dependent activator of IFN-regulatory factor (DAI), DEAD-box helicase 41 (DDX41), DNA-dependent protein kinase (DNA-PK) all detect viral DNA and trigger IFNβ transcription through activation of STING-TANK-binding kinase 1 (TBK1)-interferon regulatory factor 3 (IRF3) axis (Dempsey and Bowie, 2015). One of the remaining open questions is whether these sensors work cooperatively. Their functions are addressed with RNA interference (RNAi)-based cells and gene knock out mice individually in different host type with different stimuli, yet a systematic approach to address their functions in a single viral infection is lacking. Such cooperation has been proposed with DDX41 and IFI16, which both react to DNA transfection and HSV1 infection in human monocyte THP-1 cells (Unterholzner et al., 2010; Zhang et al., 2011). The fact that IFI16 is upregulated transcriptionally while DDX41 expression stays the same throughout the course of DNA transfection and HSV1 infection leads to the hypothesis that DDX41 might be more important in the initial sensing while IFI16 takes over this function at later stage (Unterholzner, 2013).

If HLTF is one of the viral DNA sensors, its functional redundancy should be considered with IFI16, the viral DNA sensor that recognises foreign DNA in the nucleus (Stratmann et al., 2015), since HLTF was found predominately expressed in the nucleus (Figure 3.4). In 2012, Gariano *et al.* demonstrated that transduction of IFI16 increased IFNβ production during HCMV infection in human embryonic lung fibroblasts (HELF) cells (Gariano et al., 2012). To determine whether IFI16 requires HLTF to induce IFNβ, an experiment could be envisaged whereby HLTF was depleted using siRNA with concomitant overexpression of IFI16 (i.e. via lentivirus / adenovirus), then infection with HCMV for 24 h. If HLTF cooperates with IFI16 in IFNβ induction, depletion of HLTF should impair IFNβ transcript production.

6.2.2. Is HLTF a *bona fide* viral DNA sensor?

Several findings in Chapter 4 led to the hypothesis that HLTF might be a viral DNA sensor, but more work needs to be done to first validate that HLTF modulates IFNβ induction during HCMV infection. Furthermore, two key questions need to be addressed before identifying HLTF as a *bona fide* viral DNA sensor, should HLTF's regulation of IFNβ transcription be confirmed.

One of the questions is about whether HLTF associates with HCMV DNA. Intracellular DNA sensors are assumed to have the ability to discern exogenous DNA from a cell's own genome. To date, no clear rationale has been provided to explain how the viral DNA sensor distinguish between host and foreign DNA. RNA polymerase III specifically recognises AT-rich dsDNA, which is not a common feature of dsDNA virus genome (Ablasser et al., 2009; Chiu et al., 2009). Structural analysis of IFI16 DNA binding domain reveals that IFI16 binds to the dsDNA sugar-phosphate backbone, suggesting a viral detection regardless of genome sequence (Jin et al., 2012). As a dsDNA repair protein, DNA-PK specifically binds to ends of dsDNA during IFNβ induction (Ferguson et al., 2012). HLTF contains a HIRAN (HIP116, Rad5p, N-terminal) domain that associates specifically to the 3'-end of ssDNA (Achar et al., 2015; Hishiki et al., 2015; Kile et al., 2015), but how this feature coordinates viral DNA sensing remain elusive.

The other question is how HLTF activates the signal cascade that eventually results in IRF3 phosphorylation. IFI16, DDX41, and cGAS all achieve this through interacting with STING. IFI16 and DDX41 both directly binds to STING even though they do not share any domain homology, while cGAS synthesises a secondary messenger cyclic guanosine monophosphate–adenosine monophosphate (cGAMP) to communicate with STING (Sun et al., 2013; Unterholzner et al., 2010; Zhang et al., 2011). When studying UL145-mediated HLTF degradation, I performed immunoprecipitation of endogenous HLTF in MG132 treated HFFF-TERT (Figure 3.7). During that experiment, components identified associated with HLTF were not previously reported related to IFN induction signalling transduction. Nonetheless, there is possibility that HLTF associates with IFN induction signalling molecules such as STING and IRF3. In order to immuneprecipitate HLTF and its associated proteins during HCMV infection, I propose a SILAC-based

immunoprecipitation analysis of HLTF during ΔUL145 virus infection, which may help discover which signalling proteins are co-opted to signal infection.

6.3. Future work for this project

6.3.1. How does UL145 degrade HLTF?

In this project I identified UL145 to be responsible for HCMV-mediated HLTF degradation. In collaboration with Dr. Katie Nightingale, we discovered that the CUL4A E3 ligase complex is subverted by UL145 to degrade HLTF. Recently, UL145-mediated STAT2 degradation was characterised and the interaction between STAT2, UL145, and CRL4 adaptor protein DDB1 was identified (Le-Trilling et al., 2020). It is possible that UL145 uses the same mechanism to target HLTF, however I lack convincing evidence to demonstrate the interaction between HLTF and UL145. Unexpectedly, the IP experiment in which I identified the interaction between HLTF and UL145 was performed by immunoprecipitating endogenous as opposed to overexpressed, HA-tagged HLTF. The interaction between UL145 and HLTF was identified in 293T cells by SILAC but not conventional IP, suggesting that the affinity between HLTF and UL145 might be weak, or alternatively that UL145 degraded HLTF indirectly and did not bind to HLTF.

To determine whether HLTF and UL145 interact directly, I propose to perform fluorescence resonance energy transfer (FRET) microscopy. FRET is a distance-dependent physical process in which a donor fluorophore in its excited state non-radioactively transfers its excitation energy to a neighbouring acceptor fluorophore, thereby causing the acceptor to emit its characteristic fluorescence (Bajar et al., 2016). Since FRET is only observed when a donor fluorophore and an acceptor fluorophore are within the 1–10 nm range, the fluorophores can be conjugated with proteins to identify protein association (Miyawaki, 2011). In a cell expressing both cyan fluorescent protein (CFP) tagged UL145 and yellowish-green fluorescent protein (YFP) tagged HLTF, if UL145 and HLTF interact, YFP signal could be observed when given CFP excitation energy.

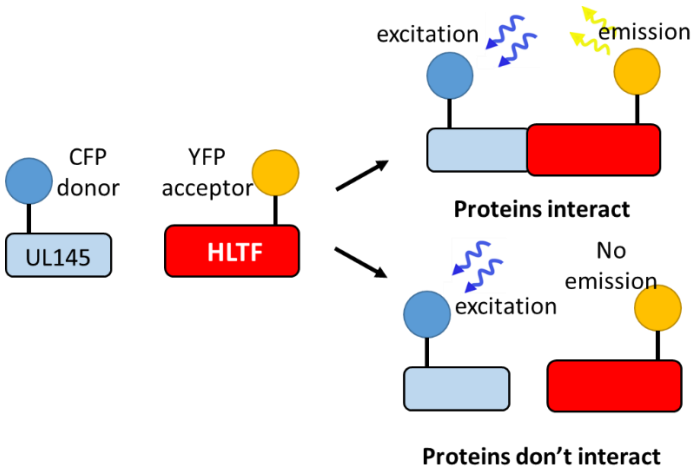

Figure 6.1. Diagram of a FRET assay examining UL145 and HLTF interaction. UL145 is fused with CFP (donor fluorophore) and HLTF is fused with YFP (donor fluorophore). If UL145 interacts with HLTF, triggering CFP results in YFP emission. IF the two proteins do not interact, no YFP signal can be observed.

However, this method requires overexpression of fluorescent protein-tagged HLTF, which in my own experience was difficult. Overexpressing HLTF might result in cell death, therefore HLTF should be driven by a conditionally regulated promoter (i.e. tetracycline regulated promoter) instead of a constitutively active promoter (spleen focus-forming virus promoter [pSFFV] was used in current experiments). If a tet-regulated system could overcome the difficulty in HLTF overexpression, it can be used in FRET microscopy and HLTF IP as previously described (subsection 3.3.2).

6.3.2. Confirmation that UL145 regulates IFNβ induction and investigation of mechanism

Temporal analysis of infection with the UL145 deletion virus suggested that UL145 might regulate IFNβ production during HCMV infection at later time points (Figure 4.22). The first follow up experiment should be an ELISA comparing WT and ΔUL145 at multiple time points throughout HCMV infection. If an increase of IFNβ production in ΔUL145 infection was validated and the acting timeframe identified, corresponding RT-qPCR should be performed to see whether UL145 regulates IFNβ induction at the transcriptional level. These assays should subsequently be repeated with shHLTF cell

lines. If HLTF participates in UL145-mediated IFNβ regulation, knocking down the HLTF gene should attenuate the up-regulation of IFNβ in ΔUL145 infection.

6.3.3. RNA/protein screen at earlier time points

In the MG132/Bortezomib screen, a shortlist of proteins that were degraded through proteasome was identified. Although incomplete, the analysis of fractionated peptides in the Leupeptin/CA-074 screen has the potential to identify host proteins degraded by lysosomes during HCMV infection. Together these screens broaden our view on HCMV-mediated protein degradation. The aim of these screens were to investigate how host proteins were down-regulated during infection. Previously the RNA/protein screen published in Nightingale *et al.* (Nightingale et al., 2018) identified that ∼18% of proteins downregulated >3-fold within 24 hr of infection were regulated primarily by mRNA levels (Figure 1.11C). However, the corresponding transcriptomic analysis at early time points is lacking. Currently the earliest time point of the RNA/protein screen is 24 hpi and all of the inhibitor screens were performed with 12 hpi samples. Therefore, a RNA/protein screen coupling RNA-sequencing and whole cell lysate proteomic analysis at multiple time points prior to 24 hpi (6, 12, 18 hpi) would provide further orthogonal data for comparison to the earlier inhibitor-based screens.

6.4. Concluding remarks

This work combined multiplexed proteomic techniques with proteasomal and lysosomal inhibitors, in search of host proteins that were actively degraded during HCMV infection. Although the lysosomal part of the project remained incomplete, the studies of HCMV-mediated proteasomal degradation led me to the discovery of a novel anti-HCMV restriction factor, HLTF. While exploring the roles of HLTF in HCMV infection, how deletion of UL145, the viral protein responsible for HLTF degradation, affects HCMV replication was intensively explored. In particular, my data pointed out a potential role of UL145 in regulation of IFNβ induction. As the main protein regulated by UL145 during HCMV infection, it is possible that UL145 modulate IFNβ via HLTF degradation. However,

much work still needs to be done before this hypothesis could be validated. Overall, work presented here expands the range of powerful screening technologies to identify HCMV restriction factor candidates by identifying virally degraded host proteins. Further investigation of these candidates will contribute to our understanding of how HCMV modulates host protein expression to evade antiviral factors.

Publications

Key manuscripts referenced in thesis

Lin KM, Nightingale K, Soday L, Antrobus R, Weekes MP. **Rapid degradation pathways of host proteins during HCMV infection revealed by quantitative proteomics.** *Front. Cell. Infect. Microbiol. (accepted, in press)*

Nightingale K, **Lin KM (co-first author)**, Ravenhill BJ, Davies C, Nobre L, Fielding CA, Ruckova E, Fletcher-Etherington A, Soday L, Nichols H, Sugrue D, Wang ECY, Moreno P, Umrania Y, Huttlin EL, Antrobus R, Davison AJ, Wilkinson GWG, Stanton RJ, Tomasec P, Weekes MP. **High-Definition Analysis of Host Protein Stability during Human Cytomegalovirus Infection Reveals Antiviral Factors and Viral Evasion Mechanisms.** *Cell Host Microbe. 2018;24(3):447-460.e11*.

Other articles published during PhD

Gruszczyk J, Kanjee U, Chan LJ, Menant S, Malleret B, Lim NTY, Schmidt CQ, Mok YF, **Lin KM**, Pearson RD, Rangel G, Smith BJ, Call MJ, Weekes MP, Griffin MDW, Murphy JM, Abraham J, Sriprawat K, Menezes MJ, Ferreira MU, Russell B, Renia L, Duraisingh MT, Tham WH. **Transferrin receptor 1 is a reticulocyte-specific receptor for Plasmodium vivax.** *Science. 2018 Jan;359(6371):48-55.*

Kanjee U, Grüring C, Chaand M, **Lin KM**, Egan E, Manzo J, Jones PL, Yu T, Barker R Jr, Weekes MP, Duraisingh MT. **CRISPR/Cas9 knockouts reveal genetic interaction between strain-transcendent erythrocyte determinants of Plasmodium falciparum invasion.** *Proc Natl Acad Sci U S A. 2017 Oct;114(44):E9356-E9365.*

References

Abate, D.A., Watanabe, S., and Mocarski, E.S. (2004). Major human cytomegalovirus structural protein pp65 (ppUL83) prevents interferon response factor 3 activation in the interferon response. Journal of virology *78*, 10995-11006.

Abe, K., Ishigami, T., Shyu, A.B., Ohno, S., Umemura, S., and Yamashita, A. (2012). Analysis of interferon-beta mRNA stability control after poly(I:C) stimulation using RNA metabolic labeling by ethynyluridine. Biochemical and biophysical research communications *428*, 44-49.

Ablasser, A., Bauernfeind, F., Hartmann, G., Latz, E., Fitzgerald, K.A., and Hornung, V. (2009). RIG-I-dependent sensing of poly(dA:dT) through the induction of an RNA polymerase III-transcribed RNA intermediate. Nat Immunol *10*, 1065-1072.

Ablasser, A., Goldeck, M., Cavlar, T., Deimling, T., Witte, G., Röhl, I., Hopfner, K.P., Ludwig, J., and Hornung, V. (2013). cGAS produces a 2'-5'-linked cyclic dinucleotide second messenger that activates STING. Nature *498*, 380-384.

Abraham, R.T. (2001). Cell cycle checkpoint signaling through the ATM and ATR kinases. Genes Dev *15*, 2177-2196.

Achar, Y.J., Balogh, D., and Haracska, L. (2011). Coordinated protein and DNA remodeling by human HLTF on stalled replication fork. Proc Natl Acad Sci U S A *108*, 14073-14078.

Achar, Y.J., Balogh, D., Neculai, D., Juhasz, S., Morocz, M., Gali, H., Dhe-Paganon, S., Venclovas, Č., and Haracska, L. (2015). Human HLTF mediates postreplication repair by its HIRAN domain-dependent replication fork remodelling. Nucleic Acids Res *43*, 10277-10291.

Adhikary, S., Marinoni, F., Hock, A., Hulleman, E., Popov, N., Beier, R., Bernard, S., Quarto, M., Capra, M., Goettig, S.*, et al.* (2005). The ubiquitin ligase HectH9 regulates transcriptional activation by Myc and is essential for tumor cell proliferation. Cell *123*, 409-421.

Adler, M., Tavalai, N., Müller, R., and Stamminger, T. (2011). Human cytomegalovirus immediate-early gene expression is restricted by the nuclear domain 10 component Sp100. The Journal of general virology *92*, 1532-1538.

Agosto, M.A., Ivanovic, T., and Nibert, M.L. (2006). Mammalian reovirus, a nonfusogenic nonenveloped virus, forms size-selective pores in a model membrane. Proc Natl Acad Sci U S A *103*, 16496-16501.

Akter, P., Cunningham, C., McSharry, B.P., Dolan, A., Addison, C., Dargan, D.J., Hassan-Walker, A.F., Emery, V.C., Griffiths, P.D., Wilkinson, G.W.*, et al.* (2003). Two novel spliced genes in human cytomegalovirus. The Journal of general virology *84*, 1117-1122.

Al-Hakim, A., Escribano-Diaz, C., Landry, M.C., O'Donnell, L., Panier, S., Szilard, R.K., and Durocher, D. (2010). The ubiquitous role of ubiquitin in the DNA damage response. DNA repair *9*, 1229-1240.

Alexander, D.E., Ward, S.L., Mizushima, N., Levine, B., and Leib, D.A. (2007). Analysis of the role of autophagy in replication of herpes simplex virus in cell culture. Journal of virology *81*, 12128-12134.

Anderholm, K.M., Bierle, C.J., and Schleiss, M.R. (2016). Cytomegalovirus Vaccines: Current Status and Future Prospects. Drugs *76*, 1625-1645.

Anders, D.G., Kacica, M.A., Pari, G., and Punturieri, S.M. (1992). Boundaries and structure of human cytomegalovirus oriLyt, a complex origin for lytic-phase DNA replication. Journal of virology *66*, 3373-3384.

Ansari, M.A., Singh, V.V., Dutta, S., Veettil, M.V., Dutta, D., Chikoti, L., Lu, J., Everly, D., and Chandran, B. (2013). Constitutive interferon-inducible protein 16-inflammasome activation during Epstein-Barr virus latency I, II, and III in B and epithelial cells. Journal of virology *87*, 8606-8623.

Aravind, L., and Koonin, E.V. (1999). DNA polymerase beta-like nucleotidyltransferase superfamily: identification of three new families, classification and evolutionary history. Nucleic Acids Res *27*, 1609-1618.

Ariza, M.E., Glaser, R., Kaumaya, P.T., Jones, C., and Williams, M.V. (2009). The EBV-encoded dUTPase activates NF-kappa B through the TLR2 and MyD88-dependent signaling pathway. J Immunol *182*, 851-859.

Azevedo, L.S., Pierrotti, L.C., Abdala, E., Costa, S.F., Strabelli, T.M., Campos, S.V., Ramos, J.F., Latif, A.Z., Litvinov, N., Maluf, N.Z.*, et al.* (2015). Cytomegalovirus infection in transplant recipients. Clinics (Sao Paulo) *70*, 515-523.

Bailey, S.G., Verrall, E., Schelcher, C., Rhie, A., Doherty, A.J., and Sinclair, A.J. (2009). Functional interaction between Epstein-Barr virus replication protein Zta and host DNA damage response protein 53BP1. Journal of virology *83*, 11116-11122.

Bajar, B.T., Wang, E.S., Zhang, S., Lin, M.Z., and Chu, J. (2016). A Guide to Fluorescent Protein FRET Pairs. Sensors (Basel, Switzerland) *16*.

Balka, K.R., Louis, C., Saunders, T.L., Smith, A.M., Calleja, D.J., D'Silva, D.B., Moghaddas, F., Tailler, M., Lawlor, K.E., Zhan, Y.*, et al.* (2020). TBK1 and IKKε Act Redundantly to Mediate STING-Induced NF-κB Responses in Myeloid Cells. Cell Rep *31*, 107492.

Bandi, P., Garcia, M.L., Booth, C.J., Chisari, F.V., and Robek, M.D. (2010). Bortezomib inhibits hepatitis B virus replication in transgenic mice. Antimicrob Agents Chemother *54*, 749-756.

Bao, W., Gu, Y., Ta, L., Wang, K., and Xu, Z. (2016). Induction of autophagy by the MG-132 proteasome inhibitor is associated with endoplasmic reticulum stress in MCF-7 cells. Mol Med Rep *13*, 796-804.

Bar-Peled, L., Schweitzer, L.D., Zoncu, R., and Sabatini, D.M. (2012). Ragulator is a GEF for the rag GTPases that signal amino acid levels to mTORC1. Cell *150*, 1196-1208.

Barber, G.N. (2015). STING: infection, inflammation and cancer. Nat Rev Immunol *15*, 760-770.

Bartek, J., and Lukas, J. (2001). Mammalian G1- and S-phase checkpoints in response to DNA damage. Current opinion in cell biology *13*, 738-747.

Bechtel, J.T., and Shenk, T. (2002). Human cytomegalovirus UL47 tegument protein functions after entry and before immediate-early gene expression. Journal of virology *76*, 1043-1050.

Benedict, C.A., Butrovich, K.D., Lurain, N.S., Corbeil, J., Rooney, I., Schneider, P., Tschopp, J., and Ware, C.F. (1999). Cutting edge: a novel viral TNF receptor superfamily member in virulent strains of human cytomegalovirus. J Immunol *162*, 6967-6970.

Benjamini, Y., and Hochberg, Y. (1995). Controlling the False Discovery Rate - a Practical and Powerful Approach to Multiple Testing. J Roy Stat Soc B Met *57*, 289-300.

Bennett, N.J., May, J.S., and Stevenson, P.G. (2005). Gamma-herpesvirus latency requires T cell evasion during episome maintenance. PLoS Biol *3*, e120.

Biolatti, M., Dell'Oste, V., Pautasso, S., Gugliesi, F., von Einem, J., Krapp, C., Jakobsen, M.R., Borgogna, C., Gariglio, M., De Andrea, M.*, et al.* (2018). Human Cytomegalovirus Tegument Protein pp65 (pUL83) Dampens Type I Interferon Production by Inactivating the DNA Sensor cGAS without Affecting STING. Journal of virology *92*.

Bjørkøy, G., Lamark, T., Brech, A., Outzen, H., Perander, M., Overvatn, A., Stenmark, H., and Johansen, T. (2005). p62/SQSTM1 forms protein aggregates degraded by autophagy and has a protective effect on huntingtin-induced cell death. The Journal of cell biology *171*, 603-614.

Blastyák, A., Hajdú, I., Unk, I., and Haracska, L. (2010). Role of double-stranded DNA translocase activity of human HLTF in replication of damaged DNA. Mol Cell Biol *30*, 684-693.

Bloom, D.C. (2016). Alphaherpesvirus Latency: A Dynamic State of Transcription and Reactivation. Adv Virus Res *94*, 53-80.

Boehme, K.W., Guerrero, M., and Compton, T. (2006). Human cytomegalovirus envelope glycoproteins B and H are necessary for TLR2 activation in permissive cells. J Immunol *177*, 7094-7102.

Bolovan-Fritts, C.A., Mocarski, E.S., and Wiedeman, J.A. (1999). Peripheral blood CD14(+) cells from healthy subjects carry a circular conformation of latent cytomegalovirus genome. Blood *93*, 394-398.

Boppana, S.B., Ross, S.A., and Fowler, K.B. (2013). Congenital cytomegalovirus infection: clinical outcome. Clin Infect Dis *57 Suppl 4*, S178-181.

Botto, S., Abraham, J., Mizuno, N., Pryke, K., Gall, B., Landais, I., Streblow, D.N., Fruh, K.J., and DeFilippis, V.R. (2019). Human Cytomegalovirus Immediate Early 86-kDa Protein Blocks Transcription and Induces Degradation of the Immature Interleukin-1β Protein during Virion-Mediated Activation of the AIM2 Inflammasome. mBio *10*.

Bouhamdan, M., Benichou, S., Rey, F., Navarro, J.M., Agostini, I., Spire, B., Camonis, J., Slupphaug, G., Vigne, R., Benarous, R.*, et al.* (1996). Human immunodeficiency virus type 1 Vpr protein binds to the uracil DNA glycosylase DNA repair enzyme. Journal of virology *70*, 697-704.

Brabec, M., Schober, D., Wagner, E., Bayer, N., Murphy, R.F., Blaas, D., and Fuchs, R. (2005). Opening of size-selective pores in endosomes during human rhinovirus

serotype 2 in vivo uncoating monitored by single-organelle flow analysis. Journal of virology *79*, 1008-1016.

Bradley, A.J., Lurain, N.S., Ghazal, P., Trivedi, U., Cunningham, C., Baluchova, K., Gatherer, D., Wilkinson, G.W., Dargan, D.J., and Davison, A.J. (2009). High-throughput sequence analysis of variants of human cytomegalovirus strains Towne and AD169. The Journal of general virology *90*, 2375-2380.

Britt, W.J. (2018). Maternal Immunity and the Natural History of Congenital Human Cytomegalovirus Infection. Viruses *10*.

Browne, E.P., and Shenk, T. (2003). Human cytomegalovirus UL83-coded pp65 virion protein inhibits antiviral gene expression in infected cells. Proc Natl Acad Sci U S A *100*, 11439-11444.

Bryant, H.E., Petermann, E., Schultz, N., Jemth, A.S., Loseva, O., Issaeva, N., Johansson, F., Fernandez, S., McGlynn, P., and Helleday, T. (2009). PARP is activated at stalled forks to mediate Mre11-dependent replication restart and recombination. Embo j *28*, 2601-2615.

Burkovics, P., Sebesta, M., Balogh, D., Haracska, L., and Krejci, L. (2014). Strand invasion by HLTF as a mechanism for template switch in fork rescue. Nucleic Acids Res *42*, 1711-1720.

Cai, M., Li, M., Wang, K., Wang, S., Lu, Q., Yan, J., Mossman, K.L., Lin, R., and Zheng, C. (2013). The herpes simplex virus 1-encoded envelope glycoprotein B activates NF-κB through the Toll-like receptor 2 and MyD88/TRAF6-dependent signaling pathway. PLoS One *8*, e54586.

Callen, E., Di Virgilio, M., Kruhlak, M.J., Nieto-Soler, M., Wong, N., Chen, H.T., Faryabi, R.B., Polato, F., Santos, M., Starnes, L.M.*, et al.* (2013). 53BP1 mediates productive and mutagenic DNA repair through distinct phosphoprotein interactions. Cell *153*, 1266-1280.

Cannon, M.J., Schmid, D.S., and Hyde, T.B. (2010). Review of cytomegalovirus seroprevalence and demographic characteristics associated with infection. Reviews in medical virology *20*, 202-213.

Castillo, J.P., Frame, F.M., Rogoff, H.A., Pickering, M.T., Yurochko, A.D., and Kowalik, T.F. (2005). Human cytomegalovirus IE1-72 activates ataxia telangiectasia mutated kinase and a p53/p21-mediated growth arrest response. Journal of virology *79*, 11467-11475.

Castro, A., Bernis, C., Vigneron, S., Labbé, J.C., and Lorca, T. (2005). The anaphase-promoting complex: a key factor in the regulation of cell cycle. Oncogene *24*, 314-325.

Ceriani, M., Scandiuzzi, C., Amigoni, L., Tisi, R., Berruti, G., and Martegani, E. (2007). Functional analysis of RalGPS2, a murine guanine nucleotide exchange factor for RalA GTPase. Exp Cell Res *313*, 2293-2307.

Cesarman, E. (2011). Gammaherpesvirus and lymphoproliferative disorders in immunocompromised patients. Cancer Lett *305*, 163-174.

Cha, T.A., Tom, E., Kemble, G.W., Duke, G.M., Mocarski, E.S., and Spaete, R.R. (1996). Human cytomegalovirus clinical isolates carry at least 19 genes not found in laboratory strains. Journal of virology *70*, 78-83.

Chandran, K., Sullivan, N.J., Felbor, U., Whelan, S.P., and Cunningham, J.M. (2005). Endosomal proteolysis of the Ebola virus glycoprotein is necessary for infection. Science *308*, 1643-1645.

Chapman, H.A., Riese, R.J., and Shi, G.P. (1997). Emerging roles for cysteine proteases in human biology. Annu Rev Physiol *59*, 63-88.

Charpak-Amikam, Y., Kubsch, T., Seidel, E., Oiknine-Djian, E., Cavaletto, N., Yamin, R., Schmiedel, D., Wolf, D., Gribaudo, G., Messerle, M.*, et al.* (2017). Human cytomegalovirus escapes immune recognition by NK cells through the downregulation of B7-H6 by the viral genes US18 and US20. Sci Rep *7*, 8661.

Chaumorcel, M., Lussignol, M., Mouna, L., Cavignac, Y., Fahie, K., Cotte-Laffitte, J., Geballe, A., Brune, W., Beau, I., Codogno, P.*, et al.* (2012). The human cytomegalovirus protein TRS1 inhibits autophagy via its interaction with Beclin 1. Journal of virology *86*, 2571-2584.

Chaurushiya, M.S., Lilley, C.E., Aslanian, A., Meisenhelder, J., Scott, D.C., Landry, S., Ticau, S., Boutell, C., Yates, J.R., 3rd, Schulman, B.A.*, et al.* (2012). Viral E3 ubiquitin ligase-mediated degradation of a cellular E3: viral mimicry of a cellular phosphorylation mark targets the RNF8 FHA domain. Mol Cell *46*, 79-90.

Chee, M.S., Bankier, A.T., Beck, S., Bohni, R., Brown, C.M., Cerny, R., Horsnell, T., Hutchison, C.A., 3rd, Kouzarides, T., Martignetti, J.A.*, et al.* (1990). Analysis of the protein-coding content of the sequence of human cytomegalovirus strain AD169. Current topics in microbiology and immunology *154*, 125-169.

Chen, D., Kon, N., Li, M., Zhang, W., Qin, J., and Gu, W. (2005). ARF-BP1/Mule is a critical mediator of the ARF tumor suppressor. Cell *121*, 1071-1083.

Chen, Y.R., Liu, M.T., Chang, Y.T., Wu, C.C., Hu, C.Y., and Chen, J.Y. (2008). Epstein-Barr virus latent membrane protein 1 represses DNA repair through the PI3K/Akt/FOXO3a pathway in human epithelial cells. Journal of virology *82*, 8124-8137.

Cheng, S., Caviness, K., Buehler, J., Smithey, M., Nikolich-Žugich, J., and Goodrum, F. (2017). Transcriptome-wide characterization of human cytomegalovirus in natural infection and experimental latency. Proc Natl Acad Sci U S A *114*, E10586-e10595.

Cherrier, L., Nasar, A., Goodlet, K.J., Nailor, M.D., Tokman, S., and Chou, S. (2018). Emergence of letermovir resistance in a lung transplant recipient with ganciclovir-resistant cytomegalovirus infection. Am J Transplant *18*, 3060-3064.

Chiu, Y.H., Macmillan, J.B., and Chen, Z.J. (2009). RNA polymerase III detects cytosolic DNA and induces type I interferons through the RIG-I pathway. Cell *138*, 576-591.

Choi, H.J., Park, A., Kang, S., Lee, E., Lee, T.A., Ra, E.A., Lee, J., Lee, S., and Park, B. (2018). Human cytomegalovirus-encoded US9 targets MAVS and STING signaling to evade type I interferon immune responses. Nature communications *9*, 125.

Christensen, M.H., Jensen, S.B., Miettinen, J.J., Luecke, S., Prabakaran, T., Reinert, L.S., Mettenleiter, T., Chen, Z.J., Knipe, D.M., Sandri-Goldin, R.M.*, et al.* (2016). HSV-1 ICP27

targets the TBK1-activated STING signalsome to inhibit virus-induced type I IFN expression. Embo j *35*, 1385-1399.

Chui, A.J., Okondo, M.C., Rao, S.D., Gai, K., Griswold, A.R., Johnson, D.C., Ball, D.P., Taabazuing, C.Y., Orth, E.L., Vittimberga, B.A*., et al.* (2019). N-terminal degradation activates the NLRP1B inflammasome. Science *364*, 82-85.

Colletti, K.S., Xu, Y., Cei, S.A., Tarrant, M., and Pari, G.S. (2004). Human cytomegalovirus UL84 oligomerization and heterodimerization domains act as transdominant inhibitors of oriLyt-dependent DNA replication: evidence that IE2-UL84 and UL84-UL84 interactions are required for lytic DNA replication. Journal of virology *78*, 9203-9214.

Compton, T., Kurt-Jones, E.A., Boehme, K.W., Belko, J., Latz, E., Golenbock, D.T., and Finberg, R.W. (2003). Human cytomegalovirus activates inflammatory cytokine responses via CD14 and Toll-like receptor 2. Journal of virology *77*, 4588-4596.

Compton, T., Nowlin, D.M., and Cooper, N.R. (1993). Initiation of human cytomegalovirus infection requires initial interaction with cell surface heparan sulfate. Virology *193*, 834-841.

Condit, R. (2013). Principles of Virology. In Fields virology, B.N. Fields, D.M. Knipe, and P.M. Howley, eds. (Philidelphia: Lippincott Williams & Wilkins).

Cornélie, S., Hoebeke, J., Schacht, A.M., Bertin, B., Vicogne, J., Capron, M., and Riveau, G. (2004). Direct evidence that toll-like receptor 9 (TLR9) functionally binds plasmid DNA by specific cytosine-phosphate-guanine motif recognition. J Biol Chem *279*, 15124-15129.

Dargan, D.J., Douglas, E., Cunningham, C., Jamieson, F., Stanton, R.J., Baluchova, K., McSharry, B.P., Tomasec, P., Emery, V.C., Percivalle, E*., et al.* (2010). Sequential mutations associated with adaptation of human cytomegalovirus to growth in cell culture. The Journal of general virology *91*, 1535-1546.

Dargan, D.J., Jamieson, F.E., MacLean, J., Dolan, A., Addison, C., and McGeoch, D.J. (1997). The published DNA sequence of human cytomegalovirus strain AD169 lacks 929 base pairs affecting genes UL42 and UL43. Journal of virology *71*, 9833-9836.

Davalos, A.R., Kaminker, P., Hansen, R.K., and Campisi, J. (2004). ATR and ATM-dependent movement of BLM helicase during replication stress ensures optimal ATM activation and 53BP1 focus formation. Cell cycle (Georgetown, Tex) *3*, 1579-1586.

Davison, A.J., Dolan, A., Akter, P., Addison, C., Dargan, D.J., Alcendor, D.J., McGeoch, D.J., and Hayward, G.S. (2003). The human cytomegalovirus genome revisited: comparison with the chimpanzee cytomegalovirus genome. The Journal of general virology *84*, 17-28.

DeFilippis, V.R., Alvarado, D., Sali, T., Rothenburg, S., and Früh, K. (2010). Human cytomegalovirus induces the interferon response via the DNA sensor ZBP1. Journal of virology *84*, 585-598.

Deigendesch, N., Koch-Nolte, F., and Rothenburg, S. (2006). ZBP1 subcellular localization and association with stress granules is controlled by its Z-DNA binding domains. Nucleic Acids Res *34*, 5007-5020.

Delboy, M.G., and Nicola, A.V. (2011). A pre-immediate-early role for tegument ICP0 in the proteasome-dependent entry of herpes simplex virus. Journal of virology *85*, 5910-5918.

Delboy, M.G., Roller, D.G., and Nicola, A.V. (2008). Cellular proteasome activity facilitates herpes simplex virus entry at a postpenetration step. Journal of virology *82*, 3381-3390.

Dell'Oste, V., Gatti, D., Gugliesi, F., De Andrea, M., Bawadekar, M., Lo Cigno, I., Biolatti, M., Vallino, M., Marschall, M., Gariglio, M*., et al.* (2014). Innate nuclear sensor IFI16 translocates into the cytoplasm during the early stage of in vitro human cytomegalovirus infection and is entrapped in the egressing virions during the late stage. Journal of virology *88*, 6970-6982.

Dempsey, A., and Bowie, A.G. (2015). Innate immune recognition of DNA: A recent history. Virology *479-480*, 146-152.

Deshaies, R.J., and Joazeiro, C.A. (2009). RING domain E3 ubiquitin ligases. Annu Rev Biochem *78*, 399-434.

Dey, M., Ahmed, A.U., and Lesniak, M.S. (2015). Cytomegalovirus and glioma: putting the cart before the horse. J Neurol Neurosurg Psychiatry *86*, 191-199.

Dhont, L., Mascaux, C., and Belayew, A. (2016). The helicase-like transcription factor (HLTF) in cancer: loss of function or oncomorphic conversion of a tumor suppressor? Cell Mol Life Sci *73*, 129-147.

Dhuruvasan, K., Sivasubramanian, G., and Pellett, P.E. (2011). Roles of host and viral microRNAs in human cytomegalovirus biology. Virus Res *157*, 180-192.

Dickey, J.S., Redon, C.E., Nakamura, A.J., Baird, B.J., Sedelnikova, O.A., and Bonner, W.M. (2009). H2AX: functional roles and potential applications. Chromosoma *118*, 683-692.

Didcock, L., Young, D.F., Goodbourn, S., and Randall, R.E. (1999). The V protein of simian virus 5 inhibits interferon signalling by targeting STAT1 for proteasome-mediated degradation. Journal of virology *73*, 9928-9933.

Dieci, G., Fiorino, G., Castelnuovo, M., Teichmann, M., and Pagano, A. (2007). The expanding RNA polymerase III transcriptome. Trends Genet *23*, 614-622.

Dikic, I. (2017). Proteasomal and Autophagic Degradation Systems. Annu Rev Biochem *86*, 193-224.

Diner, B.A., Lum, K.K., Toettcher, J.E., and Cristea, I.M. (2016). Viral DNA Sensors IFI16 and Cyclic GMP-AMP Synthase Possess Distinct Functions in Regulating Viral Gene Expression, Immune Defenses, and Apoptotic Responses during Herpesvirus Infection. mBio *7*.

Ding, H., Descheemaeker, K., Marynen, P., Nelles, L., Carvalho, T., Carmo-Fonseca, M., Collen, D., and Belayew, A. (1996). Characterization of a helicase-like transcription factor involved in the expression of the human plasminogen activator inhibitor-1 gene. DNA Cell Biol *15*, 429-442.

Ding, Y., Zhang, Y., Xu, C., Tao, Q.H., and Chen, Y.G. (2013). HECT domain-containing E3 ubiquitin ligase NEDD4L negatively regulates Wnt signaling by targeting dishevelled for proteasomal degradation. J Biol Chem *288*, 8289-8298.

Dolan, A., Cunningham, C., Hector, R.D., Hassan-Walker, A.F., Lee, L., Addison, C., Dargan, D.J., McGeoch, D.J., Gatherer, D., Emery, V.C*., et al.* (2004). Genetic content of wild-type human cytomegalovirus. The Journal of general virology *85*, 1301-1312.

Dunn, C., Chalupny, N.J., Sutherland, C.L., Dosch, S., Sivakumar, P.V., Johnson, D.C., and Cosman, D. (2003). Human cytomegalovirus glycoprotein UL16 causes intracellular sequestration of NKG2D ligands, protecting against natural killer cell cytotoxicity. J Exp Med *197*, 1427-1439.

Dziurzynski, K., Chang, S.M., Heimberger, A.B., Kalejta, R.F., McGregor Dallas, S.R., Smit, M., Soroceanu, L., and Cobbs, C.S. (2012). Consensus on the role of human cytomegalovirus in glioblastoma. Neuro Oncol *14*, 246-255.

Elder, E., and Sinclair, J. (2019). HCMV latency: what regulates the regulators? Med Microbiol Immunol *208*, 431-438.

Elias, J.E., and Gygi, S.P. (2007). Target-decoy search strategy for increased confidence in large-scale protein identifications by mass spectrometry. Nat Methods *4*, 207-214.

Eng, J.K., McCormack, A.L., and Yates, J.R. (1994). An approach to correlate tandem mass spectral data of peptides with amino acid sequences in a protein database. J Am Soc Mass Spectrom *5*, 976-989.

English, L., Chemali, M., Duron, J., Rondeau, C., Laplante, A., Gingras, D., Alexander, D., Leib, D., Norbury, C., Lippé, R*., et al.* (2009). Autophagy enhances the presentation of endogenous viral antigens on MHC class I molecules during HSV-1 infection. Nat Immunol *10*, 480-487.

Erice, A. (1999). Resistance of Human Cytomegalovirus to Antiviral Drugs. Clinical Microbiology Reviews *12*, 286-297.

Eskelinen, E.L., Reggiori, F., Baba, M., Kovács, A.L., and Seglen, P.O. (2011). Seeing is believing: the impact of electron microscopy on autophagy research. Autophagy *7*, 935-956.

Eskelinen, E.L., Tanaka, Y., and Saftig, P. (2003). At the acidic edge: emerging functions for lysosomal membrane proteins. Trends Cell Biol *13*, 137-145.

Everett, R.D., and Chelbi-Alix, M.K. (2007). PML and PML nuclear bodies: implications in antiviral defence. Biochimie *89*, 819-830.

Fang, D., Elly, C., Gao, B., Fang, N., Altman, Y., Joazeiro, C., Hunter, T., Copeland, N., Jenkins, N., and Liu, Y.C. (2002). Dysregulation of T lymphocyte function in itchy mice: a role for Itch in TH2 differentiation. Nat Immunol *3*, 281-287.

Fang, R., Wang, C., Jiang, Q., Lv, M., Gao, P., Yu, X., Mu, P., Zhang, R., Bi, S., Feng, J.M*., et al.* (2017). NEMO-IKKβ Are Essential for IRF3 and NF-κB Activation in the cGAS-STING Pathway. J Immunol *199*, 3222-3233.

Fehr, A.R., Gualberto, N.C., Savaryn, J.P., Terhune, S.S., and Yu, D. (2012). Proteasome-dependent disruption of the E3 ubiquitin ligase anaphase-promoting complex by HCMV protein pUL21a. PLoS pathogens *8*, e1002789.

Feire, A.L., Koss, H., and Compton, T. (2004). Cellular integrins function as entry receptors for human cytomegalovirus via a highly conserved disintegrin-like domain. Proc Natl Acad Sci U S A *101*, 15470-15475.

Ferguson, B.J., Mansur, D.S., Peters, N.E., Ren, H., and Smith, G.L. (2012). DNA-PK is a DNA sensor for IRF-3-dependent innate immunity. Elife *1*, e00047.

Fernandez-Capetillo, O., Lee, A., Nussenzweig, M., and Nussenzweig, A. (2004). H2AX: the histone guardian of the genome. DNA repair *3*, 959-967.

Fielding, C.A., Aicheler, R., Stanton, R.J., Wang, E.C., Han, S., Seirafian, S., Davies, J., McSharry, B.P., Weekes, M.P., Antrobus, P.R.*, et al.* (2014). Two novel human cytomegalovirus NK cell evasion functions target MICA for lysosomal degradation. PLoS pathogens *10*, e1004058.

Fielding, C.A., Weekes, M.P., Nobre, L.V., Ruckova, E., Wilkie, G.S., Paulo, J.A., Chang, C., Suárez, N.M., Davies, J.A., Antrobus, R.*, et al.* (2017). Control of immune ligands by members of a cytomegalovirus gene expansion suppresses natural killer cell activation. Elife *6*.

Fish, K.N., Soderberg-Naucler, C., Mills, L.K., Stenglein, S., and Nelson, J.A. (1998). Human cytomegalovirus persistently infects aortic endothelial cells. Journal of virology *72*, 5661-5668.

Fletcher-Etherington, A., Nobre, L., Nightingale, K., Antrobus, R., Nichols, J., Davison, A.J., Stanton, R.J., and Weekes, M.P. (2020). Human cytomegalovirus protein pUL36: A dual cell death pathway inhibitor. Proc Natl Acad Sci U S A *117*, 18771-18779.

Fliss, P.M., Jowers, T.P., Brinkmann, M.M., Holstermann, B., Mack, C., Dickinson, P., Hohenberg, H., Ghazal, P., and Brune, W. (2012). Viral mediated redirection of NEMO/IKKγ to autophagosomes curtails the inflammatory cascade. PLoS pathogens *8*, e1002517.

Fortunato, E.A., Sanchez, V., Yen, J.Y., and Spector, D.H. (2002). Infection of cells with human cytomegalovirus during S phase results in a blockade to immediate-early gene expression that can be overcome by inhibition of the proteasome. Journal of virology *76*, 5369-5379.

Frank, S.R., Köllmann, C.P., Luong, P., Galli, G.G., Zou, L., Bernards, A., Getz, G., Calogero, R.A., Frödin, M., and Hansen, S.H. (2018). p190 RhoGAP promotes contact inhibition in epithelial cells by repressing YAP activity. The Journal of cell biology *217*, 3183-3201.

Fu, Y., Comella, N., Tognazzi, K., Brown, L.F., Dvorak, H.F., and Kocher, O. (1999). Cloning of DLM-1, a novel gene that is up-regulated in activated macrophages, using RNA differential display. Gene *240*, 157-163.

Fu, Y.Z., Su, S., Gao, Y.Q., Wang, P.P., Huang, Z.F., Hu, M.M., Luo, W.W., Li, S., Luo, M.H., Wang, Y.Y.*, et al.* (2017). Human Cytomegalovirus Tegument Protein UL82

Inhibits STING-Mediated Signaling to Evade Antiviral Immunity. Cell Host Microbe *21*, 231-243.

Fuchs, W., Granzow, H., Klupp, B.G., Kopp, M., and Mettenleiter, T.C. (2002). The UL48 tegument protein of pseudorabies virus is critical for intracytoplasmic assembly of infectious virions. Journal of virology *76*, 6729-6742.

Gandhi, M.K., and Khanna, R. (2004). Human cytomegalovirus: clinical aspects, immune regulation, and emerging treatments. Lancet Infect Dis *4*, 725-738.

Ganley, I.G., Wong, P.M., Gammoh, N., and Jiang, X. (2011). Distinct autophagosomal-lysosomal fusion mechanism revealed by thapsigargin-induced autophagy arrest. Mol Cell *42*, 731-743.

Gao, D., Wu, J., Wu, Y.T., Du, F., Aroh, C., Yan, N., Sun, L., and Chen, Z.J. (2013a). Cyclic GMP-AMP synthase is an innate immune sensor of HIV and other retroviruses. Science *341*, 903-906.

Gao, M., Labuda, T., Xia, Y., Gallagher, E., Fang, D., Liu, Y.C., and Karin, M. (2004). Jun turnover is controlled through JNK-dependent phosphorylation of the E3 ligase Itch. Science *306*, 271-275.

Gao, P., Ascano, M., Wu, Y., Barchet, W., Gaffney, B.L., Zillinger, T., Serganov, A.A., Liu, Y., Jones, R.A., Hartmann, G.*, et al.* (2013b). Cyclic [G(2',5')pA(3',5')p] is the metazoan second messenger produced by DNA-activated cyclic GMP-AMP synthase. Cell *153*, 1094-1107.

Gariano, G.R., Dell'Oste, V., Bronzini, M., Gatti, D., Luganini, A., De Andrea, M., Gribaudo, G., Gariglio, M., and Landolfo, S. (2012). The intracellular DNA sensor IFI16 gene acts as restriction factor for human cytomegalovirus replication. PLoS pathogens *8*, e1002498.

Gaspar, M., and Shenk, T. (2006). Human cytomegalovirus inhibits a DNA damage response by mislocalizing checkpoint proteins. Proc Natl Acad Sci U S A *103*, 2821-2826.

Gatherer, D., Seirafian, S., Cunningham, C., Holton, M., Dargan, D.J., Baluchova, K., Hector, R.D., Galbraith, J., Herzyk, P., Wilkinson, G.W.*, et al.* (2011). High-resolution human cytomegalovirus transcriptome. Proc Natl Acad Sci U S A *108*, 19755-19760.

Gawn, J.M., and Greaves, R.F. (2002). Absence of IE1 p72 protein function during low-multiplicity infection by human cytomegalovirus results in a broad block to viral delayed-early gene expression. Journal of virology *76*, 4441-4455.

Gong, X., Kaushal, S., Ceccarelli, E., Bogdanova, N., Neville, C., Nguyen, T., Clark, H., Khatib, Z.A., Valentine, M., Look, A.T.*, et al.* (1997). Developmental regulation of Zbu1, a DNA-binding member of the SWI2/SNF2 family. Dev Biol *183*, 166-182.

Goodrum, F., Reeves, M., Sinclair, J., High, K., and Shenk, T. (2007). Human cytomegalovirus sequences expressed in latently infected individuals promote a latent infection in vitro. Blood *110*, 937-945.

Goubau, D., Deddouche, S., and Reis e Sousa, C. (2013). Cytosolic sensing of viruses. Immunity *38*, 855-869.

Grainger, L., Cicchini, L., Rak, M., Petrucelli, A., Fitzgerald, K.D., Semler, B.L., and Goodrum, F. (2010). Stress-inducible alternative translation initiation of human cytomegalovirus latency protein pUL138. Journal of virology *84*, 9472-9486.

Granato, M., Santarelli, R., Farina, A., Gonnella, R., Lotti, L.V., Faggioni, A., and Cirone, M. (2014). Epstein-barr virus blocks the autophagic flux and appropriates the autophagic machinery to enhance viral replication. Journal of virology *88*, 12715-12726.

Greaves, R.F., and Mocarski, E.S. (1998). Defective growth correlates with reduced accumulation of a viral DNA replication protein after low-multiplicity infection by a human cytomegalovirus ie1 mutant. Journal of virology *72*, 366-379.

Greene, W., Zhang, W., He, M., Witt, C., Ye, F., and Gao, S.J. (2012). The ubiquitin/proteasome system mediates entry and endosomal trafficking of Kaposi's sarcoma-associated herpesvirus in endothelial cells. PLoS pathogens *8*, e1002703.

Griffiths, P., Baraniak, I., and Reeves, M. (2015). The pathogenesis of human cytomegalovirus. J Pathol *235*, 288-297.

Groll, M., Berkers, C.R., Ploegh, H.L., and Ovaa, H. (2006). Crystal structure of the boronic acid-based proteasome inhibitor bortezomib in complex with the yeast 20S proteasome. Structure *14*, 451-456.

Gruhne, B., Kamranvar, S.A., Masucci, M.G., and Sompallae, R. (2009a). EBV and genomic instability--a new look at the role of the virus in the pathogenesis of Burkitt's lymphoma. Seminars in cancer biology *19*, 394-400.

Gruhne, B., Sompallae, R., and Masucci, M.G. (2009b). Three Epstein-Barr virus latency proteins independently promote genomic instability by inducing DNA damage, inhibiting DNA repair and inactivating cell cycle checkpoints. Oncogene *28*, 3997-4008.

Guggemoos, S., Hangel, D., Hamm, S., Heit, A., Bauer, S., and Adler, H. (2008). TLR9 contributes to antiviral immunity during gammaherpesvirus infection. J Immunol *180*, 438-443.

Guo, H., Callaway, J.B., and Ting, J.P. (2015). Inflammasomes: mechanism of action, role in disease, and therapeutics. Nat Med *21*, 677-687.

Gupta, A., Jha, S., Engel, D.A., Ornelles, D.A., and Dutta, A. (2013). Tip60 degradation by adenovirus relieves transcriptional repression of viral transcriptional activator EIA. Oncogene *32*, 5017-5025.

Haas, T., Metzger, J., Schmitz, F., Heit, A., Müller, T., Latz, E., and Wagner, H. (2008). The DNA sugar backbone 2' deoxyribose determines toll-like receptor 9 activation. Immunity *28*, 315-323.

Hahn, G., Revello, M.G., Patrone, M., Percivalle, E., Campanini, G., Sarasini, A., Wagner, M., Gallina, A., Milanesi, G., Koszinowski, U.*, et al.* (2004). Human cytomegalovirus UL131-128 genes are indispensable for virus growth in endothelial cells and virus transfer to leukocytes. Journal of virology *78*, 10023-10033.

Haince, J.F., McDonald, D., Rodrigue, A., Déry, U., Masson, J.Y., Hendzel, M.J., and Poirier, G.G. (2008). PARP1-dependent kinetics of recruitment of MRE11 and NBS1 proteins to multiple DNA damage sites. J Biol Chem *283*, 1197-1208.

Hakki, M., Marshall, E.E., De Niro, K.L., and Geballe, A.P. (2006). Binding and nuclear relocalization of protein kinase R by human cytomegalovirus TRS1. Journal of virology *80*, 11817-11826.

Halary, F., Amara, A., Lortat-Jacob, H., Messerle, M., Delaunay, T., Houlès, C., Fieschi, F., Arenzana-Seisdedos, F., Moreau, J.F., and Déchanet-Merville, J. (2002). Human cytomegalovirus binding to DC-SIGN is required for dendritic cell infection and target cell trans-infection. Immunity *17*, 653-664.

Harari, D., Orr, I., Rotkopf, R., Baranzini, S.E., and Schreiber, G. (2015). A robust type I interferon gene signature from blood RNA defines quantitative but not qualitative differences between three major IFNβ drugs in the treatment of multiple sclerosis. Hum Mol Genet *24*, 3192-3205.

Harrison, S.C. (2005). Mechanism of membrane fusion by viral envelope proteins. Adv Virus Res *64*, 231-261.

Hashimoto, H., Hishiki, A., Hara, K., and Kikuchi, S. (2017). Structural basis for the molecular interactions in DNA damage tolerances. Biophysics and physicobiology *14*, 199-205.

He, J., Tang, F., Liu, L., Chen, L., Li, J., Ou, D., Zhang, L., Li, Z., Feng, D., Li, W*., et al.* (2017). Positive regulation of TAZ expression by EBV-LMP1 contributes to cell proliferation and epithelial-mesenchymal transition in nasopharyngeal carcinoma. Oncotarget *8*, 52333-52344.

Helmer, R.A., Foreman, O., Dertien, J.S., Panchoo, M., Bhakta, S.M., and Chilton, B.S. (2013a). Role of helicase-like transcription factor (hltf) in the G2/m transition and apoptosis in brain. PLoS One *8*, e66799.

Helmer, R.A., Martínez-Zaguilán, R., Dertien, J.S., Fulford, C., Foreman, O., Peiris, V., and Chilton, B.S. (2013b). Helicase-like transcription factor (Hltf) regulates G2/M transition, Wt1/Gata4/Hif-1a cardiac transcription networks, and collagen biogenesis. PLoS One *8*, e80461.

Hemmi, H., Takeuchi, O., Kawai, T., Kaisho, T., Sato, S., Sanjo, H., Matsumoto, M., Hoshino, K., Wagner, H., Takeda, K*., et al.* (2000). A Toll-like receptor recognizes bacterial DNA. Nature *408*, 740-745.

Hensel, G.M., Meyer, H.H., Buchmann, I., Pommerehne, D., Schmolke, S., Plachter, B., Radsak, K., and Kern, H.F. (1996). Intracellular localization and expression of the human cytomegalovirus matrix phosphoprotein pp71 (ppUL82): evidence for its translocation into the nucleus. The Journal of general virology *77 (Pt 12)*, 3087-3097.

Heo, J., Dogra, P., Masi, T.J., Pitt, E.A., de Kruijf, P., Smit, M.J., and Sparer, T.E. (2015). Novel Human Cytomegalovirus Viral Chemokines, vCXCL-1s, Display Functional Selectivity for Neutrophil Signaling and Function. J Immunol *195*, 227-236.

Hesketh G.G., W.L., Davis L.J., Bright N.A., Luzio J.P. (2018). The Lysosome and Intracellular Signalling. In Endocytosis and Signaling, P.I. Lamaze C., ed. (Springer, Cham).

Hinz, A., and Galla, H.J. (2005). Viral membrane penetration: lytic activity of a nodaviral fusion peptide. Eur Biophys J *34*, 285-293.

Hishiki, A., Hara, K., Ikegaya, Y., Yokoyama, H., Shimizu, T., Sato, M., and Hashimoto, H. (2015). Structure of a Novel DNA-binding Domain of Helicase-like Transcription Factor (HLTF) and Its Functional Implication in DNA Damage Tolerance. J Biol Chem *290*, 13215-13223.

Honda, K., Takaoka, A., and Taniguchi, T. (2006). Type I interferon [corrected] gene induction by the interferon regulatory factor family of transcription factors. Immunity *25*, 349-360.

Howe, J.G., and Shu, M.D. (1989). Epstein-Barr virus small RNA (EBER) genes: unique transcription units that combine RNA polymerase II and III promoter elements. Cell *57*, 825-834.

Howley, P.M. (2006). Warts, cancer and ubiquitylation: lessons from the papillomaviruses. Trans Am Clin Climatol Assoc *117*, 113-126; discussion 126-117.

Hrecka, K., Hao, C., Shun, M.C., Kaur, S., Swanson, S.K., Florens, L., Washburn, M.P., and Skowronski, J. (2016). HIV-1 and HIV-2 exhibit divergent interactions with HLTF and UNG2 DNA repair proteins. Proc Natl Acad Sci U S A *113*, E3921-3930.

Huang da, W., Sherman, B.T., and Lempicki, R.A. (2009). Systematic and integrative analysis of large gene lists using DAVID bioinformatics resources. Nat Protoc *4*, 44-57.

Huang, Z.F., Zou, H.M., Liao, B.W., Zhang, H.Y., Yang, Y., Fu, Y.Z., Wang, S.Y., Luo, M.H., and Wang, Y.Y. (2018). Human Cytomegalovirus Protein UL31 Inhibits DNA Sensing of cGAS to Mediate Immune Evasion. Cell Host Microbe *24*, 69-80.e64.

Huh, Y.H., Kim, Y.E., Kim, E.T., Park, J.J., Song, M.J., Zhu, H., Hayward, G.S., and Ahn, J.H. (2008). Binding STAT2 by the acidic domain of human cytomegalovirus IE1 promotes viral growth and is negatively regulated by SUMO. Journal of virology *82*, 10444-10454.

Huibregtse, J.M., Scheffner, M., Beaudenon, S., and Howley, P.M. (1995). A family of proteins structurally and functionally related to the E6-AP ubiquitin-protein ligase. Proc Natl Acad Sci U S A *92*, 2563-2567.

Humar, A., and Michaels, M. (2006). American Society of Transplantation recommendations for screening, monitoring and reporting of infectious complications in immunosuppression trials in recipients of organ transplantation. Am J Transplant *6*, 262-274.

Hung, C.H., Chen, L.W., Wang, W.H., Chang, P.J., Chiu, Y.F., Hung, C.C., Lin, Y.J., Liou, J.Y., Tsai, W.J., Hung, C.L.*, et al.* (2014). Regulation of autophagic activation by Rta of Epstein-Barr virus via the extracellular signal-regulated kinase pathway. Journal of virology *88*, 12133-12145.

Huotari, J., and Helenius, A. (2011). Endosome maturation. Embo j *30*, 3481-3500.

Hurley, J.H., and Young, L.N. (2017). Mechanisms of Autophagy Initiation. Annu Rev Biochem *86*, 225-244.

Husain, M., and Moss, B. (2005). Role of receptor-mediated endocytosis in the formation of vaccinia virus extracellular enveloped particles. Journal of virology *79*, 4080-4089.

Hwang, S., Kim, K.S., Flano, E., Wu, T.T., Tong, L.M., Park, A.N., Song, M.J., Sanchez, D.J., O'Connell, R.M., Cheng, G.*, et al.* (2009). Conserved herpesviral kinase promotes viral persistence by inhibiting the IRF-3-mediated type I interferon response. Cell Host Microbe *5*, 166-178.

Ishikawa, H., and Barber, G.N. (2011). The STING pathway and regulation of innate immune signaling in response to DNA pathogens. Cell Mol Life Sci *68*, 1157-1165.

Ishov, A.M., and Maul, G.G. (1996). The periphery of nuclear domain 10 (ND10) as site of DNA virus deposition. The Journal of cell biology *134*, 815-826.

Ivashkiv, L.B., and Donlin, L.T. (2014). Regulation of type I interferon responses. Nat Rev Immunol *14*, 36-49.

Iwakiri, D., and Takada, K. (2010). Role of EBERs in the pathogenesis of EBV infection. Adv Cancer Res *107*, 119-136.

Jackson, S.E., Mason, G.M., and Wills, M.R. (2011). Human cytomegalovirus immunity and immune evasion. Virus Res *157*, 151-160.

Jean Beltran, P.M., and Cristea, I.M. (2014). The life cycle and pathogenesis of human cytomegalovirus infection: lessons from proteomics. Expert Rev Proteomics *11*, 697-711.

Jenkins, C., Abendroth, A., and Slobedman, B. (2004). A novel viral transcript with homology to human interleukin-10 is expressed during latent human cytomegalovirus infection. Journal of virology *78*, 1440-1447.

Jin, S.M., and Youle, R.J. (2012). PINK1- and Parkin-mediated mitophagy at a glance. J Cell Sci *125*, 795-799.

Jin, T., Perry, A., Jiang, J., Smith, P., Curry, J.A., Unterholzner, L., Jiang, Z., Horvath, G., Rathinam, V.A., Johnstone, R.W.*, et al.* (2012). Structures of the HIN domain:DNA complexes reveal ligand binding and activation mechanisms of the AIM2 inflammasome and IFI16 receptor. Immunity *36*, 561-571.

Johnson, K.E., Chikoti, L., and Chandran, B. (2013). Herpes simplex virus 1 infection induces activation and subsequent inhibition of the IFI16 and NLRP3 inflammasomes. Journal of virology *87*, 5005-5018.

Jovic, M., Sharma, M., Rahajeng, J., and Caplan, S. (2010). The early endosome: a busy sorting station for proteins at the crossroads. Histol Histopathol *25*, 99-112.

Juckem, L.K., Boehme, K.W., Feire, A.L., and Compton, T. (2008). Differential initiation of innate immune responses induced by human cytomegalovirus entry into fibroblast cells. J Immunol *180*, 4965-4977.

Judith, D., Mostowy, S., Bourai, M., Gangneux, N., Lelek, M., Lucas-Hourani, M., Cayet, N., Jacob, Y., Prévost, M.C., Pierre, P.*, et al.* (2013). Species-specific impact of the autophagy machinery on Chikungunya virus infection. EMBO Rep *14*, 534-544.

Kabeya, Y., Mizushima, N., Ueno, T., Yamamoto, A., Kirisako, T., Noda, T., Kominami, E., Ohsumi, Y., and Yoshimori, T. (2000). LC3, a mammalian homologue of yeast Apg8p, is localized in autophagosome membranes after processing. Embo j *19*, 5720-5728.

Kamranvar, S.A., Gruhne, B., Szeles, A., and Masucci, M.G. (2007). Epstein-Barr virus promotes genomic instability in Burkitt's lymphoma. Oncogene *26*, 5115-5123.

Kamura, T., Maenaka, K., Kotoshiba, S., Matsumoto, M., Kohda, D., Conaway, R.C., Conaway, J.W., and Nakayama, K.I. (2004). VHL-box and SOCS-box domains determine binding specificity for Cul2-Rbx1 and Cul5-Rbx2 modules of ubiquitin ligases. Genes Dev *18*, 3055-3065.

Kang, H.R., Cheong, W.C., Park, J.E., Ryu, S., Cho, H.J., Youn, H., Ahn, J.H., and Song, M.J. (2014). Murine gammaherpesvirus 68 encoding open reading frame 11 targets TANK binding kinase 1 to negatively regulate the host type I interferon response. Journal of virology *88*, 6832-6846.

Kang, T.H., Lindsey-Boltz, L.A., Reardon, J.T., and Sancar, A. (2010). Circadian control of XPA and excision repair of cisplatin-DNA damage by cryptochrome and HERC2 ubiquitin ligase. Proc Natl Acad Sci U S A *107*, 4890-4895.

Kang, W., Huang, T., Zhou, Y., Zhang, J., Lung, R.W.M., Tong, J.H.M., Chan, A.W.H., Zhang, B., Wong, C.C., Wu, F.*, et al.* (2018). miR-375 is involved in Hippo pathway by targeting YAP1/TEAD4-CTGF axis in gastric carcinogenesis. Cell death & disease *9*, 92.

Kapasi, A.J., and Spector, D.H. (2008). Inhibition of the Cyclin-Dependent Kinases at the Beginning of Human Cytomegalovirus Infection Specifically Alters the Levels and Localization of the RNA Polymerase II Carboxyl-Terminal Domain Kinases cdk9 and cdk7 at the Viral Transcriptosome. Journal of virology *82*, 394-407.

Kawai, T., and Akira, S. (2006). TLR signaling. Cell Death Differ *13*, 816-825.

Kawai, T., and Akira, S. (2010). The role of pattern-recognition receptors in innate immunity: update on Toll-like receptors. Nat Immunol *11*, 373-384.

Kazunori Handa, M.T., Michio Yamagishi, Sadafumi Ohmura, Jiro Sawada, Ichiro Tanaka (1978). Isolation and Characterization of E-64, a New Thiol Protease Inhibitor. Agricultural and Biological Chemistry *42*, 523-528.

Kerur, N., Veettil, M.V., Sharma-Walia, N., Bottero, V., Sadagopan, S., Otageri, P., and Chandran, B. (2011). IFI16 acts as a nuclear pathogen sensor to induce the inflammasome in response to Kaposi Sarcoma-associated herpesvirus infection. Cell Host Microbe *9*, 363-375.

Kile, A.C., Chavez, D.A., Bacal, J., Eldirany, S., Korzhnev, D.M., Bezsonova, I., Eichman, B.F., and Cimprich, K.A. (2015). HLTF's Ancient HIRAN Domain Binds 3' DNA Ends to Drive Replication Fork Reversal. Mol Cell *58*, 1090-1100.

Kim, J.E., Kim, Y.E., Stinski, M.F., Ahn, J.H., and Song, Y.J. (2017). Human Cytomegalovirus IE2 86 kDa Protein Induces STING Degradation and Inhibits cGAMP-Mediated IFN-β Induction. Frontiers in microbiology *8*, 1854.

Kim, T., Pazhoor, S., Bao, M., Zhang, Z., Hanabuchi, S., Facchinetti, V., Bover, L., Plumas, J., Chaperot, L., Qin, J.*, et al.* (2010). Aspartate-glutamate-alanine-histidine box motif (DEAH)/RNA helicase A helicases sense microbial DNA in human plasmacytoid dendritic cells. Proc Natl Acad Sci U S A *107*, 15181-15186.

Kim, Y.C., and Guan, K.L. (2015). mTOR: a pharmacologic target for autophagy regulation. The Journal of clinical investigation *125*, 25-32.

Kim, Y.E., and Ahn, J.H. (2010). Role of the specific interaction of UL112-113 p84 with UL44 DNA polymerase processivity factor in promoting DNA replication of human cytomegalovirus. Journal of virology *84*, 8409-8421.

Kim, Y.E., Lee, J.H., Kim, E.T., Shin, H.J., Gu, S.Y., Seol, H.S., Ling, P.D., Lee, C.H., and Ahn, J.H. (2011). Human cytomegalovirus infection causes degradation of Sp100 proteins that suppress viral gene expression. Journal of virology *85*, 11928-11937.

Kirisako, T., Kamei, K., Murata, S., Kato, M., Fukumoto, H., Kanie, M., Sano, S., Tokunaga, F., Tanaka, K., and Iwai, K. (2006). A ubiquitin ligase complex assembles linear polyubiquitin chains. Embo j *25*, 4877-4887.

Kisselev, A.F., and Goldberg, A.L. (2001). Proteasome inhibitors: from research tools to drug candidates. Chem Biol *8*, 739-758.

Kitada, T., Asakawa, S., Hattori, N., Matsumine, H., Yamamura, Y., Minoshima, S., Yokochi, M., Mizuno, Y., and Shimizu, N. (1998). Mutations in the parkin gene cause autosomal recessive juvenile parkinsonism. Nature *392*, 605-608.

Korioth, F., Maul, G.G., Plachter, B., Stamminger, T., and Frey, J. (1996). The nuclear domain 10 (ND10) is disrupted by the human cytomegalovirus gene product IE1. Exp Cell Res *229*, 155-158.

Koshizuka, T., Kobayashi, T., Ishioka, K., and Suzutani, T. (2018). Herpesviruses possess conserved proteins for interaction with Nedd4 family ubiquitin E3 ligases. Sci Rep *8*, 4447.

Koshizuka, T., Tanaka, K., and Suzutani, T. (2016). Degradation of host ubiquitin E3 ligase Itch by human cytomegalovirus UL42. The Journal of general virology *97*, 196-208.

Krishna, B.A., Wills, M.R., and Sinclair, J.H. (2019). Advances in the treatment of cytomegalovirus. Br Med Bull *131*, 5-17.

Krug, A., French, A.R., Barchet, W., Fischer, J.A., Dzionek, A., Pingel, J.T., Orihuela, M.M., Akira, S., Yokoyama, W.M., and Colonna, M. (2004a). TLR9-dependent recognition of MCMV by IPC and DC generates coordinated cytokine responses that activate antiviral NK cell function. Immunity *21*, 107-119.

Krug, A., Luker, G.D., Barchet, W., Leib, D.A., Akira, S., and Colonna, M. (2004b). Herpes simplex virus type 1 activates murine natural interferon-producing cells through toll-like receptor 9. Blood *103*, 1433-1437.

Krzyzaniak, M.A., Zumstein, M.T., Gerez, J.A., Picotti, P., and Helenius, A. (2013). Host cell entry of respiratory syncytial virus involves macropinocytosis followed by proteolytic activation of the F protein. PLoS pathogens *9*, e1003309.

Kubiczkova, L., Pour, L., Sedlarikova, L., Hajek, R., and Sevcikova, S. (2014). Proteasome inhibitors - molecular basis and current perspectives in multiple myeloma. J Cell Mol Med *18*, 947-961.

Kudoh, A., Fujita, M., Zhang, L., Shirata, N., Daikoku, T., Sugaya, Y., Isomura, H., Nishiyama, Y., and Tsurumi, T. (2005). Epstein-Barr virus lytic replication elicits ATM checkpoint signal transduction while providing an S-phase-like cellular environment. J Biol Chem *280*, 8156-8163.

Kudoh, A., Iwahori, S., Sato, Y., Nakayama, S., Isomura, H., Murata, T., and Tsurumi, T. (2009). Homologous recombinational repair factors are recruited and loaded onto the viral DNA genome in Epstein-Barr virus replication compartments. Journal of virology *83*, 6641-6651.

Kumari, P., Saha, I., Narayanan, A., Narayanan, S., Takaoka, A., Kumar, N.S., Tailor, P., and Kumar, H. (2017). Essential role of HCMV deubiquitinase in promoting oncogenesis by targeting anti-viral innate immune signaling pathways. Cell death & disease *8*, e3078.

Kuriakose, T., and Kanneganti, T.D. (2018). ZBP1: Innate Sensor Regulating Cell Death and Inflammation. Trends Immunol *39*, 123-134.

Kwun, H.J., da Silva, S.R., Shah, I.M., Blake, N., Moore, P.S., and Chang, Y. (2007). Kaposi's sarcoma-associated herpesvirus latency-associated nuclear antigen 1 mimics Epstein-Barr virus EBNA1 immune evasion through central repeat domain effects on protein processing. Journal of virology *81*, 8225-8235.

Laguette, N., Brégnard, C., Hue, P., Basbous, J., Yatim, A., Larroque, M., Kirchhoff, F., Constantinou, A., Sobhian, B., and Benkirane, M. (2014). Premature activation of the SLX4 complex by Vpr promotes G2/M arrest and escape from innate immune sensing. Cell *156*, 134-145.

Laguette, N., Sobhian, B., Casartelli, N., Ringeard, M., Chable-Bessia, C., Ségéral, E., Yatim, A., Emiliani, S., Schwartz, O., and Benkirane, M. (2011). SAMHD1 is the dendritic- and myeloid-cell-specific HIV-1 restriction factor counteracted by Vpx. Nature *474*, 654-657.

Lahouassa, H., Blondot, M.L., Chauveau, L., Chougui, G., Morel, M., Leduc, M., Guillonneau, F., Ramirez, B.C., Schwartz, O., and Margottin-Goguet, F. (2016). HIV-1 Vpr degrades the HLTF DNA translocase in T cells and macrophages. Proc Natl Acad Sci U S A *113*, 5311-5316.

Lam, E., Stein, S., and Falck-Pedersen, E. (2014). Adenovirus detection by the cGAS/STING/TBK1 DNA sensing cascade. Journal of virology *88*, 974-981.

Landy, A. (1989). Dynamic, structural, and regulatory aspects of lambda site-specific recombination. Annu Rev Biochem *58*, 913-949.

Laplante, M., and Sabatini, D.M. (2012). mTOR signaling in growth control and disease. Cell *149*, 274-293.

Lasfar, A., Lewis-Antes, A., Smirnov, S.V., Anantha, S., Abushahba, W., Tian, B., Reuhl, K., Dickensheets, H., Sheikh, F., Donnelly, R.P*., et al.* (2006). Characterization of the mouse IFN-lambda ligand-receptor system: IFN-lambdas exhibit antitumor activity against B16 melanoma. Cancer research *66*, 4468-4477.

Lawrence, T. (2009). The nuclear factor NF-kappaB pathway in inflammation. Cold Spring Harb Perspect Biol *1*, a001651.

Le-Trilling, V.T.K., Becker, T., Nachshon, A., Stern-Ginossar, N., Schöler, L., Voigt, S., Hengel, H., and Trilling, M. (2020). The Human Cytomegalovirus pUL145 Isoforms Act as Viral DDB1-Cullin-Associated Factors to Instruct Host Protein Degradation to Impede Innate Immunity. Cell Rep *30*, 2248-2260.e2245.

Le, V.T.K., Trilling, M., Wilborn, M., Hengel, H., and Zimmermann, A. (2008). Human cytomegalovirus interferes with signal transducer and activator of transcription (STAT) 2 protein stability and tyrosine phosphorylation. The Journal of general virology *89*, 2416-2426.

Lecker, S.H., Goldberg, A.L., and Mitch, W.E. (2006). Protein degradation by the ubiquitin-proteasome pathway in normal and disease states. J Am Soc Nephrol *17*, 1807-1819.

Lee, A.J., and Ashkar, A.A. (2018). The Dual Nature of Type I and Type II Interferons. Front Immunol *9*, 2061.

Lee, H.R., Huh, Y.H., Kim, Y.E., Lee, K., Kim, S., and Ahn, J.H. (2007). N-terminal determinants of human cytomegalovirus IE1 protein in nuclear targeting and disrupting PML-associated subnuclear structures. Biochemical and biophysical research communications *356*, 499-504.

Lee, M.S., and Kim, Y.J. (2007). Signaling pathways downstream of pattern-recognition receptors and their cross talk. Annu Rev Biochem *76*, 447-480.

Leoni, V., Gianni, T., Salvioli, S., and Campadelli-Fiume, G. (2012). Herpes simplex virus glycoproteins gH/gL and gB bind Toll-like receptor 2, and soluble gH/gL is sufficient to activate NF-κB. Journal of virology *86*, 6555-6562.

Leupin, O., Bontron, S., Schaeffer, C., and Strubin, M. (2005). Hepatitis B virus X protein stimulates viral genome replication via a DDB1-dependent pathway distinct from that leading to cell death. Journal of virology *79*, 4238-4245.

Levine, B., and Kroemer, G. (2008). Autophagy in the pathogenesis of disease. Cell *132*, 27-42.

Li, R., Zhu, J., Xie, Z., Liao, G., Liu, J., Chen, M.R., Hu, S., Woodard, C., Lin, J., Taverna, S.D.*, et al.* (2011). Conserved herpesvirus kinases target the DNA damage response pathway and TIP60 histone acetyltransferase to promote virus replication. Cell Host Microbe *10*, 390-400.

Li, T., Chen, J., and Cristea, I.M. (2013a). Human cytomegalovirus tegument protein pUL83 inhibits IFI16-mediated DNA sensing for immune evasion. Cell Host Microbe *14*, 591-599.

Li, T., Diner, B.A., Chen, J., and Cristea, I.M. (2012). Acetylation modulates cellular distribution and DNA sensing ability of interferon-inducible protein IFI16. Proc Natl Acad Sci U S A *109*, 10558-10563.

Li, T., Robert, E.I., van Breugel, P.C., Strubin, M., and Zheng, N. (2010). A promiscuous alpha-helical motif anchors viral hijackers and substrate receptors to the CUL4-DDB1 ubiquitin ligase machinery. Nat Struct Mol Biol *17*, 105-111.

Li, X.D., Wu, J., Gao, D., Wang, H., Sun, L., and Chen, Z.J. (2013b). Pivotal roles of cGAS-cGAMP signaling in antiviral defense and immune adjuvant effects. Science *341*, 1390-1394.

Li, Z., Pei, X.H., Yan, J., Yan, F., Cappell, K.M., Whitehurst, A.W., and Xiong, Y. (2014). CUL9 mediates the functions of the 3M complex and ubiquitylates survivin to maintain genome integrity. Mol Cell *54*, 805-819.

Liang, Q., Seo, G.J., Choi, Y.J., Kwak, M.J., Ge, J., Rodgers, M.A., Shi, M., Leslie, B.J., Hopfner, K.P., Ha, T.*, et al.* (2014). Crosstalk between the cGAS DNA sensor and Beclin-1 autophagy protein shapes innate antimicrobial immune responses. Cell Host Microbe *15*, 228-238.

Lilley, C.E., Carson, C.T., Muotri, A.R., Gage, F.H., and Weitzman, M.D. (2005). DNA repair proteins affect the lifecycle of herpes simplex virus 1. Proc Natl Acad Sci U S A *102*, 5844-5849.

Lilley, C.E., Chaurushiya, M.S., Boutell, C., Landry, S., Suh, J., Panier, S., Everett, R.D., Stewart, G.S., Durocher, D., and Weitzman, M.D. (2010). A viral E3 ligase targets RNF8 and RNF168 to control histone ubiquitination and DNA damage responses. Embo j *29*, 943-955.

Lio, C.W., McDonald, B., Takahashi, M., Dhanwani, R., Sharma, N., Huang, J., Pham, E., Benedict, C.A., and Sharma, S. (2016). cGAS-STING Signaling Regulates Initial Innate Control of Cytomegalovirus Infection. Journal of virology *90*, 7789-7797.

Liu, G., Yu, F.X., Kim, Y.C., Meng, Z., Naipauer, J., Looney, D.J., Liu, X., Gutkind, J.S., Mesri, E.A., and Guan, K.L. (2015). Kaposi sarcoma-associated herpesvirus promotes tumorigenesis by modulating the Hippo pathway. Oncogene *34*, 3536-3546.

Liu, X., Yang, N., Figel, S.A., Wilson, K.E., Morrison, C.D., Gelman, I.H., and Zhang, J. (2013). PTPN14 interacts with and negatively regulates the oncogenic function of YAP. Oncogene *32*, 1266-1273.

Ljungman, P., Griffiths, P., and Paya, C. (2002). Definitions of cytomegalovirus infection and disease in transplant recipients. Clin Infect Dis *34*, 1094-1097.

Lugrin, J., and Martinon, F. (2018). The AIM2 inflammasome: Sensor of pathogens and cellular perturbations. Immunol Rev *281*, 99-114.

Lund, J., Sato, A., Akira, S., Medzhitov, R., and Iwasaki, A. (2003). Toll-like receptor 9-mediated recognition of Herpes simplex virus-2 by plasmacytoid dendritic cells. J Exp Med *198*, 513-520.

Luo, M.H., Rosenke, K., Czornak, K., and Fortunato, E.A. (2007). Human cytomegalovirus disrupts both ataxia telangiectasia mutated protein (ATM)- and ATM-Rad3-related kinase-mediated DNA damage responses during lytic infection. Journal of virology *81*, 1934-1950.

Lurain, N.S., Kapell, K.S., Huang, D.D., Short, J.A., Paintsil, J., Winkfield, E., Benedict, C.A., Ware, C.F., and Bremer, J.W. (1999). Human cytomegalovirus UL144 open reading frame: sequence hypervariability in low-passage clinical isolates. Journal of virology *73*, 10040-10050.

Lussignol, M., Queval, C., Bernet-Camard, M.F., Cotte-Laffitte, J., Beau, I., Codogno, P., and Esclatine, A. (2013). The herpes simplex virus 1 Us11 protein inhibits autophagy through its interaction with the protein kinase PKR. Journal of virology *87*, 859-871.

Lüttichau, H.R. (2010). The cytomegalovirus UL146 gene product vCXCL1 targets both CXCR1 and CXCR2 as an agonist. J Biol Chem *285*, 9137-9146.

Lutz-Nicoladoni, C., Wolf, D., and Sopper, S. (2015). Modulation of Immune Cell Functions by the E3 Ligase Cbl-b. Front Oncol *5*, 58.

Luzio, J.P., Hackmann, Y., Dieckmann, N.M., and Griffiths, G.M. (2014). The biogenesis of lysosomes and lysosome-related organelles. Cold Spring Harb Perspect Biol *6*, a016840.

Luzio, J.P., Pryor, P.R., and Bright, N.A. (2007). Lysosomes: fusion and function. Nat Rev Mol Cell Biol *8*, 622-632.

Lydeard, J.R., Schulman, B.A., and Harper, J.W. (2013). Building and remodelling Cullin-RING E3 ubiquitin ligases. EMBO Rep *14*, 1050-1061.

Macleod, K.F., Sherry, N., Hannon, G., Beach, D., Tokino, T., Kinzler, K., Vogelstein, B., and Jacks, T. (1995). p53-dependent and independent expression of p21 during cell growth, differentiation, and DNA damage. Genes Dev *9*, 935-944.

Mahajan, M.C., and Weissman, S.M. (2002). DNA-dependent adenosine triphosphatase (helicaselike transcription factor) activates beta-globin transcription in K562 cells. Blood *99*, 348-356.

Marty, F.M., Ljungman, P., Chemaly, R.F., Maertens, J., Dadwal, S.S., Duarte, R.F., Haider, S., Ullmann, A.J., Katayama, Y., Brown, J.*, et al.* (2017). Letermovir Prophylaxis for Cytomegalovirus in Hematopoietic-Cell Transplantation. N Engl J Med *377*, 2433-2444.

Matsuoka, S., Rotman, G., Ogawa, A., Shiloh, Y., Tamai, K., and Elledge, S.J. (2000). Ataxia telangiectasia-mutated phosphorylates Chk2 in vivo and in vitro. Proc Natl Acad Sci U S A *97*, 10389-10394.

Maul, G.G. (2008). Initiation of cytomegalovirus infection at ND10. Current topics in microbiology and immunology *325*, 117-132.

Maxfield, F.R. (2014). Role of endosomes and lysosomes in human disease. Cold Spring Harb Perspect Biol *6*, a016931.

Maxson, M.E., and Grinstein, S. (2014). The vacuolar-type H^+-ATPase at a glance - more than a proton pump. J Cell Sci *127*, 4987-4993.

Maya, R., Balass, M., Kim, S.T., Shkedy, D., Leal, J.F., Shifman, O., Moas, M., Buschmann, T., Ronai, Z., Shiloh, Y.*, et al.* (2001). ATM-dependent phosphorylation of Mdm2 on serine 395: role in p53 activation by DNA damage. Genes Dev *15*, 1067-1077.

McAlister, G.C., Nusinow, D.P., Jedrychowski, M.P., Wühr, M., Huttlin, E.L., Erickson, B.K., Rad, R., Haas, W., and Gygi, S.P. (2014). MultiNotch MS3 enables accurate, sensitive, and multiplexed detection of differential expression across cancer cell line proteomes. Anal Chem *86*, 7150-7158.

McFarlane, S., Aitken, J., Sutherland, J.S., Nicholl, M.J., Preston, V.G., and Preston, C.M. (2011). Early induction of autophagy in human fibroblasts after infection with human cytomegalovirus or herpes simplex virus 1. Journal of virology *85*, 4212-4221.

McGeoch, D.J., and Gatherer, D. (2005). Integrating reptilian herpesviruses into the family herpesviridae. Journal of virology *79*, 725-731.

Melchjorsen, J., Rintahaka, J., Søby, S., Horan, K.A., Poltajainen, A., Østergaard, L., Paludan, S.R., and Matikainen, S. (2010). Early innate recognition of herpes simplex virus in human primary macrophages is mediated via the MDA5/MAVS-dependent and

MDA5/MAVS/RNA polymerase III-independent pathways. Journal of virology *84*, 11350-11358.

Meng, B., and Lever, A.M. (2013). Wrapping up the bad news: HIV assembly and release. Retrovirology *10*, 5.

Meng, Z., Moroishi, T., and Guan, K.L. (2016). Mechanisms of Hippo pathway regulation. Genes Dev *30*, 1-17.

Mercer, J., and Helenius, A. (2012). Gulping rather than sipping: macropinocytosis as a way of virus entry. Curr Opin Microbiol *15*, 490-499.

Merkl, P.E., and Knipe, D.M. (2019). Role for a Filamentous Nuclear Assembly of IFI16, DNA, and Host Factors in Restriction of Herpesviral Infection. mBio *10*.

Mettenleiter, T.C. (2002). Herpesvirus assembly and egress. Journal of virology *76*, 1537-1547.

Metzger, M.B., Pruneda, J.N., Klevit, R.E., and Weissman, A.M. (2014). RING-type E3 ligases: master manipulators of E2 ubiquitin-conjugating enzymes and ubiquitination. Biochimica et biophysica acta *1843*, 47-60.

Miyahira, A.K., Shahangian, A., Hwang, S., Sun, R., and Cheng, G. (2009). TANK-binding kinase-1 plays an important role during in vitro and in vivo type I IFN responses to DNA virus infections. J Immunol *182*, 2248-2257.

Miyawaki, A. (2011). Development of probes for cellular functions using fluorescent proteins and fluorescence resonance energy transfer. Annu Rev Biochem *80*, 357-373.

Mocarski, E.J. (2007). Betaherpes viral genes and their functions. In Human Herpesviruses: Biology, Therapy, and Immunoprophylaxis, A.C.-F. Arvin, G.; Mocarski, E.; Moore, P. S.; Roizman, B.; Whitley, R.; Yamanishi, K., ed. (Cambridge: Cambridge University Press).

Mocarski, E.S., Jr, Shenk, T., Griffiths, P.D., and Pass, R.F. (2013). Cytomegaloviruses. In Fields' virology, B.N. Fields, D.M. Knipe, and P.M. Howley, eds. (Philadelphia: Wolters Kluwer/Lippincott Williams & Wilkins Health).

Mocarski, E.S., Prichard, M.N., Tan, C.S., and Brown, J.M. (1997). Reassessing the Organization of the UL42 – UL43 Region of the Human Cytomegalovirus Strain AD169 Genome. Virology *239*, 169-175.

Montaser, M., Lalmanach, G., and Mach, L. (2002). CA-074, but not its methyl ester CA-074Me, is a selective inhibitor of cathepsin B within living cells. Biol Chem *383*, 1305-1308.

Morrone, S.R., Wang, T., Constantoulakis, L.M., Hooy, R.M., Delannoy, M.J., and Sohn, J. (2014). Cooperative assembly of IFI16 filaments on dsDNA provides insights into host defense strategy. Proc Natl Acad Sci U S A *111*, E62-71.

Motegi, A., Liaw, H.J., Lee, K.Y., Roest, H.P., Maas, A., Wu, X., Moinova, H., Markowitz, S.D., Ding, H., Hoeijmakers, J.H.*, et al.* (2008). Polyubiquitination of proliferating cell nuclear antigen by HLTF and SHPRH prevents genomic instability from stalled replication forks. Proc Natl Acad Sci U S A *105*, 12411-12416.

Mouna, L., Hernandez, E., Bonte, D., Brost, R., Amazit, L., Delgui, L.R., Brune, W., Geballe, A.P., Beau, I., and Esclatine, A. (2016). Analysis of the role of autophagy inhibition by two complementary human cytomegalovirus BECN1/Beclin 1-binding proteins. Autophagy *12*, 327-342.

Murata, M., Miyashita, S., Yokoo, C., Tamai, M., Hanada, K., Hatayama, K., Towatari, T., Nikawa, T., and Katunuma, N. (1991). Novel epoxysuccinyl peptides. Selective inhibitors of cathepsin B, in vitro. FEBS Lett *280*, 307-310.

Nailwal, H., and Chan, F.K. (2019). Necroptosis in anti-viral inflammation. Cell Death Differ *26*, 4-13.

Nakatogawa, H. (2013). Two ubiquitin-like conjugation systems that mediate membrane formation during autophagy. Essays Biochem *55*, 39-50.

Nevels, M., Nitzsche, A., and Paulus, C. (2011). How to control an infectious bead string: nucleosome-based regulation and targeting of herpesvirus chromatin. Reviews in medical virology *21*, 154-180.

Nightingale, K., Lin, K.M., Ravenhill, B.J., Davies, C., Nobre, L., Fielding, C.A., Ruckova, E., Fletcher-Etherington, A., Soday, L., Nichols, H.*, et al.* (2018). High-Definition Analysis of Host Protein Stability during Human Cytomegalovirus Infection Reveals Antiviral Factors and Viral Evasion Mechanisms. Cell Host Microbe *24*, 447-460.e411.

Nikitin, P.A., Yan, C.M., Forte, E., Bocedi, A., Tourigny, J.P., White, R.E., Allday, M.J., Patel, A., Dave, S.S., Kim, W.*, et al.* (2010). An ATM/Chk2-mediated DNA damage-responsive signaling pathway suppresses Epstein-Barr virus transformation of primary human B cells. Cell Host Microbe *8*, 510-522.

Nobre, L.V., Nightingale, K., Ravenhill, B.J., Antrobus, R., Soday, L., Nichols, J., Davies, J.A., Seirafian, S., Wang, E.C., Davison, A.J.*, et al.* (2019). Human cytomegalovirus interactome analysis identifies degradation hubs, domain associations and viral protein functions. Elife *8*.

Nowag, H., Guhl, B., Thriene, K., Romao, S., Ziegler, U., Dengjel, J., and Münz, C. (2014). Macroautophagy Proteins Assist Epstein Barr Virus Production and Get Incorporated Into the Virus Particles. EBioMedicine *1*, 116-125.

Orlikowski, D., Porcher, R., Sivadon-Tardy, V., Quincampoix, J.C., Raphaël, J.C., Durand, M.C., Sharshar, T., Roussi, J., Caudie, C., Annane, D.*, et al.* (2011). Guillain-Barré syndrome following primary cytomegalovirus infection: a prospective cohort study. Clin Infect Dis *52*, 837-844.

Orvedahl, A., Alexander, D., Tallóczy, Z., Sun, Q., Wei, Y., Zhang, W., Burns, D., Leib, D.A., and Levine, B. (2007). HSV-1 ICP34.5 confers neurovirulence by targeting the Beclin 1 autophagy protein. Cell Host Microbe *1*, 23-35.

Orvedahl, A., MacPherson, S., Sumpter, R., Jr., Tallóczy, Z., Zou, Z., and Levine, B. (2010). Autophagy protects against Sindbis virus infection of the central nervous system. Cell Host Microbe *7*, 115-127.

Orzalli, M.H., DeLuca, N.A., and Knipe, D.M. (2012). Nuclear IFI16 induction of IRF-3 signaling during herpesviral infection and degradation of IFI16 by the viral ICP0 protein. Proc Natl Acad Sci U S A *109*, E3008-3017.

Paijo, J., Döring, M., Spanier, J., Grabski, E., Nooruzzaman, M., Schmidt, T., Witte, G., Messerle, M., Hornung, V., Kaever, V.*, et al.* (2016). cGAS Senses Human Cytomegalovirus and Induces Type I Interferon Responses in Human Monocyte-Derived Cells. PLoS pathogens *12*, e1005546.

Palhegyi, A.M., Seranova, E., Dimova, S., Hoque, S., and Sarkar, S. (2019). Biomedical Implications of Autophagy in Macromolecule Storage Disorders. Front Cell Dev Biol *7*, 179.

Paludan, C., Schmid, D., Landthaler, M., Vockerodt, M., Kube, D., Tuschl, T., and Münz, C. (2005). Endogenous MHC class II processing of a viral nuclear antigen after autophagy. Science *307*, 593-596.

Pari, G.S., and Anders, D.G. (1993). Eleven loci encoding trans-acting factors are required for transient complementation of human cytomegalovirus oriLyt-dependent DNA replication. Journal of virology *67*, 6979-6988.

Park, M.Y., Kim, Y.E., Seo, M.R., Lee, J.R., Lee, C.H., and Ahn, J.H. (2006). Interactions among four proteins encoded by the human cytomegalovirus UL112-113 region regulate their intranuclear targeting and the recruitment of UL44 to prereplication foci. Journal of virology *80*, 2718-2727.

Parker, G.A., Touitou, R., and Allday, M.J. (2000). Epstein-Barr virus EBNA3C can disrupt multiple cell cycle checkpoints and induce nuclear division divorced from cytokinesis. Oncogene *19*, 700-709.

Paulus, C., Krauss, S., and Nevels, M. (2006). A human cytomegalovirus antagonist of type I IFN-dependent signal transducer and activator of transcription signaling. Proc Natl Acad Sci U S A *103*, 3840-3845.

Pellett, P.E., and Roizman, B. (2013). Herpesviridae. In Fields' virology, B.N. Fields, D.M. Knipe, and P.M. Howley, eds. (Philadelphia: Wolters Kluwer/Lippincott Williams & Wilkins Health).

Penfold, M.E., Dairaghi, D.J., Duke, G.M., Saederup, N., Mocarski, E.S., Kemble, G.W., and Schall, T.J. (1999). Cytomegalovirus encodes a potent alpha chemokine. Proc Natl Acad Sci U S A *96*, 9839-9844.

Peng, C.Y., Graves, P.R., Thoma, R.S., Wu, Z., Shaw, A.S., and Piwnica-Worms, H. (1997). Mitotic and G2 checkpoint control: regulation of 14-3-3 protein binding by phosphorylation of Cdc25C on serine-216. Science *277*, 1501-1505.

Peters, N.E., Ferguson, B.J., Mazzon, M., Fahy, A.S., Krysztofinska, E., Arribas-Bosacoma, R., Pearl, L.H., Ren, H., and Smith, G.L. (2013). A mechanism for the inhibition of DNA-PK-mediated DNA sensing by a virus. PLoS pathogens *9*, e1003649.

Petroski, M.D., and Deshaies, R.J. (2005). Function and regulation of cullin-RING ubiquitin ligases. Nat Rev Mol Cell Biol *6*, 9-20.

Pham, T.H., Kwon, K.M., Kim, Y.E., Kim, K.K., and Ahn, J.H. (2013). DNA sensing-independent inhibition of herpes simplex virus 1 replication by DAI/ZBP1. Journal of virology *87*, 3076-3086.

Platanias, L.C. (2005). Mechanisms of type-I- and type-II-interferon-mediated signalling. Nat Rev Immunol *5*, 375-386.

Poole, E., Juss, J.K., Krishna, B., Herre, J., Chilvers, E.R., and Sinclair, J. (2015). Alveolar Macrophages Isolated Directly From Human Cytomegalovirus (HCMV)-Seropositive Individuals Are Sites of HCMV Reactivation In Vivo. J Infect Dis *211*, 1936-1942.

Powers, C., DeFilippis, V., Malouli, D., and Fruh, K. (2008). Cytomegalovirus immune evasion. Current topics in microbiology and immunology *325*, 333-359.

Price, C.T., Al-Quadan, T., Santic, M., Rosenshine, I., and Abu Kwaik, Y. (2011). Host proteasomal degradation generates amino acids essential for intracellular bacterial growth. Science *334*, 1553-1557.

Prod'homme, V., Sugrue, D.M., Stanton, R.J., Nomoto, A., Davies, J., Rickards, C.R., Cochrane, D., Moore, M., Wilkinson, G.W.G., and Tomasec, P. (2010). Human cytomegalovirus UL141 promotes efficient downregulation of the natural killer cell activating ligand CD112. The Journal of general virology *91*, 2034-2039.

Qing, P., Han, L., Bin, L., Yan, L., and Ping, W.X. (2011). USP7 regulates the stability and function of HLTF through deubiquitination. Journal of cellular biochemistry *112*, 3856-3862.

Raftery, M.J., Möncke-Buchner, E., Matsumura, H., Giese, T., Winkelmann, A., Reuter, M., Terauchi, R., Schönrich, G., and Krüger, D.H. (2009). Unravelling the interaction of human cytomegalovirus with dendritic cells by using SuperSAGE. The Journal of general virology *90*, 2221-2233.

Raiborg, C., and Stenmark, H. (2009). The ESCRT machinery in endosomal sorting of ubiquitylated membrane proteins. Nature *458*, 445-452.

Rappsilber, J., Mann, M., and Ishihama, Y. (2007). Protocol for micro-purification, enrichment, pre-fractionation and storage of peptides for proteomics using StageTips. Nat Protoc *2*, 1896-1906.

Rasmussen, S.B., Sørensen, L.N., Malmgaard, L., Ank, N., Baines, J.D., Chen, Z.J., and Paludan, S.R. (2007). Type I interferon production during herpes simplex virus infection is controlled by cell-type-specific viral recognition through Toll-like receptor 9, the mitochondrial antiviral signaling protein pathway, and novel recognition systems. Journal of virology *81*, 13315-13324.

Rathinam, V.A., Jiang, Z., Waggoner, S.N., Sharma, S., Cole, L.E., Waggoner, L., Vanaja, S.K., Monks, B.G., Ganesan, S., Latz, E.*, et al.* (2010). The AIM2 inflammasome is essential for host defense against cytosolic bacteria and DNA viruses. Nat Immunol *11*, 395-402.

Rebsamen, M., Heinz, L.X., Meylan, E., Michallet, M.C., Schroder, K., Hofmann, K., Vazquez, J., Benedict, C.A., and Tschopp, J. (2009). DAI/ZBP1 recruits RIP1 and RIP3 through RIP homotypic interaction motifs to activate NF-kappaB. EMBO Rep *10*, 916-922.

Reeves, M., Murphy, J., Greaves, R., Fairley, J., Brehm, A., and Sinclair, J. (2006). Autorepression of the human cytomegalovirus major immediate-early promoter/enhancer at late times of infection is mediated by the recruitment of chromatin remodeling enzymes by IE86. Journal of virology *80*, 9998-10009.

Reeves, M.B. (2011). Chromatin-mediated regulation of cytomegalovirus gene expression. Virus Res *157*, 134-143.

Reeves, M.B., and Sinclair, J.H. (2013). Circulating dendritic cells isolated from healthy seropositive donors are sites of human cytomegalovirus reactivation in vivo. Journal of virology *87*, 10660-10667.

Revello, M.G., and Gerna, G. (2010). Human cytomegalovirus tropism for endothelial/epithelial cells: scientific background and clinical implications. Reviews in medical virology *20*, 136-155.

Rodrigues, L., Filipe, J., Seldon, M.P., Fonseca, L., Anrather, J., Soares, M.P., and Simas, J.P. (2009). Termination of NF-kappaB activity through a gammaherpesvirus protein that assembles an EC5S ubiquitin-ligase. Embo j *28*, 1283-1295.

Rosenke, K., and Fortunato, E.A. (2004). Bromodeoxyuridine-labeled viral particles as a tool for visualization of the immediate-early events of human cytomegalovirus infection. Journal of virology *78*, 7818-7822.

Sagnier, S., Daussy, C.F., Borel, S., Robert-Hebmann, V., Faure, M., Blanchet, F.P., Beaumelle, B., Biard-Piechaczyk, M., and Espert, L. (2015). Autophagy restricts HIV-1 infection by selectively degrading Tat in CD4+ T lymphocytes. Journal of virology *89*, 615-625.

Saitoh, T., Fujita, N., Hayashi, T., Takahara, K., Satoh, T., Lee, H., Matsunaga, K., Kageyama, S., Omori, H., Noda, T.*, et al.* (2009). Atg9a controls dsDNA-driven dynamic translocation of STING and the innate immune response. Proc Natl Acad Sci U S A *106*, 20842-20846.

Salsman, J., Jagannathan, M., Paladino, P., Chan, P.K., Dellaire, G., Raught, B., and Frappier, L. (2012). Proteomic profiling of the human cytomegalovirus UL35 gene products reveals a role for UL35 in the DNA repair response. Journal of virology *86*, 806-820.

Salvant, B.S., Fortunato, E.A., and Spector, D.H. (1998). Cell cycle dysregulation by human cytomegalovirus: influence of the cell cycle phase at the time of infection and effects on cyclin transcription. Journal of virology *72*, 3729-3741.

Sánchez-Tena, S., Cubillos-Rojas, M., Schneider, T., and Rosa, J.L. (2016). Functional and pathological relevance of HERC family proteins: a decade later. Cell Mol Life Sci *73*, 1955-1968.

Sanchez, V., Angeletti, P.C., Engler, J.A., and Britt, W.J. (1998). Localization of human cytomegalovirus structural proteins to the nuclear matrix of infected human fibroblasts. Journal of virology *72*, 3321-3329.

Sanchez, V., and Spector, D.H. (2008). Subversion of cell cycle regulatory pathways. Current topics in microbiology and immunology *325*, 243-262.

Santos, C.A. (2016). Cytomegalovirus and Other β-Herpesviruses. Semin Nephrol *36*, 351-361.

Sarisky, R.T., and Hayward, G.S. (1996). Evidence that the UL84 gene product of human cytomegalovirus is essential for promoting oriLyt-dependent DNA replication and

formation of replication compartments in cotransfection assays. Journal of virology *70*, 7398-7413.

Satheshkumar, P.S., Anton, L.C., Sanz, P., and Moss, B. (2009). Inhibition of the ubiquitin-proteasome system prevents vaccinia virus DNA replication and expression of intermediate and late genes. Journal of virology *83*, 2469-2479.

Sato, S., Sugiyama, M., Yamamoto, M., Watanabe, Y., Kawai, T., Takeda, K., and Akira, S. (2003). Toll/IL-1 receptor domain-containing adaptor inducing IFN-beta (TRIF) associates with TNF receptor-associated factor 6 and TANK-binding kinase 1, and activates two distinct transcription factors, NF-kappa B and IFN-regulatory factor-3, in the Toll-like receptor signaling. J Immunol *171*, 4304-4310.

Sato, Y., Kamura, T., Shirata, N., Murata, T., Kudoh, A., Iwahori, S., Nakayama, S., Isomura, H., Nishiyama, Y., and Tsurumi, T. (2009a). Degradation of phosphorylated p53 by viral protein-ECS E3 ligase complex. PLoS pathogens *5*, e1000530.

Sato, Y., Shirata, N., Kudoh, A., Iwahori, S., Nakayama, S., Murata, T., Isomura, H., Nishiyama, Y., and Tsurumi, T. (2009b). Expression of Epstein-Barr virus BZLF1 immediate-early protein induces p53 degradation independent of MDM2, leading to repression of p53-mediated transcription. Virology *388*, 204-211.

Schoggins, J.W., MacDuff, D.A., Imanaka, N., Gainey, M.D., Shrestha, B., Eitson, J.L., Mar, K.B., Richardson, R.B., Ratushny, A.V., Litvak, V.*, et al.* (2014). Pan-viral specificity of IFN-induced genes reveals new roles for cGAS in innate immunity. Nature *505*, 691-695.

Schreiner, S., and Wodrich, H. (2013). Virion factors that target Daxx to overcome intrinsic immunity. Journal of virology *87*, 10412-10422.

Scigelova, M., Hornshaw, M., Giannakopulos, A., and Makarov, A. (2011). Fourier transform mass spectrometry. Mol Cell Proteomics *10*, M111.009431.

Šedý, J.R., Bjordahl, R.L., Bekiaris, V., Macauley, M.G., Ware, B.C., Norris, P.S., Lurain, N.S., Benedict, C.A., and Ware, C.F. (2013). CD160 activation by herpesvirus entry mediator augments inflammatory cytokine production and cytolytic function by NK cells. J Immunol *191*, 828-836.

Seo, J.Y., and Cresswell, P. (2013). Viperin regulates cellular lipid metabolism during human cytomegalovirus infection. PLoS pathogens *9*, e1003497.

Seo, J.Y., Yaneva, R., Hinson, E.R., and Cresswell, P. (2011). Human cytomegalovirus directly induces the antiviral protein viperin to enhance infectivity. Science *332*, 1093-1097.

Seth, P. (1994). Adenovirus-dependent release of choline from plasma membrane vesicles at an acidic pH is mediated by the penton base protein. Journal of virology *68*, 1204-1206.

Settembre, C., Fraldi, A., Medina, D.L., and Ballabio, A. (2013). Signals from the lysosome: a control centre for cellular clearance and energy metabolism. Nat Rev Mol Cell Biol *14*, 283-296.

Sewatanon, J., and Ling, P.D. (2013). Murine gammaherpesvirus 68 ORF75c contains ubiquitin E3 ligase activity and requires PML SUMOylation but not other known cellular PML regulators, CK2 and E6AP, to mediate PML degradation. Virology *440*, 140-149.

Shadfan, M., Lopez-Pajares, V., and Yuan, Z.M. (2012). MDM2 and MDMX: Alone and together in regulation of p53. Transl Cancer Res *1*, 88-89.

Sharifi, H.J., Furuya, A.K., Jellinger, R.M., Nekorchuk, M.D., and de Noronha, C.M. (2014). Cullin4A and cullin4B are interchangeable for HIV Vpr and Vpx action through the CRL4 ubiquitin ligase complex. Journal of virology *88*, 6944-6958.

Shen, Y., Zhu, H., and Shenk, T. (1997). Human cytomagalovirus IE1 and IE2 proteins are mutagenic and mediate "hit-and-run" oncogenic transformation in cooperation with the adenovirus E1A proteins. Proc Natl Acad Sci U S A *94*, 3341-3345.

Sheridan, P.L., Schorpp, M., Voz, M.L., and Jones, K.A. (1995). Cloning of an SNF2/SWI2-related protein that binds specifically to the SPH motifs of the SV40 enhancer and to the HIV-1 promoter. J Biol Chem *270*, 4575-4587.

Shieh, S.Y., Ahn, J., Tamai, K., Taya, Y., and Prives, C. (2000). The human homologs of checkpoint kinases Chk1 and Cds1 (Chk2) phosphorylate p53 at multiple DNA damage-inducible sites. Genes Dev *14*, 289-300.

Shirata, N., Kudoh, A., Daikoku, T., Tatsumi, Y., Fujita, M., Kiyono, T., Sugaya, Y., Isomura, H., Ishizaki, K., and Tsurumi, T. (2005). Activation of ataxia telangiectasia-mutated DNA damage checkpoint signal transduction elicited by herpes simplex virus infection. J Biol Chem *280*, 30336-30341.

Shnayder, M., Nachshon, A., Krishna, B., Poole, E., Boshkov, A., Binyamin, A., Maza, I., Sinclair, J., Schwartz, M., and Stern-Ginossar, N. (2018). Defining the Transcriptional Landscape during Cytomegalovirus Latency with Single-Cell RNA Sequencing. mBio *9*.

Shpilka, T., Mizushima, N., and Elazar, Z. (2012). Ubiquitin-like proteins and autophagy at a glance. J Cell Sci *125*, 2343-2348.

Sijmons, S., Thys, K., Mbong Ngwese, M., Van Damme, E., Dvorak, J., Van Loock, M., Li, G., Tachezy, R., Busson, L., Aerssens, J.*, et al.* (2015a). High-throughput analysis of human cytomegalovirus genome diversity highlights the widespread occurrence of gene-disrupting mutations and pervasive recombination. Journal of virology.

Sijmons, S., Thys, K., Mbong Ngwese, M., Van Damme, E., Dvorak, J., Van Loock, M., Li, G., Tachezy, R., Busson, L., Aerssens, J.*, et al.* (2015b). High-throughput analysis of human cytomegalovirus genome diversity highlights the widespread occurrence of gene-disrupting mutations and pervasive recombination. Journal of virology *89*, 7673-7695.

Simanek, A.M., Dowd, J.B., Pawelec, G., Melzer, D., Dutta, A., and Aiello, A.E. (2011). Seropositivity to cytomegalovirus, inflammation, all-cause and cardiovascular disease-related mortality in the United States. PLoS One *6*, e16103.

Simonsen, A., and Tooze, S.A. (2009). Coordination of membrane events during autophagy by multiple class III PI3-kinase complexes. The Journal of cell biology *186*, 773-782.

Sinclair, J. (2010). Chromatin structure regulates human cytomegalovirus gene expression during latency, reactivation and lytic infection. Biochimica et biophysica acta *1799*, 286-295.

Sinclair, J., and Sissons, P. (2006). Latency and reactivation of human cytomegalovirus. The Journal of general virology *87*, 1763-1779.

Sinzger, C., Hahn, G., Digel, M., Katona, R., Sampaio, K.L., Messerle, M., Hengel, H., Koszinowski, U., Brune, W., and Adler, B. (2008). Cloning and sequencing of a highly productive, endotheliotropic virus strain derived from human cytomegalovirus TB40/E. The Journal of general virology *89*, 359-368.

Siracusano, G., Venuti, A., Lombardo, D., Mastino, A., Esclatine, A., and Sciortino, M.T. (2016). Early activation of MyD88-mediated autophagy sustains HSV-1 replication in human monocytic THP-1 cells. Sci Rep *6*, 31302.

Sirbu, B.M., and Cortez, D. (2013). DNA damage response: three levels of DNA repair regulation. Cold Spring Harb Perspect Biol *5*, a012724.

Sissons, J.G., and Carmichael, A.J. (2002). Clinical aspects and management of cytomegalovirus infection. J Infect *44*, 78-83.

Skaar, J.R., Pagan, J.K., and Pagano, M. (2013). Mechanisms and function of substrate recruitment by F-box proteins. Nat Rev Mol Cell Biol *14*, 369-381.

Skaletskaya, A., Bartle, L.M., Chittenden, T., McCormick, A.L., Mocarski, E.S., and Goldmacher, V.S. (2001). A cytomegalovirus-encoded inhibitor of apoptosis that suppresses caspase-8 activation. Proc Natl Acad Sci U S A *98*, 7829-7834.

Sloan, E., Orr, A., and Everett, R.D. (2016). MORC3, a Component of PML Nuclear Bodies, Has a Role in Restricting Herpes Simplex Virus 1 and Human Cytomegalovirus. Journal of virology *90*, 8621-8633.

Slobedman, B., Cao, J.Z., Avdic, S., Webster, B., McAllery, S., Cheung, A.K., Tan, J.C., and Abendroth, A. (2010). Human cytomegalovirus latent infection and associated viral gene expression. Future Microbiol *5*, 883-900.

Slobedman, B., and Mocarski, E.S. (1999). Quantitative analysis of latent human cytomegalovirus. Journal of virology *73*, 4806-4812.

Sluimer, J., and Distel, B. (2018). Regulating the human HECT E3 ligases. Cell Mol Life Sci *75*, 3121-3141.

Smith, G. (2012). Herpesvirus transport to the nervous system and back again. Annual review of microbiology *66*, 153-176.

Smith, G.C., and Jackson, S.P. (1999). The DNA-dependent protein kinase. Genes Dev *13*, 916-934.

Sobhy, H. (2017). A comparative review of viral entry and attachment during large and giant dsDNA virus infections. Arch Virol *162*, 3567-3585.

Soucy, T.A., Smith, P.G., Milhollen, M.A., Berger, A.J., Gavin, J.M., Adhikari, S., Brownell, J.E., Burke, K.E., Cardin, D.P., Critchley, S.*, et al.* (2009). An inhibitor of NEDD8-activating enzyme as a new approach to treat cancer. Nature *458*, 732-736.

Spaete, R.R., Gehrz, R.C., and Landini, M.P. (1994). Human cytomegalovirus structural proteins. The Journal of general virology *75 (Pt 12)*, 3287-3308.

Spit, M., Rieser, E., and Walczak, H. (2019). Linear ubiquitination at a glance. J Cell Sci *132*.

Sridharan, H., Ragan, K.B., Guo, H., Gilley, R.P., Landsteiner, V.J., Kaiser, W.J., and Upton, J.W. (2017). Murine cytomegalovirus IE3-dependent transcription is required for DAI/ZBP1-mediated necroptosis. EMBO Rep *18*, 1429-1441.

Stanton, R.J., Baluchova, K., Dargan, D.J., Cunningham, C., Sheehy, O., Seirafian, S., McSharry, B.P., Neale, M.L., Davies, J.A., Tomasec, P.*, et al.* (2010). Reconstruction of the complete human cytomegalovirus genome in a BAC reveals RL13 to be a potent inhibitor of replication. The Journal of clinical investigation *120*, 3191-3208.

Stanton, R.J., McSharry, B.P., Rickards, C.R., Wang, E.C., Tomasec, P., and Wilkinson, G.W. (2007). Cytomegalovirus destruction of focal adhesions revealed in a high-throughput Western blot analysis of cellular protein expression. Journal of virology *81*, 7860-7872.

Stempel, M., Chan, B., Juranić Lisnić, V., Krmpotić, A., Hartung, J., Paludan, S.R., Füllbrunn, N., Lemmermann, N.A., and Brinkmann, M.M. (2019). The herpesviral antagonist m152 reveals differential activation of STING-dependent IRF and NF-κB signaling and STING's dual role during MCMV infection. Embo j *38*.

Stern-Ginossar, N., Weisburd, B., Michalski, A., Le, V.T., Hein, M.Y., Huang, S.X., Ma, M., Shen, B., Qian, S.B., Hengel, H.*, et al.* (2012). Decoding human cytomegalovirus. Science *338*, 1088-1093.

Stetson, D.B., and Medzhitov, R. (2006). Type I interferons in host defense. Immunity *25*, 373-381.

Stratmann, S.A., Morrone, S.R., van Oijen, A.M., and Sohn, J. (2015). The innate immune sensor IFI16 recognizes foreign DNA in the nucleus by scanning along the duplex. Elife *4*, e11721.

Suda, H., Aoyagi, T., Hamada, M., Takeuchi, T., and Umezawa, H. (1972). Antipain, a new protease inhibitor isolated from actinomycetes. The Journal of antibiotics *25*, 263-266.

Sun, L., Wu, J., Du, F., Chen, X., and Chen, Z.J. (2013). Cyclic GMP-AMP synthase is a cytosolic DNA sensor that activates the type I interferon pathway. Science *339*, 786-791.

Sun, X., Yau, V.K., Briggs, B.J., and Whittaker, G.R. (2005). Role of clathrin-mediated endocytosis during vesicular stomatitis virus entry into host cells. Virology *338*, 53-60.

Sun, Z., Lu, Y., Ruan, Q., Ji, Y., He, R., Qi, Y., Ma, Y., and Huang, Y. (2007). Human cytomegalovirus UL145 gene is highly conserved among clinical strains. J Biosci *32*, 1111-1118.

Suzuki, T., Takahashi, T., Guo, C.T., Hidari, K.I., Miyamoto, D., Goto, H., Kawaoka, Y., and Suzuki, Y. (2005). Sialidase activity of influenza A virus in an endocytic pathway enhances viral replication. Journal of virology *79*, 11705-11715.

Taisne, C., Lussignol, M., Hernandez, E., Moris, A., Mouna, L., and Esclatine, A. (2019). Human cytomegalovirus hijacks the autophagic machinery and LC3 homologs in order to optimize cytoplasmic envelopment of mature infectious particles. Sci Rep *9*, 4560.

Takaoka, A., Wang, Z., Choi, M.K., Yanai, H., Negishi, H., Ban, T., Lu, Y., Miyagishi, M., Kodama, T., Honda, K.*, et al.* (2007). DAI (DLM-1/ZBP1) is a cytosolic DNA sensor and an activator of innate immune response. Nature *448*, 501-505.

Takeshita, F., Leifer, C.A., Gursel, I., Ishii, K.J., Takeshita, S., Gursel, M., and Klinman, D.M. (2001). Cutting edge: Role of Toll-like receptor 9 in CpG DNA-induced activation of human cells. J Immunol *167*, 3555-3558.

Tallóczy, Z., Jiang, W., Virgin, H.W.t., Leib, D.A., Scheuner, D., Kaufman, R.J., Eskelinen, E.L., and Levine, B. (2002). Regulation of starvation- and virus-induced autophagy by the eIF2alpha kinase signaling pathway. Proc Natl Acad Sci U S A *99*, 190-195.

Tallóczy, Z., Virgin, H.W.t., and Levine, B. (2006). PKR-dependent autophagic degradation of herpes simplex virus type 1. Autophagy *2*, 24-29.

Tamura, T., Yanai, H., Savitsky, D., and Taniguchi, T. (2008). The IRF family transcription factors in immunity and oncogenesis. Annu Rev Immunol *26*, 535-584.

Tan, N.G., Ardley, H.C., Scott, G.B., Rose, S.A., Markham, A.F., and Robinson, P.A. (2003). Human homologue of ariadne promotes the ubiquitylation of translation initiation factor 4E homologous protein, 4EHP. FEBS Lett *554*, 501-504.

Tanaka, K. (2009). The proteasome: overview of structure and functions. Proc Jpn Acad Ser B Phys Biol Sci *85*, 12-36.

Tanner, N.K., and Linder, P. (2001). DExD/H box RNA helicases: from generic motors to specific dissociation functions. Mol Cell *8*, 251-262.

Tavalai, N., Adler, M., Scherer, M., Riedl, Y., and Stamminger, T. (2011). Evidence for a dual antiviral role of the major nuclear domain 10 component Sp100 during the immediate-early and late phases of the human cytomegalovirus replication cycle. Journal of virology *85*, 9447-9458.

Tavalai, N., and Stamminger, T. (2011). Intrinsic cellular defense mechanisms targeting human cytomegalovirus. Virus Res *157*, 128-133.

Thottacherry, J.J., Sathe, M., Prabhakara, C., and Mayor, S. (2019). Spoiled for Choice: Diverse Endocytic Pathways Function at the Cell Surface. Annu Rev Cell Dev Biol *35*, 55-84.

Tibbetts, R.S., Cortez, D., Brumbaugh, K.M., Scully, R., Livingston, D., Elledge, S.J., and Abraham, R.T. (2000). Functional interactions between BRCA1 and the checkpoint kinase ATR during genotoxic stress. Genes Dev *14*, 2989-3002.

Tibbetts, S.A., Loh, J., Van Berkel, V., McClellan, J.S., Jacoby, M.A., Kapadia, S.B., Speck, S.H., and Virgin, H.W.t. (2003). Establishment and maintenance of gammaherpesvirus latency are independent of infective dose and route of infection. Journal of virology *77*, 7696-7701.

Tokunaga, F., Sakata, S., Saeki, Y., Satomi, Y., Kirisako, T., Kamei, K., Nakagawa, T., Kato, M., Murata, S., Yamaoka, S*., et al.* (2009). Involvement of linear polyubiquitylation of NEMO in NF-kappaB activation. Nat Cell Biol *11*, 123-132.

Tomasec, P., Wang, E.C., Davison, A.J., Vojtesek, B., Armstrong, M., Griffin, C., McSharry, B.P., Morris, R.J., Llewellyn-Lacey, S., Rickards, C*., et al.* (2005). Downregulation of natural killer cell-activating ligand CD155 by human cytomegalovirus UL141. Nat Immunol *6*, 181-188.

Tong, J., Yan, X., and Yu, L. (2010). The late stage of autophagy: cellular events and molecular regulation. Protein & cell *1*, 907-915.

Tooze, S.A., Abada, A., and Elazar, Z. (2014). Endocytosis and autophagy: exploitation or cooperation? Cold Spring Harb Perspect Biol *6*, a018358.

Towatari, T., Nikawa, T., Murata, M., Yokoo, C., Tamai, M., Hanada, K., and Katunuma, N. (1991). Novel epoxysuccinyl peptides. A selective inhibitor of cathepsin B, in vivo. FEBS Lett *280*, 311-315.

Tran, K., Kamil, J.P., Coen, D.M., and Spector, D.H. (2010a). Inactivation and disassembly of the anaphase-promoting complex during human cytomegalovirus infection is associated with degradation of the APC5 and APC4 subunits and does not require UL97-mediated phosphorylation of Cdh1. Journal of virology *84*, 10832-10843.

Tran, K., Mahr, J.A., and Spector, D.H. (2010b). Proteasome subunits relocalize during human cytomegalovirus infection, and proteasome activity is necessary for efficient viral gene transcription. Journal of virology *84*, 3079-3093.

Tsubuki, S., Saito, Y., Tomioka, M., Ito, H., and Kawashima, S. (1996). Differential inhibition of calpain and proteasome activities by peptidyl aldehydes of di-leucine and tri-leucine. J Biochem *119*, 572-576.

Turk, V., Stoka, V., Vasiljeva, O., Renko, M., Sun, T., Turk, B., and Turk, D. (2012). Cysteine cathepsins: from structure, function and regulation to new frontiers. Biochimica et biophysica acta *1824*, 68-88.

Ulane, C.M., and Horvath, C.M. (2002). Paramyxoviruses SV5 and HPIV2 assemble STAT protein ubiquitin ligase complexes from cellular components. Virology *304*, 160-166.

Umashankar, M., Petrucelli, A., Cicchini, L., Caposio, P., Kreklywich, C.N., Rak, M., Bughio, F., Goldman, D.C., Hamlin, K.L., Nelson, J.A*., et al.* (2011). A novel human cytomegalovirus locus modulates cell type-specific outcomes of infection. PLoS pathogens *7*, e1002444.

Unk, I., Hajdú, I., Fátyol, K., Hurwitz, J., Yoon, J.H., Prakash, L., Prakash, S., and Haracska, L. (2008). Human HLTF functions as a ubiquitin ligase for proliferating cell nuclear antigen polyubiquitination. Proc Natl Acad Sci U S A *105*, 3768-3773.

Unterholzner, L. (2013). The interferon response to intracellular DNA: why so many receptors? Immunobiology *218*, 1312-1321.

Unterholzner, L., Keating, S.E., Baran, M., Horan, K.A., Jensen, S.B., Sharma, S., Sirois, C.M., Jin, T., Latz, E., Xiao, T.S*., et al.* (2010). IFI16 is an innate immune sensor for intracellular DNA. Nat Immunol *11*, 997-1004.

Upadhyayula, S., and Michaels, M.G. (2013). Ganciclovir, Foscarnet, and Cidofovir: Antiviral Drugs Not Just for Cytomegalovirus. J Pediatric Infect Dis Soc *2*, 286-290.

Upton, J.W., Kaiser, W.J., and Mocarski, E.S. (2010). Virus inhibition of RIP3-dependent necrosis. Cell Host Microbe *7*, 302-313.

Valiya Veettil, M., Sadagopan, S., Kerur, N., Chakraborty, S., and Chandran, B. (2010). Interaction of c-Cbl with myosin IIA regulates Bleb associated macropinocytosis of Kaposi's sarcoma-associated herpesvirus. PLoS pathogens *6*, e1001238.

Van Damme, E., and Van Loock, M. (2014). Functional annotation of human cytomegalovirus gene products: an update. Frontiers in microbiology *5*, 218.

Vanarsdall, A.L., and Johnson, D.C. (2012). Human cytomegalovirus entry into cells. Current opinion in virology *2*.

Vandevenne, P., Lebrun, M., El Mjiyad, N., Ote, I., Di Valentin, E., Habraken, Y., Dortu, E., Piette, J., and Sadzot-Delvaux, C. (2011). The varicella-zoster virus ORF47 kinase interferes with host innate immune response by inhibiting the activation of IRF3. PLoS One *6*, e16870.

Varnum, S.M., Streblow, D.N., Monroe, M.E., Smith, P., Auberry, K.J., Pasa-Tolic, L., Wang, D., Camp, D.G., 2nd, Rodland, K., Wiley, S*., et al.* (2004). Identification of proteins in human cytomegalovirus (HCMV) particles: the HCMV proteome. Journal of virology *78*, 10960-10966.

Vincent, H.A., Ziehr, B., and Moorman, N.J. (2017). Mechanism of Protein Kinase R Inhibition by Human Cytomegalovirus pTRS1. Journal of virology *91*.

Voges, D., Zwickl, P., and Baumeister, W. (1999). The 26S proteasome: a molecular machine designed for controlled proteolysis. Annu Rev Biochem *68*, 1015-1068.

Wack, A., Terczyńska-Dyla, E., and Hartmann, R. (2015). Guarding the frontiers: the biology of type III interferons. Nat Immunol *16*, 802-809.

Waisner, H., and Kalamvoki, M. (2019). The ICP0 Protein of Herpes Simplex Virus 1 (HSV-1) Downregulates Major Autophagy Adaptor Proteins Sequestosome 1 and Optineurin during the Early Stages of HSV-1 Infection. Journal of virology *93*.

Wang, D., and Shenk, T. (2005). Human cytomegalovirus virion protein complex required for epithelial and endothelial cell tropism. Proc Natl Acad Sci U S A *102*, 18153-18158.

Wang, D., Xu, Q., Yuan, Q., Jia, M., Niu, H., Liu, X., Zhang, J., Young, C.Y., and Yuan, H. (2019). Proteasome inhibition boosts autophagic degradation of ubiquitinated-AGR2 and enhances the antitumor efficiency of bevacizumab. Oncogene *38*, 3458-3474.

Wang, J.T., Doong, S.L., Teng, S.C., Lee, C.P., Tsai, C.H., and Chen, M.R. (2009). Epstein-Barr virus BGLF4 kinase suppresses the interferon regulatory factor 3 signaling pathway. Journal of virology *83*, 1856-1869.

Wang, W., Taylor, S.L., Leisenfelder, S.A., Morton, R., Moffat, J.F., Smirnov, S., and Zhu, H. (2005). Human cytomegalovirus genes in the 15-kilobase region are required for viral replication in implanted human tissues in SCID mice. Journal of virology *79*, 2115-2123.

Wang, W., Xu, L., Su, J., Peppelenbosch, M.P., and Pan, Q. (2017). Transcriptional Regulation of Antiviral Interferon-Stimulated Genes. Trends Microbiol *25*, 573-584.

Wang, X., Huong, S.M., Chiu, M.L., Raab-Traub, N., and Huang, E.S. (2003). Epidermal growth factor receptor is a cellular receptor for human cytomegalovirus. Nature *424*, 456-461.

Wang, Y., Argiles-Castillo, D., Kane, E.I., Zhou, A., and Spratt, D.E. (2020). HECT E3 ubiquitin ligases - emerging insights into their biological roles and disease relevance. J Cell Sci *133*.

Weekes, M.P., Tan, S.Y., Poole, E., Talbot, S., Antrobus, R., Smith, D.L., Montag, C., Gygi, S.P., Sinclair, J.H., and Lehner, P.J. (2013). Latency-associated degradation of the MRP1 drug transporter during latent human cytomegalovirus infection. Science *340*, 199-202.

Weekes, Michael P., Tomasec, P., Huttlin, Edward L., Fielding, Ceri A., Nusinow, D., Stanton, Richard J., Wang, Eddie C.Y., Aicheler, R., Murrell, I., Wilkinson, Gavin W.G.*, et al.* (2014). Quantitative Temporal Viromics: An Approach to Investigate Host-Pathogen Interaction. Cell *157*, 1460-1472.

Wenzel, D.M., Lissounov, A., Brzovic, P.S., and Klevit, R.E. (2011). UBCH7 reactivity profile reveals parkin and HHARI to be RING/HECT hybrids. Nature *474*, 105-108.

West, A.P., Koblansky, A.A., and Ghosh, S. (2006). Recognition and signaling by toll-like receptors. Annu Rev Cell Dev Biol *22*, 409-437.

Wickham, T.J., Mathias, P., Cheresh, D.A., and Nemerow, G.R. (1993). Integrins alpha v beta 3 and alpha v beta 5 promote adenovirus internalization but not virus attachment. Cell *73*, 309-319.

Wiertz, E.J., Jones, T.R., Sun, L., Bogyo, M., Geuze, H.J., and Ploegh, H.L. (1996a). The human cytomegalovirus US11 gene product dislocates MHC class I heavy chains from the endoplasmic reticulum to the cytosol. Cell *84*, 769-779.

Wiertz, E.J., Tortorella, D., Bogyo, M., Yu, J., Mothes, W., Jones, T.R., Rapoport, T.A., and Ploegh, H.L. (1996b). Sec61-mediated transfer of a membrane protein from the endoplasmic reticulum to the proteasome for destruction. Nature *384*, 432-438.

Wiggin, G.R., Soloaga, A., Foster, J.M., Murray-Tait, V., Cohen, P., and Arthur, J.S. (2002). MSK1 and MSK2 are required for the mitogen- and stress-induced phosphorylation of CREB and ATF1 in fibroblasts. Mol Cell Biol *22*, 2871-2881.

Wilkinson, D.E., and Weller, S.K. (2004). Recruitment of cellular recombination and repair proteins to sites of herpes simplex virus type 1 DNA replication is dependent on the composition of viral proteins within prereplicative sites and correlates with the induction of the DNA damage response. Journal of virology *78*, 4783-4796.

Wu, J., Sun, L., Chen, X., Du, F., Shi, H., Chen, C., and Chen, Z.J. (2013). Cyclic GMP-AMP is an endogenous second messenger in innate immune signaling by cytosolic DNA. Science *339*, 826-830.

Wu, J.J., Li, W., Shao, Y., Avey, D., Fu, B., Gillen, J., Hand, T., Ma, S., Liu, X., Miley, W.*, et al.* (2015). Inhibition of cGAS DNA Sensing by a Herpesvirus Virion Protein. Cell Host Microbe *18*, 333-344.

Xagorari, A., and Chlichlia, K. (2008). Toll-like receptors and viruses: induction of innate antiviral immune responses. The open microbiology journal *2*, 49-59.

Xiao, Z., Chen, Z., Gunasekera, A.H., Sowin, T.J., Rosenberg, S.H., Fesik, S., and Zhang, H. (2003). Chk1 mediates S and G2 arrests through Cdc25A degradation in response to DNA-damaging agents. J Biol Chem *278*, 21767-21773.

Yan, J., Shun, M.C., Hao, C., Zhang, Y., Qian, J., Hrecka, K., DeLucia, M., Monnie, C., Ahn, J., and Skowronski, J. (2018). HIV-1 Vpr Reprograms CLR4(DCAF1) E3 Ubiquitin Ligase to Antagonize Exonuclease 1-Mediated Restriction of HIV-1 Infection. mBio *9*.

Yan, J., Shun, M.C., Zhang, Y., Hao, C., and Skowronski, J. (2019). HIV-1 Vpr counteracts HLTF-mediated restriction of HIV-1 infection in T cells. Proc Natl Acad Sci U S A *116*, 9568-9577.

Yang, Q., Liu, T.T., Lin, H., Zhang, M., Wei, J., Luo, W.W., Hu, Y.H., Zhong, B., Hu, M.M., and Shu, H.B. (2017). TRIM32-TAX1BP1-dependent selective autophagic degradation of TRIF negatively regulates TLR3/4-mediated innate immune responses. PLoS pathogens *13*, e1006600.

Yang, Z., and Klionsky, D.J. (2010). Eaten alive: a history of macroautophagy. Nat Cell Biol *12*, 814-822.

Yasuma, T., Oi, S., Choh, N., Nomura, T., Furuyama, N., Nishimura, A., Fujisawa, Y., and Sohda, T. (1998). Synthesis of peptide aldehyde derivatives as selective inhibitors of human cathepsin L and their inhibitory effect on bone resorption. J Med Chem *41*, 4301-4308.

Yatim, N., and Albert, Matthew L. (2011). Dying to Replicate: The Orchestration of the Viral Life Cycle, Cell Death Pathways, and Immunity. Immunity *35*, 478-490.

Yu, D., Smith, G.A., Enquist, L.W., and Shenk, T. (2002). Construction of a self-excisable bacterial artificial chromosome containing the human cytomegalovirus genome and mutagenesis of the diploid TRL/IRL13 gene. Journal of virology *76*, 2316-2328.

Zhang, G., Raghavan, B., Kotur, M., Cheatham, J., Sedmak, D., Cook, C., Waldman, J., and Trgovcich, J. (2007). Antisense transcription in the human cytomegalovirus transcriptome. Journal of virology *81*, 11267-11281.

Zhang, W., Matrisian, L.M., Holmbeck, K., Vick, C.C., and Rosenthal, E.L. (2006). Fibroblast-derived MT1-MMP promotes tumor progression in vitro and in vivo. BMC Cancer *6*, 52.

Zhang, X., Shi, H., Wu, J., Zhang, X., Sun, L., Chen, C., and Chen, Z.J. (2013). Cyclic GMP-AMP containing mixed phosphodiester linkages is an endogenous high-affinity ligand for STING. Mol Cell *51*, 226-235.

Zhang, X.H., Tee, L.Y., Wang, X.G., Huang, Q.S., and Yang, S.H. (2015). Off-target Effects in CRISPR/Cas9-mediated Genome Engineering. Molecular therapy Nucleic acids *4*, e264.

Zhang, Z., Yuan, B., Bao, M., Lu, N., Kim, T., and Liu, Y.J. (2011). The helicase DDX41 senses intracellular DNA mediated by the adaptor STING in dendritic cells. Nat Immunol *12*, 959-965.

Zhao, B., Wei, X., Li, W., Udan, R.S., Yang, Q., Kim, J., Xie, J., Ikenoue, T., Yu, J., Li, L.*, et al.* (2007). Inactivation of YAP oncoprotein by the Hippo pathway is involved in cell contact inhibition and tissue growth control. Genes Dev *21*, 2747-2761.

Zhao, J., Zeng, Y., Xu, S., Chen, J., Shen, G., Yu, C., Knipe, D., Yuan, W., Peng, J., Xu, W.*, et al.* (2016). A Viral Deamidase Targets the Helicase Domain of RIG-I to Block RNA-Induced Activation. Cell Host Microbe *20*, 770-784.

Zhou, X., DeLucia, M., Hao, C., Hrecka, K., Monnie, C., Skowronski, J., and Ahn, J. (2017). HIV-1 Vpr protein directly loads helicase-like transcription factor (HLTF) onto the CRL4-DCAF1 E3 ubiquitin ligase. J Biol Chem *292*, 21117-21127.

Zhu, H., Shen, Y., and Shenk, T. (1995). Human cytomegalovirus IE1 and IE2 proteins block apoptosis. Journal of virology *69*, 7960-7970.

Zhu, H., Zheng, C., Xing, J., Wang, S., Li, S., Lin, R., and Mossman, K.L. (2011). Varicella-zoster virus immediate-early protein ORF61 abrogates the IRF3-mediated innate immune response through degradation of activated IRF3. Journal of virology *85*, 11079-11089.

Zimmermann, C., Krämer, N., Krauter, S., Strand, D., Sehn, E., Wolfrum, U., Freiwald, A., Butter, F., and Plachter, B. (2020). Autophagy interferes with human cytomegalovirus genome replication, morphogenesis, and progeny release. Autophagy, 1-17.

Zubarev, R.A., and Makarov, A. (2013). Orbitrap mass spectrometry. Anal Chem *85*, 5288-5296.

Appendices

Appendix table 1. Proteins identified to be rescued by MG132 at 12, 18, 24 hpi.

The uniprot accession code, gene name, full gene name, number of peptide identified, MG132 rescued ratio, and Benjimini corrected significance A p value of proteins identified to be rescued by MG132 at 12, 18, or 24 hpi are listed. A given protein was considered rescued by MG132 if its MG132 rescue ratio was greater than 1.5 and p value was less than 0.01.

Proteins rescued by MG132 at 12hpi					
Uniprot	**Gene Symbol**	**Description**	Peptides	MG132 rescue ratio	Rescue ratio p-value
Q9H0V9-2	LMAN2L	Isoform 2 of VIP36-like protein	1	4.65	6.73E-08
Q6ZN30	BNC2	Zinc finger protein basonuclin-2	6	3.75	2.72E-06
Q9H1A4	ANAPC1	Anaphase-promoting complex subunit 1	6	3.43	1.09E-05
Q15678	PTPN14	Tyrosine-protein phosphatase non-receptor type 14	9	3.29	2.04E-05
Q9NRY4	ARHGAP35	Rho GTPase-activating protein 35	20	3.02	6.91E-05
Q14527	HLTF	Helicase-like transcription factor	5	3.02	6.91E-05
Q9Y485	DMXL1	DmX-like protein 1	5	3.01	7.23E-05
Q15392	DHCR24	Delta(24)-sterol reductase	9	2.99	7.92E-05
O43734	TRAF3IP2	Adapter protein CIKS	1	2.95	9.52E-05
Q86X27	RALGPS2	Ras-specific guanine nucleotide-releasing factor RalGPS2	4	2.85	1.51E-04
Q96NE9	FRMD6	FERM domain-containing protein 6	6	2.78	2.09E-04
Q9UKI2	CDC42EP3	Cdc42 effector protein 3	4	2.77	2.19E-04
Q9H3M7	TXNIP	Thioredoxin-interacting protein	7	2.74	2.53E-04
Q7Z2Z1	TICRR	Treslin	1	2.71	2.91E-04
Q96SB3	PPP1R9B	Neurabin-2	15	2.64	4.04E-04
Q3MIT2	PUS10	Putative tRNA pseudouridine synthase Pus10	1	2.56	5.90E-04
Q9UJX5-3	ANAPC4	Isoform 3 of Anaphase-promoting complex subunit 4	3	2.56	5.90E-04

Q9UJX4	ANAPC5	Anaphase-promoting complex subunit 5	3	2.55	6.18E-04
P46934-4	NEDD4	Isoform 4 of E3 ubiquitin-protein ligase NEDD4	8	2.51	7.48E-04
Q86SQ0	PHLDB2	Pleckstrin homology-like domain family B member 2	26	2.50	7.84E-04
Q8NB16	MLKL	Mixed lineage kinase domain-like protein	3	2.49	8.22E-04
Q7Z3E5	ARMC9	LisH domain-containing protein ARMC9	11	2.41	1.20E-03
Q9HAU0-6	PLEKHA5	Isoform 6 of Pleckstrin homology domain-containing family A member 5	10	2.38	1.39E-03
Q8WV24	PHLDA1	Pleckstrin homology-like domain family A member 1	1	2.37	1.46E-03
Q9UHI8	ADAMTS1	A disintegrin and metalloproteinase with thrombospondin motifs 1	12	2.37	1.46E-03
Q96PU5	NEDD4L	E3 ubiquitin-protein ligase NEDD4-like	3	2.35	1.61E-03
O75676	RPS6KA4	Ribosomal protein S6 kinase alpha-4	4	2.34	1.68E-03
Q9Y4F9	FAM65B	Protein FAM65B	5	2.33	1.77E-03
O75486	SUPT3H	Transcription initiation protein SPT3 homolog	1	2.31	1.94E-03
Q9HA65	TBC1D17	TBC1 domain family member 17	4	2.29	2.14E-03
Q96J02	ITCH	E3 ubiquitin-protein ligase Itchy homolog	5	2.24	2.72E-03
Q14149	MORC3	MORC family CW-type zinc finger protein 3	13	2.21	3.15E-03
Q86XF0	DHFRL1	Dihydrofolate reductase, mitochondrial	3	2.16	4.00E-03
P78357	CNTNAP1	Contactin-associated protein 1	10	2.15	4.20E-03
Q5T5X7	BEND3	BEN domain-containing protein 3	3	2.14	4.41E-03
P30307	CDC25C	M-phase inducer phosphatase 3	1	2.11	5.10E-03
P23497-4	SP100	Isoform Sp100-C of Nuclear autoantigen Sp-100	17	2.11	5.10E-03
Q9P0V3	SH3BP4	SH3 domain-binding protein 4	14	2.09	5.61E-03
P17302	GJA1	Gap junction alpha-1 protein	9	2.05	6.81E-03
P84022	SMAD3	Mothers against decapentaplegic homolog 3	2	2.05	6.81E-03
Q9Y2U5	MAP3K2	Mitogen-activated protein kinase kinase kinase 2	3	2.05	6.81E-03
Q14865	ARID5B	AT-rich interactive domain-containing protein 5B	13	2.04	7.15E-03
Q99962	SH3GL2	Endophilin-A1	1	2.04	7.15E-03
Q96JM2-3	ZNF462	Isoform 3 of Zinc finger protein 462	1	2.01	8.26E-03

Q14511	NEDD9	Enhancer of filamentation 1	3	1.98	9.55E-03
Q8TAM2	TTC8	Tetratricopeptide repeat protein 8	2	1.98	9.55E-03
		Proteins rescued by MG132 at 18hpi			
Uniprot	Gene Symbol	Description	Peptides	MG132 rescue ratio	Rescue ratio p-value
Q9H0V9-2	LMAN2L	Isoform 2 of VIP36-like protein	1	4.65	6.73E-08
Q6ZN30	BNC2	Zinc finger protein basonuclin-2	6	3.75	2.72E-06
Q9H1A4	ANAPC1	Anaphase-promoting complex subunit 1	6	3.43	1.09E-05
Q15678	PTPN14	Tyrosine-protein phosphatase non-receptor type 14	9	3.29	2.04E-05
Q9NRY4	ARHGAP35	Rho GTPase-activating protein 35	20	3.02	6.91E-05
Q14527	HLTF	Helicase-like transcription factor	5	3.02	6.91E-05
Q9Y485	DMXL1	DmX-like protein 1	5	3.01	7.23E-05
Q15392	DHCR24	Delta(24)-sterol reductase	9	2.99	7.92E-05
O43734	TRAF3IP2	Adapter protein CIKS	1	2.95	9.52E-05
Q86X27	RALGPS2	Ras-specific guanine nucleotide-releasing factor RalGPS2	4	2.85	1.51E-04
Q96NE9	FRMD6	FERM domain-containing protein 6	6	2.78	2.09E-04
Q9UKI2	CDC42EP3	Cdc42 effector protein 3	4	2.77	2.19E-04
Q9H3M7	TXNIP	Thioredoxin-interacting protein	7	2.74	2.53E-04
Q7Z2Z1	TICRR	Treslin	1	2.71	2.91E-04
Q96SB3	PPP1R9B	Neurabin-2	15	2.64	4.04E-04
Q3MIT2	PUS10	Putative tRNA pseudouridine synthase Pus10	1	2.56	5.90E-04
Q9UJX5-3	ANAPC4	Isoform 3 of Anaphase-promoting complex subunit 4	3	2.56	5.90E-04
Q9UJX4	ANAPC5	Anaphase-promoting complex subunit 5	3	2.55	6.18E-04
P46934-4	NEDD4	Isoform 4 of E3 ubiquitin-protein ligase NEDD4	8	2.51	7.48E-04
Q86SQ0	PHLDB2	Pleckstrin homology-like domain family B member 2	26	2.50	7.84E-04
Q8NB16	MLKL	Mixed lineage kinase domain-like protein	3	2.49	8.22E-04
Q7Z3E5	ARMC9	LisH domain-containing protein ARMC9	11	2.41	1.20E-03
Q9HAU0-6	PLEKHA5	Isoform 6 of Pleckstrin homology domain-containing family A member 5	10	2.38	1.39E-03

Q8WV24	PHLDA1	Pleckstrin homology-like domain family A member 1	1	2.37	1.46E-03
Q9UHI8	ADAMTS1	A disintegrin and metalloproteinase with thrombospondin motifs 1	12	2.37	1.46E-03
Q96PU5	NEDD4L	E3 ubiquitin-protein ligase NEDD4-like	3	2.35	1.61E-03
O75676	RPS6KA4	Ribosomal protein S6 kinase alpha-4	4	2.34	1.68E-03
Q9Y4F9	FAM65B	Protein FAM65B	5	2.33	1.77E-03
O75486	SUPT3H	Transcription initiation protein SPT3 homolog	1	2.31	1.94E-03
Q9HA65	TBC1D17	TBC1 domain family member 17	4	2.29	2.14E-03
Q96J02	ITCH	E3 ubiquitin-protein ligase Itchy homolog	5	2.24	2.72E-03
Q14149	MORC3	MORC family CW-type zinc finger protein 3	13	2.21	3.15E-03
Q86XF0	DHFRL1	Dihydrofolate reductase, mitochondrial	3	2.16	4.00E-03
P78357	CNTNAP1	Contactin-associated protein 1	10	2.15	4.20E-03
Q5T5X7	BEND3	BEN domain-containing protein 3	3	2.14	4.41E-03
P30307	CDC25C	M-phase inducer phosphatase 3	1	2.11	5.10E-03
P23497-4	SP100	Isoform Sp100-C of Nuclear autoantigen Sp-100	17	2.11	5.10E-03
Q9P0V3	SH3BP4	SH3 domain-binding protein 4	14	2.09	5.61E-03
P17302	GJA1	Gap junction alpha-1 protein	9	2.05	6.81E-03
P84022	SMAD3	Mothers against decapentaplegic homolog 3	2	2.05	6.81E-03
Q9Y2U5	MAP3K2	Mitogen-activated protein kinase kinase kinase 2	3	2.05	6.81E-03
Q14865	ARID5B	AT-rich interactive domain-containing protein 5B	13	2.04	7.15E-03
Q99962	SH3GL2	Endophilin-A1	1	2.04	7.15E-03
Q96JM2-3	ZNF462	Isoform 3 of Zinc finger protein 462	1	2.01	8.26E-03
Q14511	NEDD9	Enhancer of filamentation 1	3	1.98	9.55E-03
Q8TAM2	TTC8	Tetratricopeptide repeat protein 8	2	1.98	9.55E-03
		Proteins rescued by MG132 at 24 hpi			
Uniprot	Gene Symbol	Description	Peptides	MG132 rescue ratio	Rescue ratio p-value
Q5T5X7	BEND3	BEN domain-containing protein 3	1	5.62	5.54E-19
P54756	EPHA5	Ephrin type-A receptor 5	2	3.66	1.44E-11
P41220	RGS2	Regulator of G-protein signaling 2	2	3.12	2.61E-09

P01100	FOS	Proto-oncogene c-Fos	3	2.91	2.08E-08
P09603	CSF1	Macrophage colony-stimulating factor 1	2	2.75	1.03E-07
O95067	CCNB2	G2/mitotic-specific cyclin-B2	2	2.72	1.39E-07
O76061	STC2	Stanniocalcin-2	1	2.61	4.18E-07
P52799	EFNB2	Ephrin-B2	4	2.51	1.15E-06
P55040	GEM	GTP-binding protein GEM	1	2.36	5.21E-06
Q14527	HLTF	Helicase-like transcription factor	9	2.33	7.05E-06
P28360	MSX1	Homeobox protein MSX-1	3	2.18	3.20E-05
P54753	EPHB3	Ephrin type-B receptor 3	6	2.17	3.53E-05
Q13322	GRB10	Growth factor receptor-bound protein 10	3	2.13	5.28E-05
A6ZKI3	FAM127A	Protein FAM127A	2	2.08	8.71E-05
P48740-2	MASP1	Isoform 2 of Mannan-binding lectin serine protease 1	7	2.07	9.63E-05
Q96JG8-4	MAGED4	Isoform 4 of Melanoma-associated antigen D4	5	2.04	1.30E-04
Q9NTJ4-4	MAN2C1	Isoform 4 of Alpha-mannosidase 2C1	1	2.03	1.43E-04
Q15048	LRRC14	Leucine-rich repeat-containing protein 14	1	1.99	2.14E-04
P08697	SERPINF2	Alpha-2-antiplasmin	1	1.95	3.17E-04
Q86Y39	NDUFA11	NADH dehydrogenase [ubiquinone] 1 alpha subcomplex subunit 11	5	1.91	4.71E-04
O95243	MBD4	Methyl-CpG-binding domain protein 4	7	1.90	5.19E-04
O15194	CTDSPL	CTD small phosphatase-like protein	1	1.89	5.73E-04
Q15014	MORF4L2	Mortality factor 4-like protein 2	13	1.87	6.96E-04
Q9Y561	LRP12	Low-density lipoprotein receptor-related protein 12	3	1.85	8.46E-04
Q9Y4G2	PLEKHM1	Pleckstrin homology domain-containing family M member 1	3	1.82	1.13E-03
Q14149	MORC3	MORC family CW-type zinc finger protein 3	11	1.81	1.25E-03
O43164	PJA2	E3 ubiquitin-protein ligase Praja-2	7	1.81	1.25E-03
Q86VI3	IQGAP3	Ras GTPase-activating-like protein IQGAP3	20	1.81	1.25E-03
Q9BRS2	RIOK1	Serine/threonine-protein kinase RIO1	3	1.80	1.37E-03
Q9NQS7	INCENP	Inner centromere protein	4	1.79	1.51E-03

Q7Z5L7-3	PODN	Isoform 3 of Podocan	2	1.79	1.51E-03
Q9H2G9	BLZF1	Golgin-45	12	1.79	1.51E-03
O75689-2	ADAP1	Isoform 2 of Arf-GAP with dual PH domain-containing protein 1	1	1.77	1.83E-03
Q86YV9	HPS6	Hermansky-Pudlak syndrome 6 protein	2	1.76	2.02E-03
Q9Y5G0	PCDHGB5	Protocadherin gamma-B5	7	1.76	2.02E-03
O14939	PLD2	Phospholipase D2	1	1.75	2.22E-03
Q66K89	E4F1	Transcription factor E4F1	1	1.74	2.44E-03
Q6PID6	TTC33	Tetratricopeptide repeat protein 33	4	1.74	2.44E-03
P23497-4	SP100	Isoform Sp100-C of Nuclear autoantigen Sp-100	21	1.74	2.44E-03
Q8IX01	SUGP2	SURP and G-patch domain-containing protein 2	17	1.74	2.44E-03
Q9H1A4	ANAPC1	Anaphase-promoting complex subunit 1	11	1.71	3.25E-03
Q15831	STK11	Serine/threonine-protein kinase STK11	1	1.70	3.57E-03
P55899	FCGRT	IgG receptor FcRn large subunit p51	4	1.69	3.92E-03
Q99962	SH3GL2	Endophilin-A1	1	1.69	3.92E-03
Q9NYF3	FAM53C	Protein FAM53C	3	1.68	4.31E-03
Q8N4S0	CCDC82	Coiled-coil domain-containing protein 82	4	1.68	4.31E-03
Q9BY41	HDAC8	Histone deacetylase 8	1	1.67	4.73E-03
O60238	BNIP3L	BCL2/adenovirus E1B 19 kDa protein-interacting protein 3-like	2	1.67	4.73E-03
O14730	RIOK3	Serine/threonine-protein kinase RIO3	7	1.67	4.73E-03
Q8NB16	MLKL	Mixed lineage kinase domain-like protein	7	1.64	6.26E-03
Q03113	GNA12	Guanine nucleotide-binding protein subunit alpha-12	6	1.64	6.26E-03
Q99715	COL12A1	Collagen alpha-1(XII) chain	147	1.63	6.87E-03
Q9UKU6	TRHDE	Thyrotropin-releasing hormone-degrading ectoenzyme	9	1.63	6.87E-03
Q8N0W4-2	NLGN4X	Isoform 2 of Neuroligin-4, X-linked	1	1.63	6.87E-03
O96006	ZBED1	Zinc finger BED domain-containing protein 1	5	1.62	7.53E-03
P28347	TEAD1	Transcriptional enhancer factor TEF-1	1	1.62	7.53E-03

Q13671	RIN1	Ras and Rab interactor 1	9	1.61	8.26E-03
Q14094	CCNI	Cyclin-I	2	1.60	9.05E-03
P01008	SERPINC1	Antithrombin-III	2	1.59	9.91E-03
Q53HC5	KLHL26	Kelch-like protein 26	2	1.59	9.91E-03

Uniprot	Gene Symbol	Description	Peptides	MG132 rescue ratio	Rescue ratio p-value
Q99418	CYTH2	Cytohesin-2	1	3.57	1.11E-19
Q5T7W7	TSTD2	Thiosulfate sulfurtransferase/rhodanese-like domain-containing protein 2	1	2.70	1.11E-12
P12107	COL11A1	Collagen alpha-1(XI) chain	1	2.61	6.07E-12
Q5T5X7	BEND3	BEN domain-containing protein 3	3	2.48	7.07E-11
Q9UJX6	ANAPC2	Anaphase-promoting complex subunit 2	1	2.26	4.44E-09
Q6UUV9-2	CRTC1	Isoform 2 of CREB-regulated transcription coactivator 1	1	2.23	7.78E-09
Q9BRT8	CBWD1	COBW domain-containing protein 1	1	2.00	5.48E-07
Q14527	HLTF	Helicase-like transcription factor	8	1.95	1.36E-06
Q9NZ94	NLGN3	Neuroligin-3	1	1.88	4.78E-06
P09603	CSF1	Macrophage colony-stimulating factor 1	1	1.86	6.82E-06
Q8N4S0	CCDC82	Coiled-coil domain-containing protein 82	5	1.85	8.14E-06
A6ZKI3	FAM127A	Protein FAM127A	3	1.77	3.31E-05
A1A4S6	ARHGAP10	Rho GTPase-activating protein 10	7	1.76	3.94E-05
Q8IX01	SUGP2	SURP and G-patch domain-containing protein 2	12	1.76	3.94E-05
O00221	NFKBIE	NF-kappa-B inhibitor epsilon	3	1.72	7.82E-05
Q14653	IRF3	Interferon regulatory factor 3	3	1.70	1.10E-04
Q86XP1	DGKH	Diacylglycerol kinase eta	1	1.69	1.30E-04
Q8IVF5-2	TIAM2	Isoform 2 of T-lymphoma invasion and metastasis-inducing protein 2	1	1.69	1.30E-04
Q9UHW5-2	GPN3	Isoform 2 of GPN-loop GTPase 3	1	1.68	1.54E-04
Q99962	SH3GL2	Endophilin-A1	1	1.68	1.54E-04

P98174	FGD1	FYVE, RhoGEF and PH domain-containing protein 1	4	1.67	1.82E-04
Q9UK97	FBXO9	F-box only protein 9	2	1.66	2.15E-04
Q9Y4K3	TRAF6	TNF receptor-associated factor 6	2	1.65	2.54E-04
Q8IYR2	SMYD4	SET and MYND domain-containing protein 4	1	1.65	2.54E-04
P52799	EFNB2	Ephrin-B2	4	1.64	3.00E-04
Q15038	DAZAP2	DAZ-associated protein 2	1	1.64	3.00E-04
O14641	DVL2	Segment polarity protein dishevelled homolog DVL-2	11	1.63	3.54E-04
Q86VP3-2	PACS2	Isoform 2 of Phosphofurin acidic cluster sorting protein 2	2	1.63	3.54E-04
Q8WWN8	ARAP3	Arf-GAP with Rho-GAP domain, ANK repeat and PH domain-containing protein 3	3	1.61	4.91E-04
Q8WV24	PHLDA1	Pleckstrin homology-like domain family A member 1	1	1.61	4.91E-04
Q8N2Q7	NLGN1	Neuroligin-1	2	1.59	6.79E-04
O60566-3	BUB1B	Isoform 3 of Mitotic checkpoint serine/threonine-protein kinase BUB1 beta	1	1.56	1.10E-03
O95243	MBD4	Methyl-CpG-binding domain protein 4	6	1.55	1.29E-03
Q96JK2	DCAF5	DDB1- and CUL4-associated factor 5	6	1.54	1.51E-03
P32754	HPD	4-hydroxyphenylpyruvate dioxygenase	1	1.54	1.51E-03
Q13490	BIRC2	Baculoviral IAP repeat-containing protein 2	7	1.54	1.51E-03
Q12882	DPYD	Dihydropyrimidine dehydrogenase [NADP(+)]	6	1.53	1.76E-03
Q53GA4	PHLDA2	Pleckstrin homology-like domain family A member 2	3	1.52	2.06E-03
Q6PID6	TTC33	Tetratricopeptide repeat protein 33	6	1.52	2.06E-03
Q8IWZ6	BBS7	Bardet-Biedl syndrome 7 protein	2	1.52	2.06E-03
Q15678	PTPN14	Tyrosine-protein phosphatase non-receptor type 14	3	1.51	2.40E-03
Q8TDX6	CSGALNACT1	Chondroitin sulfate N-acetylgalactosaminyltransferase 1	1	1.51	2.40E-03
Q03113	GNA12	Guanine nucleotide-binding protein subunit alpha-12	1	1.51	2.40E-03
P48740-2	MASP1	Isoform 2 of Mannan-binding lectin serine protease 1	11	1.51	2.40E-03
Q9HAD4	WDR41	WD repeat-containing protein 41	4	1.50	2.80E-03
Q7Z3E5	ARMC9	LisH domain-containing protein ARMC9	6	1.50	2.80E-03

P78560	CRADD	Death domain-containing protein CRADD	1	1.50	2.80E-03

Appendix table 2. Proteins identified to be degraded by pSILAC screen.

The uniprot accession code, gene name, full gene name of proteins identified to be degraded over 6 or 18 h of HCMV infection are listed. The rate of protein decline in mock- and HCMV-infected samples was therefore estimated using exponential regression in Excel and the formula: [relative protein abundance] (t) = $e^{Kdeg \cdot t}$ where Kdeg is the rate constant for degradation, and should be negative for degraded proteins. In cases where $Kdeg_{mock}$ was greater than 0, a fold change (FC_{CMV}) in protein abundance in the HCMV-infected sample at 6 or 18 hpi was instead used, defined by $FC_{HCMV} = e^{-Kdeg(CMV) \cdot t}$ A protein was considered down-regulated if $r_{deg} = Kdeg_{HCMV}/Kdeg_{mock} > 1.5$ (when $Kdeg_{mock} < 0$) or $FC_{HCMV} > 1.5$ (when $Kdeg_{mock} > 0$). P-values of r_{deg} (when $Kdeg_{mock} < 0$) and FC_{HCMV} (when $Kdeg_{mock} > 0$) were estimated and corrected for multiple hypothesis testing using the method of Benjamini-Hochberg. P-value of r_{deg} or FC_{HCMV} should <0.05 for a protein to be selected.

Uniprot	Gene Symbol	Description	0-6h peptides	0-18h peptides	6h r_{deg} or FC_{HCMV}	18h r_{deg} or FC_{HCMV}	p-value 0-6h Medium	p-value 0-18h Medium
Q14527	HLTF	Helicase-like transcription factor	10	5	4.26	1.76	1.14E-09	4.83E-02
Q8IX01	SUGP2	SURP and G-patch domain-containing protein 2	17	16	9.59	2.30	2.25E-02	5.12E-12
Q96J02	ITCH	E3 ubiquitin-protein ligase Itchy homolog	9	12	2.34	2.46	3.38E-02	6.32E-05
Q14149	MORC3	MORC family CW-type zinc finger protein 3	9	11	2.45	2.57	6.46E-05	5.36E-11
Q9Y485	DMXL1	DmX-like protein 1	1	6	2.09	5.32	1.81E-02	5.22E-12
Q92896-2	GLG1	Isoform 2 of Golgi apparatus protein 1	35	36	3.22	4.75	1.08E-25	6.02E-20
Q8NB16	MLKL	Mixed lineage kinase domain-like protein	5	3	1.82	11.43	6.68E-07	8.88E-04
Q99832	CCT7	T-complex protein 1 subunit eta	50	50	2.69	1.70	4.67E-02	4.31E-04
P16070	CD44	CD44 antigen	64	62	3.73	6.83	1.79E-06	1.15E-02
Q9UER7	DAXX	Death domain-associated protein 6	2	3	3.46	4.28	1.14E-06	6.43E-03
P11717	IGF2R	Cation-independent mannose-6-phosphate receptor	57	63	3.83	3.17	1.08E-02	3.72E-03

Q8NEM7-3	SUPT20H	Isoform 3 of Transcription factor SPT20 homolog	3	2	6.94	3.68	8.10E-03	4.16E-03
Q53ET0	CRTC2	CREB-regulated transcription coactivator 2	4	2	1.70		1.19E-02	8.03E-01
P16403	HIST1H1C	Histone H1.2	9	17	2.53	0.52	2.80E-02	4.67E-01
P51805	PLXNA3	Plexin-A3	1	1	1.98	0.79	4.25E-02	5.67E-01
Q7Z333-4	SETX	Isoform 4 of Probable helicase senataxin	3	1	3.88	2.41	2.78E-02	1.96E-01
Q9Y4K3	TRAF6	TNF receptor-associated factor 6	3	2	3.13	6.92	2.56E-02	4.28E-01
O00257	CBX4	E3 SUMO-protein ligase CBX4	4		2.14		2.37E-02	
Q9Y4F5	CEP170B	Centrosomal protein of 170 kDa protein B	1	5	24.09	2.02	7.90E-04	7.21E-01
P41240	CSK	Tyrosine-protein kinase CSK	10	10	6.35	1.16	3.20E-02	7.31E-01
P27707	DCK	Deoxycytidine kinase	7	8	4.01	0.89	3.10E-02	8.05E-02
Q8N9I9-2	DTX3	Isoform 2 of Probable E3 ubiquitin-protein ligase DTX3	1		1.75		1.14E-02	
Q70Z53-3	FRA10AC1	Isoform 3 of Protein FRA10AC1	3	3	3.74	0.77	3.19E-02	7.83E-02
P14649	MYL6B	Myosin light chain 6B	8	21	2.69	0.33	3.62E-02	1.88E-01
P55209	NAP1L1	Nucleosome assembly protein 1-like 1	58	35	1.98	0.57	6.59E-03	4.00E-01
O43776	NARS	Asparagine--tRNA ligase, cytoplasmic	22	39	1.54	4.66	3.89E-02	1.57E-01
P36639	NUDT1	7,8-dihydro-8-oxoguanine triphosphatase	6	3	10.44	-5.97	1.05E-02	9.67E-01
Q9H5K3	POMK	Protein O-mannose kinase	2	3	1.67	1.36	1.94E-02	5.42E-01
Q9Y371	SH3GLB1	Endophilin-B1	7	8	1.56	1.11	3.14E-02	5.54E-01
P52630	STAT2	Signal transducer and activator of transcription 2	7	6	3.21	1.29	7.15E-04	1.01E-04
P16949	STMN1	Stathmin	29	49	1.60	4.51	8.71E-03	2.84E-01
O75663	TIPRL	TIP41-like protein	8	14	1.79	1.02	2.45E-02	4.42E-01

Q9Y2K1	ZBTB1	Zinc finger and BTB domain-containing protein 1	1		1.78		1.15E-02	
O43707	ACTN4	Alpha-actinin-4	179	259	1.74	1.32	2.33E-02	2.16E-05
P54819	AK2	Adenylate kinase 2, mitochondrial	24	30	2.55	-1.61	9.94E-03	2.20E-01
Q9UIJ7	AK3	GTP:AMP phosphotransferase AK3, mitochondrial	9	13	2.23	-0.93	1.72E-02	2.44E-03
Q13740-2	ALCAM	Isoform 2 of CD166 antigen	64	46	2.59	3.30	1.22E-02	7.24E-01
Q9NVI7-2	ATAD3A	Isoform 2 of ATPase family AAA domain-containing protein 3A	8	18	2.67	-3.73	3.39E-02	6.09E-02
P78537	BLOC1S1	Biogenesis of lysosome-related organelles complex 1 subunit 1	3	1	2.47	0.51	1.07E-02	7.14E-01
Q12830	BPTF	Nucleosome-remodeling factor subunit BPTF	15	33	1.61	0.46	1.08E-02	6.00E-08
Q05682-4	CALD1	Isoform 4 of Caldesmon	4	8	2.24		2.16E-03	2.50E-01
Q05682-3	CALD1	Isoform 3 of Caldesmon	3	1	3.21	0.57	1.34E-03	4.64E-01
Q76M96-2	CCDC80	Isoform 2 of Coiled-coil domain-containing protein 80	3	9	1.63	1.06	1.51E-03	3.53E-01
Q9ULG6-5	CCPG1	Isoform 5 of Cell cycle progression protein 1	3	6	2.42	0.85	1.22E-02	1.66E-04
Q9H3Q1	CDC42EP4	Cdc42 effector protein 4	10	6	3.22	0.90	1.12E-02	4.33E-01
Q9NZZ3	CHMP5	Charged multivesicular body protein 5	9	9	1.75	0.45	1.57E-02	4.67E-01
Q9Y3Y2-3	CHTOP	Isoform 2 of Chromatin target of PRMT1 protein	9	7	1.82	0.22	4.82E-02	2.79E-01
P20674	COX5A	Cytochrome c oxidase subunit 5A, mitochondrial	7	17	1.58	-1.18	4.87E-02	3.51E-01
P51398	DAP3	28S ribosomal protein S29, mitochondrial	13	13	14.88	-0.23	1.60E-03	3.12E-01
Q9NX74	DUS2	tRNA-dihydrouridine(20) synthase [NAD(P)+]-like	8	3	1.75	0.61	8.37E-03	3.09E-01
Q9GZT9	EGLN1	Egl nine homolog 1	7	11	1.61	1.26	2.07E-02	3.85E-02

Q96AY2-2	EME1	Isoform 2 of Crossover junction endonuclease EME1	1	2	6.26		1.07E-02	7.69E-01
P06733	ENO1	Alpha-enolase	209	220	3.90		4.54E-04	3.21E-02
P58107	EPPK1	Epiplakin	6	4	1.62	6.15	3.56E-02	2.13E-01
P60520	GABARAPL2	Gamma-aminobutyric acid receptor-associated protein-like 2	9	10	6.16	1.14	4.45E-02	2.09E-01
Q8NBF1	GLIS1	Zinc finger protein GLIS1	1		2.35		1.44E-02	
Q5T3I0-3	GPATCH4	Isoform 3 of G patch domain-containing protein 4	6	5	2.82	0.48	3.22E-02	3.94E-02
Q6P1K8	GTF2H2C	General transcription factor IIH subunit 2-like protein	3	4	2.78		1.57E-02	8.30E-01
P16402	HIST1H1D	Histone H1.3	40	60	1.66	0.41	2.99E-02	2.88E-01
P31943	HNRNPH1	Heterogeneous nuclear ribonucleoprotein H	24	45	9.99	-0.96	1.31E-02	4.96E-01
P55795	HNRNPH2	Heterogeneous nuclear ribonucleoprotein H2	4	19	2.03		2.49E-02	9.47E-03
Q9HBG6-5	IFT122	Isoform 5 of Intraflagellar transport protein 122 homolog	7	5	1.86	5.50	7.86E-03	4.82E-01
Q16891-2	IMMT	Isoform 2 of MICOS complex subunit MIC60	3	8	4.11	1.06	4.33E-02	3.69E-03
Q14678	KANK1	KN motif and ankyrin repeat domain-containing protein 1	10	3	1.61	1.27	5.31E-03	7.34E-01
O60870	KIN	DNA/RNA-binding protein KIN17	5	5	10.02	0.49	2.95E-02	5.04E-04
Q9UHV7	MED13	Mediator of RNA polymerase II transcription subunit 13	3	2	12.70	1.32	3.63E-02	6.53E-01
P42568	MLLT3	Protein AF-9	1	2	6.13	0.58	1.92E-03	9.19E-03
P82650	MRPS22	28S ribosomal protein S22, mitochondrial	14	9	15.82	0.35	1.33E-02	2.40E-01
P35579	MYH9	Myosin-9	632	738	17.58	1.46	1.50E-03	1.44E-05
O75376	NCOR1	Nuclear receptor corepressor 1	12	18	2.40	0.54	3.71E-02	4.63E-06

O00483	NDUFA4	Cytochrome c oxidase subunit NDUFA4	4	9	2.63	0.95	1.48E-04	4.21E-01
P08651	NFIC	Nuclear factor 1 C-type	8	10	2.15	0.86	4.60E-03	1.00E+00
O60551	NMT2	Glycylpeptide N-tetradecanoyltransferase 2	12	14	1.51	0.06	3.26E-02	9.62E-01
O95478	NSA2	Ribosome biogenesis protein NSA2 homolog	2	3	2.77	0.77	2.21E-02	3.38E-02
P22059	OSBP	Oxysterol-binding protein 1	13	19	3.79	0.71	3.99E-02	3.35E-01
Q8TE49-2	OTUD7A	Isoform 2 of OTU domain-containing protein 7A	1	2	1.62	1.14	1.64E-02	4.22E-02
Q9UKK3	PARP4	Poly [ADP-ribose] polymerase 4	33	33	1.61	0.91	2.32E-02	1.31E-01
P57721	PCBP3	Poly(rC)-binding protein 3	25	17	5.26	1.23	9.28E-03	1.07E-01
Q9Y263	PLAA	Phospholipase A-2-activating protein	14	15	1.87	0.79	2.54E-02	4.96E-01
Q9UNA4	POLI	DNA polymerase iota	4		2.20		5.80E-03	
P24928	POLR2A	DNA-directed RNA polymerase II subunit RPB1	29	31	2.12	1.11	4.65E-05	9.81E-07
O15514	POLR2D	DNA-directed RNA polymerase II subunit RPB4	5	4	6.94	0.77	3.93E-02	2.55E-01
O15355	PPM1G	Protein phosphatase 1G	15	19	2.18	0.32	9.74E-03	7.67E-01
P63151-2	PPP2R2A	Isoform 2 of Serine/threonine-protein phosphatase 2A 55 kDa regulatory subunit B alpha isoform	12	21	59.69	0.38	2.28E-02	1.94E-01
Q99460	PSMD1	26S proteasome non-ATPase regulatory subunit 1	78	67	2.38	5.76	5.50E-04	5.14E-02
Q15185	PTGES3	Prostaglandin E synthase 3	22	27	1.75		2.93E-02	1.41E-01
P51149	RAB7A	Ras-related protein Rab-7a	36	33	2.60	3.58	2.04E-02	6.87E-02
C9J798	RASA4B	Ras GTPase-activating protein 4B	5	3	1.72	0.99	7.30E-03	5.30E-01
Q9H7B2	RPF2	Ribosome production factor 2 homolog	7	4	3.84	1.94	4.79E-03	4.36E-01
P46778	RPL21	60S ribosomal protein L21	37	37	1.65	1.03	2.82E-04	5.05E-02

P62424	RPL7A	60S ribosomal protein L7a	52	57	3.16	1.18	2.09E-03	1.48E-01
P46783	RPS10	40S ribosomal protein S10	38	42	6.02	-0.46	1.14E-02	3.17E-01
P62841	RPS15	40S ribosomal protein S15	22	18	1.73	-0.90	4.41E-03	8.76E-03
P62244	RPS15A	40S ribosomal protein S15a	22	13	4.14		2.70E-03	3.17E-01
Q9UBE0	SAE1	SUMO-activating enzyme subunit 1	27	26	3.09	-0.12	1.60E-02	9.16E-02
O00422	SAP18	Histone deacetylase complex subunit SAP18	14	10	4.18	0.35	4.47E-02	1.70E-01
Q9HCN8	SDF2L1	Stromal cell-derived factor 2-like protein 1	1	2	2.15		3.42E-02	3.13E-01
Q9BRK5	SDF4	45 kDa calcium-binding protein	16	11	1.57	0.52	3.49E-04	4.64E-04
O94979-8	SEC31A	Isoform 8 of Protein transport protein Sec31A	46	57	1.80	0.93	3.02E-02	1.99E-03
O43765	SGTA	Small glutamine-rich tetratricopeptide repeat-containing protein alpha	8	15	4.38	0.97	2.76E-02	8.37E-01
Q5HYK7	SH3D19	SH3 domain-containing protein 19	11	10	1.88	0.41	2.88E-02	9.45E-03
P48067-2	SLC6A9	Isoform GlyT-1A of Sodium- and chloride-dependent glycine transporter 1	2	1	1.68	1.73	1.12E-02	8.86E-01
O75391	SPAG7	Sperm-associated antigen 7	13	8	1.81	0.71	2.52E-02	1.89E-02
Q96I99	SUCLG2	Succinate--CoA ligase [GDP-forming] subunit beta, mitochondrial	40	46	1.72	0.61	3.96E-02	3.32E-01
Q96BN2	TADA1	Transcriptional adapter 1	1		2.61		2.07E-03	
Q6I9Y2	THOC7	THO complex subunit 7 homolog	10	4	1.68	-0.43	9.11E-03	7.88E-03
O94972	TRIM37	E3 ubiquitin-protein ligase TRIM37	1		2.26		8.31E-03	
Q969M7-2	UBE2F	Isoform 2 of NEDD8-conjugating enzyme UBE2F	2	2	1.89	0.55	3.98E-02	1.67E-01
Q9NVE5-3	USP40	Isoform 3 of Ubiquitin carboxyl-terminal hydrolase 40	6	5	3.52	-1.06	3.24E-02	6.37E-02
P08670	VIM	Vimentin	408	370	2.18		6.01E-04	7.24E-02

Q7Z5K2-3	WAPL	Isoform 3 of Wings apart-like protein homolog	15	17	3.02	0.86	4.96E-02	1.53E-02
Q9H1J7	WNT5B	Protein Wnt-5b	9	4	2.92	0.72	6.22E-03	2.46E-01
Q68DK2	ZFYVE26	Zinc finger FYVE domain-containing protein 26	6	4	2.69	-1.78	4.10E-02	3.84E-01
Q15326	ZMYND11	Zinc finger MYND domain-containing protein 11	6	7	2.27	1.66	3.94E-04	3.51E-01
Q9H1A4	ANAPC1	Anaphase-promoting complex subunit 1	6	6	1.24	10.60	3.20E-02	9.86E-09
Q9UJX4	ANAPC5	Anaphase-promoting complex subunit 5	6	2	1.67	4.63	1.20E-01	3.38E-03
Q9NRY4	ARHGAP35	Rho GTPase-activating protein 35	18	36	1.83	4.20	1.02E-02	1.09E-21
Q9HAU0-6	PLEKHA5	Isoform 6 of Pleckstrin homology domain-containing family A member 5	7	10		4.40	5.11E-01	2.60E-03
Q96SB3	PPP1R9B	Neurabin-2	8	11	1.50	5.56	5.52E-03	5.12E-12
Q15392	DHCR24	Delta(24)-sterol reductase	13	15		9.24	3.28E-01	1.29E-07
P16333	NCK1	Cytoplasmic protein NCK1	13	10	0.18	2.40	4.13E-01	2.09E-06
P13797	PLS3	Plastin-3	109	94		2.47	4.83E-01	9.41E-06
P17612	PRKACA	cAMP-dependent protein kinase catalytic subunit alpha	6	8		1.61	4.88E-02	2.55E-02
P60891	PRPS1	Ribose-phosphate pyrophosphokinase 1	14	11	1.68	30.28	3.30E-01	3.47E-02
P23497-4	SP100	Isoform Sp100-C of Nuclear autoantigen Sp-100	13	5	1.14	3.40	7.33E-03	8.96E-05
Q9H4A3-7	WNK1	Isoform 6 of Serine/threonine-protein kinase WNK1	28	29	1.34	2.24	3.96E-01	4.57E-04
Q9UJX5-3	ANAPC4	Isoform 3 of Anaphase-promoting complex subunit 4	2	3	-0.38	5.32	7.37E-01	4.30E-03
P78357	CNTNAP1	Contactin-associated protein 1	3	4	1.26	2.61	1.18E-02	2.50E-03
Q8TE73	DNAH5	Dynein heavy chain 5, axonemal		3		2.49		1.78E-02

Q15678	PTPN14	Tyrosine-protein phosphatase non-receptor type 14	4	3	1.83	1.77	2.59E-01	2.68E-02
Q86X27	RALGPS2	Ras-specific guanine nucleotide-releasing factor RalGPS2	7	7		5.69	3.14E-02	2.42E-05
O75676	RPS6KA4	Ribosomal protein S6 kinase alpha-4	7	6	1.78	2.43	1.50E-01	1.17E-05
O96006	ZBED1	Zinc finger BED domain-containing protein 1	4	3	1.15	2.06	8.00E-02	6.47E-03
Q2M2I8	AAK1	AP2-associated protein kinase 1	12	26	0.57	14.39	4.51E-01	4.26E-02
Q9Y6D5	ARFGEF2	Brefeldin A-inhibited guanine nucleotide-exchange protein 2	8	13	-1.07	2.79	2.61E-01	4.81E-03
P31939	ATIC	Bifunctional purine biosynthesis protein PURH	45	49	1.18	2.95	9.37E-01	1.86E-04
Q7L1Q6-3	BZW1	Isoform 3 of Basic leucine zipper and W2 domain-containing protein 1	35	47		2.34	6.78E-01	3.37E-02
P16152	CBR1	Carbonyl reductase [NADPH] 1	46	26		4.60	4.63E-01	4.21E-02
P14324	FDPS	Farnesyl pyrophosphate synthase	7	12		1.62	7.56E-01	1.60E-02
Q4V328	GRIPAP1	GRIP1-associated protein 1	12	14	1.48	1.85	7.88E-01	5.06E-03
Q13907-2	IDI1	Isoform 2 of Isopentenyl-diphosphate Delta-isomerase 1	10	12		1.94	4.87E-01	2.86E-03
P46821	MAP1B	Microtubule-associated protein 1B	184	246	-0.56	2.36	2.36E-01	1.38E-08
Q15691	MAPRE1	Microtubule-associated protein RP/EB family member 1	27	27		2.85	2.11E-01	1.33E-02
P61244	MAX	Protein max	1	1	1.50	2.03	9.69E-01	4.64E-02
Q96RE7	NACC1	Nucleus accumbens-associated protein 1	6	8	-8.43	10.58	1.11E-01	2.56E-02
Q16537	PPP2R5E	Serine/threonine-protein phosphatase 2A 56 kDa regulatory subunit epsilon isoform	4	5		2.72	7.86E-02	4.64E-03
P63098	PPP3R1	Calcineurin subunit B type 1	9	12	0.58	1.59	2.51E-01	2.98E-02

P04049-2	RAF1	Isoform 2 of RAF proto-oncogene serine/threonine-protein kinase	3	7	-4.00	2.08	5.62E-01	7.72E-03
P08134	RHOC	Rho-related GTP-binding protein RhoC	16	20		2.88	2.66E-01	7.64E-09
Q9NR31	SAR1A	GTP-binding protein SAR1a	9	10		5.20	6.15E-01	1.76E-02
Q8IXJ6	SIRT2	NAD-dependent protein deacetylase sirtuin-2	2	1	1.26	9.80	4.77E-01	4.70E-02
Q14258	TRIM25	E3 ubiquitin/ISG15 ligase TRIM25	24	35		4.07	5.05E-01	6.88E-06
Q16222	UAP1	UDP-N-acetylhexosamine pyrophosphorylase	20	22	0.77	1.61	3.80E-01	3.73E-02
P61088	UBE2N	Ubiquitin-conjugating enzyme E2 N	30	23		4.81	3.36E-04	1.02E-05
Q5T4S7-2	UBR4	Isoform 2 of E3 ubiquitin-protein ligase UBR4	78	80		1.54	7.76E-01	5.25E-03
P23381	WARS	Tryptophan--tRNA ligase, cytoplasmic	30	38		4.01	6.36E-01	4.16E-05
P54577	YARS	Tyrosine--tRNA ligase, cytoplasmic	60	63		12.40	1.12E-02	4.91E-03
P31946	YWHAB	14-3-3 protein beta/alpha	27	22	-1.13	4.73	6.30E-01	7.87E-04
Q9Y6B6	SAR1B	GTP-binding protein SAR1b	16	12		1.54	5.05E-02	2.58E-03
P35611-3	ADD1	Isoform 3 of Alpha-adducin	29	19	-83.43	2.64	6.82E-01	1.32E-05
Q9UEY8	ADD3	Gamma-adducin	15	20	0.39	1.64	9.24E-01	3.83E-05
P63010-2	AP2B1	Isoform 2 of AP-2 complex subunit beta	65	101		2.50	4.09E-01	4.16E-05
Q8N392	ARHGAP18	Rho GTPase-activating protein 18	27	27	2.60	4.47	3.64E-01	9.68E-03
Q9NVJ2	ARL8B	ADP-ribosylation factor-like protein 8B	15	9		11.11	8.47E-01	5.19E-04
Q8NHH9	ATL2	Atlastin-2	4	8	1.50	2.29	1.21E-01	4.43E-02
P20020-3	ATP2B1	Isoform B of Plasma membrane calcium-transporting ATPase 1	49	82	1.95	16.03	9.53E-01	4.80E-02
O75964	ATP5L	ATP synthase subunit g, mitochondrial	9	5	-1.46	40.92	4.31E-01	2.84E-02
P61421	ATP6V0D1	V-type proton ATPase subunit d 1	4	8	-1.00	3.10	3.63E-01	2.84E-02

P54289	CACNA2D1	Voltage-dependent calcium channel subunit alpha-2/delta-1	17	21	-3.96	2.28	2.51E-01	1.57E-03
Q86VP6	CAND1	Cullin-associated NEDD8-dissociated protein 1	65	66		5.94	6.17E-01	9.54E-04
P17655	CAPN2	Calpain-2 catalytic subunit	52	44	-5.18	3.40	7.77E-01	1.02E-05
P40227	CCT6A	T-complex protein 1 subunit zeta	59	30	1.53	2.81	2.50E-03	2.90E-04
P14209	CD99	CD99 antigen	4	9	0.79	1.70	6.27E-02	2.06E-02
P60953	CDC42	Cell division control protein 42 homolog	25	23		4.89	6.19E-01	2.66E-05
Q9Y5S2	CDC42BPB	Serine/threonine-protein kinase MRCK beta	16	33		2.80	8.82E-02	7.59E-04
Q8NCH0	CHST14	Carbohydrate sulfotransferase 14		2		1.97		3.98E-02
Q07065	CKAP4	Cytoskeleton-associated protein 4	67	88	2.47	4.18	2.56E-01	2.49E-02
O96005	CLPTM1	Cleft lip and palate transmembrane protein 1	5	18		1.58	4.48E-01	4.20E-03
Q00610	CLTC	Clathrin heavy chain 1	165	133		4.41	6.67E-01	2.46E-10
P21964	COMT	Catechol O-methyltransferase	15	8		90.75	2.79E-02	4.31E-03
Q9Y678	COPG1	Coatomer subunit gamma-1	51	59		2.83	8.24E-02	8.46E-04
Q9BT78	COPS4	COP9 signalosome complex subunit 4	25	23		3.43	3.48E-04	1.33E-02
Q9ULV4-3	CORO1C	Isoform 3 of Coronin-1C	53	80	1.35	1.77	2.00E-01	2.06E-02
Q99829	CPNE1	Copine-1	14	16	1.56	4.57	3.24E-01	2.85E-02
O75718	CRTAP	Cartilage-associated protein	22	30		32.40	2.31E-02	2.16E-02
P35221	CTNNA1	Catenin alpha-1	48	57	1.22	1.59	1.56E-01	6.55E-15
Q14247	CTTN	Src substrate cortactin	61	74	-0.26	2.03	7.38E-01	3.36E-02
Q96KC8	DNAJC1	DnaJ homolog subfamily C member 1	2	6	2.54	1.58	5.71E-01	4.83E-02
Q96N67	DOCK7	Dedicator of cytokinesis protein 7	30	38		2.39	3.39E-01	4.23E-02
Q9Y3R5	DOPEY2	Protein dopey-2	7	8		1.85	9.73E-01	3.58E-02
P26641-2	EEF1G	Isoform 2 of Elongation factor 1-gamma	70	56		1.91	6.33E-01	1.27E-02

P13639	EEF2	Elongation factor 2	256	285		2.29	9.82E-02	3.40E-05
Q9NZN4	EHD2	EH domain-containing protein 2	76	61		2.42	9.96E-01	8.32E-03
Q9NZN3	EHD3	EH domain-containing protein 3	19	12		124.38	5.65E-01	2.38E-02
Q15717-2	ELAVL1	Isoform 2 of ELAV-like protein 1	17	17		2.96	2.59E-01	4.27E-02
P50402	EMD	Emerin	9	14	7.37	2.29	6.44E-01	3.60E-02
Q9H2F5	EPC1	Enhancer of polycomb homolog 1	2	4	0.93	2.89	9.77E-01	4.43E-02
Q96CN4-2	EVI5L	Isoform 2 of EVI5-like protein	9	5		4.83	3.00E-01	1.16E-03
Q8IWE2	FAM114A1	Protein NOXP20	32	37	0.53	20.67	9.79E-01	2.87E-02
Q96TA1	FAM129B	Niban-like protein 1	61	71		8.08	8.54E-03	6.06E-08
Q96AC1-3	FERMT2	Isoform 3 of Fermitin family homolog 2	57	54		2.29	7.46E-02	2.63E-04
P07954	FH	Fumarate hydratase, mitochondrial	49	51		3.09	4.03E-02	3.50E-02
Q9NZ56	FMN2	Formin-2	5	14		2.02	8.45E-02	3.88E-02
Q13283	G3BP1	Ras GTPase-activating protein-binding protein 1	38	37	0.45	2.00	6.13E-02	1.68E-02
P11413-2	G6PD	Isoform Long of Glucose-6-phosphate 1-dehydrogenase	41	44	1.27	2.34	1.23E-01	3.73E-02
Q8N4A0	GALNT4	Polypeptide N-acetylgalactosaminyltransferase 4	3	7		3.42	1.91E-01	4.28E-02
P04062	GBA	Glucosylceramidase	11	7		1.79	8.92E-01	2.40E-02
Q92820	GGH	Gamma-glutamyl hydrolase	5	10		1.60	4.75E-01	2.35E-02
O94923	GLCE	D-glucuronyl C5-epimerase	3	5	1.51	2.59	3.11E-01	3.32E-02
O94925	GLS	Glutaminase kidney isoform, mitochondrial	20	30	-5.43	1.86	1.22E-01	1.14E-02
Q68CQ7	GLT8D1	Glycosyltransferase 8 domain-containing protein 1	9	14	1.39	3.32	9.82E-01	1.70E-03
P04899-4	GNAI2	Isoform sGi2 of Guanine nucleotide-binding protein G(i) subunit alpha-2	16	15		6.14	8.68E-02	2.20E-02

P62879	GNB2	Guanine nucleotide-binding protein G(I)/G(S)/G(T) subunit beta-2	27	15		1.65	3.29E-01	1.19E-05
Q9HAV0	GNB4	Guanine nucleotide-binding protein subunit beta-4	3	3		3.43	5.15E-01	4.87E-02
P63218	GNG5	Guanine nucleotide-binding protein G(I)/G(S)/G(O) subunit gamma-5	2	4	-3.49	2.04	6.48E-01	1.16E-03
Q14789-2	GOLGB1	Isoform 2 of Golgin subfamily B member 1	83	124	0.59	2.72	4.81E-02	8.81E-16
O00461	GOLIM4	Golgi integral membrane protein 4	15	17	3.91	3.70	1.91E-01	1.88E-02
P17174	GOT1	Aspartate aminotransferase, cytoplasmic	18	18		3.16	1.59E-01	6.26E-03
Q8TED1	GPX8	Probable glutathione peroxidase 8	9	14	-0.52	1.70	5.44E-01	6.51E-03
O43390-2	HNRNPR	Isoform 2 of Heterogeneous nuclear ribonucleoprotein R	51	56	1.60	7.15	2.18E-01	3.85E-02
P34932	HSPA4	Heat shock 70 kDa protein 4	133	151	1.50	26.40	2.28E-01	1.63E-02
P38646	HSPA9	Stress-70 protein, mitochondrial	102	138	0.85	100.73	2.03E-01	6.51E-03
Q9Y547	HSPB11	Intraflagellar transport protein 25 homolog	5	2		2.12	2.98E-01	2.45E-02
Q7Z6Z7	HUWE1	E3 ubiquitin-protein ligase HUWE1	45	56	1.76	1.54	1.91E-01	1.98E-02
O00410-3	IPO5	Isoform 3 of Importin-5	51	63		1.66	4.91E-01	1.50E-03
P23229-6	ITGA6	Isoform Alpha-6X1X2A of Integrin alpha-6	14	16	0.11	2.39	4.03E-01	4.02E-02
Q14571	ITPR2	Inositol 1,4,5-trisphosphate receptor type 2	12	18		2.05	2.32E-01	4.70E-02
P52294	KPNA1	Importin subunit alpha-5	10	12	-7.10	2.16	5.96E-01	8.06E-03
Q14974	KPNB1	Importin subunit beta-1	36	39	1.55	4.49	1.36E-01	2.63E-04
P42704	LRPPRC	Leucine-rich PPR motif-containing protein, mitochondrial	82	86		4.92	9.60E-01	8.74E-08
P78559-2	MAP1A	Isoform 2 of Microtubule-associated protein 1A	86	129	1.37	1.67	3.93E-01	2.60E-03

P27816-4	MAP4	Isoform 4 of Microtubule-associated protein 4	6	11	0.29	2.09	1.11E-02	6.80E-03
Q99549-2	MPHOSPH8	Isoform 2 of M-phase phosphoprotein 8	9	7		1.84	7.36E-02	4.93E-02
Q9NZW5	MPP6	MAGUK p55 subfamily member 6	5	8	1.45	2.09	7.34E-01	3.47E-02
Q86UE4	MTDH	Protein LYRIC	39	47	-0.27	4.91	5.64E-01	3.83E-03
Q15746-2	MYLK	Isoform 2 of Myosin light chain kinase, smooth muscle	84	82		1.74	4.21E-01	2.21E-02
P54920	NAPA	Alpha-soluble NSF attachment protein	26	18	0.48	3.54	8.24E-01	7.91E-03
Q6ZNB6	NFXL1	NF-X1-type zinc finger protein NFXL1	7	12	1.45	3.26	5.62E-01	2.57E-02
Q13423	NNT	NAD(P) transhydrogenase, mitochondrial	51	56	-4.23	4.68	4.06E-01	7.01E-03
P46459	NSF	Vesicle-fusing ATPase	54	51	-0.51	3.64	3.92E-01	5.89E-03
Q02818	NUCB1	Nucleobindin-1	24	19	0.94	1.63	1.85E-02	3.01E-03
P80303-2	NUCB2	Isoform 2 of Nucleobindin-2	36	28		13.35	1.23E-01	5.09E-07
Q13177	PAK2	Serine/threonine-protein kinase PAK 2	27	31	0.41	2.72	6.00E-01	1.26E-02
O95340-2	PAPSS2	Isoform B of Bifunctional 3'-phosphoadenosine 5'-phosphosulfate synthase 2	12	26	0.83	2.27	8.38E-01	3.90E-04
Q9NVD7	PARVA	Alpha-parvin	15	21	0.65	2.32	7.28E-01	1.17E-02
O95613	PCNT	Pericentrin	18	21	1.44	1.55	1.05E-01	2.23E-02
P42356	PI4KA	Phosphatidylinositol 4-kinase alpha	17	22	5.00	1.58	2.60E-01	2.44E-02
Q8IY17-4	PNPLA6	Isoform 4 of Neuropathy target esterase	6	9	1.13	5.62	5.74E-05	1.10E-05
O75569	PRKRA	Interferon-inducible double-stranded RNA-dependent protein kinase activator A	3	14		2.05	1.51E-01	1.87E-02
P07602-3	PSAP	Isoform Sap-mu-9 of Prosaposin	31	51	0.45	38.25	1.49E-03	4.48E-03

P62333	PSMC6	26S protease regulatory subunit 10B	22	21	0.22	6.87	7.90E-01	1.55E-02
Q13200	PSMD2	26S proteasome non-ATPase regulatory subunit 2	48	63		3.05	2.14E-01	3.33E-03
Q9Y3E5	PTRH2	Peptidyl-tRNA hydrolase 2, mitochondrial	7	8		2.49	2.83E-02	2.97E-02
P61106	RAB14	Ras-related protein Rab-14	14	20		3.50	8.19E-01	1.33E-02
Q9ULC3	RAB23	Ras-related protein Rab-23	6	10	-4.14	7.09	6.39E-02	2.58E-04
P51148-2	RAB5C	Isoform 2 of Ras-related protein Rab-5C	36	22		3.83	9.37E-01	1.87E-02
P61006	RAB8A	Ras-related protein Rab-8A	17	30		6.36	3.48E-01	2.08E-03
P61224	RAP1B	Ras-related protein Rap-1b	11	29		4.76	4.45E-02	1.63E-03
P54136	RARS	Arginine--tRNA ligase, cytoplasmic	52	85		28.33	2.29E-01	2.80E-02
Q9NWS8	RMND1	Required for meiotic nuclear division protein 1 homolog	3	6		1.52	3.01E-01	7.04E-03
Q96AT9	RPE	Ribulose-phosphate 3-epimerase	4	2	0.04	4.27	6.87E-01	2.64E-02
P62829	RPL23	60S ribosomal protein L23	32	20	0.56	4.21	3.09E-02	2.94E-02
Q9P2E9	RRBP1	Ribosome-binding protein 1	141	165	0.86	2.61	2.23E-01	2.48E-26
Q9NQC3	RTN4	Reticulon-4	32	15		3.23	1.36E-02	1.77E-02
P06703	S100A6	Protein S100-A6	40	36		20.63	1.68E-02	1.63E-05
P55735-3	SEC13	Isoform 3 of Protein SEC13 homolog	17	14		5.49	2.83E-03	2.72E-03
Q92503-2	SEC14L1	Isoform 2 of SEC14-like protein 1	4	2	1.20	1.84	2.64E-02	1.33E-02
O75396	SEC22B	Vesicle-trafficking protein SEC22b	20	18	0.32	1.60	1.32E-01	1.62E-02
O94855-2	SEC24D	Isoform 2 of Protein transport protein Sec24D	18	24		4.08	3.14E-01	4.15E-03
Q8NC51-3	SERBP1	Isoform 3 of Plasminogen activator inhibitor 1 RNA-binding protein	3	10		2.45	6.69E-02	3.32E-02
O75368	SH3BGRL	SH3 domain-binding glutamic acid-rich-like protein	10	23		3.62	3.63E-01	1.01E-03

Q2TAY7	SMU1	WD40 repeat-containing protein SMU1	8	10	2.00	8.62	1.89E-01	8.33E-03
P57768	SNX16	Sorting nexin-16	1	2	0.88	4.74	6.63E-02	2.15E-02
Q9H930	SP140L	Nuclear body protein SP140-like protein	3	1	1.23	1.87	5.27E-02	2.88E-02
Q13813-2	SPTAN1	Isoform 2 of Spectrin alpha chain, non-erythrocytic 1	217	226	0.83	2.51	4.89E-01	9.15E-14
P43307	SSR1	Translocon-associated protein subunit alpha	14	15		11.63	2.14E-02	4.02E-02
P50502	ST13	Hsc70-interacting protein	41	29	0.70	1.51	2.63E-02	2.64E-03
P55854-2	SUMO3	Isoform 2 of Small ubiquitin-related modifier 3	7	6	-0.05	3.62	9.59E-02	6.00E-03
O94901-9	SUN1	Isoform 9 of SUN domain-containing protein 1	2	12	11.33	2.48	1.19E-01	1.28E-02
Q8WXH0-2	SYNE2	Isoform 2 of Nesprin-2	92	95	3.73	3.16	5.59E-01	2.00E-07
O75529	TAF5L	TAF5-like RNA polymerase II p300/CBP-associated factor-associated factor 65 kDa subunit 5L		2		4.97		2.10E-03
Q99805	TM9SF2	Transmembrane 9 superfamily member 2	6	9	1.39	3.28	1.05E-01	1.15E-04
P49755	TMED10	Transmembrane emp24 domain-containing protein 10	25	19	-1.72	5.45	1.39E-01	7.73E-04
Q15363	TMED2	Transmembrane emp24 domain-containing protein 2	13	22		1.51	1.26E-02	4.42E-07
Q9BVC6	TMEM109	Transmembrane protein 109	3	5	2.18	5.78	2.31E-01	3.96E-02
Q86WV6	TMEM173	Stimulator of interferon genes protein	3	16		8.33	4.99E-01	1.29E-03
Q6NUQ4	TMEM214	Transmembrane protein 214	18	31		1.67	8.80E-02	1.21E-02
Q53FP2	TMEM35A	Transmembrane protein 35A	3	3		1.81	3.59E-01	3.47E-02
Q6ZXV5	TMTC3	Transmembrane and TPR repeat-containing protein 3	11	27	1.57	2.03	6.61E-01	1.12E-03

Q9Y320	TMX2	Thioredoxin-related transmembrane protein 2	5	10	-1.64	1.88	4.28E-02	1.01E-02
Q9H496	TOR1AIP2	Torsin-1A-interacting protein 2, isoform IFRG15		1		26.03		2.50E-02
P09493-6	TPM1	Isoform 6 of Tropomyosin alpha-1 chain	8	11	0.36	3.93	8.74E-02	1.03E-05
P09493-3	TPM1	Isoform 3 of Tropomyosin alpha-1 chain	27	46	0.90	1.98	5.39E-06	2.96E-07
P07951-2	TPM2	Isoform 2 of Tropomyosin beta chain	10	35	0.14	2.21	2.92E-05	8.55E-04
P07951	TPM2	Tropomyosin beta chain	7	13	0.47	4.76	1.28E-04	1.87E-02
O95361	TRIM16	Tripartite motif-containing protein 16	14	9	1.19	1.56	3.31E-01	1.65E-02
Q13630	TSTA3	GDP-L-fucose synthase	4	4		1.76	7.55E-01	2.00E-02
Q9UHD9	UBQLN2	Ubiquilin-2	4	5		1.51	1.59E-01	7.14E-03
Q8IWV7	UBR1	E3 ubiquitin-protein ligase UBR1	10	13		3.14	8.39E-01	2.72E-02
Q9NZ43	USE1	Vesicle transport protein USE1	6	7	1.97	1.56	2.57E-01	4.78E-02
O95183	VAMP5	Vesicle-associated membrane protein 5	1	9	1.07	6.89	9.89E-02	3.01E-02
Q6EMK4	VASN	Vasorin	1	4	1.24	1.64	1.24E-01	7.80E-03
O75436	VPS26A	Vacuolar protein sorting-associated protein 26A	16	22		9.37	2.54E-02	1.19E-02
Q9H6S0	YTHDC2	Probable ATP-dependent RNA helicase YTHDC2	13	9	1.85	1.81	4.37E-02	2.99E-02
Q9UBQ5	EIF3K	Eukaryotic translation initiation factor 3 subunit K	7	9		1.59	1.05E-01	4.54E-02
P08473	MME	Neprilysin	62	80	1.33	1.55	2.94E-01	2.89E-03

Appendix table 3. Proteins identified to be downregulated on protein level but not RNA level at 24 or 72 hpi.

The uniprot accession code, gene name, full gene name, number of peptide identified, fold changes of protein and RNA abundance and p-values of fold changes are listed here. p-values that a given protein was expressed significantly differently at 24 or 72 h compared to mock infection were estimated using Benjamini-Hochberg-corrected significance A value. A Benjamini-Hochberg corrected student's t-test was used to estimate the p-value for the hypothesis that a given transcript was expressed significantly differently at 24 or 72 h compared to mock infection

Proteins identified to be downregulated solely on protein level at 24 hpi							
Uniprot	**Gene Symbol**	**Description**	**Protein peptides**	**Protein FC 24h**	**RNA FC 24h**	**Protein 24h vs mock p-value**	**RNA 24h vs mock p-value**
Q8WW38	ZFPM2	Zinc finger protein ZFPM2	1	0.11	6.50	4.73E-06	1.52E-02
P51587	BRCA2	Breast cancer type 2 susceptibility protein	1	0.12	1.91	4.86E-06	2.76E-03
Q9H1A4	ANAPC1	Anaphase-promoting complex subunit 1	1	0.20	2.60	5.53E-04	1.84E-03
Q16670	ZSCAN26	Zinc finger and SCAN domain-containing protein 26	1	0.21	1.11	6.80E-04	1.67E-01
Q9NRY4	ARHGAP35	Rho GTPase-activating protein 35	11	0.25	1.07	2.69E-03	4.42E-01
Q9Y5G0	PCDHGB5	Protocadherin gamma-B5	1	0.25	1.08	3.03E-03	5.55E-01
P15531-2	NME1	Isoform 2 of Nucleoside diphosphate kinase A	1	0.27	1.30	4.69E-03	2.09E-01
Q15003	NCAPH	Condensin complex subunit 2	1	0.27	1.27	4.83E-03	2.09E-01
Q7Z333-4	SETX	Isoform 4 of Probable helicase senataxin	4	0.27	1.21	4.94E-03	6.88E-02
Q6PIY7	PAPD4	Poly(A) RNA polymerase GLD2	1	0.28	1.41	5.25E-03	5.48E-03
Q9H4A3-7	WNK1	Isoform 6 of Serine/threonine-protein kinase WNK1	7	0.28	1.50	5.47E-03	5.03E-03

Q99759-2	MAP3K3	Isoform 2 of Mitogen-activated protein kinase kinase kinase 3	1	0.28	1.90	5.54E-03	3.76E-02
Q99961	SH3GL1	Endophilin-A2	10	0.28	1.02	6.06E-03	9.55E-01
P16333	NCK1	Cytoplasmic protein NCK1	6	0.30	1.06	8.10E-03	4.48E-01
P16403	HIST1H1C	Histone H1.2	3	0.30	1.16	8.72E-03	9.19E-01
P23921	RRM1	Ribonucleoside-diphosphate reductase large subunit	15	0.30	1.71	9.10E-03	3.33E-04
Q9Y2U5	MAP3K2	Mitogen-activated protein kinase kinase kinase 2	1	0.32	1.56	1.24E-02	5.40E-03
O75815	BCAR3	Breast cancer anti-estrogen resistance protein 3	1	0.32	1.21	1.34E-02	1.19E-01
Q9UJX4	ANAPC5	Anaphase-promoting complex subunit 5	3	0.33	1.29	1.60E-02	8.82E-03
P50748	KNTC1	Kinetochore-associated protein 1	3	0.34	1.05	1.66E-02	6.69E-01
Q9HAW0	BRF2	Transcription factor IIIB 50 kDa subunit	2	0.34	2.60	1.91E-02	3.33E-01
Q99685	MGLL	Monoglyceride lipase	8	0.35	1.10	1.98E-02	1.57E-01
O95081	AGFG2	Arf-GAP domain and FG repeat-containing protein 2	1	0.35	1.40	2.03E-02	1.12E-01
P17812	CTPS1	CTP synthase 1	14	0.35	1.73	2.07E-02	1.51E-02
P49327	FASN	Fatty acid synthase	80	0.35	1.15	2.08E-02	6.81E-01
Q9P2D6	FAM135A	Protein FAM135A	1	0.35	2.43	2.20E-02	6.22E-04
Q14527	HLTF	Helicase-like transcription factor	3	0.35	1.88	2.23E-02	3.44E-03
Q14790-9	CASP8	Isoform 9 of Caspase-8	2	0.36	1.50	2.28E-02	1.15E-02
Q9BPX3	NCAPG	Condensin complex subunit 3	5	0.36	1.46	2.39E-02	1.05E-02
Q9BVJ7	DUSP23	Dual specificity protein phosphatase 23	1	0.36	1.00	2.52E-02	9.98E-01
A1A4S6	ARHGAP10	Rho GTPase-activating protein 10	5	0.37	1.13	2.75E-02	2.34E-01

Q05209	PTPN12	Tyrosine-protein phosphatase non-receptor type 12	8	0.37	1.07	2.75E-02	3.97E-01
Q96PU5	NEDD4L	E3 ubiquitin-protein ligase NEDD4-like	3	0.37	2.00	2.77E-02	4.25E-03
Q8IXW5	RPAP2	Putative RNA polymerase II subunit B1 CTD phosphatase RPAP2	1	0.37	1.17	2.81E-02	1.21E-01
Q9P1F3	ABRACL	Costars family protein ABRACL	1	0.37	1.46	2.95E-02	2.84E-03
Q14558-2	PRPSAP1	Isoform 2 of Phosphoribosyl pyrophosphate synthase-associated protein 1	5	0.38	1.26	3.14E-02	1.68E-01
P60891	PRPS1	Ribose-phosphate pyrophosphokinase 1	4	0.39	2.13	3.49E-02	2.26E-03
Q9BV44	THUMPD3	THUMP domain-containing protein 3	3	0.39	1.42	3.52E-02	2.18E-02
O60879	DIAPH2	Protein diaphanous homolog 2	4	0.39	1.08	3.78E-02	2.96E-01
Q13480-2	GAB1	Isoform 2 of GRB2-associated-binding protein 1	1	0.39	1.03	3.83E-02	7.08E-01
O94804	STK10	Serine/threonine-protein kinase 10	10	0.39	1.03	3.85E-02	9.27E-01
O60610	DIAPH1	Protein diaphanous homolog 1	19	0.40	1.66	4.06E-02	1.84E-02
P11908-2	PRPS2	Isoform 2 of Ribose-phosphate pyrophosphokinase 2	7	0.40	1.57	4.13E-02	1.80E-03
P56945-6	BCAR1	Isoform 6 of Breast cancer anti-estrogen resistance protein 1	4	0.40	1.17	4.20E-02	3.24E-01
P13797	PLS3	Plastin-3	43	0.40	1.01	4.25E-02	9.49E-01
O60281	ZNF292	Zinc finger protein 292	1	0.40	1.15	4.27E-02	1.07E-01
Q13509	TUBB3	Tubulin beta-3 chain	55	0.40	3.67	4.28E-02	1.00E-01
P48163	ME1	NADP-dependent malic enzyme	14	0.40	1.41	4.32E-02	1.20E-03
Q9NR46-2	SH3GLB2	Isoform 2 of Endophilin-B2	2	0.40	1.78	4.34E-02	3.75E-01
Q6ZUT9-2	DENND5B	Isoform 2 of DENN domain-containing protein 5B	1	0.40	1.73	4.36E-02	1.51E-03

P18510-3	IL1RN	Isoform 3 of Interleukin-1 receptor antagonist protein	1	0.41	1.65	4.44E-02	2.63E-02
Q14142	TRIM14	Tripartite motif-containing protein 14	1	0.41	1.90	4.45E-02	5.73E-03
Q9NWQ9	C14orf119	Uncharacterized protein C14orf119	1	0.41	1.24	4.47E-02	9.16E-02
O95772	STARD3NL	MLN64 N-terminal domain homolog	3	0.41	1.63	4.55E-02	2.79E-03
Q8IVD9	NUDCD3	NudC domain-containing protein 3	4	0.41	1.25	4.88E-02	6.11E-01
Q92882	OSTF1	Osteoclast-stimulating factor 1	3	0.41	1.32	4.93E-02	1.96E-02
Q8IX01	SUGP2	SURP and G-patch domain-containing protein 2	8	0.41	1.49	4.93E-02	1.17E-01
Q6AWC2-6	WWC2	Isoform 6 of Protein WWC2	1	0.41	1.49	4.96E-02	5.66E-03

Proteins identified to be downregulated solely on protein level at 72 hpi

Uniprot	**Gene Symbol**	**Description**	**Protein peptides**	**Protein FC 72h**	**RNA FC 72h**	**Protein 72h vs mock p-value**	**RNA 72h vs mock p-value**
Q9H1A4	ANAPC1	Anaphase-promoting complex subunit 1	1	0.07	1.54	5.34E-04	2.83E-02
P78348-1	ASIC1	Isoform 1 of Acid-sensing ion channel 1	2	0.08	1.53	8.72E-04	2.64E-01
Q8WW38	ZFPM2	Zinc finger protein ZFPM2	1	0.09	56.68	1.65E-03	1.94E-03
P16403	HIST1H1C	Histone H1.2	3	0.09	2.65	1.98E-03	4.61E-01
Q96SB3	PPP1R9B	Neurabin-2	8	0.10	1.36	2.91E-03	1.56E-01
O95081	AGFG2	Arf-GAP domain and FG repeat-containing protein 2	1	0.11	3.21	3.41E-03	3.25E-03
Q7Z333-4	SETX	Isoform 4 of Probable helicase senataxin	4	0.14	1.14	9.52E-03	2.28E-01
Q53ET0	CRTC2	CREB-regulated transcription coactivator 2	1	0.14	1.77	9.87E-03	6.44E-02

Q8WUI4-8	HDAC7	Isoform 8 of Histone deacetylase 7	1	0.14	1.15	1.05E-02	5.72E-01
Q9UJX4	ANAPC5	Anaphase-promoting complex subunit 5	3	0.14	1.12	1.07E-02	5.60E-02
P51587	BRCA2	Breast cancer type 2 susceptibility protein	1	0.14	1.31	1.09E-02	7.60E-02
Q8IX01	SUGP2	SURP and G-patch domain-containing protein 2	8	0.15	2.33	1.32E-02	2.10E-03
P51805	PLXNA3	Plexin-A3	2	0.15	1.70	1.38E-02	7.13E-02
Q9P2D6	FAM135A	Protein FAM135A	1	0.16	1.79	1.70E-02	5.99E-04
P02458	COL2A1	Collagen alpha-1(II) chain	13	0.16	102.16	1.80E-02	1.74E-03
Q00537-2	CDK17	Isoform 2 of Cyclin-dependent kinase 17	1	0.17	1.35	1.87E-02	5.01E-03
Q08AD1	CAMSAP2	Calmodulin-regulated spectrin-associated protein 2	3	0.17	1.52	2.06E-02	3.63E-04
Q9H4A3-7	WNK1	Isoform 6 of Serine/threonine-protein kinase WNK1	7	0.17	1.99	2.11E-02	5.52E-04
Q8N5C8	TAB3	TGF-beta-activated kinase 1 and MAP3K7-binding protein 3	1	0.17	2.35	2.17E-02	3.77E-04
Q9Y2U5	MAP3K2	Mitogen-activated protein kinase kinase kinase 2	1	0.17	1.96	2.22E-02	9.81E-04
Q99576	TSC22D3	TSC22 domain family protein 3	2	0.18	1.23	2.31E-02	2.61E-02
Q14527	HLTF	Helicase-like transcription factor	3	0.18	2.08	2.45E-02	8.10E-05
P06753	TPM3	Tropomyosin alpha-3 chain	24	0.19	2.58	3.14E-02	2.08E-04
O76041	NEBL	Nebulette	1	0.22	75.62	4.56E-02	1.17E-04
Q9HAU0-6	PLEKHA5	Isoform 6 of Pleckstrin homology domain-containing family A member 5	4	0.22	1.68	4.66E-02	5.07E-03
P17612	PRKACA	cAMP-dependent protein kinase catalytic subunit alpha	6	0.22	1.01	4.67E-02	9.25E-01
Q86WN1	FCHSD1	F-BAR and double SH3 domains protein 1	2	0.22	3.47	4.69E-02	4.64E-04

P05413	FABP3	Fatty acid-binding protein, heart	5	0.22	2.12	4.78E-02	1.80E-02
P22694-2	PRKACB	Isoform 2 of cAMP-dependent protein kinase catalytic subunit beta	9	0.22	1.45	4.83E-02	8.48E-04
Q8WU10	PYROXD1	Pyridine nucleotide-disulfide oxidoreductase domain-containing protein 1	1	0.22	1.24	5.00E-02	3.10E-01

Appendix table 4. Proteins identified to be degraded during HCMV infection in at least two out of three screens (high confidence).

Seven proteins passed the selection criteria of all 3 screens and 28 proteins passed 2 screens. “Y” means the protein was identified to be degraded in that particular screen, and “N” means that the protein did not. “N/A” means that the protein was not quantified in that particular screen.

Uniprot	Gene Symbol	Description	Screens degraded (stringent criteria)	MG132 Screen	pSILAC screen	RNA/Protein
Q9H1A4	ANAPC1	Anaphase-promoting complex subunit 1	3	Y	Y	Y
Q9UJX4	ANAPC5	Anaphase-promoting complex subunit 5	3	Y	Y	Y
Q9NRY4	ARHGAP35	Rho GTPase-activating protein 35	3	Y	Y	Y
Q14527	HLTF	Helicase-like transcription factor	3	Y	Y	Y
Q9HAU0-6	PLEKHA5	Isoform 6 of Pleckstrin homology domain-containing family A member 5	3	Y	Y	Y
Q96SB3	PPP1R9B	Neurabin-2	3	Y	Y	Y
Q8IX01	SUGP2	SURP and G-patch domain-containing protein 2	3	Y	Y	Y
Q53ET0	CRTC2	CREB-regulated transcription coactivator 2	2	N	Y	Y
Q15392	DHCR24	Delta(24)-sterol reductase	2	Y	Y	N
P16403	HIST1H1C	Histone H1.2	2	N	Y	Y
Q96J02	ITCH	E3 ubiquitin-protein ligase Itchy homolog	2	Y	Y	N
Q9Y2U5	MAP3K2	Mitogen-activated protein kinase kinase kinase 2	2	Y	Y	N
Q14149	MORC3	MORC family CW-type zinc finger protein 3	2	Y	Y	N
P16333	NCK1	Cytoplasmic protein NCK1	2	N	Y	Y
P13797	PLS3	Plastin-3	2	N	Y	Y
P51805	PLXNA3	Plexin-A3	2	N	Y	Y
P17612	PRKACA	cAMP-dependent protein kinase catalytic subunit alpha	2	N	Y	Y
P60891	PRPS1	Ribose-phosphate pyrophosphokinase 1	2	N	Y	Y

Q7Z333-4	SETX	Isoform 4 of Probable helicase senataxin	2	N	Y	Y
P23497-4	SP100	Isoform Sp100-C of Nuclear autoantigen Sp-100	2	Y	Y	N
Q9Y4K3	TRAF6	TNF receptor-associated factor 6	2	Y	Y	N
Q9H4A3-7	WNK1	Isoform 6 of Serine/threonine-protein kinase WNK1	2	N	Y	Y
Q9UJX5-3	ANAPC4	Isoform 3 of Anaphase-promoting complex subunit 4	2	Y	Y	N/A
A1A4S6	ARHGAP10	Rho GTPase-activating protein 10	2	Y	N	Y
P78357	CNTNAP1	Contactin-associated protein 1	2	Y	Y	N
Q9Y485	DMXL1	DmX-like protein 1	2	Y	Y	N/A
Q8TE73	DNAH5	Dynein heavy chain 5, axonemal	2	Y	Y	N
Q92896-2	GLG1	Isoform 2 of Golgi apparatus protein 1	2	N	Y	Y
Q8NB16	MLKL	Mixed lineage kinase domain-like protein	2	Y	Y	N/A
Q96PU5	NEDD4L	E3 ubiquitin-protein ligase NEDD4-like	2	Y	N/A	Y
Q9Y5G0	PCDHGB5	Protocadherin gamma-B5	2	Y	N/A	Y
Q15678	PTPN14	Tyrosine-protein phosphatase non-receptor type 14	2	Y	Y	N
Q86X27	RALGPS2	Ras-specific guanine nucleotide-releasing factor RalGPS2	2	Y	Y	N/A
O75676	RPS6KA4	Ribosomal protein S6 kinase alpha-4	2	Y	Y	N
O96006	ZBED1	Zinc finger BED domain-containing protein 1	2	Y	Y	N/A